



---

Publicly Accessible Penn Dissertations

---


Summer 8-12-2011

# Cryptophane Derivatives as Gas Sensors and Hyperpolarized Xenon-129 Biosensors

Najat S. Khan

University of Pennsylvania, najat@sas.upenn.edu

Follow this and additional works at: <http://repository.upenn.edu/edissertations>

 Part of the [Biochemistry Commons](#), and the [Organic Chemistry Commons](#)

---

## Recommended Citation

Khan, Najat S., "Cryptophane Derivatives as Gas Sensors and Hyperpolarized Xenon-129 Biosensors" (2011). *Publicly Accessible Penn Dissertations*. 393.

<http://repository.upenn.edu/edissertations/393>

This paper is posted at ScholarlyCommons. <http://repository.upenn.edu/edissertations/393>

For more information, please contact [libraryrepository@pobox.upenn.edu](mailto:libraryrepository@pobox.upenn.edu).

---

# Cryptophane Derivatives as Gas Sensors and Hyperpolarized Xenon-129 Biosensors

## Abstract

### ABSTRACT

#### CRYPTOPHANE DERIVATIVES AS GAS SENSORS AND HYPERPOLARIZED XENON-129 BIOSENSORS

Najat S. Khan

Professor Ivan J. Dmochowski

This thesis describes the progress in the development of cryptophanes for three different applications: encapsulation of noble gases,  $^{129}\text{Xe}$  NMR biosensing for cancer detection, and the construction of molecular devices. A new water-soluble organic host molecule, tris-(triazole ethylamine) cryptophane, was synthesized for noble gas detection. This host was found to bind xenon with the highest affinity to date ( $K_A = 42,000 \pm 2,000 \text{ M}^{-1}$  at 293 K). The same host was employed in the development of a radiometric assay for measuring the association constant of radon binding to a discrete molecular species,  $K_A = 49,000 \pm 12,000 \text{ M}^{-1}$  at 293 K. For cancer detection by hyperpolarized  $^{129}\text{Xe}$  MRI, a new folate-conjugated cryptophane biosensor was developed that targets folate receptors (FR) overexpressed in a majority of cancer cells. The biosensor was relatively non-toxic at low micromolar concentrations required for imaging and was shown to selectively target cancer cells overexpressing FR. Flow cytometry results indicated a 10-fold higher cellular internalization in KB cells (FR+) than in HT-1080 cells (FR-). Finally, a smaller cavity tribenzylamine hemicryptophane was synthesized where the molecular structure and motions of the cage closely resembled that of molecular gyroscopes. It also provided a vehicle for exploring the structure and properties of multiple *p*-phenylene rotators within one molecule. The compact size and molecular motions of this gyroscope-inspired tribenzylamine hemicryptophane make it an attractive starting point for controlling the direction and coupling of rotators within molecular systems.

## Degree Type

Dissertation

## Degree Name

Doctor of Philosophy (PhD)

## Graduate Group

Chemistry

## First Advisor

Dr. Ivan J. Dmochowski

---

**Second Advisor**

Dr. Virgil Percec

**Third Advisor**

Dr. David Christianson, Dr. Bill Dailey

**Keywords**

Biosensor, Cryptophane, Folate, Hyperpolarized, Hemicryptophane, Xenon

**Subject Categories**

Biochemistry | Organic Chemistry

CRYPTOPHANE DERIVATIVES AS GAS SENSORS AND HYPERPOLARIZED  
XENON-129 BIOSENSORS

Najat S. Khan

A Dissertation

In

Chemistry

Presented to the Faculties of the University of Pennsylvania in Partial  
Fulfillment of the Requirements for the Degree of Doctor of Philosophy

2011

---

Professor Ivan J. Dmochowski  
Supervisor of Dissertation

---

Professor Gary Molander  
Graduate Group Chair

Committee Members:

Dr. Virgil Percec, Roy Vagelos Chair and Professor of Chemistry  
Dr. David W. Christianson, Roy and Diana Vagelos Professor of Chemistry and  
Chemical Biology  
Dr. Bill Dailey, Associate Professor of Chemistry Organic Chemistry

CRYPTOPHANE DERIVATIVES AS GAS SENSORS AND HYPERPOLARIZED  
XENON-129 BIOSENSORS ©

2011

NAJAT S. KHAN

*For my grandparents, Dada, Dadi, Nana, Nani,  
and my parents, Ammu and Akke*

## ACKNOWLEDGEMENTS

I would like to first thank my dissertation advisor, Professor Ivan Dmochowski for providing the opportunity to work on several challenging and very rewarding projects. I greatly appreciate his continuous support and advice in all aspects of my thesis work as well as my future career goals. His open door policy has led to extremely useful discussions that I will take with me in my future endeavors. I would also like to thank my committee members, Dr. Virgil Percec, Dr. David Christianson and Dr. William Dailey for their helpful comments and insights over the past four years.

I would also like to thank the wonderful members of the Dmochowski lab. It has been a pleasure to work with past and current members of the lab, and over the years I have made many close friends. What has always stood out for me about our lab has been how well we all work together. Everyone is eager and willing to help, whether it is research related or issues of a more personal nature. A few people have really helped me along my path especially our postdoc Dr. Olena Taratula with whom I have worked closely throughout the last three years. Her strong work ethic and in-depth knowledge of chemistry has truly been an inspiration. Outside of lab she has been a very dear friend and her optimistic nature has made many difficult decisions seem easy. Julie Gripenburg and I joined Penn the same year and I couldn't have asked for a more caring and helpful friend. We have shared many experiences together and through the tough times I cannot imagine persevering without her sound advice. I have thoroughly enjoyed working with the other members of "Team Cryptophane": Brittany Riggle aka "Riggle", Yubin Bai,

David Jacobson aka “Tall” David, Jenny Chambers, Dr. Qien Wei, Dr. Garry Seward, Tara Kaufmann, and of course Dr. Aru Hill. Without Aru patiently teaching me all the essential organic laboratory skills, I could not have synthesized a single cryptophane. Also, thank you to the rest of the Dmochowski group members for making lab such an enjoyable experience: Jasmina Cheung-Lau (thanks for the daily laughs from the “Question of the Day”), Brittani Ruble and Dr. Ashley Fiamengo (thanks for helping me print and assemble this thesis), Katie Liao, Weiren Liu, and Dr. XinJing Tang.

I would also like to thank my classmates and friends including Julia Sandell and Ollie (therapy chats), Sara Braun, Lillian Rozin, Ariane Perez-Gavilan aka “PG”, Genette McGrew, Joshua Stecher, Chris and Jen MacDermaid, Alia Orbin, Stephen Gonzales, Jose Manuel Perez-Aguilar aka “Pepe”, Mark Fegley, Anne Wagner, Emily Berkley, Julie Aaron, and Sabreena Rahman.

For always being there through my ups and downs that is the graduate school experience, I would like to thank Blake Willmarth. Not only did he patiently listen to how things never worked in research, but he had the right advice to cheer me up and put everything into perspective. His support and efforts to keep me as happy as I could be every single day is something that I will never forget. Also, thanks to my handsome puppy Bo and rabbit Cheddar for putting a smile on my face everyday!

Lastly, I would like to thank my parents, Dr. Shamsheer Ali Khan and Dr. Nazma Begum, and my sister Dr. Jihan Khan and brother-in-law Vikram Mathur. Growing up in



three different countries, I admired how my parents were always up to the challenge and worked extremely hard to achieve the very best for themselves and our family. I am very lucky to have a mother who has exemplified the core values that I believe helped me throughout my graduate career: hard work, discipline, and constant willingness to learn more. My father has always been supportive through all my challenges and constantly reminded me to confidently face up to whatever may lie ahead. This unfailing belief in me along with their confidence in my choices in life is what has helped me be the person I am today. And I couldn't ask for a more perfect older sister to guide me through this process. Her clear views and calming demeanor have constantly helped to guide me in the right direction. To the newest member of the family, I would like to thank Vikram for being a great addition to my support system. Finally, I would like to thank my grandparents; I will always cherish their perseverance and hard work that they put in to help my family and myself be where we are today.

# ABSTRACT

## CRYPTOPHANE DERIVATIVES AS GAS SENSORS AND HYPERPOLARIZED XENON-129 BIOSENSORS

Najat S. Khan

Professor Ivan J. Dmochowski

This thesis describes the progress in the development of cryptophanes for three different applications: encapsulation of noble gases,  $^{129}\text{Xe}$  NMR biosensing for cancer detection, and the construction of molecular devices. A new water-soluble organic host molecule, tris-(triazole ethylamine) cryptophane, was synthesized for noble gas detection. This host was found to bind xenon with the highest affinity to date ( $K_A = 42,000 \pm 2,000 \text{ M}^{-1}$  at 293 K). The same host was employed in the development of a radiometric assay for measuring the association constant of radon binding to a discrete molecular species,  $K_A = 49,000 \pm 12,000 \text{ M}^{-1}$  at 293 K. For cancer detection by hyperpolarized  $^{129}\text{Xe}$  MRI, a new folate-conjugated cryptophane biosensor was developed that targets folate receptors (FR) overexpressed in a majority of cancer cells. The biosensor was relatively non-toxic at low micromolar concentrations required for imaging and was shown to selectively target cancer cells overexpressing FR. Flow cytometry results indicated a 10-fold higher cellular internalization in KB cells (FR+) than in HT-1080 cells (FR-). Finally, a smaller cavity tribenzylamine hemicryptophane was synthesized where the molecular structure and motions of the cage closely resembled that of molecular gyroscopes. It also provided a vehicle for exploring the structure and properties of multiple *p*-phenylene rotators

within one molecule. The compact size and molecular motions of this gyroscope-inspired tribenzylamine hemicryptophane make it an attractive starting point for controlling the direction and coupling of rotators within molecular systems.

## TABLE OF CONTENTS

<b>TITLE.....</b>	<b>i</b>
<b>DEDICATION.....</b>	<b>ii</b>
<b>ACKNOWLEDGEMENTS.....</b>	<b>iii</b>
<b>ABSTRACT.....</b>	<b>vi</b>
<b>TABLE OF CONTENTS.....</b>	<b>viii</b>
<b>LIST OF SCHEMES, FIGURES, AND TABLES.....</b>	<b>ix</b>
<b>CHAPTER 1:</b>	
<b>Introduction.....</b>	<b>1</b>
1.1 The role of cryptophanes in host-guest chemistry.....	1
1.2 Development of $^{129}\text{Xe}$ biosensors.....	9
1.3 Hemicryptophanes: a new application in the development of molecular devices.....	20
1.4 References.....	25
<b>CHAPTER 2: Measurement of Xenon and Radon Binding to a Cryptophane</b>	
<b>Molecular Host .....</b>	<b>36</b>
Abstract.....	37
Introduction.....	38
Results and Discussion.....	41
Conclusions.....	58
Experimental Procedures.....	61
Acknowledgements.....	72
References.....	73

<b>CHAPTER 3: Targeting The Folate Receptor with a Folate-Conjugated Cryptophane for Cancer Detection.....</b>	<b>79</b>
Abstract.....	80
Introduction.....	81
Results and Discussion.....	87
Conclusions.....	105
Experimental Procedures.....	106
Acknowledgements.....	123
References.....	124
<b>CHAPTER 4: Multiple Hindered Rotators in a Gyroscope-Inspired Tribenzylamine Hemicryptophane.....</b>	<b>129</b>
Abstract.....	130
Introduction.....	131
Results and Discussion.....	138
Conclusions.....	154
Experimental Procedures.....	155
Acknowledgements.....	170
References.....	171
<b>CHAPTER 5: Summary and Future Directions.....</b>	<b>178</b>
<b>APPENDIX A: X-ray Crystallographic Report.....</b>	<b>196</b>

<b>Figure 1.1.</b> Structure of Cryptophane-A.....	3
<b>Figure 1.2.</b> Two superimposed crystal structures of a triallyl cryptophane .....	5
<b>Figure 1.3.</b> Water-soluble cryptophanes.....	7
<b>Figure 1.4.</b> $^{129}\text{Xe}$ NMR biosensing concept.....	12
<b>Figure 1.5.</b> Biotin-conjugated $^{129}\text{Xe}$ biosensor.....	16
<b>Figure 1.6.</b> Benzenesulfonamide-conjugated $^{129}\text{Xe}$ biosensor.....	17
<b>Figure 1.7.</b> Examples of molecular devices and components.....	22
<b>Figure 2.1.</b> Structure of TTAC and TTPC.....	40
<b>Figure 2.2.</b> Synthesis of tris-(triazole ethylamine) cryptophane-A (TTEC).....	41
<b>Figure 2.3.</b> Enthalpogram of xenon binding to TTEC at pH 7.5.....	43
<b>Figure 2.4.</b> Diagrammatic representation of the radon binding affinity measurement....	45
<b>Figure 2.5.</b> Radon binding to TTEC.....	49
<b>Figure 2.6.</b> Structure of Tripropargyl cryptophane-Xe complex.....	51
<b>Figure 2.7.</b> Enthalpogram of xenon binding to TTEC at pH 2.5.....	54
<b>Figure 2.8.</b> Hyperpolarized $^{129}\text{Xe}$ NMR spectrum of TTEC at pH 7.5.....	55
<b>Figure 2.9.</b> Hyperpolarized $^{129}\text{Xe}$ NMR spectrum of TTEC at pH 2.5.....	56
<b>Figure 2.10.</b> Titration curve of TTEC.....	57
<b>Figure 3.1.</b> Scheme of FR $\alpha$ -mediated endocytosis of a folic acid drug conjugate.....	85
<b>Figure 3.2.</b> Structure of the FR $\alpha$ -targeting $^{129}\text{Xe}$ NMR biosensor.....	87
<b>Scheme 3.1.</b> 5-step synthesis of $\alpha$ -[2-(trimethylsilyl)ethoxy]-2- <i>N</i> -[2-(trimethylsilyl)- ethoxycarbonyl]folic acid.....	90
<b>Scheme 3.2.</b> 3-step synthesis of a cyclotriguaiacylene (CTG) unit.....	91

<b>Scheme 3.3.</b> Synthesis of [3-propargyloxy-4-(2-iodoethoxy)phenyl]methanol (D Linker) and [4-(2-iodoethoxy)-3-methoxyphenyl]methanol (A Linker).....	92
<b>Scheme 3.4.</b> Synthesis of monopropargylated derivative of cryptophane-A.....	93
<b>Scheme 3.5.</b> Synthesis of unlabeled and Cy3-labeled biosensor <b>24</b> and <b>25</b> .....	94
<b>Figure 3.3.</b> Cytotoxicity assays for folate-conjugated cryptophane biosensor.....	95
<b>Figure 3.4.</b> Confocal Laser Scanning Microscopy of Cy3-labeled <b>25</b> in KB, HeLa, and HT-1080 cells.....	98
<b>Figure 3.5.</b> Flow cytometry of Cy3-labeled <b>25</b> in KB and HT-1080 cells.....	100
<b>Figure 3.6.</b> Hyperpolarized $^{129}\text{Xe}$ NMR spectrum of <b>24</b> .....	102
<b>Figure 4.1.</b> Examples of molecular components.....	130
<b>Scheme 4.1.</b> Gyroscope-inspired tribenzylamine hemicryptophane ( <b>5</b> ).....	135
<b>Scheme 4.2.</b> Three-step synthesis of tribenzylamine hemicryptophane ( <b>5</b> ).....	138
<b>Figure 4.2.</b> Crystal structure analysis of ( <b>5</b> ).....	140
<b>Figure 4.3.</b> Molecular dynamics (MD) simulations in the absence and presence of xenon atom.....	143
<b>Figure 4.4.</b> Computational modeling and cavity volume calculations using GRASP....	145
<b>Figure 4.5.</b> $^1\text{H}$ VT-NMR spectra of <b>5</b> measured in $\text{CD}_2\text{Cl}_2$ .....	147
<b>Figure 4.6.</b> $^1\text{H}$ - $^1\text{H}$ NOESY spectrum of <b>5</b> in $\text{CDCl}_3$ .....	148
<b>Figure 4.7.-4.8.</b> Analysis of the molecular dynamics simulations .....	150
<b>Figure 4.9.</b> Orthogonal views of 30 superimposed structures from MD simulations....	152
<b>Figure 4.10.</b> Minimized energy structures of <b>5</b> .....	154

# CHAPTER 1: INTRODUCTION

## 1.1. The role of cryptophanes in host-guest chemistry

Host-guest chemistry involves the encapsulation of neutral and charged species by a variety of synthetic molecular systems.<sup>1</sup> This host-guest association is a key aspect of many applications in chemistry and biochemistry and has helped to elucidate many of the fundamentals of molecular recognition<sup>2-9</sup> and complexation among biological systems in Nature.<sup>10-16</sup> One of the first model studies of molecular recognition involved the binding of ammonium ions by crown ethers in solution by Pederson et al.<sup>17</sup> Since then, there has been a rapid growth in the synthesis of various organic hosts and investigation of their binding to guest molecules. Examples of organic synthetic host molecules include calixarenes,<sup>18-22</sup> cavitands,<sup>23</sup> cyclodextrins,<sup>24,25</sup> crown ethers,<sup>24,25</sup> carcerands,<sup>26</sup> and cryptophanes.<sup>1</sup> Due to the different molecular structures of these hosts, a wide variety of cavities with guest-binding properties are present, which has led to applications in drug delivery,<sup>27</sup> molecular recognition,<sup>23</sup> storage and separation,<sup>28</sup> and catalysis.<sup>29-31</sup>

Cryptophane-A is a molecular cage that was first developed by André Collet in 1981.<sup>32,33</sup> Since then, extensive research has been performed with this cage and its derivatives in the field of host-guest chemistry.<sup>1</sup> It is a chiral molecule with  $D_3$  symmetry, which is formed when two CTV (cyclotrimeratrylene) units are joined by three ethylene linkers (Figure 1.1). Guests are encapsulated within the cavity due to the presence of the three portals in the equatorial region of the cage. Previous work has shown that the size



and nature of the cavity can be tuned by varying the molecular structure as well as the length of the linkers.<sup>34</sup> The internal volume has been estimated to be  $87 \text{ \AA}^3$  (Figure 1.1), based on high-resolution X-ray crystallographic studies.<sup>35,36</sup> Cryptophane-A has been shown to reversibly bind to a variety of neutral small molecules (e.g. methane,  $K_A = 130 \text{ M}^{-1}$  in  $\text{C}_2\text{D}_2\text{Cl}_4$  at 298 K; chloroform,  $K_A = 230 \text{ M}^{-1}$  in  $\text{C}_2\text{D}_2\text{Cl}_4$  at 298 K; and xenon,  $K_A = 3900 \text{ M}^{-1}$  in  $\text{C}_2\text{D}_2\text{Cl}_4$  at 278 K).<sup>37,38</sup>

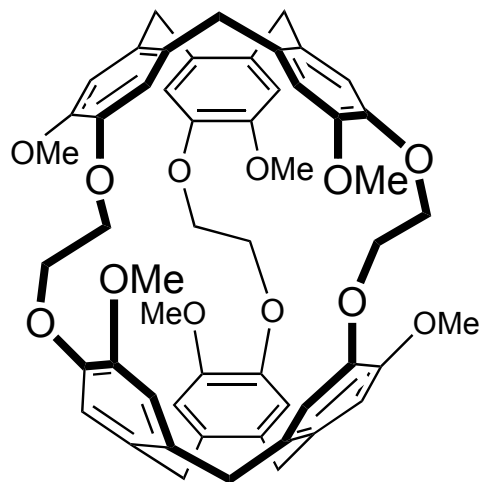


**Figure 1.1.** Cryptophane-A consists of two CTV units, which are joined by three ethylene linkers to give an internal volume of  $87 \text{ \AA}^3$ .

High-resolution X-ray structures of cryptophane-A and trifunctionalized derivative complexes have been reported with water, methanol, xenon and chloroform in the Dmochowski group.<sup>36</sup> In the case of methanol and xenon, the cavity is underfilled with a packing coefficient (defined as guest volume divided by host internal volume) of 0.39 and 0.47 respectively, whereas it is overfilled with chloroform as the guest (0.73).<sup>36</sup> According to Rebek's "55% rule", the volume of the guest and host are both critical for encapsulation processes to occur. By studying a variety of host-guest complexes they were able to determine that optimal binding is reached when the packing coefficient is  $0.55 \pm 0.09$  in organic liquids.<sup>35</sup> It is therefore not surprising that xenon binds with the highest affinity to cryptophane since the packing coefficient at 0.47 is closest to the empirically determined value reported by Rebek et al. This is also supported by the fact that X-ray structures indicated nearly optimized van der Waals interactions between xenon and the six cyclotriguaiacylene (CTG) phenyl moieties (experimental average = 4.31 Å, optimal van der Waals interaction distance for Xe and phenyl carbon is 3.86 Å).<sup>36</sup> In order to accommodate guests of different sizes, the crystal structures indicate that the trifunctionalized cryptophanes are able to increase the internal cavity volume by more than 20% by the expansion of two of the three ethylene linkers (Figure 1.2).<sup>36</sup> This study provided the first example of xenon-cryptophane association in the solid state and further demonstrated the role of cryptophanes as organic hosts that are capable of undergoing 'induced fit' to optimize binding via London forces to guest molecules.

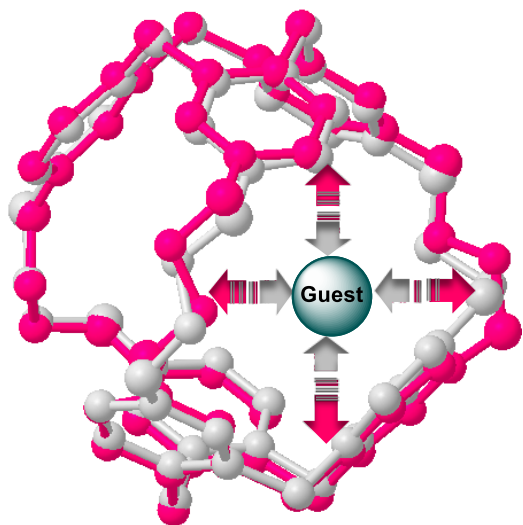


**Figure 1.2.** Side view of two superimposed crystal structures of a cryptophane-A derivative, triallyl cryptophane. The cryptophane is shown encapsulating MeOH (grey) and  $\text{CDCl}_3$  (pink). Guests, hydrogens and side chains were removed for easier viewing. Figure adapted from Taratula et al.<sup>36</sup>

In order to eventually perform *in vivo* studies, water-soluble versions of cryptophane-A have also been synthesized: Huber's hexa-acid cryptophanes ( $K_A = 6,800 \text{ M}^{-1}$  at 293 K) where the six methoxy groups were replaced by  $-\text{OCH}_2\text{CO}_2\text{H}$  groups,<sup>39</sup> tris-(triazole propionic acid) cryptophane (TTPC) ( $K_A = 17,000 \text{ M}^{-1}$  at 293 K),<sup>40</sup> and triacetate-functionalized cryptophane (TAAC) ( $K_A = 33,000 \text{ M}^{-1}$  at 293 K) (Figure 1.3).<sup>41</sup> The binding of xenon to TTPC and TAAC was measured by isothermal titration calorimetry (ITC) and fluorescence quenching.<sup>40,41</sup> TAAC has three carboxylate groups close to the cryptophane core and was determined to have the highest binding affinity for xenon of any host molecule in buffer.<sup>41</sup> The higher binding affinity in aqueous buffer compared to organic solvents is due to the higher enthalpic and entropic contributions in buffer. The higher enthalpic contributions arise from increased van der Waals interactions due to a more compact shape in water (assisted by the flexible ethylene linkers) whereas the desolvation of the water shell around xenon upon binding to cryptophane accounts for the high entropic contribution (Figure 1.3).<sup>40,41</sup>

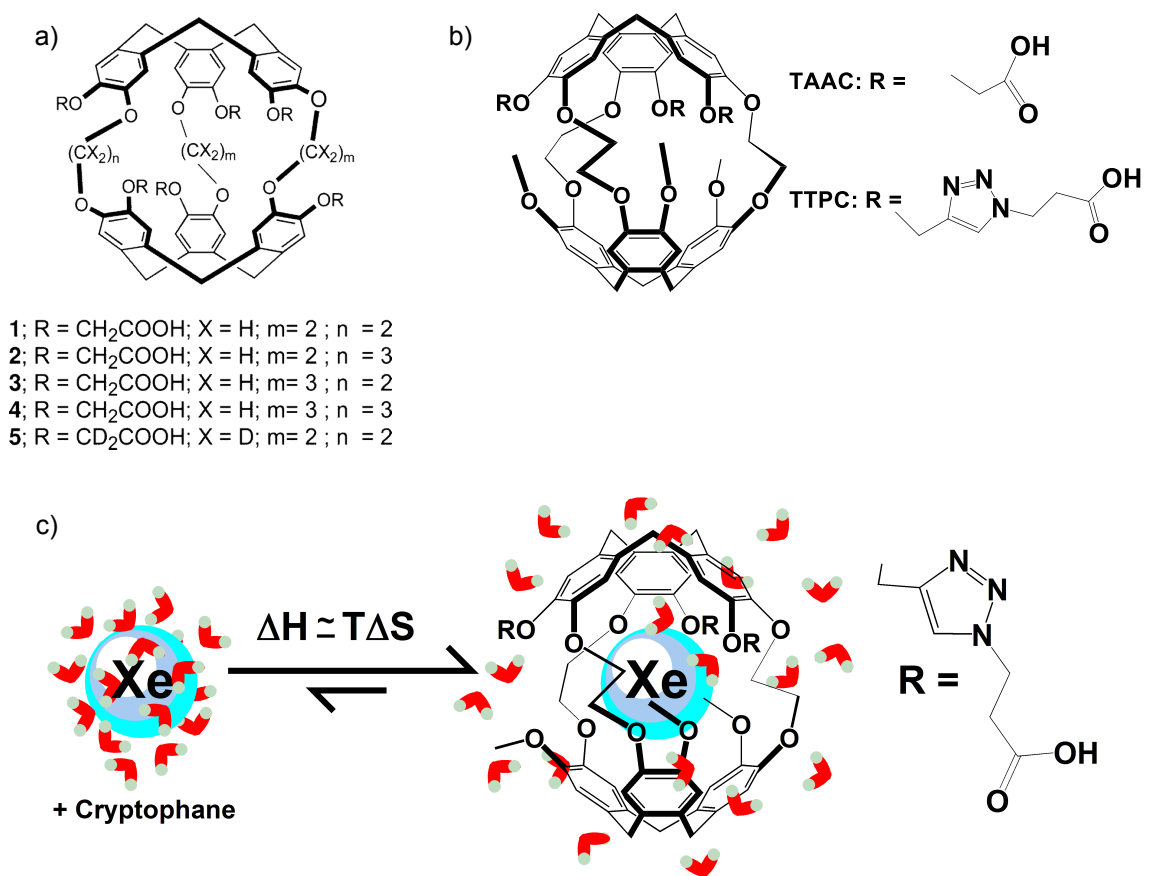


**Figure 1.3.** Water-soluble cryptophanes a) Huber's hexa-acid cryptophanes, b) TAAC and TTPC, c) A major contributor to xenon binding is entropy which arises from the desolvation of Xe. Roughly 20 water molecules make up the first solvation sphere of the Xe atom in aqueous solution. Figure adapted from Huber and Hill, et al.<sup>39-41</sup>

This thesis outlines the synthesis and development of a new water-soluble amine-based cryptophane-A derivative with the goals of expanding the variety of neutral molecules reversibly binding to cryptophanes and determining the substituent effects on xenon binding affinity. The binding of radon and xenon to this molecule was investigated. Although both radon and xenon are noble gases, unlike xenon, all 35 isotopes of radon are radioactive. Radon is formed as an intermediate species resulting from the decay of uranium-238, which is found in the Earth's crust. It is considered to be an indoor air pollutant since exposure to radon (due to high levels of accumulation within homes) leads to the incidence of lung cancers in many geographic regions.<sup>42</sup> Despite this, there is currently no literature data for the binding of radon to a discrete molecular species. So far, only the adsorption of radon to bulk substrates such as charcoal, silica gel and ice,<sup>43</sup> and on the formation of radon halides<sup>44</sup> has been determined. Therefore, a novel sensitive assay was developed in the Dmochowski lab to determine the binding of radon to cryptophane. Additionally, the binding of xenon to the same host was also investigated using isothermal titration calorimetry (ITC).

## 1.2. Development of targeted $^{129}\text{Xe}$ biosensors

Among the small, neutral molecules that are reversibly encapsulated by cryptophanes, xenon has garnered the most attention. This is because of the promising potential of using hyperpolarized (hp)  $^{129}\text{Xe}$  biosensors as novel contrast agents for magnetic resonance imaging (MRI) and spectroscopy (MRS).<sup>45</sup> Although MRI is one of the most widely used non-invasive tools for imaging deep tissues with high spatial and temporal resolution (with approximately 30 million procedures performed per year in the U.S.), it suffers from several limitations. Because the intrinsic signals are from protons in water and fat, there is usually low sensitivity and high background noise present. Lungs are difficult to image due to low proton concentration whereas in the brain, multiple lipid bilayers decrease sensitivity due to high proton noise, resulting in poor signal-to-noise ratios.<sup>46,47</sup> As a result, several small tumors may remain undetected until they have progressed and become larger, which then may hurt patient prognosis. To overcome this problem, MRI contrast agents are currently used to increase the signal-to-noise ratio and include gadolinium chelates,<sup>48-50</sup> iron oxide nanoparticles<sup>51-54</sup> and manganese chelates.<sup>55</sup> Contrast agents are generally paramagnetic species that increase signal-to-noise ratio by changing the longitudinal ( $T_1$ ) or transverse ( $T_2$ ) relaxation times of neighboring water molecules. Gadolinium contrast agents (e.g. Omniscan) are most frequently used and account for 40-50% of MRI scans.<sup>49</sup> Although they do improve the contrast of MRI images, they are not targeted towards specific biomarkers. Since they depend on relative changes for imaging, Gd contrast agents are less effective at multiplexing and detecting proteins at low concentrations.<sup>56,57</sup> Additionally, U.S. and European agencies have issued



advisories against Gd agents based on the toxicity risks posed to patients with impaired renal function who may develop nephrogenic systemic fibrosis/nephrogenic fibrosing dermopathy (NSF/NFD).<sup>58</sup> This disease has recently “disappeared”, due to greater awareness of NSF and the risks posed to the dialysis patient population. Other contrast agents include iron oxide nanoparticles, which are effective at imaging liver lesions, but are plagued by low sensitivity due to small changes in  $T_2$ .<sup>54</sup> Manganese chelates are also used but tend to accumulate in the liver and have low sensitivity due to small changes in  $T_1$ .<sup>55</sup> As a result of low sensitivity and toxicity concerns, alternative nonproton-based, hyperpolarized MRI agents such as  $^{129}\text{Xe}$ ,  $^{13}\text{C}$ ,  $^{83}\text{Kr}$  and  $^3\text{He}$  are currently being explored.<sup>59-62</sup>

$^{129}\text{Xe}$  is an attractive MRI contrast agent since it is spin- $\frac{1}{2}$  (26.5% isotopic abundance), non-toxic, inert (below its anesthetic threshold, which is 70% by volume of inhaled gas mixtures), has millimolar solubility ( $\sim 5$  mM) in water<sup>63</sup> and is very polarizable. The polarizability of the 56 electron cloud is reflected by the large chemical shift window ( $> 300$  ppm).<sup>64</sup> This allows for the simultaneous detection of different species (i.e., multiplexing), which is currently not possible with untargeted  $^1\text{H}$  MRI contrast agents. Since most diseases lead to overexpression of a variety of biomarkers, the ability to perform multiplexed detection through MRI would greatly increase the effectiveness and sensitivity of this imaging modality. Additionally, hp  $^{129}\text{Xe}$  can be generated through spin-exchange optical pumping (SEOP) to increase NMR signal by more than 10,000-fold. This helps to increase the sensitivity of MRI.<sup>65</sup> SEOP polarizes  $^{129}\text{Xe}$  gas by transferring angular momentum from circularly polarized light to rubidium.

The nuclear spin from polarized rubidium is then transferred to the nuclear spin of xenon through dipolar coupling (Figure 1.4a). As a result, a > 10,000-fold signal enhancement is achieved relative to the normal Boltzmann distribution of nuclear spins.<sup>65,66</sup> The hyperpolarized state has a spin–lattice relaxation time  $T_1$  of roughly 70 min.<sup>67</sup> However, the  $T_1$  value is significantly reduced in the presence of paramagnetic species such as iron and oxygen. As a result, the  $T_1$  value is only 4 seconds in deoxygenated blood and 13 seconds in oxygenated blood.<sup>68</sup> Despite this, several *in vivo* MRI imaging studies with hp  $^{129}\text{Xe}$  gas have already been performed. In cases where  $^{129}\text{Xe}$  gas was introduced via inhalation, organs such as the brain and lungs were successfully imaged.<sup>47,69-76</sup> It has also been possible to image organs by introducing  $^{129}\text{Xe}$  via direct intravenous<sup>77</sup> and arterial<sup>71</sup> routes in rodents. Additionally, since it is now possible to deliver over 50% hp  $^{129}\text{Xe}$  at flow rates of 1–2 L/min, the potential for performing MRI where hp  $^{129}\text{Xe}$  gas is continuously replenished via inhalation has further increased.<sup>78,79</sup> This would allow for organs such as the brain and the lungs to be imaged over extended periods of time. It has also been reported that the hyperpolarized lifetime of xenon can be increased to 20-30 seconds by co-injecting with intralipids or emulsions, which may allow for the possibility to image a wider variety of organs.<sup>71,80</sup>

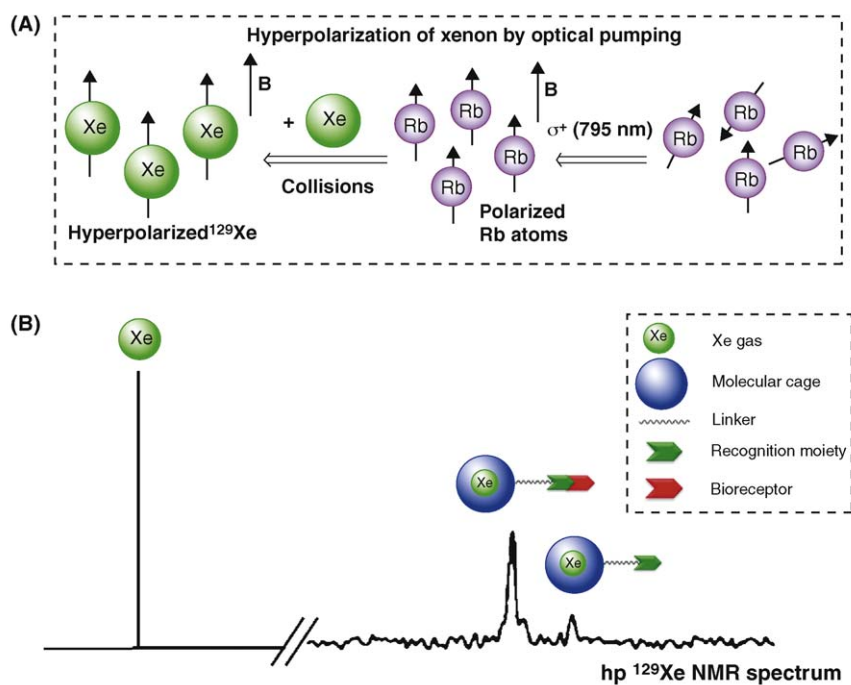


**Figure 1.4.** a) The process of spin-exchange optical pumping to produce hp  $^{129}\text{Xe}$  gas, b) Schematic representation illustrating the primary concept of  $^{129}\text{Xe}$  NMR biosensing whereby there is a distinct shift in  $^{129}\text{Xe}$  NMR resonance upon binding to the targeted biomarker. Adapted from Taratula et al.<sup>45</sup>

In order to perform biosensing applications with water-soluble cryptophane-based  $^{129}\text{Xe}$  contrast agents, two major strategies have been pursued: 1) localization of  $^{129}\text{Xe}$  signals at the desired target to enhance signal-to-noise and, 2) multiplexing, which would allow for the simultaneous detection of various disease biomarkers.<sup>45,81</sup> The first strategy requires the synthesis of water-soluble cryptophane-A derivatives that bind tightly to xenon. As mentioned earlier, our lab has worked extensively on developing high affinity water-soluble cryptophane-A derivatives for *in vivo* applications where it is crucial for Xe to bind preferentially to cryptophanes and outcompete other proteins and fatty tissues present in the body. The binding affinity of Xe for proteins tends to be low and ranges from  $10\text{ M}^{-1}$  for hemoglobin to  $200\text{ M}^{-1}$  for myoglobin<sup>82,83</sup> whereas the affinity for water-soluble, tri-substituted cryptophanes synthesized in our lab ranges from 17,000 to 33,000  $\text{M}^{-1}$  in buffer and 22,000  $\text{M}^{-1}$  in blood plasma at 293 K.<sup>40,41</sup> The second strategy of multiplexing has also been developed in recent years where targeted cryptophane biosensors have been synthesized by conjugating the host molecule with a ligand that targets a biologically relevant biomarker (Figure 1.4b). The unbound biosensor has a unique NMR resonance and upon binding to the biomarker, additional  $^{129}\text{Xe}$  NMR peaks are formed that can be easily differentiated from the initial NMR resonance of the unbound biosensor. If a large variety of such biosensors could be developed where each targets a specific biosensor and had a unique chemical shift upon binding, a large number of targets could be investigated simultaneously, thereby leading to a more sensitive and accurate diagnosis.

The first example of such a targeted  $^{129}\text{Xe}$  biosensor consisted of a biotin-conjugated cryptophane which gave a unique resonance at 70 ppm in solution.<sup>81</sup> Upon binding to streptavidin, a new peak was formed at  $\sim 72.5$  ppm (Figure 1.5). Therefore, a  $\sim 2.5$  ppm shift illustrates that the polarizable xenon atom is able to detect a difference in the chemical environment upon binding.<sup>81</sup> Since xenon has a large chemical shift window, this proof-of-concept experiment indicated the potential of  $^{129}\text{Xe}$  NMR biosensors for multiplexing, whereby multiple biomarkers that indicate cancer formation can be simultaneously detected using MRI. Following this example, our lab developed an enzyme-responsive  $^{129}\text{Xe}$  biosensor that targeted the enzyme matrix metalloproteinase-7 (MMP-7).<sup>84</sup> MMP-7 is an important target since it is responsible for degrading extracellular matrix and is highly upregulated near tumors of the colon and breast.<sup>85-87</sup> Upon proteolysis of the peptide (MMP-7 substrate), two new NMR peaks (the biosensor consisted of two diastereomers) were formed 0.3 and 0.5 ppm upfield from the uncleaved NMR peak.<sup>84</sup> Although the change in chemical shift was not very significant for *in vivo* applications, this study illustrated that enzymatic activity can be detected by using  $^{129}\text{Xe}$  NMR biosensors. Larger chemical shifts differences (3.0 to 7.5 ppm) upon binding were observed with a *p*-benzenesulfonamide-conjugated  $^{129}\text{Xe}$  biosensor used to target carbonic anhydrase isozymes I and II (Figure 1.6a, b).<sup>88</sup> X-ray crystallography studies by the Christianson lab confirmed the presence of one xenon atom in the cryptophane cage as well as the binding of the benzenesulfonamide moiety in the carbonic anhydrase II binding site (Figure 1.6c).<sup>89</sup> It is also interesting to note that for the 6-bond linker moiety, xenon was able to differentiate CA I from CA II (which have slightly different chemical shifts) while for the 7-bond linker, xenon was not only able to distinguish between the

two isozymes, but was also able to differentiate between the two diastereomers of the biosensor when bound to CA II.<sup>88</sup> Therefore, the sensitivity of these contrast agents coupled with the significant chemical shift changes upon binding to biomarkers makes them promising candidates for  $^{129}\text{Xe}$  NMR biosensing.

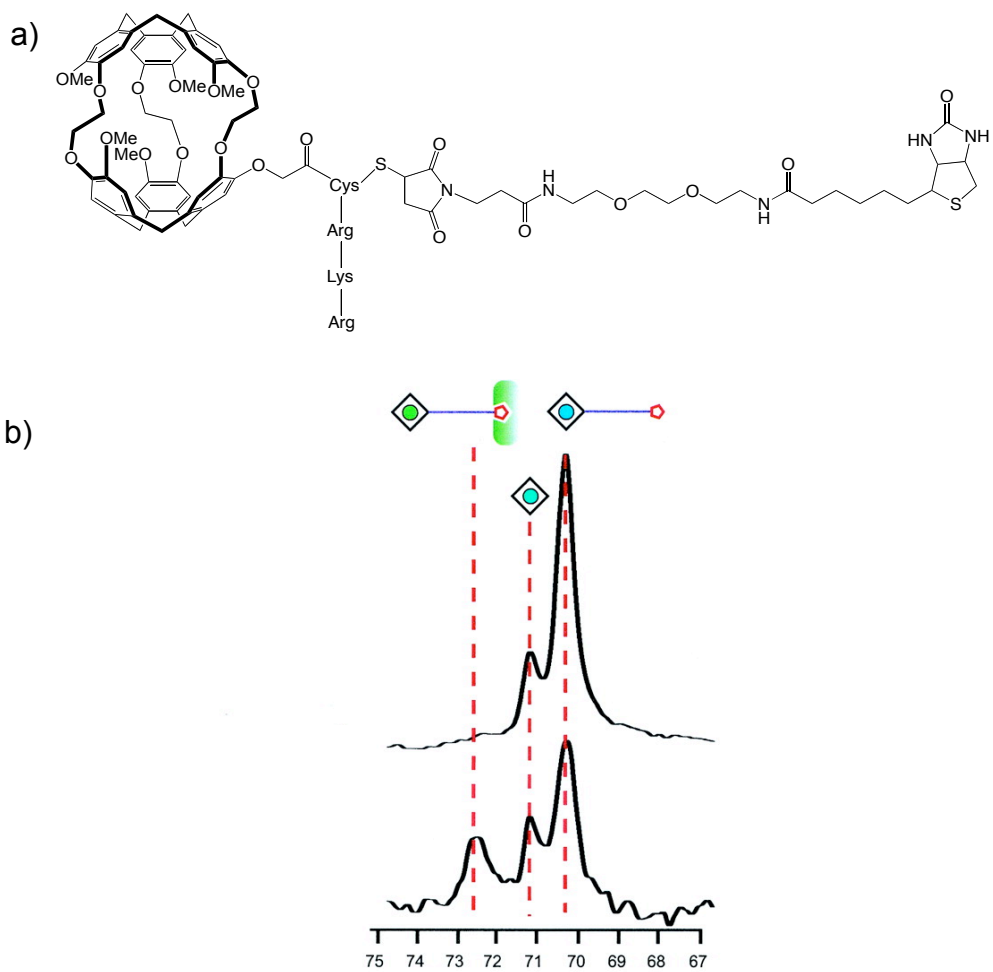


**Figure 1.5.** a) Biotin-conjugated  $^{129}\text{Xe}$  biosensor, b)  $^{129}\text{Xe}$  NMR resonance for the biosensor shifts from 70.2 to 72.5 ppm when biotin binds to streptavidin. Figure adapted from Spence, et al.<sup>81</sup>

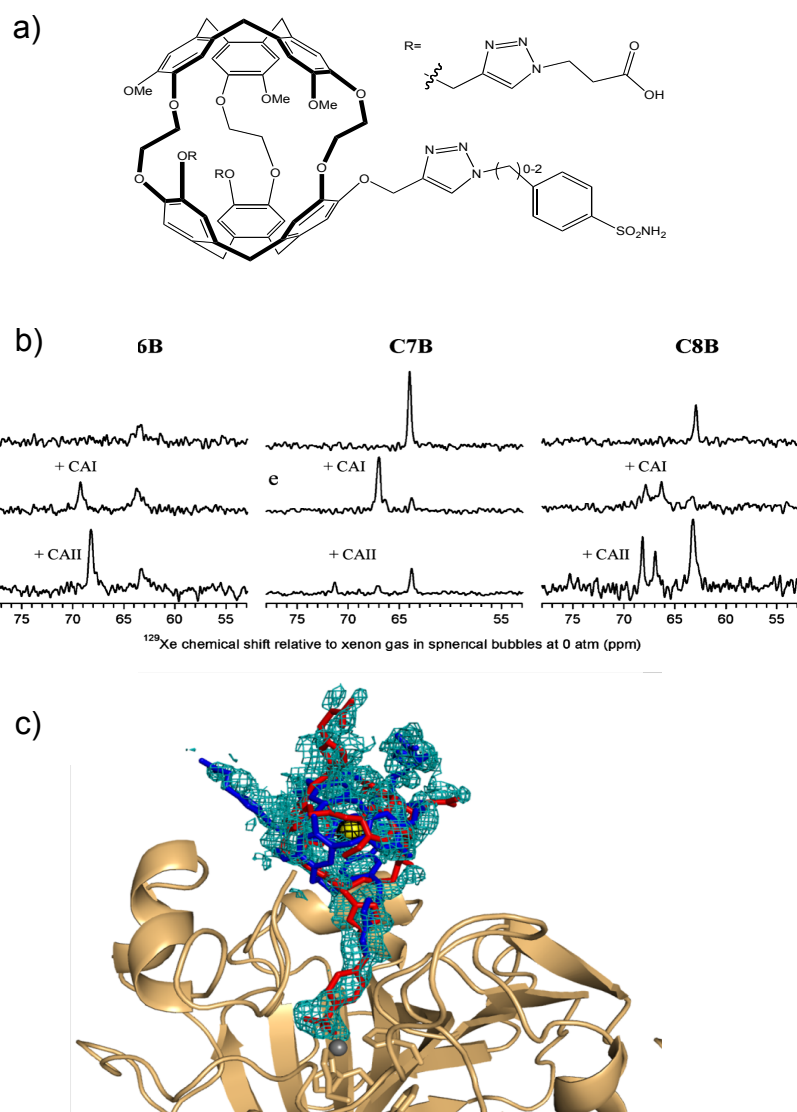


**Figure 1.6.** a) Chemical structure of a benzenesulfonamide-conjugated cryptophane with a variable length linker that targets CA, b)  $^{129}\text{Xe}$  NMR spectroscopy showing the biosensors binding to CA I and II, c) Crystal structure showing the binding of the C8B biosensor to CAII where the Xe atom (green) is bound to cryptophane and the targeting sulfonamidate anion is coordinated to  $\text{Zn}^{2+}$  (gray). Adapted from Aaron and Chambers, et al.<sup>88,89</sup>



In order to pursue biological applications with  $^{129}\text{Xe}$  NMR biosensors, our lab performed the first successful delivery of water-soluble cryptophanes to cancer and normal cells by conjugating cryptophanes with cationic cell penetrating peptides which are able to cross cell membranes.<sup>90-92</sup> The cellular delivery of the cryptophanes was confirmed by using confocal laser scanning microscopy. In order to target specific cancer biomarkers, the next step involved conjugating cryptophanes with targeting moieties and performing biological studies to determine cytotoxicity as well as the selectivity of delivering these biosensors to cancer cells overexpressing the targeted biomarkers.

This thesis outlines the work done towards the development of a  $^{129}\text{Xe}$  biosensor to target the cancer biomarker, folate binding protein (FBP). FBP is a membrane-bound glycosylphosphatidylinositol (GPI)-linked membrane glycoprotein, which is highly upregulated (3-5 million copies/cell) in colon, breast, ovarian and brain tumors whereas it is underexpressed in most normal tissues.<sup>93-96</sup> It is upregulated in fast growing cancer cells as folic acid, an essential component for one-carbon transfer reactions, has a high affinity for FBP and is transported into cells via folate-receptor mediated endocytosis. Previous studies have shown that FBP can effectively deliver folic acid-conjugated nanoparticles and imaging agents into cells.<sup>94</sup> In this thesis, a new water-soluble cryptophane-A derivative was conjugated to a selectively protected ( $\gamma$ -conjugate) folate moiety. Confocal laser scanning microscopy, flow cytometry, cytotoxicity assays and hyperpolarized  $^{129}\text{Xe}$  NMR spectroscopy were performed to determine cellular viability, cellular delivery and the selectivity in delivering the biosensor to cancer cells overexpressing FBP. These studies are crucial for the development of a library of targeted

cryptophane-based  $^{129}\text{Xe}$  biosensors, each of which can be selectively delivered to the desired biomarkers, thereby enabling *in vivo* multiplexing during MRI.

### 1.3. Hemicyptophanes: a new application in the development of molecular devices

Related molecules to cryptophanes are hemicyptophanes, where one of the two CTV units is replaced by a N, O, S, or P atom to add different functionalities into the cage. As a result, the internal cavity tends to be dissymmetric.<sup>97</sup> Hemicyptophanes have found a wide range of applications as organic hosts, metalloreceptors and catalysts. Recent examples of hemicyptophanes include the synthesis of chiral trialkanamine-based hemicyptophanes, which can act as metalloreceptors by forming an oxovanadium complex.<sup>98</sup> Another type of hemicyptophane modified with a thiophosphorylated group has been confirmed by crystallographic analysis to encapsulate toluene.<sup>97</sup> Additionally, the Ugi-type multi-component macrocyclization reaction was employed to synthesize diverse hemicyptophanes by using polyfunctional building blocks.<sup>99</sup> Zn(II)-included hemicyptophane has also been shown to have significant catalytic activity in the hydrolysis of methyl *para*-nitrocarbonate.<sup>100</sup> Triamide hemicyptophanes have also shown strong affinity for ion-pairs due to their heteroditopic character.<sup>101</sup>

This thesis outlines a potentially new application for hemicyptophanes in the field of molecular devices and components. In recent years, there has been an explosive growth in the development of chemical systems that rely on electronic, chemical or mechanical effects to mimic the functions of macroscopic devices.<sup>102</sup> These systems have not only allowed for the development of molecular-level machines,<sup>102</sup> but also have provided a platform for understanding complex biological machines, e.g. bacterial

flagella, ATPase pumps, etc.<sup>103-110</sup> Examples of such molecular mechanical systems include brakes, gears, propellers, turnstiles, and gyroscopes (Figure 1.7).<sup>105,111-114</sup>

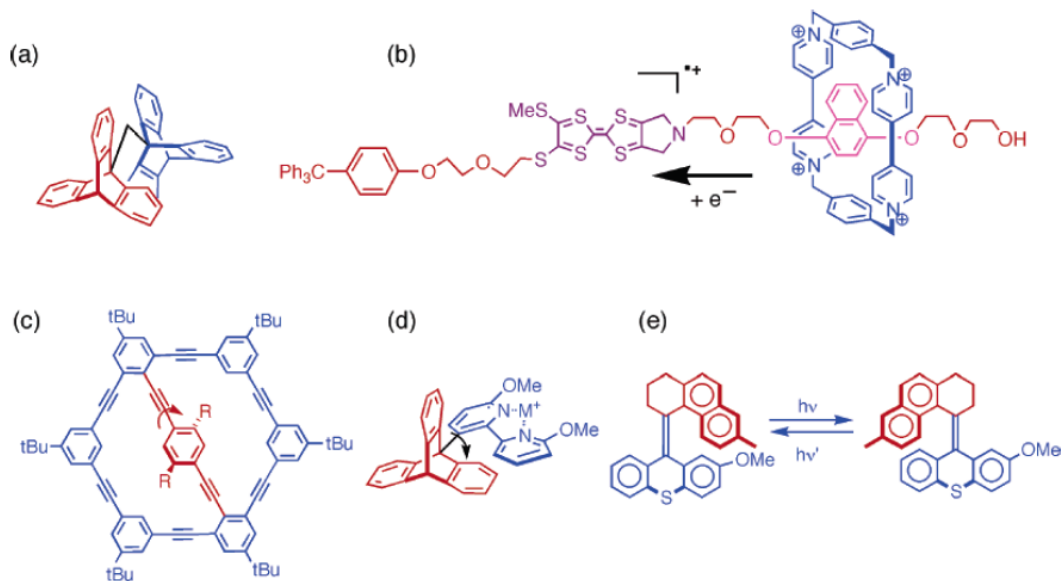


**Figure 1.7.** Examples of molecular devices and components that rely on chemical, electronic and structural changes to mimic macroscopic devices. a) Mislow and Iwamura's "molecular bevel gears",<sup>113</sup> b) Stoddart's "shuttles",<sup>115</sup> c) Moore's "molecular turnstiles",<sup>116</sup> d) Kelly's "brakes",<sup>117</sup> and e) Feringa's photochemically driven "motors".<sup>118</sup> Figure adapted from Khuong et al.<sup>119</sup>

In this thesis, a novel hemicryptophane was designed where one of the two CTV units was replaced by a tribenzylamine moiety. Although the new hemicryptophane was originally developed for host-guest applications, binding experiments revealed that the three rotating phenylene groups in the cage prevented the binding of small gaseous guests and solvent molecules at standard conditions. Upon further investigation, it was determined that the molecular structure and motions of this hemicryptophane closely resembled that of molecular gyroscopes. The criteria of designing molecular gyroscopes include rotary elements (rotators) that are connected to a static framework (stator). Among the several molecular gyroscopes that have been previously synthesized, one example consists of using metal-centered motifs to create gyroscopes where the central rotator is protected by a three-spoke stator.<sup>102,120-124</sup> Another example includes the synthesis of amphidynamic crystals by Garcia-Garibay and coworkers where the central rotator of a solid-state gyroscope is protected by bulky substituents that form the stator.<sup>125-134</sup> In both cases the rotator is protected by the stator to allow for low-barrier rotation. Yet due to the intercalation of solvent molecules or steric effects in solid-state studies, these gyroscopes have encountered undesirable barriers to rotation. Therefore, in this thesis we outline the design of a novel hemicryptophane, which unlike previous examples, has multiple, proximate rotators within one molecular system with an internal cavity small enough to deter the inclusion of solvent and gaseous molecules that could hamper rotation of the rotators. Also, we investigated the rate of rotation by <sup>1</sup>H variable temperature (VT) NMR spectroscopy and molecular dynamics (MD) simulations. The results outlined in this thesis indicate that hemicryptophanes make for compelling initial motifs for the synthesis of future molecular gyroscopes where the rotation could be

controlled in a unidirectional fashion by incorporating either bulky substituents or dipole moments in the rotators.

## REFERENCES

- (1) Brotin, T.; Dutasta, J. P. *Chem. Rev.* **2009**, *109*, 88-130.
- (2) Babine, R. E.; Bender, S. L. *Chem. Rev.* **1997**, *97*, 1359-1472.
- (3) Bohm, H.-J.; Klebe, G. *Angew. Chem. Int. Ed. Engl.* **1996**, *35*, 2588-2614.
- (4) Fox, T.; Thomas, B. E., IV; McCarrick, M.; Kollman, P. A. *J. Phys. Chem.* **1996**, *100*, 10779-10783.
- (5) Houk, K. N.; Nakamura, K.; Sheu, C.; Keating, A. E. *Science* **1996**, *273*, 627-629.
- (6) Mordasini Denti, T. Z.; van Gunsteren, W. F.; Diederich, F. *J. Am. Chem. Soc.* **1996**, 6044-6051.
- (7) Nakamura, K.; Sheu, C.; Keating, A. E.; Houk, K. N.; Sherman, J. C.; Chapman, R. G.; Jorgensen, W. L. *J. Am. Chem. Soc.* **1997**, *119*, 4321-4322.
- (8) Sheu, C.; Houk, K. N. *J. Am. Chem. Soc.* **1996**, *118*, 8056-8070.
- (9) Wallimann, P.; Mattei, S.; Seiler, P.; Diederich, F. *Helv. Chim. Acta* **1997**, *80*, 2368-2390.
- (10) Dougherty, D. A. *Science* **1996**, *271*, 163-168.
- (11) Dougherty, D. A.; Stauffer, D. A. *Science* **1990**, *250*, 1558-1560.
- (12) Ma, J. C.; Dougherty, D. A. *Chem. Rev.* **1997**, *97*, 1303-1324.
- (13) Mecozzi, S.; West, A. P., Jr.; Dougherty, D. A. *Proc. Natl. Acad. Sci. U. S. A.* **1996**, *93*, 10566-10571.
- (14) Meric, R.; Lehn, J.-M.; J.-P., V. *J.-P. Bull. Soc. Chim. Fr.* **1994**, *131*, 579-583.
- (15) Murayama, K.; Aoki, K. *J. Chem. Soc., Chem. Commun.* **1997**, 119-120.



- (16) Kirchoff, P. D.; Dutasta, J.-P.; Collet, A.; McCammon, J. A. *J. Am. Chem. Soc.* **1999**, *121*, 381-390.
- (17) Pedersen, C. J. *J. Am. Chem. Soc.* **1967**, *89*, 7017-7036.
- (18) Fenyvesi, E.; Szente, L.; Russel, N. R.; McNamara, M. *Comprehensive Supramolecular Chemistry*; Pergamon: New York, NY, **1996**; Vol. 3.
- (19) Shinkai, S. *Tetrahedron* **1993**, *49*, 8933-8968.
- (20) Linnane, P.; Shinkai, S. *Chem. Ind.* **1994**, 811-814.
- (21) Bohmer, V. *Angew. Chem. Int. Ed. Engl.* **1995**, *34*, 713-745.
- (22) Gutsche, C. D. *Aldrichimica Acta* **1995**, *28*, 3-9.
- (23) Cram, D. J.; Cram, J. M.; The Royal Society of Chemistry: Thomas Graham House, Science Park: Cambridge, U.K., 1994.
- (24) Murakami, Y.; Kikuchi Ji, J.; Hisaeda, Y.; Hayashida, O. *Chem. Rev.* **1996**, *96*, 721-758.
- (25) Rekharsky, M. V.; Inoue, Y. *Chem. Rev.* **1998**, *98*, 1875-1918.
- (26) Conn, M. M.; Rebek, J. *Chem. Rev.* **1997**, *97*, 1647-1668.
- (27) Fromming, K. H.; Atwood, J. L.; Lehn, J.-M.; Davies, J. E. D.; MacNicol, D. D.; Vogtle, F. *Comprehensive Supramolecular Chemistry* **1996**, *10*, 445.
- (28) Rudkevitch, D. M.; Leontiev, A. V. *Aust. J. Chem.* **2004**, *57*, 713-722.
- (29) Pluth, M. D.; Bergman, R. G.; Raymond, K. N. *Science* **2007**, *316*, 85-88.
- (30) Sanders, J. K. M. *Chem.-Eur. J.* **1998**, *4*, 1378-1383.
- (31) Vriezema, D. M.; Comellas Aragone`s, M.; Elemans, J. A. A. W.; Cornelissen, J. J. L. M.; Rowan, A. E.; Nolte, R. J. M. *Chem. Rev.* **2005**, *105*, 1445-1489.
- (32) Gabard, J.; Collet, A. *J. Chem. Soc. Chem. Commun.* **1981**, 1137-1139.

- (33) Collet, A. *Comp. Supramol. Chem.* **2** **1996**, 325-365.
- (34) Brotin, T.; Devic, T.; Lesage, A.; Emsley, L.; Collet, A. *Chem. Eur. J.* **2001**, *7*, 1561-1573.
- (35) Mecozzi, S.; Rebek, J. *Chem. Eur. J.* **1998**, *4*, 1016-1022.
- (36) Taratula, O.; Hill, P. A.; Khan, N. S.; Carroll, P. J.; Dmochowski, I. J. *Nat. Commun.* **2010**, *1*:148.
- (37) Garel, L.; Dutasta, J. P.; Collet, A. *Angew. Chem. Int. Ed.* **1993**, *32*, 1169-1171.
- (38) Bartik K, L. M., Dutasta JP, Collet A, Reisse J. *J. Am. Chem. Soc.* **1998**, *120*, 784-791.
- (39) Huber, G.; Brotin, T.; Dubois, L.; Desvaux, H.; Dutasta, J. P.; Berthault, P. *J. Am. Chem. Soc.* **2006**, *128*, 6239-6246.
- (40) Hill, P. A.; Wei, Q.; Eckenhoff, R. G.; Dmochowski, I. J. *J. Am. Chem. Soc.* **2007**, *129*, 9262-9263.
- (41) Hill, P. A.; Wei, Q.; Troxler, T.; Dmochowski, I. J. *J. Am. Chem. Soc.* **2009**, *131*, 3069-3077.
- (42) Darby, S.; Hill, D.; Auvinen, A.; Barros-Dios, J. M.; Baysson, H.; Bochicchio, F.; Deo, H.; Falk, R.; Forastiere, F.; Hakama, M.; Heid, I.; Kreienbrock, L.; Kreuzer, M.; Lagarde, F.; Mäkeläinen, I.; Muirhead, C.; Oberaigner, W.; Pershagen, G.; Ruano-Ravina, A.; Ruosteenoja, E.; Schaffrath Rosario, A.; Tirmarche, M.; Tomášek, L.; Whitley, E.; Wichmann, H. E.; Doll, R. *Brit. Med. J.* **2005**, *330*, 223-227.
- (43) Eichler, B.; Zimmermann, H. P.; Gäggeler, H. W. *J. Phys. Chem.* **2000**, *104*, 3126-3131.

- (44) Avrorin, V. V.; Krasikova, R. N.; Nefedov, V. D.; Toropova, M. A. *Russ. Chem. Rev.* **1982**, *51*, 12-20
- (45) Taratula, O.; Dmochowski, I. J. *Curr. Opin. Chem. Biol.*, **2010**, *14*, 97-104.
- (46) Krings, T.; Schreckenberger, M.; Rohde, V.; Foltys, H.; Spetzger, U.; Sabri, O.; Reinges, M. H. T.; Kemeny, S.; Meyer, P. T.; Moller-Hartmann, W.; Kornith, M.; Gilsbach, J. M.; Buell, U.; Thron, A. *J. Neurol. Neurosurg. Psychiat.* **2001**, *71*, 762-771.
- (47) Ruppert, K.; Mata, J. F.; Brookeman, J. R.; Hagspiel, K. D.; Mugler, J. P. *Magn. Reson. Med.* **2004**, *51*, 676-687.
- (48) Chan, K. W.-Y.; Wong, W.-T. *Coord. Chem. Rev.* **2007**, *251*, 2428-2451.
- (49) Raymond, K. N.; Pierre, V. C. *Bioconjug. Chem.* **2004**, *16*, 3-8.
- (50) Urbanczyk-Pearson, L. M.; Femia, F. J.; Smith, J.; Parigi, G.; Duimstra, J. A.; Eckermann, A. L.; Luchinat, C.; Meade, T. J. *Inorg. Chem.* **2008**, *47*, 56-68.
- (51) Amstad, E.; Gillich, T.; Bilecka, I.; Textor, M.; Reimhult, E. *Nano. Lett.* **2009**, *9*, 4042-4048.
- (52) Perez, J. M.; Josephson, L.; Weissleder, R. *Chembiochem* **2004**, *5*, 261-264.
- (53) Slotkin, J.; Cahill, K.; Tharin, S.; Shapiro, E. *Neurotherapeutics* **2009**, *4*, 428-433.
- (54) Wang, Y. X.; Hussain, S. M.; Krestin, G. P. *Eur. Radiol.* **2001**, *11*, 2319-2331.

- (55) Tan, M.; Wu, X.; Jeong, E. K.; Chen, Q.; Parker, D. L.; Lu, Z. R. *Mol. Pharm.* **2010**, *7*, 936-943.
- (56) Degani, H.; Gusic, V.; Weinstein, D.; Fields, S.; Strano, S. *Nat. Med.* **1997**, *3*, 780-782.
- (57) Foster-Gareau, P.; Heyn, C.; Alejski, A.; Rutt, B. K. *Magn. Reson. Med.* **2003**, *49*, 968-971.
- (58) Broome, D. R.; Girguis, M. S.; Baron, P. W.; Cottrell, A. C.; Kjellin, I.; Kirk, G. A. *AJR Am. J. Roentgenol.* **2007**, *188*, 586-592.
- (59) Clevelanda, Z. I.; Pavlovskayaa, G. E.; Elkinsb, N. D.; Stupica, K. F.; Repineb, J. E.; Meersmann, T. *J. Magn. Reson.* **2008**, *195*, 232-237.
- (60) Golman, K.; Zandt, R. I.; Lerche, M.; Pehrson, R.; Ardenkjaer-Larsen, J. H. *Cancer Res.* **2006**, *66*, 10855-10860.
- (61) Hopkins, S. R.; Levin, D. L.; Emami, K.; Kadlecsek, S.; Yu, J.; Ishii, M.; Rizi, R. R. *J. Appl. Physiol.* **2007**, *102*, 1244-1254.
- (62) Mugler, J. P., 3rd; Driehuys, B.; Brookeman, J. R.; Cates, G. D.; Berr, S. S.; Bryant, R. G.; Daniel, T. M.; de Lange, E. E.; Downs, J. H., 3rd; Erickson, C. J.; Happer, W.; Hinton, D. P.; Kassel, N. F.; Maier, T.; Phillips, C. D.; Saam, B. T.; Sauer, K. L.; Wagshul, M. E. *Magn. Reson. Med.* **1997**, *37*, 809-815.
- (63) Clever, H. L. *Solubility Data Series* **1979**, *2*.
- (64) Raftery, D. *Annu. Rep. NMR Spectrosc.* **2006**, *57*, 205-270.
- (65) Berthault, P.; Huber, G.; Desvaux, H. *Prog. Nucl. Magn. Reson. Spec.* **2008**, *55*, 35-60.
- (66) Goodson, B. M. *J. Magn. Reson.* **2002**, *155*, 157-216.

- (67) Jameson, A. K.; Jameson, C. J.; Gutowsky, H. S. *J. Chem. Phys.* **1970**, *53*, 2310-2321.
- (68) Venkatesh, A. K.; Zhao, L.; Balamore, D.; Jolesz, F. A.; Albert, M. S. *NMR Biomed.* **2000**, *13*, 245-252.
- (69) Driehuys, B.; Cofer, G. P.; Pollaro, J.; Mackel, J. B.; Hedlund, L. W.; Johnson, G. A. *Proc. Natl. Acad. Sci. U. S. A.* **2006**, *103*, 18278-18283.
- (70) Driehuys, B.; Pollaro, J.; Cofer, G. P. *Magn. Reson. Med.* **2008**, *60*, 14-20.
- (71) Duhamel, G.; Choquet, P.; Grillon, E.; Lamalle, L.; Leviel, J. L.; Ziegler, A.; Constantinesco, A. *Magn. Reson. Med.* **2001**, *46*, 208-212.
- (72) Welsh, R. C.; Chupp, T. E.; Coulter, K. P.; Rosen, M. S.; Swanson, S. D. *Nucl. Instrum. Methods Phys. Res. A-Accel. Spectrom. Det. Assoc. Equip.* **1998**, *402*, 461-463.
- (73) Albert, M. S.; Cates, G. D.; Driehuys, B.; Happer, W.; Saam, B.; Springer, C. S., Jr.; Wishnia, A. *Nature* **1994**, *370*, 199-201.
- (74) Swanson, S. D.; Rosen, M. S.; Agranoff, B. W.; Coulter, K. P.; Welsh, R. C.; Chupp, T. E. *Magn. Reson. Med.* **1997**, *38*, 695-698.
- (75) Swanson, S. D.; Rosen, M. S.; Coulter, K. P.; Welsh, R. C.; Chupp, T. E. *Magn. Reson. Med.* **1999**, *42*, 1137-1145.
- (76) Wagshul, M. E.; Button, T. M.; Li, H. F.; Liang, Z.; Springer, C. S.; Zhong, K.; Wishnia, A. *Magn. Reson. Med.* **1996**, *36*, 183-191.
- (77) Goodson, B. M.; Song, Y.; Taylor, R. E.; Schepkin, V. D.; Brennan, K. M.; Chingas, G. C.; Budinger, T. F.; Navon, G.; Pines, A. *Proc. Natl. Acad. Sci. U. S. A.* **1997**, *94*, 14725-14729.

- (78) Ruset, I. C.; Ketel, S.; Hersman, F. W. *Phys. Rev. Lett.* **2006**, *96*, 053002.
- (79) Hersman, F. W.; Ruset, I. C.; Ketel, S.; Muradian, I.; Covrig, S. D.; Distelbrink, J.; Porter, W.; Watt, D.; Ketel, J.; Brackett, J.; Hope, A.; Patz, S. *Acad. Radiol.* **2008**, *15*, 683-692.
- (80) Duhamel, G.; Choquet, P.; Grillon, E.; Leviel, J. L.; Ziegler, A.; Constantinesco, A. *Comptes Rendus De L Academie Des Sciences Serie Ii Fascicule C-Chimie 4*, 789-794.
- (81) Spence, M. M.; Rubin, S. M.; Dimitrov, I. E.; Ruiz, E. J.; Wemmer, D. E.; Pines, A.; Yao, S. Q.; Tian, F.; Schultz, P. G. *Proc. Natl. Acad. Sci. U. S. A.* **2001**, *98*, 10654-10657.
- (82) Schiltz, M.; Fourme, R.; Prange, T. *Methods Enzymol.* **2003**, *374*, 83-119.
- (83) Tilton, R. F., Jr.; Kuntz, I. D., Jr. *Biochemistry* **1982**, *21*, 6850-6857.
- (84) Wei, Q.; Seward, G. K.; Hill, P. A.; Patton, B.; Dimitrov, I. E.; Kuzma, N. N.; Dmochowski, I. J. *J. Am. Chem. Soc.* **2006**, *128*, 13274-13283.
- (85) McIntyre, J. O.; Fingleton, B.; Wells, K. S.; Piston, D. W.; Lynch, C. C.; Gautam, S.; Matrisian, L. M. *Biochem. J.* **2004**, *377*, 617-628.
- (86) Welch, A. R.; Holman, C. M.; Huber, M.; Brenner, M. C.; Browner, M. F.; Van Wart, H. E. *Biochemistry* **1996**, *35*, 10103-10109.
- (87) Yamashita, K.; Mori, M.; Shiraishi, T.; Shibuta, K.; Sugimachi, K. *Clin. Cancer Res.* **2000**, *6*, 1169-1174.
- (88) Chambers, J. M.; Hill, P. A.; Aaron, J. A.; Han, Z.; Christianson, D. W.; Kuzma, N. N.; Dmochowski, I. J. *J. Am. Chem. Soc.* **2009**, *131*, 563-569.

- (89) Aaron, J. A.; Chambers, J. M.; Jude, K. M.; Di Costanzo, L.; Dmochowski, I. J.; Christianson, D. W. *J. Am. Chem. Soc.* **2008**, *130*, 6942-6943.
- (90) Seward, G. K.; Wei, Q.; Dmochowski, I. J. *Bioconjug. Chem.* **2008**, *19*, 2129-2135.
- (91) Lindgren, M.; Gallet, X.; Soomets, U.; Hallbrink, M.; Brakenhielm, E.; Pooga, M.; Brasseur, R.; Langel, U. *Bioconjug. Chem.* **2000**, *11*, 619-626.
- (92) Lindgren, M.; Hallbrink, M.; Prochiantz, A.; Langel, U. *Trends Pharmacol. Sci.* **2000**, *21*, 99-103.
- (93) Campbell, I. G.; Jones, T. A.; Foulkes, W. D.; Trowsdale, J. *Cancer Res.* **1991**, *51*, 5329-5338.
- (94) Hilgenbrink, A. R.; Low, P. S. *J. Pharm. Sci.* **2005**, *94*, 2135-2146.
- (95) Sudimack, J.; Lee, R. J. *Adv. Drug Deliv. Rev.* **2000**, *41*, 147-162.
- (96) Weitman, S. D.; Lark, R. H.; Coney, L. R.; Fort, D. W.; Frasca, V.; Zurawski, V. R., Jr.; Kamen, B. A. *Cancer Res.* **1992**, *52*, 3396-3401.
- (97) Gosse, I.; Dutasta, J. P.; Perrin, M.; Thozet, A. *New J. Chem.* **1999**, *23*, 545-548.
- (98) Gautier, A.; Mulatier, J. C.; Crassous, J.; Dutasta, J. P. *Org. Lett.* **2005**, *7*, 1207-1210.
- (99) Rivera, D. G.; Wessjohann, L. A. *J. Am. Chem. Soc.* **2006**, *128*, 7122-7123.
- (100) Makita, Y.; Sugimoto, K.; Furuyoshi, K.; Ikeda, K.; Fujiwara, S.; Shin-ike, T.; Ogawa, A. *Inorg. Chem.* **2010**, *49*, 7220-7222.

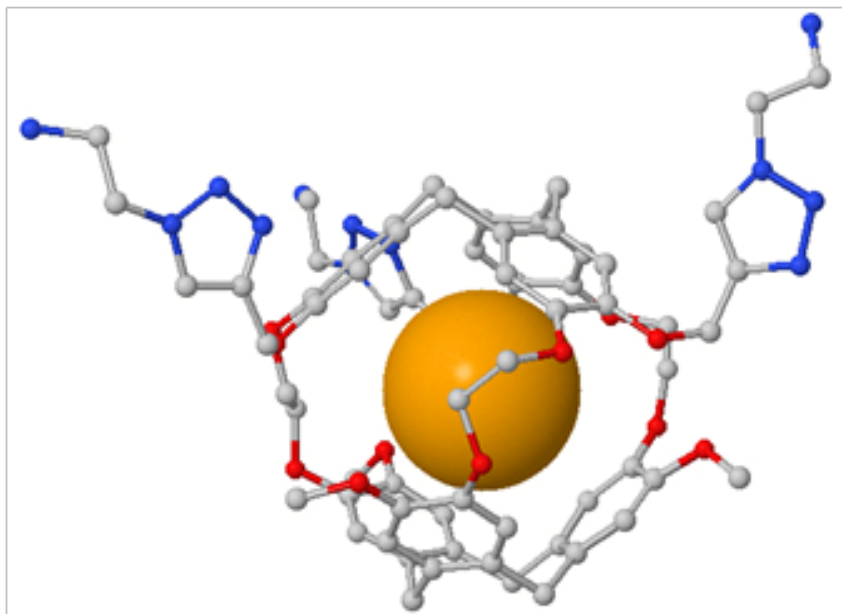
- (101) Raytchev, P. D.; Perraud, O.; Aronica, C.; Martinez, A.; Dutasta, J. P. *J. Org. Chem.* **2010**, *75*, 2099-2102.
- (102) Kay, E. R.; Leigh, D. A.; Zerbetto, F. *Angew. Chem. Int. Ed. Engl.* **2007**, *46*, 72-191.
- (103) Boyer, P. D. *Biosci. Rep.* **1998**, *18*, 97-117.
- (104) Elston, T.; Wang, H.; Oster, G. *Nature* **1998**, *391*, 510-513.
- (105) Kelly, T. R.; Sestelo, J. P. *Struct. Bond.* **2001**, *99*, 19-53.
- (106) Nakanishi-Matsui, M.; Sekiya, M.; Nakamoto, R. K.; Futai, M. *Biochim. Biophys. Acta.* **2010**, *1797*, 1343-1352.
- (107) Rice, S.; Lin, A. W.; Safer, D.; Hart, C. L.; Naber, N.; Carragher, B. O.; Cain, S. M.; Pechatnikova, E.; Wilson-Kubalek, E. M.; Whittaker, M.; Pate, E.; Cooke, R.; Taylor, E. W.; Milligan, R. A.; Vale, R. D. *Nature* **1999**, *402*, 778-784.
- (108) Sindelar, C. V.; Downing, K. H. *Proc. Natl. Acad. Sci. U. S. A* **2010**, *107*, 4111-4116.
- (109) Terashima, H.; Kojima, S.; Homma, M. *Int. Rev. Cell. Mol. Biol.* **2008**, *270*, 39-85.
- (110) Woolley, D. M. *Biol. Rev. Camb. Philos. Soc.* **2010**, *85*, 453-470.
- (111) Day, A. I.; Blanch, R. J.; Arnold, A. P.; Lorenzo, S.; Lewis, G. R.; Dance, I. *Angew. Chem. Int. Ed. Engl.* **2002**, *41*, 275-277.
- (112) Garcia-Garibay, M. A. *Proc. Natl. Acad. Sci. U. S. A* **2005**, *102*, 10771-10776.
- (113) Iwamura, H.; Mislow, K. *Acc. Chem. Res.* **1988**, *21*, 175-182.
- (114) Michl, J.; Sykes, C. H. *ACS Nano.* **2009**, *3*, 1042-1048.



- (115) Raymo, F. M.; Stoddart, J. F.; Feringa, B. L., Ed. *Switchable Catenanes and Molecular Shuttles*; Wiley-VCH: Weinheim, Germany, **2001**, 219-248.
- (116) Moore, J. S.; Bedard, T. C. *J. Am. Chem. Soc.* **1995**, *117*, 10662-10671.
- (117) Kelly, T. R.; Bowyer, M. C.; Bashkar, V.; Bebbington, D.; Lang, F.; Kim, M. H.; Jette, M. P. *J. Am. Chem. Soc.* **1994**, 3657-3658.
- (118) Feringa, B. L.; van Delden, R. A.; Koumura, N.; Geertsema, E. M. *Chem. Rev.* *100*, 1789-1816.
- (119) Khuong, T. A.; Nunez, J. E.; Godinez, C. E.; Garcia-Garibay, M. A. *Acc. Chem. Res.* **2006**, *39*, 413-422.
- (120) Nakazawa, J.; Hagiwara, J.; Mizuki, M.; Shimazaki, Y.; Tani, F.; Naruta, Y. *Angew. Chem. Int. Edit.* **2005**, *117*, 3810-3812.
- (121) Shima, T.; Hampel, F.; Gladysz, J. A. *Angew. Chem. Int. Ed. Engl.* **2004**, *43*, 5537-5540.
- (122) Skopek, K.; Barbasiewicz, M.; Hampel, F.; Gladysz, J. A. *Inorg. Chem.* **2008**, *47*, 3474-3476.
- (123) Wang, L.; Hampel, F.; Gladysz, J. A. *Angew. Chem. Int. Ed. Engl.* **2006**, *45*, 4372-4375.
- (124) Wang, L.; Shima, T.; Hampel, F.; Gladysz, J. A. *Chem. Commun.* **2006**, 4075-4077.
- (125) Cizmeciyan, D.; Yonutas, H.; Karlen, S. D.; Garcia-Garibay, M. A. *Solid. State Nucl. Magn. Reson.* **2005**, *28*, 1-8.
- (126) Dominguez, Z.; Dang, H.; Strouse, M. J.; Garcia-Garibay, M. A. *J. Am. Chem. Soc.* **2002**, *124*, 7719-7727.

- (127) Dominguez, Z.; Dang, H.; Strouse, M. J.; Garcia-Garibay, M. A. *J. Am. Chem. Soc.* **2002**, *124*, 2398-2399.
- (128) Dominguez, Z.; Khuong, T. A.; Dang, H.; Sanrame, C. N.; Nunez, J. E.; Garcia-Garibay, M. A. *J. Am. Chem. Soc.* **2003**, *125*, 8827-8837.
- (129) Garcia-Garibay, M. A. *Acc. Chem. Res.* **2003**, *36*, 491-498.
- (130) Garcia-Garibay, M. A. *Angew. Chem. Int. Ed. Engl.* **2007**, *46*, 8945-8947.
- (131) Garcia-Garibay, M. A. *Nat. Mater.* **2008**, *7*, 431-432.
- (132) Garcia-Garibay, M. A.; Dang, H. *Org. Biomol. Chem.* **2009**, *7*, 1106-1114.
- (133) Godinez, C. E.; Zepeda, G.; Garcia-Garibay, M. A. *J. Am. Chem. Soc.* **2002**, *124*, 4701-4707.
- (134) Godinez, C. E.; Zepeda, G.; Mortko, C. J.; Dang, H.; Garcia-Garibay, M. A. *J. Org. Chem.* **2004**, *69*, 1652-1662.

## CHAPTER 2: MEASUREMENT OF RADON AND XENON BINDING TO A CRYPTOPHANE MOLECULAR HOST



This paper was adapted from a manuscript submitted to *Proc. Natl. Acad. Sci. U.S.A.*

David R. Jacobson<sup>a†</sup>, Najat S. Khan<sup>a†</sup>, Ronald Collé<sup>b</sup>, Ryan Fitzgerald<sup>b</sup>, Lizbeth Laureano-Pérez<sup>b</sup>, Yubin Bai<sup>a</sup> and Ivan J. Dmochowski<sup>a,1</sup>

<sup>†</sup>These authors contributed equally to this work

<sup>a</sup>*Department of Chemistry, University of Pennsylvania, 231 South 34<sup>th</sup> St., Philadelphia, PA 19104, USA*

<sup>b</sup>*Ionizing Radiation Division, Physics Laboratory, National Institute of Standards and Technology, Gaithersburg, MD 20899, USA*

## ABSTRACT

Xenon and radon have many similar properties, a difference being that all 35 isotopes of radon ( $^{195}\text{Rn}$  through  $^{229}\text{Rn}$ ) are radioactive. Radon is a pervasive indoor air pollutant believed to cause significant incidence of lung cancer in many geographic regions, yet radon affinity for a discrete molecular species has never been determined. By comparison, the chemistry of xenon has been widely studied and applied in science and technology. Here, both noble gases were found to bind with exceptional affinity to tris-(triazole ethylamine) cryptophane, a new water-soluble organic host molecule. The cryptophane-xenon association constant,  $K_A = 42,000 \pm 2,000 \text{ M}^{-1}$  at 293 K, was determined by isothermal titration calorimetry. This represents the highest measured xenon affinity for a host molecule. The partitioning of radon between air and aqueous cryptophane solutions of varying concentration was determined radiometrically to give the cryptophane-radon association constant:  $K_A = 49,000 \pm 12,000 \text{ M}^{-1}$  at 293 K.

## INTRODUCTION

Radon and xenon were isolated by Ramsay and co-workers more than one century ago, but since that time only the chemistry of xenon has received much attention. Xenon can be harvested from the atmosphere and has wide-ranging applications, from plasma televisions to ion propulsion systems for spacecraft. Radioactive  $^{133}\text{Xe}$  is used as a tracer for measuring physiological blood flow<sup>1</sup> and also in detecting long-range fallout from nuclear weapons testing.<sup>2</sup> Stable isotope  $^{129}\text{Xe}$  has a spin- $1/2$  nucleus that can be hyperpolarized to generate very large signals for magnetic resonance imaging (MRI).<sup>3</sup> Host molecules have been identified that bind xenon with high affinity,<sup>4</sup> motivating further technological applications. Much less studied is radon, a radioactive noble gas that occurs as an intermediate species in the decay chain of uranium-238, an element ubiquitous in Earth's crust. Epidemiological studies indicate that indoor accumulation of radon may cause a 5-31% increase in lung cancer risk per 100 Bq m<sup>-3</sup> exposure.<sup>5</sup> In Europe, such a level corresponds to 2% of all cancer deaths.<sup>5</sup> The imperative to detect and remediate indoor radon motivates the study of radon chemistry, as do other scientific applications such as radon emission related to seismic activity.<sup>6</sup> Prior radon-chemical studies have focused on adsorption of the gas to bulk substrates<sup>7</sup> such as charcoal, silica gel and ice, and on the formation of radon halides.<sup>8</sup> Radon hydrates have also been found to incorporate into the crystal lattices of SO<sub>2</sub> and H<sub>2</sub>S hydrates.<sup>8</sup> Until now, no discrete molecular species has been shown to bind radon, presenting an exciting frontier in noble gas research and host-guest chemistry.

Radon is 10-15% larger by van der Waals volume than xenon ( $V_{Xe} \approx 42 \text{ \AA}^3$ ,  $V_{Rn} \approx 47 \text{ \AA}^3$ )<sup>9</sup> and exhibits higher polarizability ( $\alpha_{Xe} = 4.044 \text{ \AA}^3$ ,  $\alpha_{Rn} = 5.3 \text{ \AA}^3$ ),<sup>10</sup> which should promote binding to void spaces. These observations led us to examine binding of radon to a cryptophane organic host molecule that has well established xenon affinity.<sup>4</sup> Cryptophane-A, consisting of two cyclotriguaiacylene caps joined by three ethylene linkers, has been shown to encapsulate xenon reversibly as a host-guest complex.<sup>11</sup> Recent X-ray crystallographic studies have shown that the internal volume of trisubstituted cryptophane-A derivatives can vary by more than 20%, depending on the size of the encapsulated guest.<sup>12</sup>

Several cryptophane-A derivatives have been synthesized and shown by isothermal titration calorimetry (ITC), fluorescence quenching and NMR studies to exhibit xenon association constants as high as  $33,000 \pm 3,000 \text{ M}^{-1}$  at 293 K in phosphate-buffered water (Figure 2.1).<sup>13-16</sup> Herein, we report a new cryptophane-A derivative, tris-(triazole ethylamine) cryptophane (TTEC), with superior xenon-binding characteristics. A sensitive radiometric assay was developed for measuring radon binding to the same cryptophane.

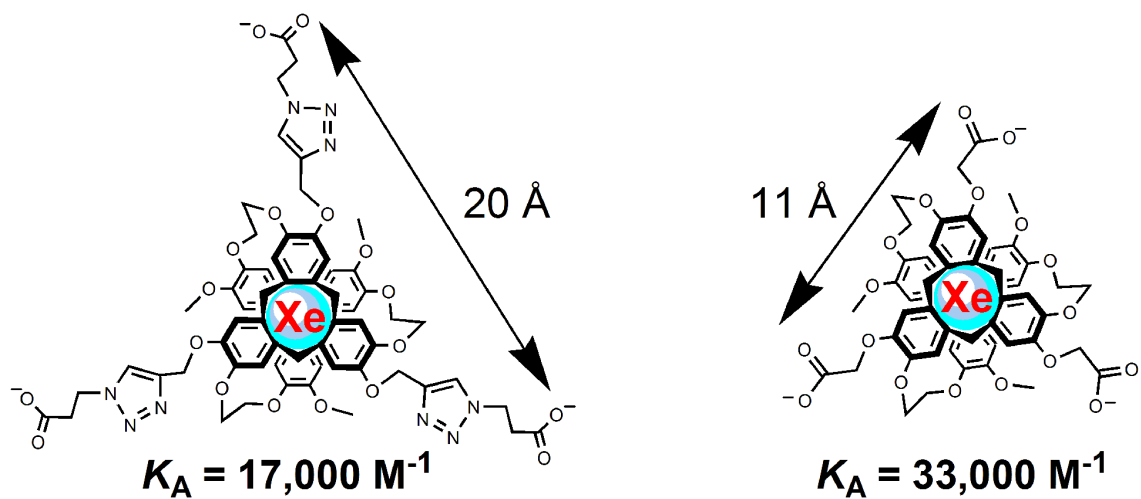


**Figure 2.1.** Water-soluble cryptophanes tris-(triazole propionic acid) (TTPC) and triacetic acid cryptophane-A (TAAC). Figure adapted from Hill, et al.<sup>15</sup>

## RESULTS AND DISCUSSION

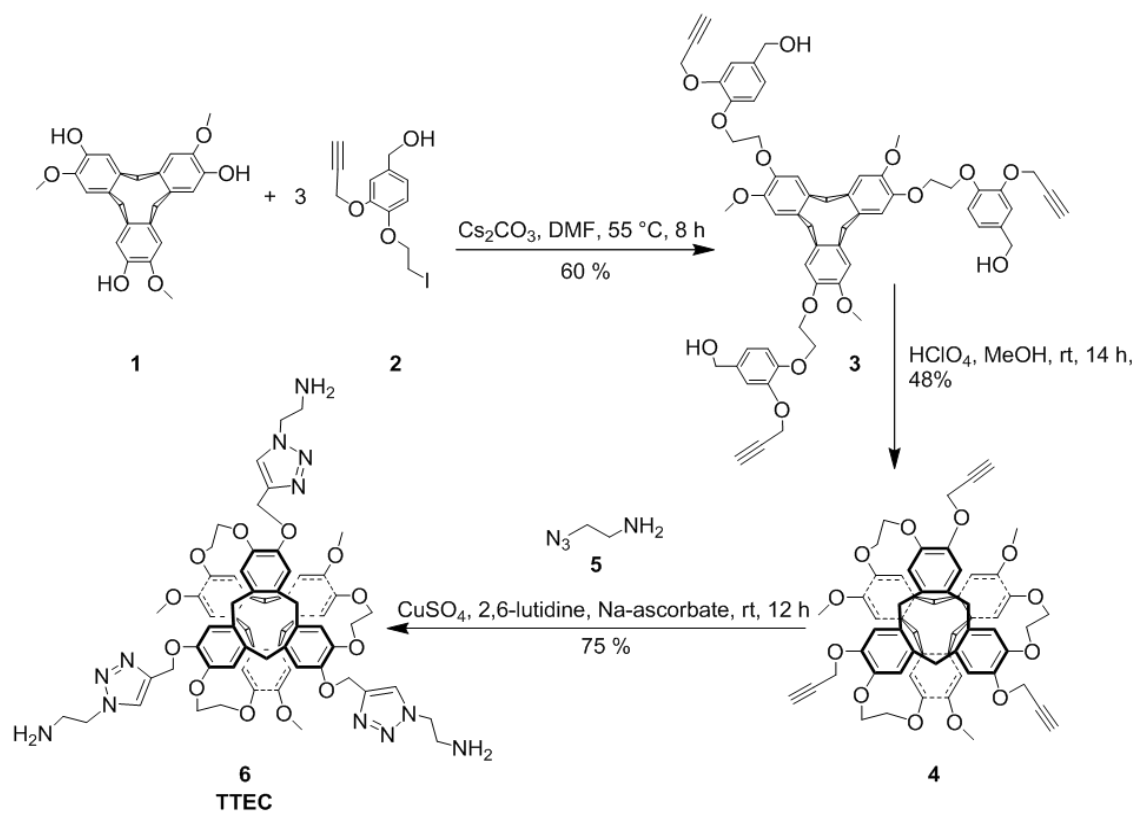


**Figure 2.2.** Synthesis of tris-(triazole ethylamine) cryptophane-A (TTEC), top view shown.



**Synthesis.** The synthetic route leading to TTEC (compound **6**) is outlined in Figure 2.2 and briefly described here. A list of reagents, general methods, and synthetic procedures are provided in the Experimental procedures section. Tripropargyl cryptophane **4** was synthesized in 10 steps in 4% overall yield according to literature procedure and matched the reported physical constants and NMR spectrum.<sup>14</sup> 2-Azidoethylamine was synthesized in 93% yield, also following literature precedent.<sup>17</sup> Reaction of **4** with three equivalents of 2-azidoethylamine was achieved via copper(I)-mediated [3 + 2] Huisgen cycloaddition<sup>18-21</sup> to give the water-soluble TTEC (**6**). TTEC was purified by HPLC (Experimental procedures section provides representative trace) and isolated in 75% yield. TTEC identity was confirmed by <sup>1</sup>H, <sup>13</sup>C, and hyperpolarized <sup>129</sup>Xe NMR spectroscopy (see Experimental procedures), in addition to matrix-assisted laser desorption/ionization mass spectrometry.

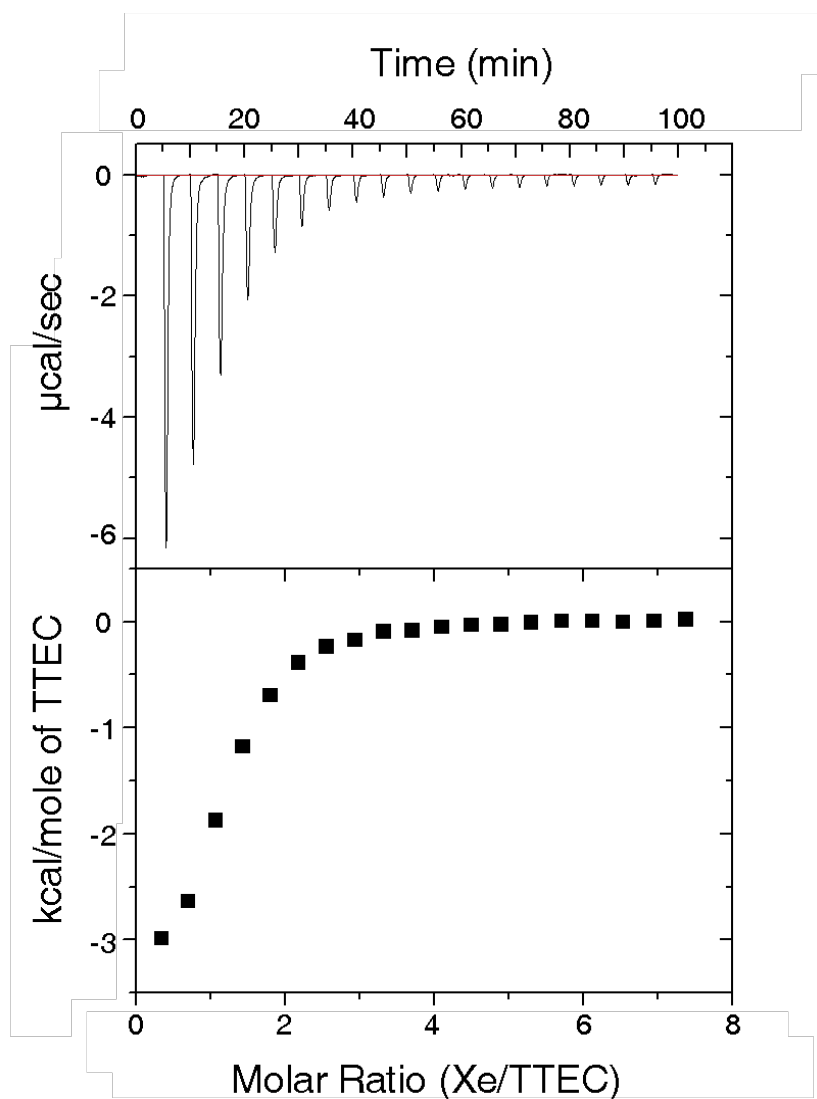


**Figure 2.3.** Enthalpogram of xenon binding to TTEC. Saturated aqueous xenon solution (5.05 mM) was titrated into 140  $\mu\text{M}$  TTEC in phosphate buffer (20 mM, pH 7.5) at 293 K.

**Xenon Binding.** To study the binding of xenon to TTEC, we utilized an ITC protocol previously developed in our laboratory.<sup>14</sup> The experiments were performed by titrating TTEC in phosphate buffer (20 mM, pH 7.5) at 293 K with saturated xenon-in-water solution (5.05 mM at 1 atm, determined from the literature).<sup>22</sup> The association constant was measured to be  $K_A = 42,000 \pm 2,000 \text{ M}^{-1}$  at 293 K, which is the highest xenon affinity measured for any synthetic or naturally occurring host molecule. The cited uncertainty interval for  $K_A$  is a standard uncertainty, assumed to correspond to a standard deviation, whose principal component was the uncertainty of the enthalpogram fit. Specifically, fitting of the enthalpogram (molar heat evolved vs. molar ratio, Figure 2.3) yielded thermodynamic parameters for the encapsulation:  $\Delta H = -14.96 \pm 0.30 \text{ kJ mol}^{-1}$ ;  $-T\Delta S = -10.97 \text{ kJ mol}^{-1}$  at 293 K. Note that enthalpic and entropic components contributed similarly to the Gibbs free energy of xenon binding at 293 K ( $\Delta G = -25.93 \text{ kJ mol}^{-1}$ ), which is believed to incorporate contributions from the dissolution of the clathrate water structure that surrounds xenon in solution, the release of one or more water molecules from the cryptophane cavity, and the non-covalent dispersion interactions between bound xenon and TTEC.

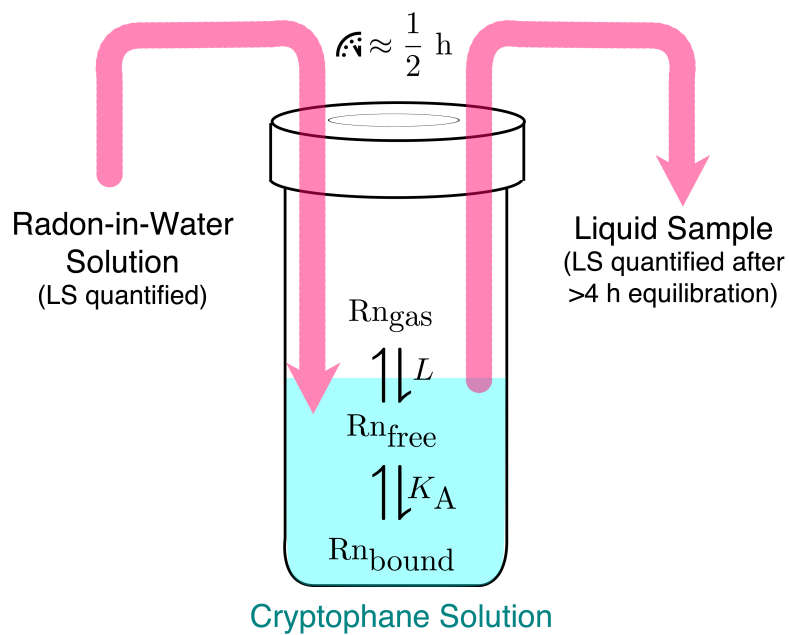


**Figure 2.4.** Diagrammatic representation of the radon binding affinity measurement, which exploits the partition of radon between aqueous and gaseous phases. ‘LS’ refers to liquid scintillation counting.  $L$  is the Ostwald coefficient of gas partition and  $K_A$  is the radon association constant to be determined.

**Radon Binding.** Studies of radon binding used  $^{222}\text{Rn}$  evolved from the decay of  $^{226}\text{Ra}$  in four capsules, akin to NIST standards disseminated as SRM 4973<sup>23</sup> and consisting of polyethylene-encapsulated  $^{226}\text{Ra}$  solution. These capsules generate a radium-free radon solution from decay of the radium and diffusion of the gaseous radon out of the capsules,<sup>24</sup> and have been used to produce very small quantities of radon for use in calibrating environmental standards, e.g. those of drinking water. In particular, only about two femtomoles of radon were available for use in our studies, rendering impractical the fluorescence quenching and ITC methods we previously used to measure xenon binding to cryptophane in water.<sup>14</sup> Instead, we devised a method (Figure 2.4) wherein the binding of radon to TTEC could be measured radiometrically by liquid scintillation, a technique with detection efficiency approaching five due to equilibrated radon progeny.<sup>25</sup> A related technique, involving gas-phase activity measurement, has been used to determine the partition of radon between water and various organic liquids.<sup>26</sup> Radon partitions between gas and liquid phases according to a known ratio: the Ostwald solubility coefficient<sup>27</sup> ( $L$ ) for that liquid and temperature. Cryptophane dissolved into the liquid phase of such a system acts as a radon sink and perturbs the system away from the Ostwald value in proportion to the binding affinity. Thirty to forty minutes were allowed for radon to partition between the gas and liquid phases, with intermittent mixing. Subsequent sampling of the liquid phase allowed determination of the “apparent partition coefficient”, and from that  $K_A$ . We begin with the standard expression of  $K_A$ :

$$K_A = \frac{[Bound]}{[TTEC]_{free}[Rn]_{free}}.$$

Because  $[Rn] \ll [TTEC]$  (femtomole vs. micromole quantities), the simplification was made that  $[TTEC]_{free} \approx [TTEC]$ . Therefore,

$$K_A = \frac{A_B}{A_{free}} \frac{1}{[TTEC]}$$

where  $A_B$  and  $A_{free}$  are the bound and free radon activities in solution, which were not independently measured. We have the definition of the Ostwald partition coefficient,

$$L = \frac{[Rn]_{free}}{[Rn]_g} = \frac{A_{free} V_g}{A_g V_l},$$

where  $V_g$  and  $V_l$  are the gas and liquid phase volumes and  $A_g$  the gas-phase radon activity.

Defining the *apparent* partition coefficient,  $L'$

$$L' = \frac{(A_{free} + A_B)V_g}{A_g V_l},$$

we arrive at the relationship,

$$L' = LK_A[TTEC] + L.$$

(1)

From LS counting before and after exposure to cryptophane, we determined  $A_g$  and  $(A_{free} + A_B)$ , which in turn yielded  $L'$ . Our  $L'$  vs.  $[TTEC]$  data were fit by linear regression to equation (1) (Figure 2.5). By this method, the affinity of TTEC for radon was found to be  $K_A = 49,000 \pm 12,000 \text{ M}^{-1}$  at 293 K. The standard uncertainty given here for  $K_A$  derived from the 95% confidence intervals on the parameters of fit to the apparent partition coefficients vs. TTEC concentration series (Equation 1 and Figure 2.5). The

uncertainty in the radon assays used to derive the partition coefficients was negligible. These data were well fit by a linear model, with  $R^2 = 0.87$ . Radon activity measured for reaction vessels containing no cryptophane deviated from this line, as expected when the  $[Rn] \ll [TTEC]$  condition no longer holds.

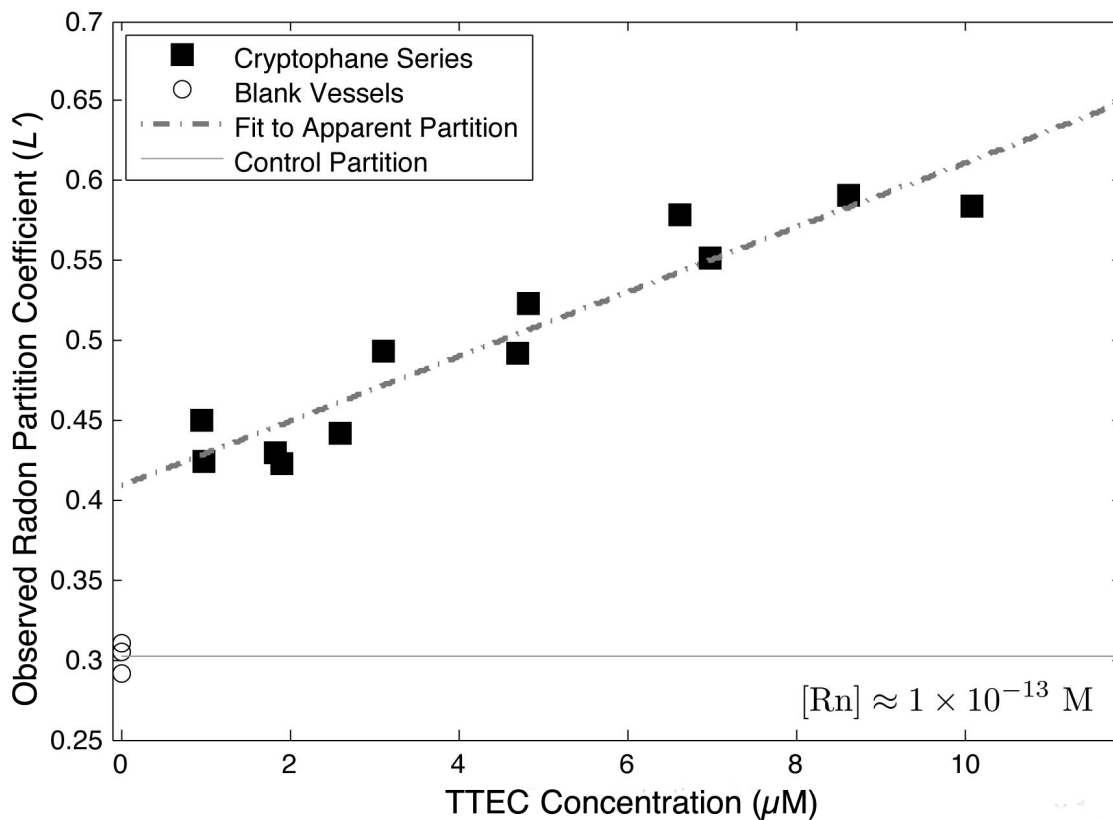


**Figure 2.5.** Apparent partition coefficient,  $L'$ , as a function of cryptophane concentration. The circles represent reaction vessels that contained no cryptophane; the squares represent a series of increasing cryptophane concentrations in the non-saturated regime, fitted to equation (1).



From these experiments, radon was found to bind TTEC with a free energy of binding 0.4 kJ/mol more negative than in the case of xenon (-26.3 vs. -25.9 kJ/mol). However, radon is also more soluble in water solution than xenon and therefore liberates less free energy upon desolvation (-20.71 kJ/mol, Rn vs. -23.18 kJ/mol, Xe; est.).<sup>28</sup> Accounting for this, we estimate that supramolecular interactions of the TTEC-Rn complex, e.g. balance of improved dispersion interactions and entropic cost of confinement, produce a free energy of binding 2.9 kJ/mol stronger than in the TTEC-Xe complex. Our previous crystallographic study showed that the internal volume of trisubstituted cryptophane-A derivatives bound to Xe is roughly 87 Å<sup>3</sup> and can expand to ~100 Å<sup>3</sup> to accommodate a much larger (71 Å<sup>3</sup>) CDCl<sub>3</sub> guest.<sup>12</sup> We can assume that TTEC bound to either Xe or Rn adopts a very similar geometry to the previous 4-Xe crystal structure (Figure 2.6).<sup>12</sup> As evidenced by this structure, Xe underfills the cryptophane cavity, interacting over tenths of angstroms with the phenyl carbon atoms in both cyclotriguaiacylene caps. The somewhat larger, more polarizable Rn atom is expected to exhibit stronger van der Waals interactions with TTEC than Xe, as supported by the measured enhancement in free energy of binding.

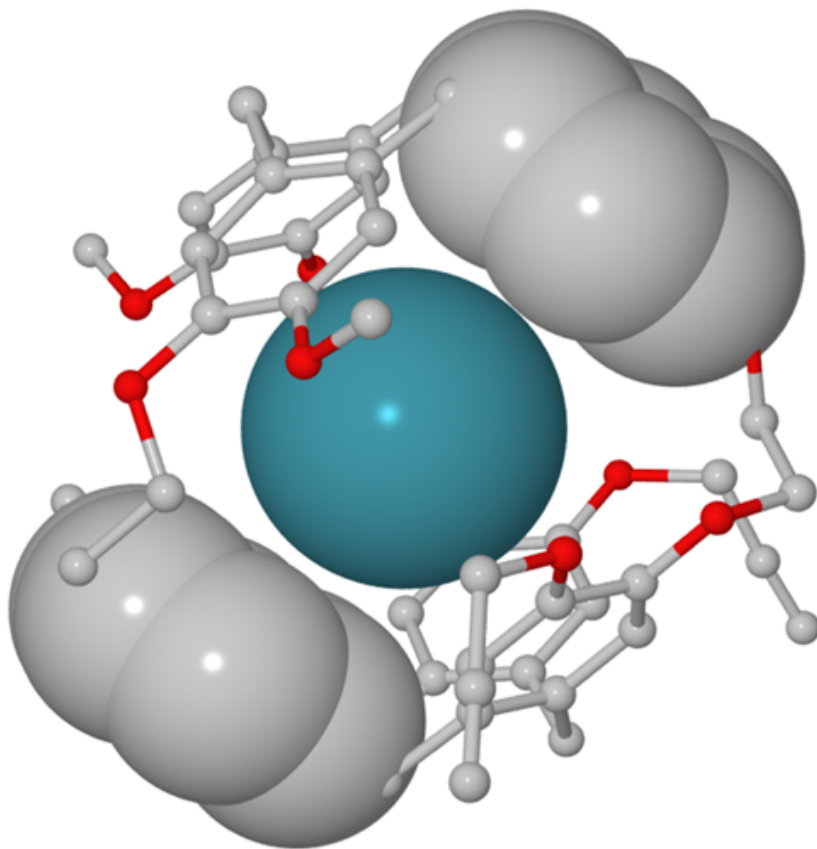


**Figure 2.6.** Structure of 4-Xe complex determined from X-ray crystallography.<sup>12</sup> van der Waals radii are shown for Xe (blue sphere) and carbon atoms of one pair of opposing phenyl groups. Hydrogen atoms have been removed for clarity. Rn is expected to bind to the same site in TTEC, while occupying 10-15% more of the interior cavity volume.

Despite the institution of government-sponsored detection and remediation programs in many countries,<sup>29</sup> contemporary assessments show that radon exposure remains the second leading cause of lung cancer, after smoking, in the United States.<sup>30,31</sup> While the environmental health risks posed by radon are well recognized, studies of radon binding to well-defined synthetic or biological targets have not been performed; studies have tended to focus on the association of radon progeny, not radon itself.<sup>32</sup> Challenges in this work have been to obtain pure <sup>222</sup>Rn and make binding measurements on very small quantities of material. In the current study, pure radon was obtained by sealing <sup>226</sup>RaCl<sub>2</sub> solution inside of polyethylene capsules permeable only to the gaseous emanation. These capsules, placed in a sealed 10.6-mL water-filled vessel, generated a useful concentration of <sup>222</sup>Rn within roughly one week as a steady state was approached. This solution provided sufficient <sup>222</sup>Rn for tens of binding measurements. This method requires the radium-filled capsules to be properly sealed, and all <sup>222</sup>Rn manipulations must be performed using gas-tight syringes inside of a laboratory fume hood. With these precautions, this method has broad utility for the study of radon binding to many different biological samples, biomolecules, or other small-molecule hosts.

The concepts of supramolecular chemistry<sup>33,34</sup> can be usefully applied to the study of radon binding. For example, many organic cavitands should bind radon with appreciable affinity, based on radon's considerable polarizability and molecular volume, which is similar to that of dichloromethane. This study showed that a water-soluble cryptophane-A derivative binds radon with considerable affinity. Indeed, TTEC may provide a nearly optimal cavity for radon as its internal volume ( $\sim 90 \text{ \AA}^3$ , assuming

modest expansion from the average 4-Xe structure)<sup>12</sup> is approximately twice the radon atomic volume.<sup>35</sup> Furthermore, in lieu of three ethylamine groups, tripropargylated **4** can be reacted with a wide variety of water-solubilizing azido-linkers that may fine-tune the host-noble gas interaction.<sup>12-14</sup>

Considering our previous study of the analogous tris(triazole propionic acid) cryptophane,<sup>14</sup> it is striking that a tris-carboxylate to tris-amine substitution at the cryptophane periphery increased the Xe association constant from 17,000 M<sup>-1</sup> to 42,000 M<sup>-1</sup> at 293 K. In order to explore the role of electrostatic interactions, we investigated xenon binding to TTEC at pH 2.5 (Figure 2.7) and 7.5 (Figure 2.3). As shown in Figures 2.8 and 2.9, hyperpolarized <sup>129</sup>Xe NMR spectroscopy gave comparable chemical shifts at 298 K for TTEC-<sup>129</sup>Xe at pH 2.5 (63.8 ppm) and pH 7.5 (64.3 ppm), which is indicative of very similar Xe binding environments within the cryptophane. Over this pH range the compound went from a state of predominantly triple protonation at pH 2.5 to mostly single protonation at pH 7.5 while remaining in solution (Figure 2.10). Slightly higher Xe binding affinity was observed by ITC at pH 7.5 than pH 2.5 ( $K_A = 42,000 \pm 2,000 \text{ M}^{-1}$  vs.  $K_A = 34,000 \pm 1,000 \text{ M}^{-1}$  at 293 K, Figure 2.7). Thus, it appears that electrostatic interactions, as well as other effects such as cryptophane solvation, are responsible for the enhanced Xe binding observed in TTEC.

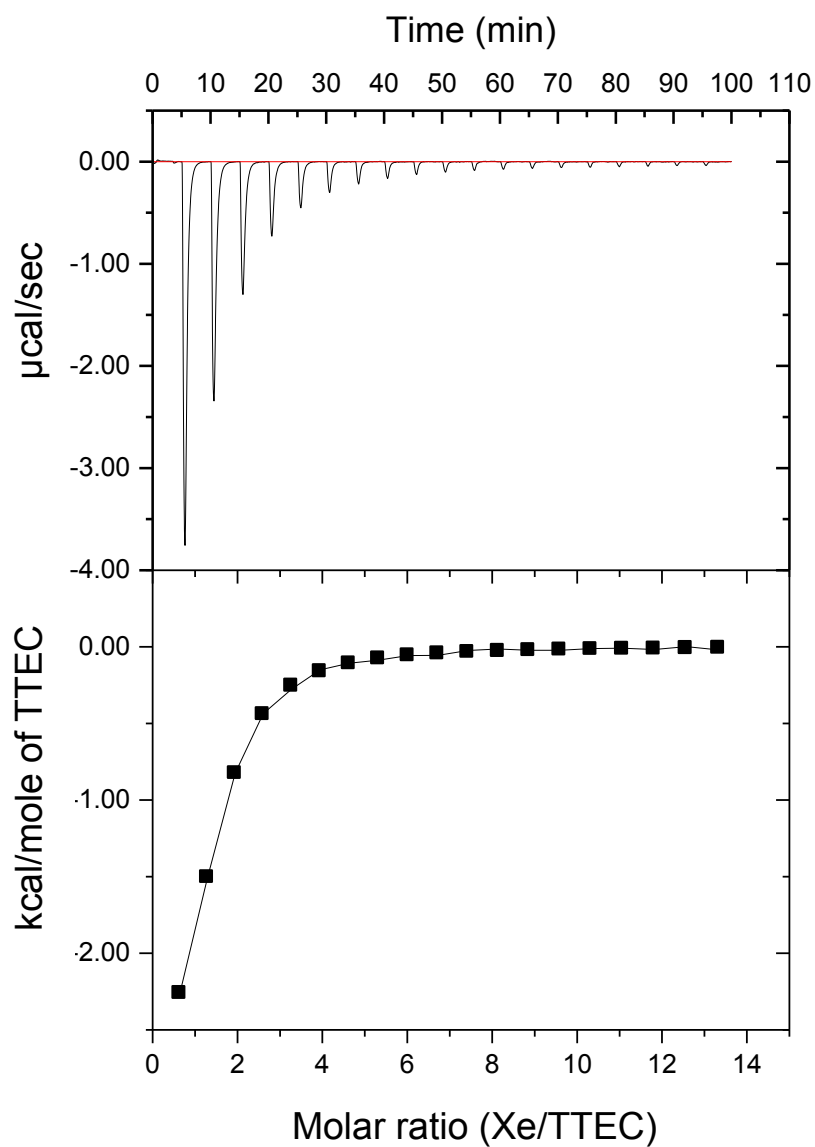


**Figure 2.7.** Enthalpogram of 83  $\mu\text{M}$  TTEC (**6**) in phosphate buffer (20 mM, pH 2.5) at 293 K titrated with saturated aqueous xenon solution (5.05 mM).

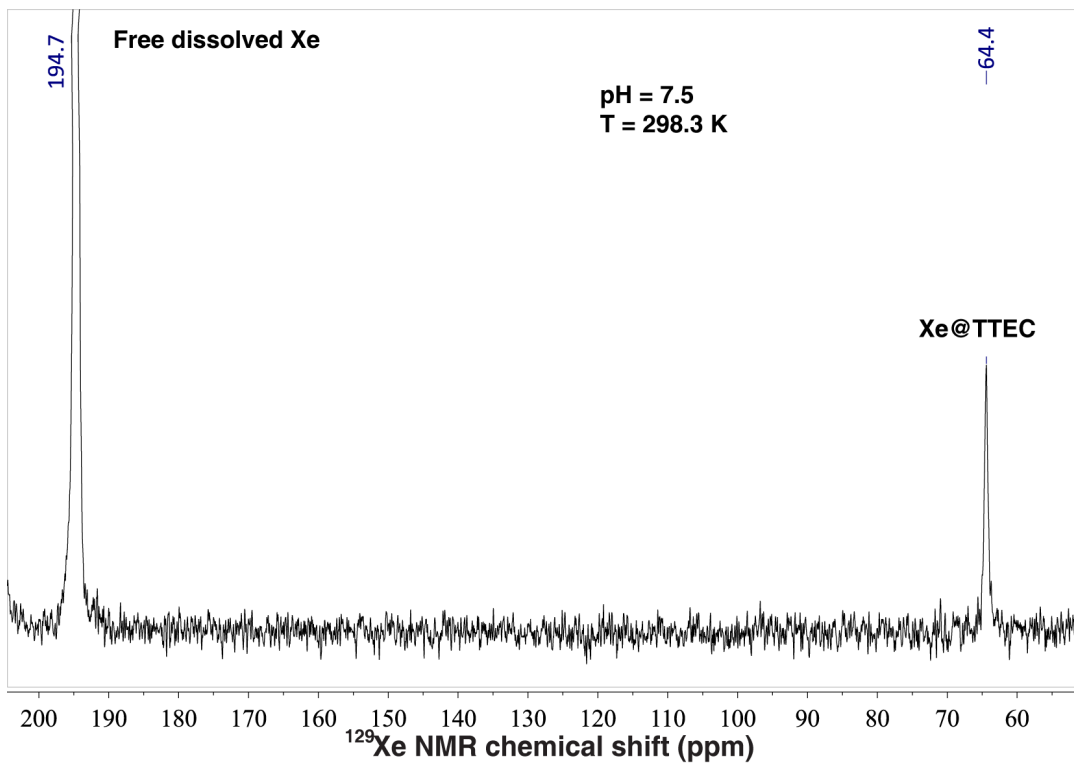


**Figure 2.8.** Hyperpolarized  $^{129}\text{Xe}$  NMR spectrum showing xenon bound to TTEC (6) in 20 mM phosphate buffer, pH 7.5.

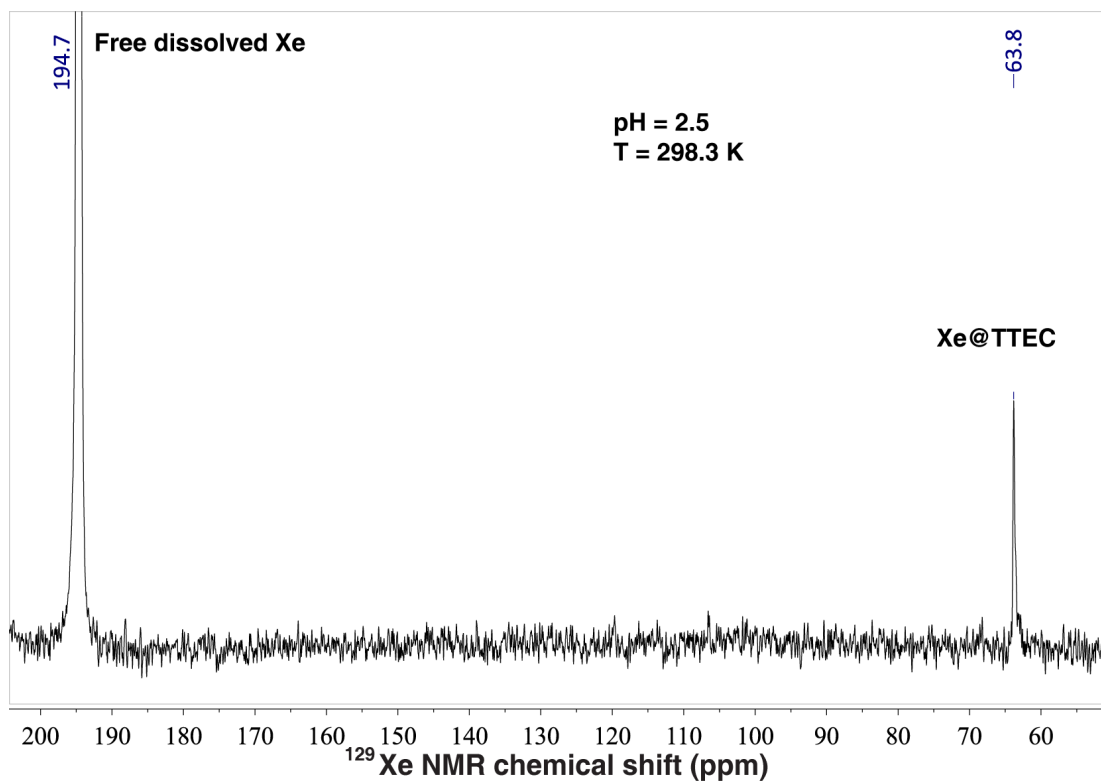


**Figure 2.9.** Hyperpolarized  $^{129}\text{Xe}$  NMR spectrum showing xenon bound to TTEC (6) in 20 mM phosphate buffer, pH 2.5.

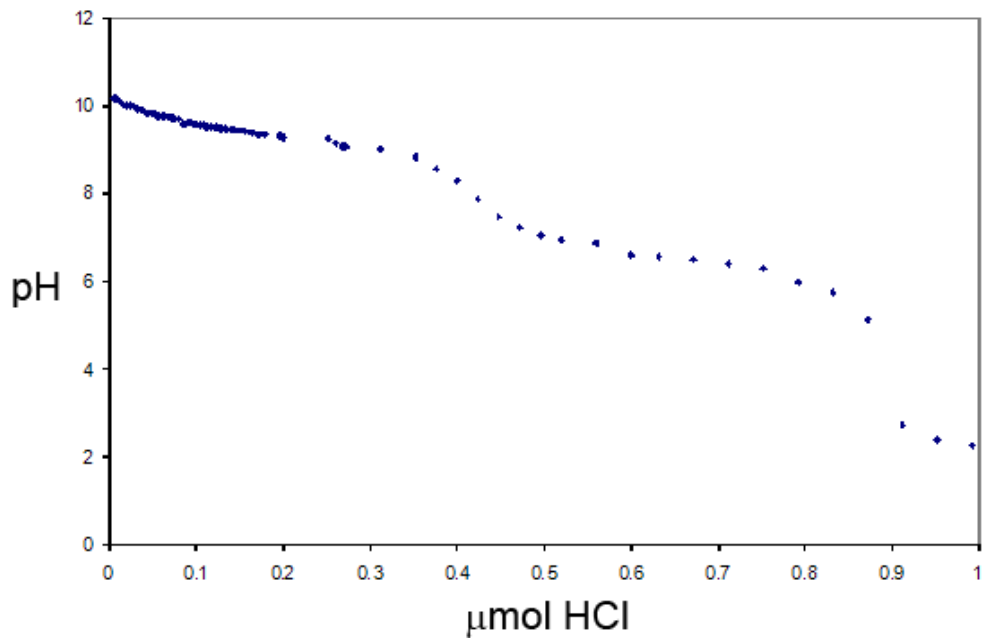


**Figure 2.10.** Titration curve showing the titration of 0.279 micromoles TTEC (**6**) in 1 mL of 100 mM NaCl with small aliquots of 50 mM HCl. The acid-base titrations were performed following the same methodology reported previously.<sup>15</sup>



## CONCLUSION

The development of high-affinity Xe-binding cages is an area of active investigation and is critical to the burgeoning field of xenon biosensing.<sup>16,36,37</sup> Synthetic host molecules designed to bind xenon in cells or *in vivo* must compete against a wide variety of biological substrates. Xenon is lipophilic and exhibits affinity for cavities in macromolecular interiors. Xenon's lipophilic behavior has been shown from its partition with long-chain hydrocarbons<sup>38,39</sup> and from its *in vitro*<sup>40</sup> and *in vivo*<sup>41</sup> partition with fatty tissue. Xenon binding to myoglobin has been well characterized by NMR spectroscopy<sup>42,43</sup> and X-ray crystallography,<sup>44</sup> and metmyoglobin-Xe association constants have been measured to be  $\sim 200 \text{ M}^{-1}$  and  $10 \text{ M}^{-1}$ .<sup>44,45</sup> Comparable affinities have been determined for other naturally occurring sites in hemoglobin,<sup>43</sup> lipoxygenase,<sup>46</sup> and lipid transfer protein,<sup>47</sup> as well as specially designed hydrophobic cavities in T4 lysozyme,<sup>48</sup> ribose-binding protein,<sup>49</sup> and other examples.<sup>50,51</sup> We showed previously that xenon binds water-soluble cryptophanes  $\sim 1.5$ -fold less avidly in human plasma than in aqueous buffer solution.<sup>14</sup> Thus, the design of higher affinity xenon-binding molecules such as TTEC extends the range of possible biological applications. Biologically targeted cryptophanes are under development as potential  $^{129}\text{Xe}$  MRI contrast agents, as demonstrated by xenon biosensors for the prototypical biotin-avidin interaction<sup>52,53</sup> and other proteins,<sup>54-56</sup> as well as cell studies.<sup>57-59</sup> This demonstration of radon binding to cryptophane raises similar possibilities of molecularly functionalized radon binders for biological, environmental, and materials applications involving radon delivery, sequestration, or detection.

Finally, it is significant that xenon and radon showed similarly tight binding for a well-defined molecular cavity (TTEC). This suggests that radon, which like xenon is known to be lipophilic,<sup>26,60</sup> also binds with appreciable affinity to many proteins, surfactants, and small air spaces in the lung and other regions of the body. Radiometric binding methods developed in the course of this work will enable quantitative comparisons of radon binding to various biomolecular targets, as a means of assessing environmental health risk. Such information may ultimately be useful in developing more effective mitigation strategies for this indoor pollutant.

## EXPERIMENTAL PROCEDURES

**Reagents.** Organic reagents and solvents were used as purchased from the following commercial sources:

*Sigma-Aldrich:* methanol, 2,6-lutidine; *Acros:* cesium carbonate, anhydrous dimethylsulfoxide (DMSO), anhydrous dimethylformamide (DMF), 70% perchloric acid, *d*<sub>6</sub>-DMSO, CDCl<sub>3</sub>; *Fisher:* sodium chloride, potassium phosphate, ethyl acetate, dichloromethane, hydrochloric acid, sodium hydroxide, sodium sulfate, acetone, hexanes; *Cambridge Isotope Laboratories:* deuterium oxide; *Airco Industrial Gases:* research-grade xenon gas.

**General Methods.** All organic reactions were carried out under nitrogen atmosphere. <sup>1</sup>H NMR (500.14 MHz) and <sup>13</sup>C NMR (125.77 MHz) spectra were obtained on a Bruker AMX 500 spectrometer at the University of Pennsylvania NMR facility. Electrospray ionization mass spectrometry was performed in low-resolution mode on a Micromass LC Platform and in high-resolution mode on a Micromass Autospec while *matrix-assisted laser desorption/ionization spectrometry* (MALDI) was performed on a Bruker Daltonic Ultraflex III MALDI-TOF-TOF at the Mass Spectrometry Center in the Chemistry Department at the University of Pennsylvania. Isothermal titration calorimetry (ITC) was performed using a MicroCal VP-ITC titration microcalorimeter (Northampton, MA). For ITC measurements in buffer, solutions were prepared with deionized (DI) water obtained from Mar Cor Premium Grade Mixed Bed Service Deionization (18.2 megohm-cm resistivity at 25 °C). Column chromatography was performed using 60 Å porosity, 40-75 µm particle size silica gel from Sorbent Technologies. Thin layer chromatography (TLC)

was performed using silica gel plates with UV light at 254 nm for detection. HPLC analysis was performed on an Agilent 1100 system equipped with a quaternary pump and diode array detector using a Varian Microsorb-MV 300-5 C8 column (4.6 × 250 mm, 5 μm). The gradient eluent was composed of two solvents: 0.1% aqueous TFA (solvent A) and a 0.1% solution of TFA in CH<sub>3</sub>CN (solvent B). UV-visible spectra were measured using a diode-array Agilent 89090A spectrophotometer.

**Synthesis.** Cyclotriguaiacylene (**1**), and [3-propargyloxy-4-(2-iodoethoxy)phenyl]methanol (**2**) were synthesized using previously published protocols.<sup>56</sup> The NMR spectra and physical constants also matched the reported literature data.<sup>56</sup>

2,7,12-Tris[2-[4-(hydroxymethyl)-2-propargyloxyphenoxy]ethoxy]-3,8,13-trimethoxy-10,15-dihydro-2H-tribenzo[a,d,g]cyclononene (**3**), and tripropargyl cryptophane (**4**) were also synthesized using previous protocols.<sup>14</sup> The identity and purity of the compounds were confirmed by matching the NMR spectra and physical constants to reported literature data.<sup>14</sup> 2-Azidoethylamine (**5**) was synthesized in 93% yield, also following literature precedent.<sup>17</sup>

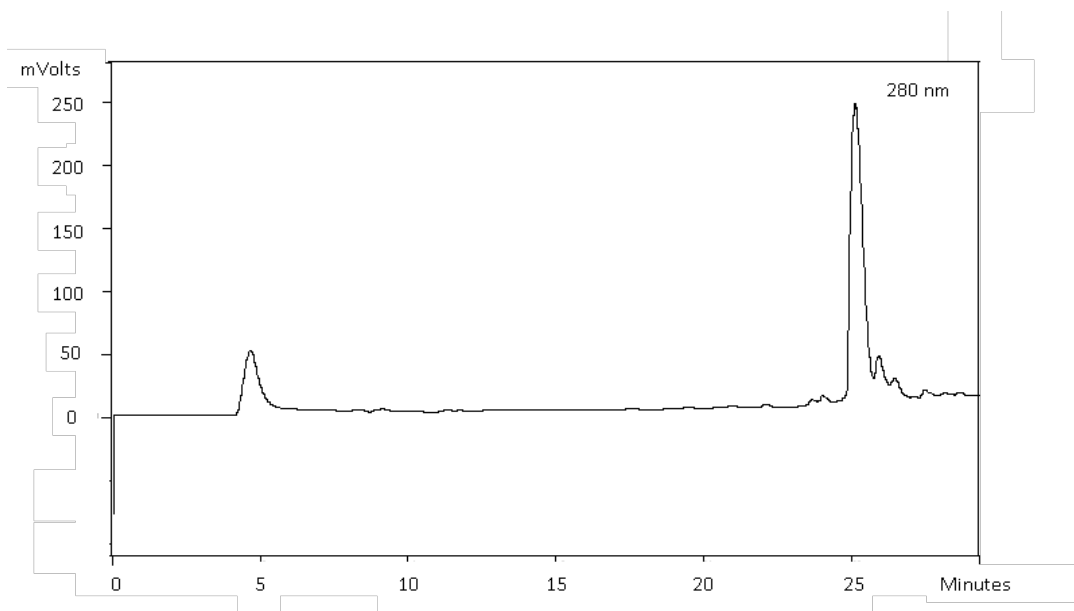
**Tris(triazole ethylamine) cryptophane (6, TTEC).** Tripropargyl cryptophane (**4**) (10.13 mg, 0.01049 mmol, 1.0 equiv.), 2-azidoethylamine (**5**) (4.47 mg, 0.0520 mmol, 5.0 equiv.), copper (II) sulfate (0.83 mg, 0.0052 mmol, 0.5 equiv.), 2,6 lutidine (0.11 mg, 0.0010 mmol, 0.1 equiv.), and sodium ascorbate (82.14 mg, 0.4146 mmol, 40 equiv.) were added to a glass vial with septum cap. Dry DMSO (0.5 mL) was added and the reaction was magnetically stirred under nitrogen overnight. The product was purified

using two methods: 1) 0.1 % TFA in DI water was added to the reaction mixture which led to the precipitation of the product TTEC (**6**) which was centrifuged and the supernatant discarded. The white pellet was resuspended in DI water and precipitated by adding 0.1 % TFA and centrifuged again to separate the supernatant. This was repeated twice after which the white precipitate was dried under vacuum; 2) The product was also purified using the HPLC gradient 0.1% TFA in 95% water: 5% acetonitrile to 0.1% TFA in 20% water: 80% acetonitrile over 75 min. This resulted in 9.73 mg (75% yield) of TTEC (**6**) as a white powder. <sup>1</sup>H NMR (500 MHz, *d*<sub>6</sub>-DMSO):  $\sigma$  8.20 (s, 3H), 7.09 (s, 3H), 6.88 (s, 3H), 6.82 (s, 3H), 6.80 (s, 3H), 5.12-5.03 (m, 6H), 4.52-4.49 (m, 6H), 4.42 (s, 6H), 4.21-4.09 (m, 18H), 3.51 (s, 9H), 3.38 (d, *J* = 13.8 Hz, 3H). H<sub>eq</sub> and  $\alpha$ -amino protons with a total integration of 6H were hidden under residual water peak. <sup>13</sup>C NMR (125 MHz, *d*<sub>6</sub>-DMSO) 148.8, 147.8, 146.0, 145.7, 143.3, 133.8, 133.5, 132.6, 131.7, 124.5, 120.7, 119.0, 117.0, 115.0, 68.8, 68.3, 62.8, 56.0, 49.3, 35.0, 29.1; MALDI MS calcd. for C<sub>66</sub>H<sub>72</sub>N<sub>12</sub>O<sub>12</sub> (M + Na<sup>+</sup>) 1247.539; found 1247.724.

**Hyperpolarized  $^{129}\text{Xe}$  NMR Spectroscopy.** A home-built version of the previously commercially available Nycomed-Amersham (now GE) IGI.Xe.2000  $^{129}\text{Xe}$  hyperpolarizer was used to generate the hyperpolarized  $^{129}\text{Xe}$  gas. A gas mixture of 89%  $\text{N}_2$ , 10% He, and 1% natural abundance Xe (Spectra Gases) was flowed through the hyperpolarizer.  $^{129}\text{Xe}$  was hyperpolarized to 10-15% after being cryogenically separated, accumulated, thawed, and collected in CAV NMR tubes (New Era). After Xe collection, NMR tubes were shaken vigorously to mix cryptophane solutions with Xe.

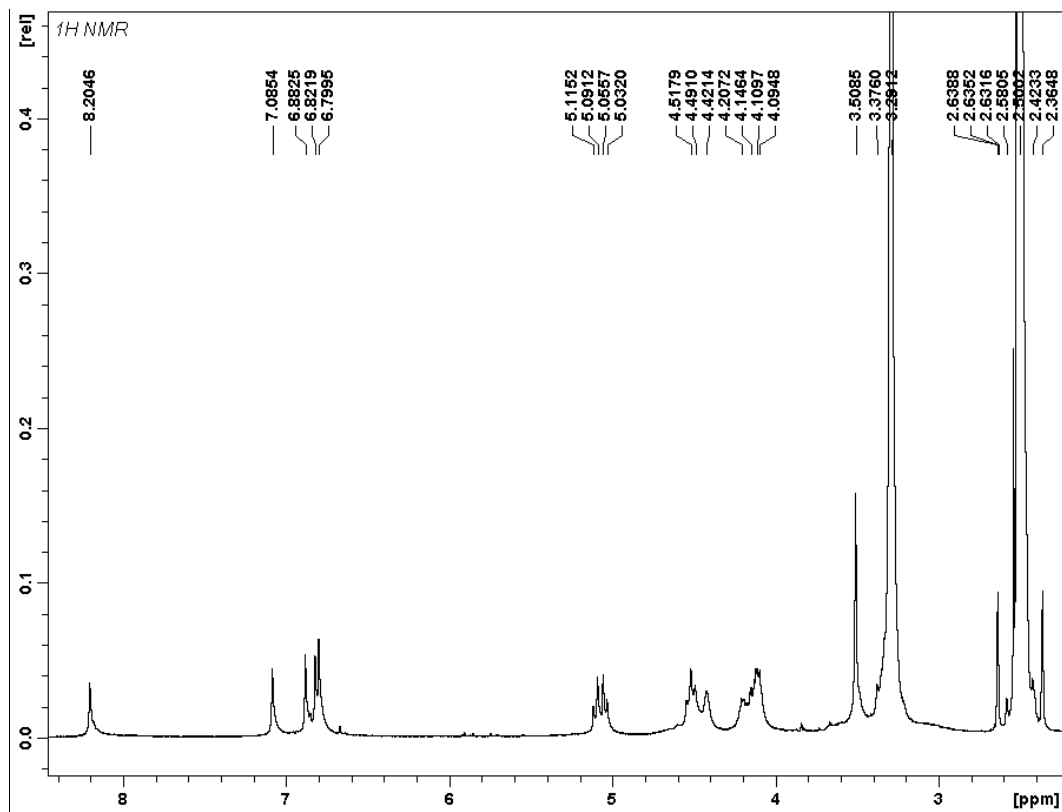
All  $^{129}\text{Xe}$  NMR measurements were carried out on a 500 MHz Bruker BioDRX NMR spectrometer at the University of Pennsylvania NMR Facility. RF pulse frequency for  $^{129}\text{Xe}$  was 138.12 MHz. Samples were observed using either a 5 mm PABBO NMR probe or a similar 10 mm probe.

$^{129}\text{Xe}$  NMR spectra were acquired using the Exchange Signal Averaging (ESA) method.<sup>61</sup> Selective pulses (90° flip angle, EBurp1 shaped) were generated at the Xe@cryptophane resonance frequencies. Each pulse lasted 5 ms, which gave a designated excitation region ~1 kHz. All spectra were signal averaged by 40 scans. A delay of 0.15 s was given between scans to allow polarized Xe to exchange in and depolarized Xe to exchange out of the cryptophane cavity. Sample temperature was controlled by VT unit on NMR spectrometer to  $27 \pm 1$  °C.



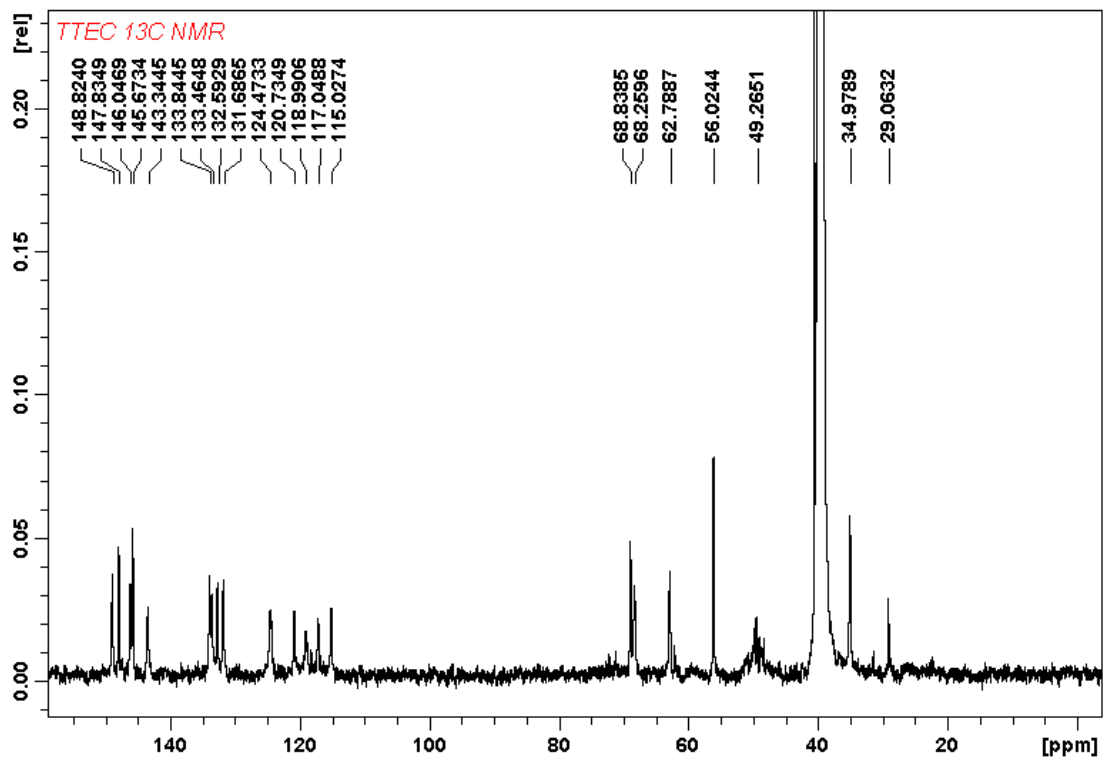
HPLC trace for TTEC (**6**). Column: Microsorb-MV 300-5 C8 250 x 4.6 mm (Varian); flow rate: 1 mL/min; injected volume: 500  $\mu$ L; wavelength detection: 280 nm. HPLC gradient 0.1% TFA in 95% water: 5% acetonitrile to 0.1% TFA in 20% water: 80% acetonitrile over 75 min. Retention time of TTEC: 25.16 min.

$^1\text{H}$  NMR of TTEC (6) in  $\text{d}_6$ -DMSO at 298K



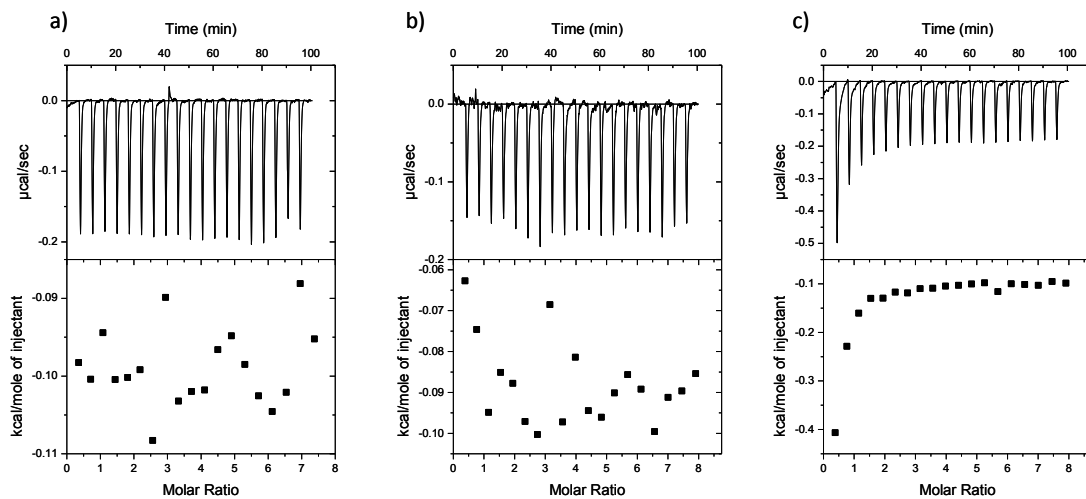


$^{13}\text{C}$  NMR of TTEC (**6**) in  $d_6$ -DMSO at 298K

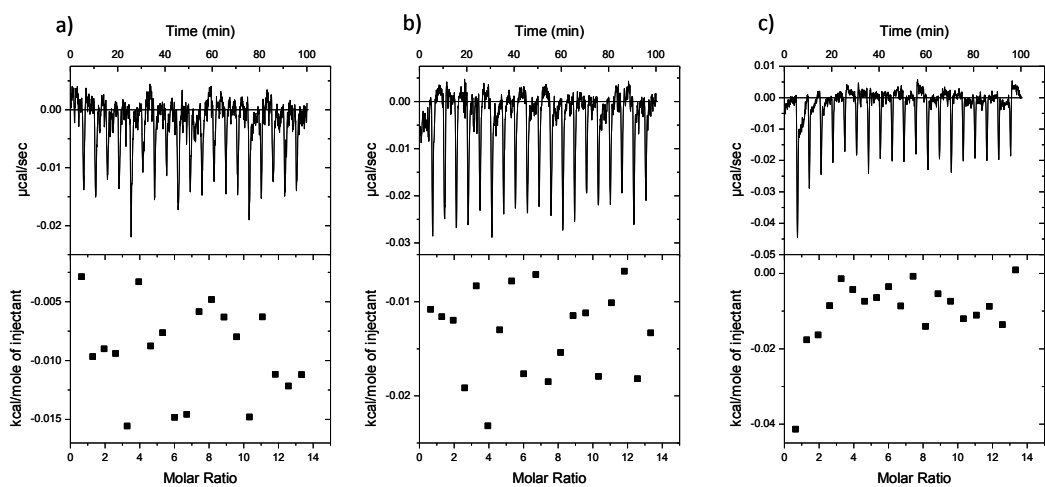


**Xenon Binding Study.** Isothermal titration calorimetry (ITC) was performed using a MicroCal VP-ITC titration microcalorimeter (Northampton, MA).<sup>62</sup> TTEC was dissolved in phosphate buffer (20 mM, pH 7.5) and the concentration (140  $\mu$ M) was determined by UV-vis spectroscopy according to the extinction coefficient of TTEC at 280 nm ( $\epsilon_{280} = 12,400 \text{ M}^{-1}\text{cm}^{-1}$ ). The preparation of saturated aqueous xenon solution and the determination of xenon concentration at 293 K were performed following the same methodology reported previously.<sup>14,22</sup> The titrations were carried out at 293 K; 1.8 mL of the TTEC in 20 mM phosphate buffer was placed in the calorimeter cell, and the saturated xenon-water solution was loaded into the microsyringe.

The titration was performed by the sequential addition of 15  $\mu$ L aliquots of xenon solution (for a total of 19 injections) at 5-min intervals. The heat of reaction per injection (micro-calories per second) was determined by integration of the peak areas (ORIGIN 7.0, MicroCal software). The values of the binding enthalpy ( $\Delta H^\circ$ ), the stoichiometry of binding ( $n$ ), and the association constant ( $K_A$ ) were obtained from fitting the heat evolved per mole of xenon injected versus the xenon/TTEC molar ratio using the same software. Three control experiments (see Experimental procedures) were performed with each phosphate buffer (20 mM) at pH 7.5 or pH 2.5: 1) saturated xenon solution titrated into buffer; 2) water titrated into TTEC-buffer solution; and 3) water titrated into buffer to determine the heats of dilution. Processes #1 and #2 were subtracted from, and #3 was added back to, the corresponding TTEC-xenon binding enthalpogram before curve fitting.



ITC buffer controls at 293 K. Buffer is 20 mM phosphate, pH 7.5. a) Water titrated into buffer. b) Water titrated into a solution of 140 μM TTEC (6) in buffer. c) Xenon-saturated water ( $[Xe] = 5.05 \text{ mM}$ ) titrated into buffer.



ITC buffer controls at 293 K. Buffer is 20 mM phosphate buffer, pH 2.5. a) Buffer titrated into buffer. b) Buffer titrated into a solution of 83  $\mu\text{M}$  TTEC (**6**) in buffer. c) Xenon-saturated buffer ( $[\text{Xe}] = 5.05 \text{ mM}$ ) titrated into buffer.

**Radon Binding Study.** Radon was generated from 63 kBq  $^{226}\text{Ra}$  in four polyethylene capsules submersed in a water-filled 10.6 mL vessel sealed with an aluminum-lined septum. Radon was allowed to accumulate in the water for 8 days prior to the experiment. The emanation fraction (i.e., the ratio of accumulated  $^{222}\text{Rn}$  to the total generated from  $^{226}\text{Ra}$  decay) for the capsules was about 30%. Stock TTEC solution concentration (48.3  $\mu\text{M}$ ) was determined by UV-vis spectroscopy and radon-in-water solution concentration (1.002 pM) by LS counting. Glass vials (1.1-mL Chromacol screw top, Supelco, Bellefonte, PA, USA) sealed with PTFE septa were filled by micropipette with varying concentrations of cryptophane solution (0.49-5.29 nmol in 120  $\mu\text{L}$ ; six concentrations, each in duplicate, and three null trials), and with radon-in-water solution (400  $\mu\text{L}$ ) from the generator, by 10-mL glass, gas-tight Hamilton syringe. The rest of the vial was left as airspace. The samples were incubated for 30-40 min at 293 K; each vial was subjected to two 5-sec vortex mixings, one each at the beginning and end of the incubation. A 400  $\mu\text{L}$  sample was withdrawn from each vial and injected beneath the surface of approximately 19 mL LS cocktail that consisted of a commercial scintillation fluid (Ultima GAB, PerkinElmer, Waltham MA, USA) having a 5% water fraction in a 22-mL Al-foil lined, glass LS vial. LS counting was done using automated equipment after allowing time for radon to equilibrate with its daughter nuclides. Each sample was counted for 1 h in two apparatuses with different operational parameters (Beckman Coulter, Brea, CA, USA; Wallac, PerkinElmer, Waltham, MA, USA). All liquid transfers by micropipette and syringe, as well as the precise volumes of the vials, were quantified gravimetrically.

The radon determinations were based on well-established LS procedures for the assay of gravimetrically-determined aliquots of aqueous solutions containing radon in radioactive equilibrium with its short-lived daughter products.<sup>23</sup> Raw LS data were corrected for background (< 0.3% correction), for the radon content in the airspace above the cocktail in the LS vials (approx. 0.7 % correction), and for radioactive decay to a common reference time. Counting was initiated after a minimum of 4 h to ensure that the radon daughters were in radioactive equilibrium. Each source was measured for 20 min over a period of 0.2 to 4.9 days on 6 to 10 occasions. The corrected net counting rates were observed to decay with the radon half-life, indicating that there was no radium leakage from the capsules. Corrected data were fitted to equation (1) by least-squares linear regression using MATLAB (Mathworks, Natick, MA, USA) to obtain  $K_A$  and  $L$ .

## **ACKNOWLEDGMENTS**

Support came from the DOD (W81XWH-04-1-0657), NIH (CA110104), a Camille and Henry Dreyfus Teacher-Scholar Award, and UPenn Chemistry Department. We thank Roderic Eckenhoff for access to ITC, George Furst for assistance with NMR spectroscopy, and Pat Carroll for rendering Figure 2.6.

## **AUTHOR CONTRIBUTIONS**

D.R.J. and N.S.K. co-wrote the manuscript. D.R.J. developed the cryptophane-radon binding measurement protocol in collaboration with R.C. and analyzed the radon-binding data in consultation with R.F. N.S.K. synthesized and characterized the reported compounds and performed ITC measurements of cryptophane-xenon binding. R.C. performed the cryptophane-radon binding measurements with help from L.L.-P. and D.R.J. Y.B. performed hyperpolarized  $^{129}\text{Xe}$  NMR spectroscopy. I.J.D. initiated this project and edited the manuscript.

## REFERENCES

- (1) Obrist, W. D.; Thompson, H. K.; Wang, H. S.; Wilkinson, W. E. *Stroke* **1975**, *6*, 245-256.
- (2) Perkins, R.; Casey, L. *Radioxenons: their role in monitoring a comprehensive test-ban treaty*. U.S. Department of Energy Department of Energy, Richland, VA, **1996**.
- (3) Oros, A.; Shah, N. J. *Phys. Med. Biol.* **2004**, *49*, R105-R153.
- (4) Brotin, T.; Dutasta, J. *J. Chem. Rev.* **2009**, *109*, 88-130.
- (5) Darby, S.; Hill, D.; Auvinen, A.; Barros-Dios, J. M.; Baysson, H.; Bochicchio, F.; Deo, H.; Falk, R.; Forastiere, F.; Hakama, M.; Heid, I.; Kreienbrock, L.; Kreuzer, M.; Lagarde, F.; Mäkeläinen, I.; Muirhead, C.; Oberaigner, W.; Pershagen, G.; Ruano-Ravina, A.; Ruosteenoja, E.; Schaffrath Rosario, A.; Tirmarche, M.; Tomášek, L.; Whitley, E.; Wichmann, H. E.; Doll, R. *Brit. Med. J.* **2005**, *330*, 223-227.
- (6) Ghosh, D.; Deb, A.; Sengupta, R. *J. Appl. Geophys.* **2009**, *69*, 67-81.
- (7) Eichler, B.; Zimmermann, H. P.; Gäggeler, H. W. *J. Phys. Chem.* **2000**, *104*, 3126-3131.
- (8) Avrorin, V. V.; Krasikova, R. N.; Nefedov, V. D.; Toropova, M. A. *Russ. Chem. Rev.* **1982**, *51*, 12-20.
- (9) Runeberg, N.; Pyykkö, P. I. *J. Quant. Chem.* **1998**, *66*, 131-140.
- (10) Lide, D. R. *CRC Handbook of Chemistry and Physics*; CRC Press: New York, **2002**.



- (11) Bartik, K.; Luhmer, M.; Dutasta, J.; Collet, A.; Reisse, J. *J. Am. Chem. Soc.* **1998**, *120*, 784-791.
- (12) Taratula, O.; Hill, P. A.; Khan, N. S.; Carroll, P. J.; Dmochowski, I. J. *Nat. Commun.* **2010**, *1*:148.
- (13) Fogarty, H. A.; Berthault, P.; Brotin, T.; Huber, G.; Desvaux, H.; Dutasta, J. P. *J. Am. Chem. Soc.* **2007**, *129*, 10332-10333.
- (14) Hill, P. A.; Wei, Q.; Eckenhoff, R. G.; Dmochowski, I. J. *J. Am. Chem. Soc.* **2007**, *129*, 9262-9263.
- (15) Hill, P. A.; Wei, Q.; Troxler, T.; Dmochowski, I. J. *J. Am. Chem. Soc.* **2009**, *131*, 3069-3077.
- (16) Fairchild, R. M.; Joseph, A. I.; Holman, K. T.; Fogarty, H. A.; Brotin, T.; Dutasta, J. P.; Boutin, C.; Huber, G.; Berthault, P. *J. Am. Chem. Soc.* **2010**, *132*, 15505-15507.
- (17) Angelos, S.; Yang, Y.-W.; Patel, K.; Stoddart, J. F.; Zink, J. I. *Angew. Chem. Int. Edit.* **2008**, *47*, 2222-2226.
- (18) Tornøe, C. W.; Christensen, C.; Meldal, M. *J. Org. Chem.* **2002**, *67*, 3057-3064.
- (19) Kolb, H. C.; Finn, M. G.; Sharpless, K. B. *Angew. Chem. Int. Edit.* **2001**, *40*, 2004-2021.
- (20) Rostovtsev, V. V.; Green, L. G.; Fokin, V. V.; Sharpless, K. B. *Angew. Chem. Int. Edit.* **2002**, *41*, 2596-2599.
- (21) Punna, S.; Kuzelka, J.; Wang, Q.; Finn, M. G. *Angew. Chem. Int. Edit.* **2005**, *44*, 2215-2220.

- (22) Clever, H. L. *Solubility Data Series*; Pergamon Press: New York, **1979**;  
Vol. 2.
- (23) NIST, National Institute of Standards and Technology. Certificate,  
Standard Reference Material 4973, Radon-222 Emanation Standard, Gaithersburg, MD,  
**2005**.
- (24) Collé, R. *Radioact. Radiochem.* **1995**, 6, 16-29.
- (25) Collé, R.; Kishore, R. *Nucl. Instr. Meth. Phys. Res.* **1997**, A391, 511-528.
- (26) Schubert, M.; Lehmann, K.; Paschke, A. *Sci. Total Environ.* **2007**, 376,  
306-316.
- (27) Battino, R. *Fluid Phase Equilibr.* **1984**, 15, 231-240.
- (28) Scharlin, P.; Battino, R.; Silla, E.; Tuñón, I.; Pascual-Ahuir, J. L. *Pure &  
Appl. Chem.* **1998**, 70, 1895-1904.
- (29) Cole, L. A. *Element of risk: the politics of radon*; Oxford University Press:  
New York, **1993**.
- (30) Pawel, D. J.; Puskin, J. S. *Health Phys.* **2004**, 87, 68-74.
- (31) Lugg, A.; Probert, D. *Appl. Energy* **1997**, 56, 93-196.
- (32) Evans, H. H.; Mencl, J.; Bakale, G.; Rao, P. S.; Jostes, R. F.; Hui, T. E.;  
Cross, F. T.; Schwartz, J. L. *Radiat. Res.* **1993**, 136, 48-56.
- (33) Lehn, J.-M. *Supramolecular Chemistry*; Wiley-VCH, **1995**.
- (34) Davis, A. V.; Yeh, R. M.; Raymond, K. N. *Proc Natl Acad Sci U.S.A.*  
**2002**, 99, 4793-4796.
- (35) Mecozzi, S.; Rebek, J. *Chem. Eur. J.* **1998**, 4, 1016-1022.

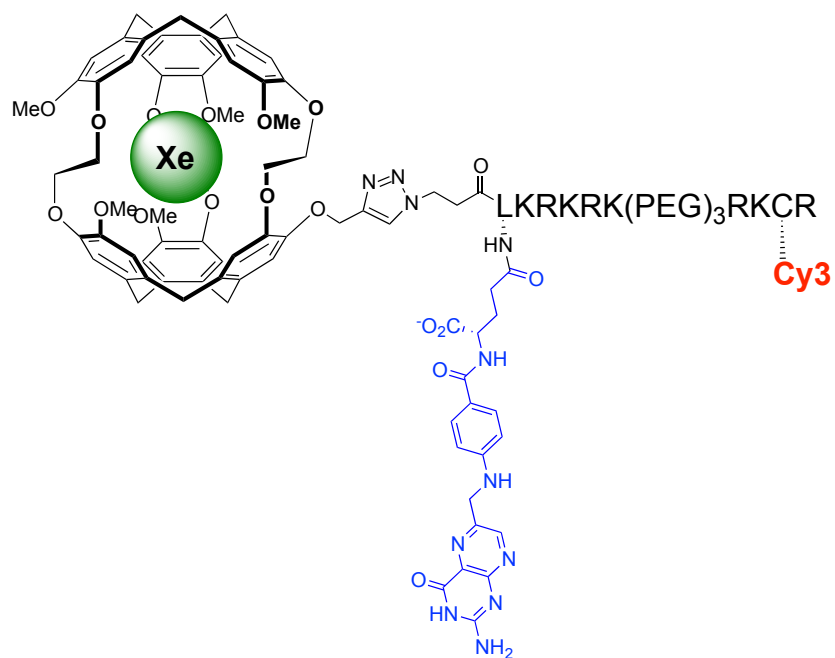
- (36) Kim, B. S.; Ko, Y. H.; Kim, Y.; Lee, H. J.; Selvapalam, N.; Lee, H. C.; Kim, K. *Chem. Commun.* **2008**, 2756-2758.
- (37) Taratula, O.; Dmochowski, I. J. *Curr. Opin. Chem. Biol.*, **2010**, *14*, 97-104.
- (38) Clever, H. L. *J. Phys. Chem.* **1958**, *62*, 375-376.
- (39) Graziano, G. *Biophys. Chem.* **2003**, *105*, 371-382.
- (40) Yeh, S. Y.; Peterson, R. E. *J. Pharm. Sci.* **1963**, *52*, 453-458.
- (41) Andersen, A. M.; Ladefoged, J. *Scand. J. Clin Lab. Invest.* **1967**, *19*, 72-78.
- (42) Rubin, S. M.; Spence, M. M.; Goodson, B. M.; Wemmer, D. E.; Pines, A. *Proc. Nat. Acad. Sci. U.S.A.* **2000**, *97*, 9472-9475.
- (43) Tilton, R. F.; Kuntz, I. D. *Biochemistry* **1982**, *21*, 6850-6857.
- (44) Tilton, R. F.; Kuntz, I. D.; Petsko, G. A. *Biochemistry* **1984**, *23*, 2849-2857.
- (45) Ewing, G. J.; Maestas, S. *J. Phys. Chem.* **1970**, *74*, 2341-2344.
- (46) Bowers, C. R.; Storhaug, V.; Webster, C. E.; Bharatam, J.; Cottone, A., 3rd; Gianna, R.; Betsey, K.; Gaffney, B. J. *J. Am. Chem. Soc.* **1999**, *121*, 9370-9377.
- (47) Dubois, L.; Da Silva, P.; Landon, C.; Huber, J. G.; Ponchet, M.; Vovelle, F.; Berthault, P.; Desvaux, H. *J. Am. Chem. Soc.* **2004**, *126*, 15738-15746.
- (48) Quillin, M. L.; Breyer, W. A.; Griswold, I. J.; Matthews, B. W. *J. Mol. Biol.* **2000**, *302*, 955-977.
- (49) Lowery, T. J.; Rubin, S. M.; Ruiz, E. J.; Pines, A.; Wemmer, D. E. *Angew. Chem. Int. Edit.* **2004**, *43*, 6320-6322.

- (50) Groger, C.; Moglich, A.; Pons, M.; Koch, B.; Hengstenberg, W.; Kalbitzer, H. R.; Brunner, E. *J. Am. Chem. Soc.* **2003**, *125*, 8726-8727.
- (51) Rubin, S. M.; Lee, S. Y.; Ruiz, E. J.; Pines, A.; Wemmer, D. E. *J. Mol. Biol.* **2002**, *322*, 425-440.
- (52) Spence, M. M.; Rubin, S. M.; Dimitrov, I. E. *Proc. Nat. Acad. Sci. U.S.A.* **2001**, *98*, 10654-10657.
- (53) Spence, M. M.; Ruiz, E. J.; Rubin, S. M.; Lowery, T. J.; Winssinger, N.; Schultz, P. G.; Wemmer, D. E.; Pines, A. *J. Am. Chem. Soc.* **2004**, *126*, 15287-15294.
- (54) Chambers, J. M.; Hill, P. A.; Aaron, J. A.; Han, Z.; Christianson, D. W.; Kuzma, N. N.; Dmochowski, I. J. *J. Am. Chem. Soc.* **2009**, *131*, 563-569.
- (55) Schlundt, A.; Kilian, W.; Beyermann, M.; Sticht, J.; Guenther, S.; Höpner, S.; Falk, K.; Roetzschke, O.; Mitschang, L.; Freund, C. *Angew. Chem. Int. Edit.* **2009**, *121*, 4206-4209.
- (56) Wei, Q.; Seward, G. K.; Hill, P. A.; Patton, B.; Dimitrov, I. E.; Kuzma, N. N.; Dmochowski, I. J. *J. Am. Chem. Soc.* **2006**, *128*, 13274-13283.
- (57) Boutina, C.; Desvauxa, H.; Carrierea, M.; Leteurtreb, F.; Jaminb, N.; Boulardb, Y.; Berthault, P. *NMR Biomed.* **2011**, *24*, 1-7.
- (58) Seward, G. K.; Bai, Y.; Khan, N. S.; Dmochowski, I. J. *Chem. Sci.* **2011**, doi: 10.1039/c1031sc00041a.
- (59) Seward, G. K.; Wei, Q.; Dmochowski, I. J. *Bioconjug. Chem.* **2008**, *19*, 2129-2135.
- (60) Nussbaum, E.; Hursh, J. B. *J. Phys. Chem.* **1958**, *62*, 81-84.

(61) Spence, M. M.; Ruiz, E. J.; Rubin, S. M.; Lowery, T. J.; Winssinger, N.; Schultz, P. G.; Wemmer, D. E.; Pines, A. *J. Am. Chem. Soc.* **2004**, *126*, 15287-15294.

(62) Certain commercial equipment, instruments, or materials are identified in this paper to foster understanding. Such identification does not imply recommendation by the National Institute of Standards and Technology, nor does it imply that the materials or equipment identified are necessarily the best available for the purpose.

**CHAPTER 3: TARGETING THE FOLATE RECEPTOR  
WITH A FOLATE-CONJUGATED CRYPTOPHANE FOR  
CANCER DETECTION**



## ABSTRACT

Folate-conjugated cryptophane enables the targeting and delivery of cryptophane to cells overexpressing folate receptors, which are overexpressed in many human cancers. The cryptophane biosensor was synthesized in 19 nonlinear steps, which included functionalization with a folate recognition moiety, solubilizing peptide group and Cy3 dye. Cellular internalization was monitored by confocal laser scanning microscopy (CLSM). A competitive blocking study confirmed cryptophane endocytosis through a folate receptor-mediated pathway. Flow cytometry revealed 10-fold higher cellular internalization in cancer cells overexpressing folate receptors (KB cells) compared to cells underexpressing folate receptors (HT-1080 cells). The biosensor was determined to be relatively non-toxic in low folate receptor expressing HT-1080 cells by MTT assay at the micromolar cryptophane concentrations typically used for hyperpolarized  $^{129}\text{Xe}$  NMR biosensing experiments. In folate overexpressing KB cells, the viability ranged from 100% to 80% from 0  $\mu\text{M}$  to 10  $\mu\text{M}$  and dropped to 50% at 38  $\mu\text{M}$ .  $^{129}\text{Xe}$  NMR studies were performed and the resulting peak at 65 ppm confirmed xenon binding to the folate-conjugated cryptophane. Studies are currently underway to detect the binding of the folate-conjugated biosensor to monomeric folate binding protein at nanomolar or picomolar concentrations using Hyper-CEST NMR techniques.

## INTRODUCTION

As mentioned in Chapter 1, magnetic resonance imaging (MRI) is a noninvasive medical imaging technique used to scan deep tissues with high spatial resolution. Although it can provide high contrast images of different tissues such as organs and bones, it is limited by low sensitivity due to the high background-to-signal ratio. In order to increase signal, especially when imaging vascular tissues or analyzing brain perfusion, gadolinium- or iron-oxide-based contrast agents are commonly used. However, there are limitations to these imaging agents. Early and accurate diagnoses of disease states increasingly rely upon information gleaned from molecular imaging of protein biomarkers or metabolic processes. There are now many examples using PET and SPECT imaging agents with readily detected radioactive nuclei.<sup>1</sup> By comparison, current MRI contrast agents have limited ability to detect proteins of low abundance in cells.<sup>2,3,4</sup> The goal of making “smart” MRI contrast agents that produce readily measured signal in response to environmental cues has led to investigation of alternate nuclei, including hyperpolarized  $^{129}\text{Xe}$ ,  $^{13}\text{C}$ ,  $^{38}\text{Kr}$  and  $^3\text{He}$ .<sup>5-8</sup>

$^{129}\text{Xe}$  is an attractive option for imaging because of its nontoxicity, chemical-shift sensitivity to its molecular environment and hyperpolarizability. Additionally, water-soluble tris-(triazole ethylamine) and tris-carboxylate derivatives of cryptophane-A have been developed that bind xenon with large association constants,  $K_A = 17,000\text{-}42,000 \text{ M}^{-1}$  in buffer at 293 K. Additionally, one cryptophane was shown to bind Xe in human plasma with appreciable affinity,  $K_A = 22,000 \text{ M}^{-1}$  at 310K.<sup>9</sup> This has led to the synthesis

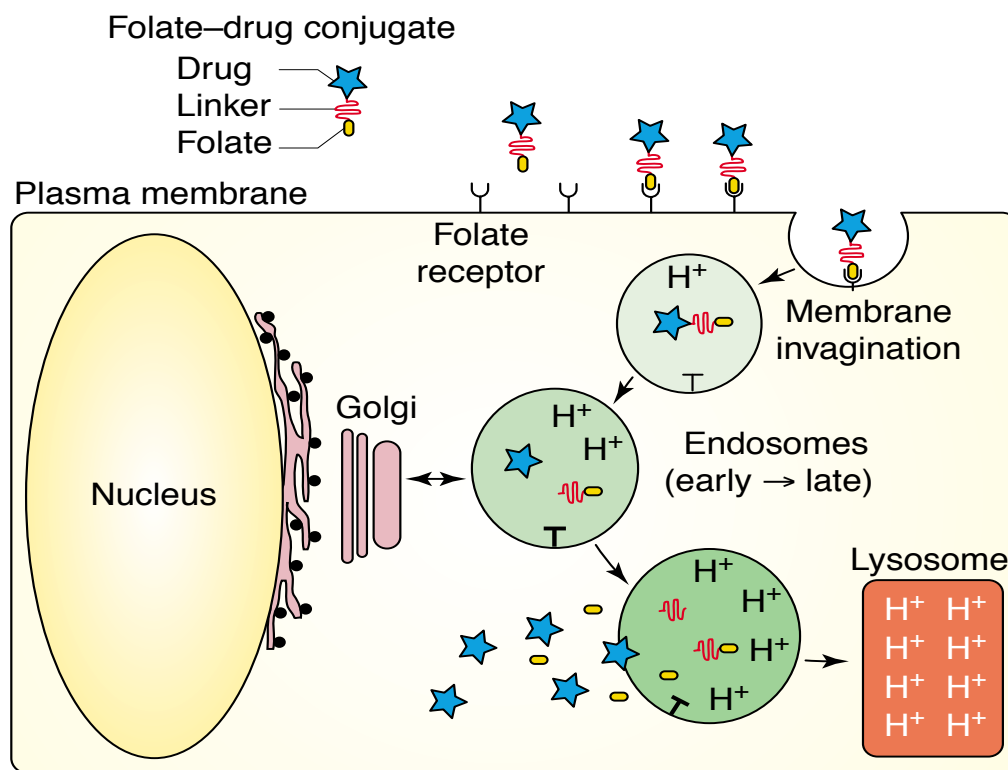


of cryptophane-based biosensors that are conjugated to various ligands via a hydroxyl or propargyl group. As mentioned in Chapter 1, these include a biotin-modified cryptophane biosensor that can detect streptavidin *in vitro*,<sup>10-13</sup> an enzyme-responsive <sup>129</sup>Xe NMR biosensor for the detection of matrix metalloproteinase-7 (MMP-7),<sup>14</sup> and a series of benzenesulfonamide-functionalized cryptophane-A derivatives that exhibited the largest isozyme-specific chemical shift changes (3.0-7.5 ppm), upon binding carbonic anhydrases I and II.<sup>15</sup> Another recent example included the synthesis of a peptide-labeled <sup>129</sup>Xe biosensor by Schlundt et al. that produced a 1 ppm downfield shift upon binding to a major histocompatibility complex (MHC) class II protein.<sup>16</sup> The delivery of cryptophanes using cell penetrating peptides or by targeting  $\alpha_v\beta_3$  integrin receptors into cancer and normal cells has also been demonstrated.<sup>17,18</sup> The cryptophanes were minimally cytotoxic and intracellular concentrations of approximately 100  $\mu$ M were achieved, which should be sufficient for *in vivo* hyperpolarized <sup>129</sup>Xe MRI studies.<sup>17,18</sup>

In cells, there are three types of transporters that are responsible for the uptake of folate. These include RFC (reduced folate carrier),<sup>19</sup> proton-coupled high affinity folate transporter,<sup>20</sup> and folate receptor (FR, also known as high affinity folate binding protein).<sup>21</sup> Folate receptors are cell surface glycosylphosphatidylinositol (GPI)-linked membrane glycoproteins with molecular weights ranging from 38,000 to 45,000 Da.<sup>22</sup> It has a high binding affinity ( $K_D \approx 0.1-1$  nM with a 1:1 stoichiometry) for folic acid and 5-methyltetrahydrofolate.<sup>22</sup> FR is mainly located on the luminal surface of polarized epithelial cells. In humans, FR has 4 different types of isoforms:  $\alpha$ ,  $\beta$ ,  $\gamma$ , and  $\delta$ , where isoforms  $\alpha$  and  $\beta$  are membrane bound.<sup>21</sup> Among them, FR $\alpha$  is overexpressed in non-

mucinous adenocarcinomas of the ovary, cervix, uterus, ependymal brain tumors, whereas normal cell lines have very low FR expression.<sup>23-26</sup> FR expression in normal tissues mostly is found in polarized epithelial cells in the proximal kidney tubules, choroid plexus, etc.<sup>25,27-31</sup> FR $\alpha$  is overexpressed in 90% of ovarian carcinomas and higher levels of expression are generally associated with poorly differentiated and aggressive tumors.<sup>31,32</sup> It is believed that FR $\alpha$  is overexpressed because the fast growth rate of cancer cells requires more folic acid.<sup>21</sup> Folic acid is an essential component of the one-carbon transfer reactions which are crucial for one-carbon, nucleic acid, and amino acid metabolism, as well as the synthesis and proliferation of cells.<sup>33</sup> For instance, in ovarian cancer cells it was possible to limit cancer cell growth by using a FA-antibody to decrease FR $\alpha$  expression.<sup>34</sup>

Although FR $\alpha$  is expressed in normal tissues, their distribution on the luminal surface of epithelial cells ensures that they are not directly accessible through the blood stream.<sup>21</sup> Therefore, it is expected that for *in vivo* studies, folate-conjugated agents will be selectively targeted to tumors overexpressing FR $\alpha$ . Previous studies have shown that FR $\alpha$  can transport folic acid as well as folic acid conjugates (e.g., imaging agents, proteins, nanoparticles) via receptor-mediated endocytosis (Figure 3.1).<sup>23</sup> Therefore, FR $\alpha$  is a potential cancer biomarker that would indicate the presence of cancerous abnormalities if detected by the folate-conjugated <sup>129</sup>Xe biosensor. Additionally, folate remains essentially unaltered after endocytosis and is stable for several hours after the uptake by cancer cells.<sup>35</sup> All of these characteristics make FR $\alpha$  an attractive marker for the <sup>129</sup>Xe biosensor to detect.



*Drug Discovery Today*

**Figure 3.1.** Scheme of the FR $\alpha$ -mediated endocytosis of a folic acid drug conjugate. Folate conjugates bind FR $\alpha$  with high affinity and are internalized into endosomes. As proton pumps acidify the lumen of late-stage endosomes, the folate conjugates are released into the cell cytosol.<sup>36</sup>

In this study, a folate-conjugated water-soluble cryptophane biosensor (Figure 3.2) was synthesized, which was envisioned to target cancer cells that are known to overexpress FR $\alpha$ . The biosensor was composed of four functional components. The first was the monopropargylated cryptophane-A derivative, which is known to bind xenon in organic and aqueous solvents.<sup>14</sup> The second part was the solubilizing moiety, which consists of a polycationic peptide (RKR) where the positive charges are deliberately broken up by a polyethyleneglycol unit (PEG). This is because polycation sequences of five or greater peptide units are known to induce non-specific uptake of peptide conjugates into cells.<sup>37</sup> The third component consisted of the Cy3 fluorescent dye, which is conjugated through a maleimide linkage to the cysteine residue on the peptide sequence. The dye was included to assist in the visualization of the biosensor in both FR+ and FR- cells by confocal laser scanning microscopy and flow cytometry. Lastly, a folate recognition moiety that has a high affinity for FR $\alpha$  was conjugated via an orthogonally protected lysine on the peptide sequence. The last step in the synthesis involved the conjugation of the N-terminal azide of the peptide-folate conjugate to monopropargylated cryptophane by a Cu(I)-catalyzed [3+2] Huisgen cycloaddition.<sup>38-40</sup> Selective cell uptake and cytotoxicity studies were performed using confocal laser scanning microscopy, flow cytometry and MTT assays for KB and HT-1080 cancer cells.

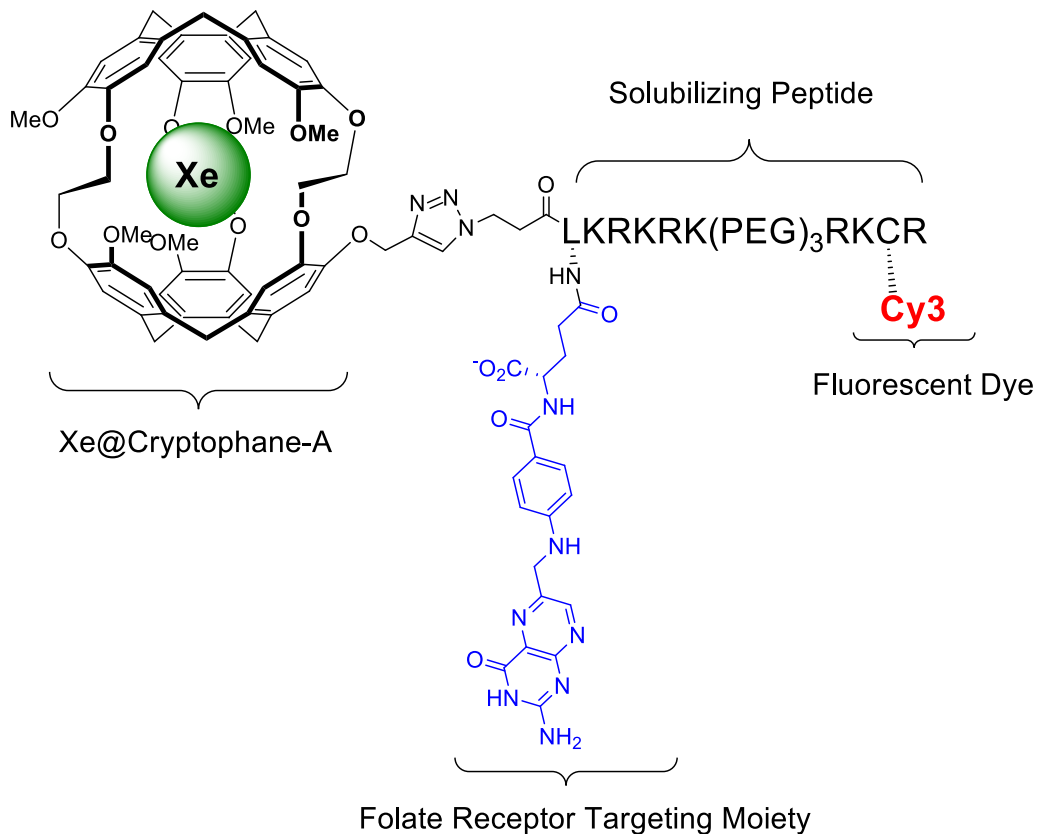


**Figure 3.2.** Structure of the FR $\alpha$ -targeting  $^{129}\text{Xe}$  NMR biosensor, with a xenon-binding cryptophane, solubilizing peptide, FR $\alpha$  targeting moiety (blue) and fluorescent Cy3 dye for *in vitro* studies (red).

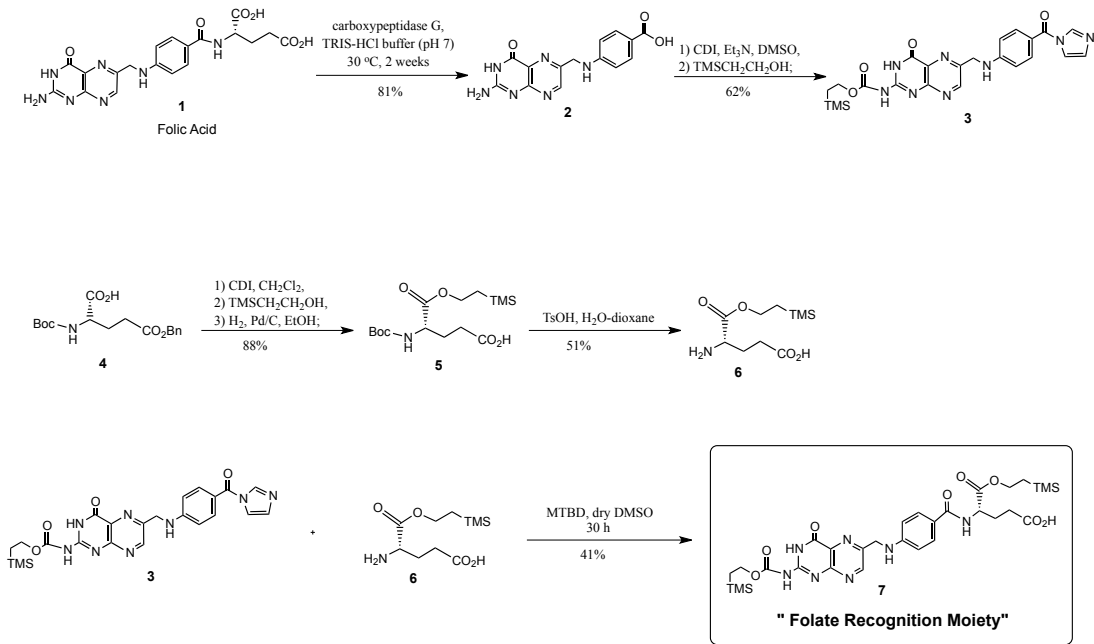
## RESULTS AND DISCUSSION

### *Synthesis and characterization of folate-cryptophane conjugate*

#### **Synthesis of $\alpha$ -[2-(Trimethylsilyl)ethoxy]-2-N-[2-(trimethylsilyl)-**

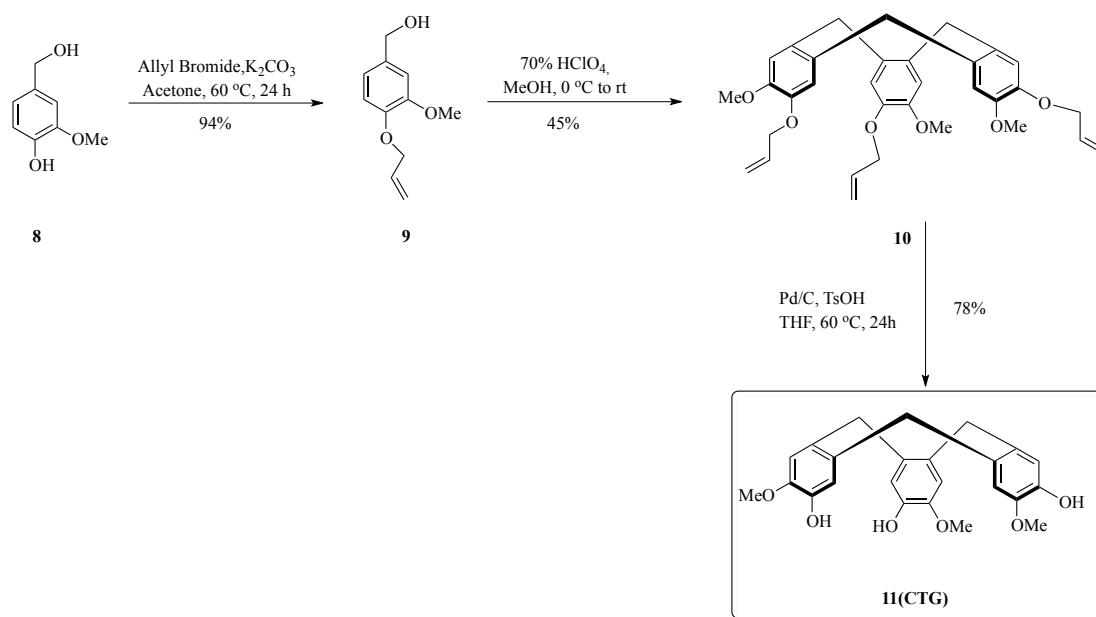
**ethoxycarbonyl]folic acid (“folate recognition moiety”).** The conjugation of folic acid to the peptide sequence with DCC would lead to the synthesis of a mixture of  $\alpha$ -folate and  $\gamma$ -folate conjugates. Because only the  $\gamma$ -conjugate is recognized by the FR $\alpha$  receptor, a selectively protected folic acid derivative **7** was synthesized in 5 nonlinear steps in 13% overall yield (Scheme 3.1).<sup>41</sup> The folate recognition moiety was prepared from two intermediates: the 2-*N*-teoc-pteronic acid derivative, where the teoc group is 2-(trimethylsilyl)ethoxycarbonyl, and the  $\alpha$ -carboxyl-protected glutamic acid.<sup>41</sup> Folic acid (**1**) undergoes enzymatic hydrolysis with carboxypeptidase-G to give pteronic acid (**2**). Carbonyldiimidazole (CDI) and 2-trimethylsilylethanol in dry dimethyl sulfoxide (DMSO) were added to the crude pteronic acid to produce the protected pteronic acid, 1-(2-*N*-teoc-pteroyl)imidazole (**3**) in 62% yield. In order to synthesize the second intermediate, the  $\alpha$ -carboxylate group in *N*-Boc-L-Glu (OBn)-OH (**4**) was protected by treating it with CDI and 2-trimethylsilylethanol while the  $\gamma$ -carboxylate group was selectively deprotected using Pd-C to give **5** in 88% yield. The *N*-Boc group was also deprotected using TsOH to give  $\alpha$ -(2-TMS-ethyl) glutamate **6** in 51% yield. Finally, **3** was treated with 1.5 equiv. of **6** and *N*-methyl-1,5,9-triazabicyclo[4.4.0]-decene (MTBD) in dry DMSO to give the folate recognition moiety in 41% yield.

The monopropargylated derivative of cryptophane-A was also synthesized in 12 nonlinear steps in 3% overall yield (Scheme 3.2, 3.3 and 3.4).<sup>14</sup>

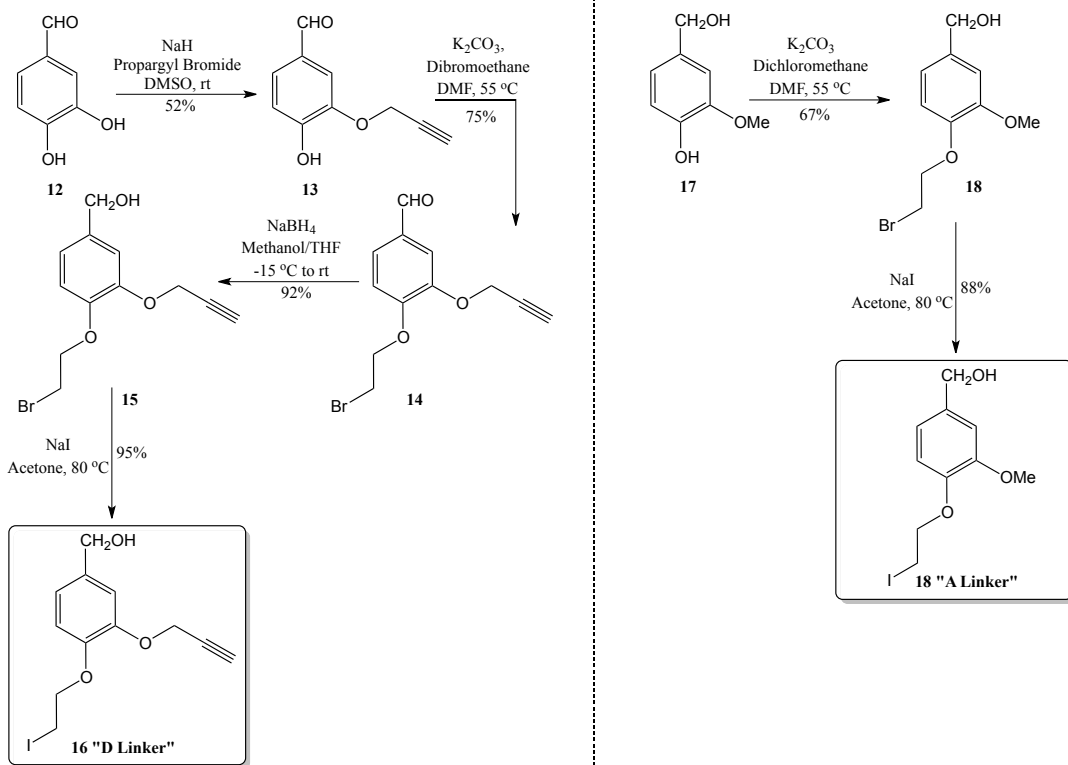


**Scheme 3.1.** 5-step synthesis of  $\alpha$ -[2-(trimethylsilyl)ethoxy]-2-*N*-[2-(trimethylsilyl)ethoxycarbonyl]folic acid. Figure adapted from Nomura et al.<sup>41</sup>

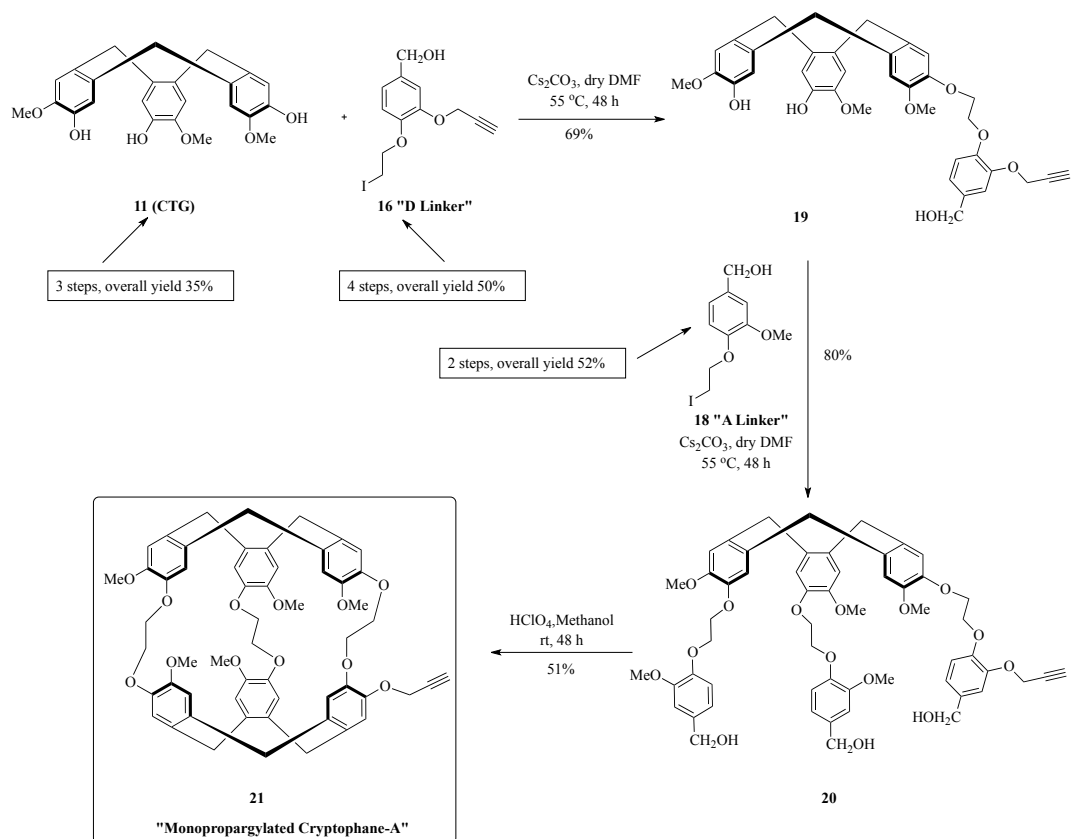




**Scheme 3.2.** 3-step synthesis of a cyclotriguaiacylene (CTG) unit. Figure adapted from Wei et al.<sup>14</sup>

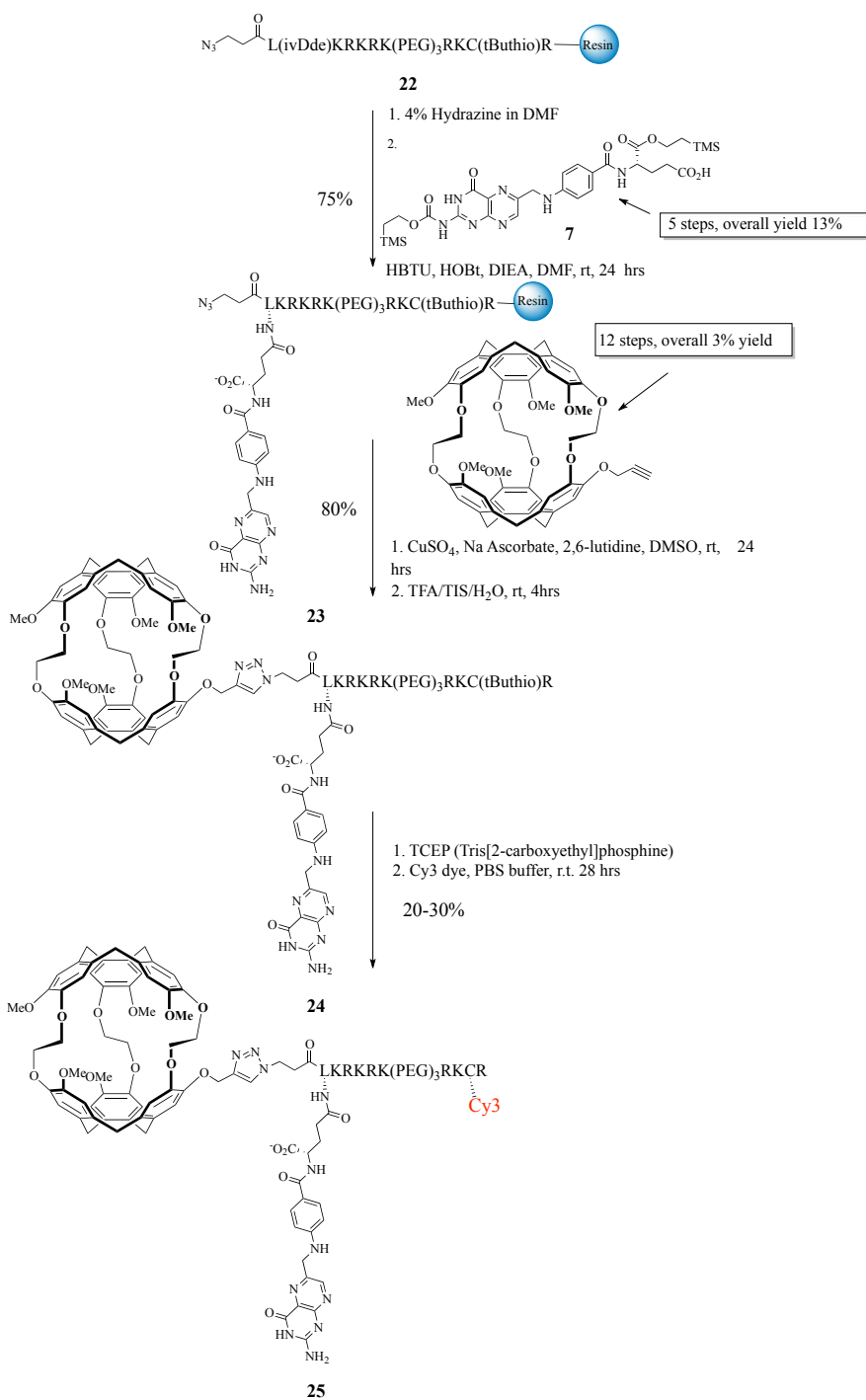


**Scheme 3.3.** Synthesis of [3-propargyloxy-4-(2-iodoethoxy)phenyl]methanol (D Linker) and [4-(2-iodoethoxy)-3-methoxyphenyl]methanol (A Linker). Figure adapted from Wei et al.<sup>14</sup>



**Scheme 3.4.** Synthesis of monopropargylated derivative of cryptophane-A. Figure adapted from Wei et al.<sup>14</sup>

The azidopeptide **22** was synthesized by standard solid-phase synthesis using Fmoc-substituted reagents.<sup>42</sup> 3-Azido propionic acid was prepared according to literature procedures and incorporated as the N-terminal residue.<sup>43</sup> The peptide **22** was synthesized in 85% yield and consisted of three polyethylene glycol units and lysine-arginine units to help solubilize the biosensor in water. The cysteine in the peptide chain was included to fluorescently label the biosensor for *in vitro* studies. The azidopeptide was orthogonally deprotected using 4% hydrazine in water and readily coupled to the  $\gamma$ -folate conjugate **7** using coupling agents in dry DMF to yield **23** in 75% yield. In order to monitor the reaction, a portion of the reaction mixture was cleaved from the resin and purified by reverse-phase HPLC (see Experimental procedures). Once the formation of the product was confirmed, **23** (on solid support) was coupled to monopropargylated cryptophane-A to give **24** by Cu(I)-catalyzed [3+2] cycloaddition. Although the yield for **24** was initially low (~20% yield), it was significantly improved to approximately 80% by using a large excess of sodium ascorbate (40 equiv.) to ensure that copper remained reduced as Cu(I) to catalyze the reaction. The product was purified by reverse-phase HPLC (see Experimental procedures) and was determined to be readily soluble in water. To fluorescently label the conjugate **24**, the cysteine was deprotected using TCEP and coupled with the maleimide functionalized Cy3 dye (excitation 550 nm and emission 575 nm). Cy3 labeling efficiencies were determined from the ratio of dye absorbance at 550 nm to the cryptophane absorbance at 280 nm. **25** was purified by reverse-phase HPLC (see Experimental procedures) and the yields at 20-30% were lower than expected. The removal of excess TCEP using a gel filtration column did not assist in increasing the yields.



**Scheme 3.5.** Synthesis of unlabeled and Cy3-labeled biosensor **24** and **25**, respectively, where a last step involved the Cu(I)-catalyzed [3+2] cycloaddition of monopropargyl-cryptophane to the folate-conjugated azidopeptide on solid support.

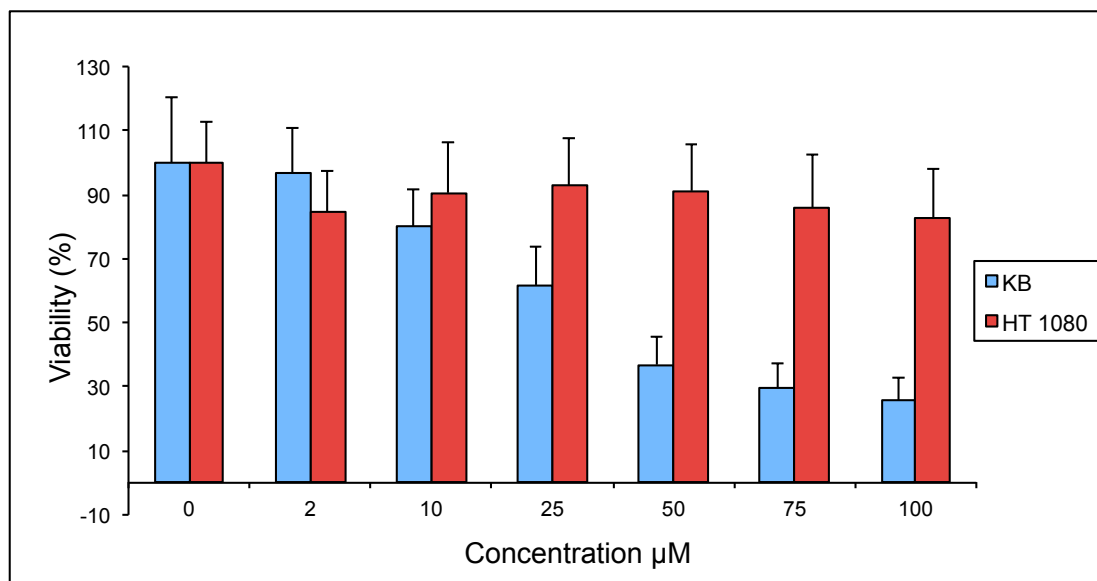


**Figure 3.3.** Cytotoxicity assays for folate-conjugated cryptophane biosensor in KB (blue), and HT-1080 cells (red). %Viability was determined via MTT assay after 24 h incubation with increasing concentrations of **24**, as compared to untreated cells.

In order to perform cell cytotoxicity and uptake studies, two cell lines were selected. KB cells (a cell line derived from human carcinoma of the nasopharynx) were selected because they are known to highly overexpress FR $\alpha$  while HT-1080 cells (a fibrosarcoma cell line) are known to underexpress FR $\alpha$  relative to KB cells. The cytotoxicity of **24** was evaluated by adding increasing concentrations (0 to 100  $\mu$ M) of the folate-cryptophane conjugate **24** to KB (FR+) and HT-1080 (FR-) cells, as shown in Figure 3.3. In KB cells, the viability (scaled to 100% at 0  $\mu$ M) decreased from 80% at 10  $\mu$ M to 50% at 38  $\mu$ M. Maximum toxicity in KB cells (23% viability) was found when the cells were incubated with the highest concentration of **24** (100  $\mu$ M). Cell viabilities determined when 0-10  $\mu$ M of the biosensor was added to KB cells were comparable to those seen with fluorescent contrast agents such as folate-substituted poly(*p*-phenyleneethynylene).<sup>44</sup> At concentrations  $\sim$ 2  $\mu$ M, **25** exhibited sufficient fluorescence intensity to be detected inside the intracellular domain both via confocal microscopy and flow cytometry and was also minimally cytotoxic. The viability of HT-1080 cells ranged from 100% at 0  $\mu$ M to 82% at 100  $\mu$ M of **24**. The higher viability of HT-1080 cells indicates minimal toxicity in human cell lines that do not overexpress FR $\alpha$ . In general, **24** was more cytotoxic to cancer cells that are FR+ than those that are FR-. This is likely due to the higher levels of FR $\alpha$  that are expressed on KB cells versus HT-1080 cells, which in turn causes increased intracellular accumulation of biosensor **24**. Similar trends were seen in a previous study where a cyclic RGD peptide-conjugated cryptophane was determined to be more toxic in cell lines overexpressing the targeted  $\alpha_v\beta_3$  integrin receptors (60% toxicity in ASPC-1 cells versus 30% toxicity in HFL-1 cells) after 24 h incubation at 100  $\mu$ M concentration.

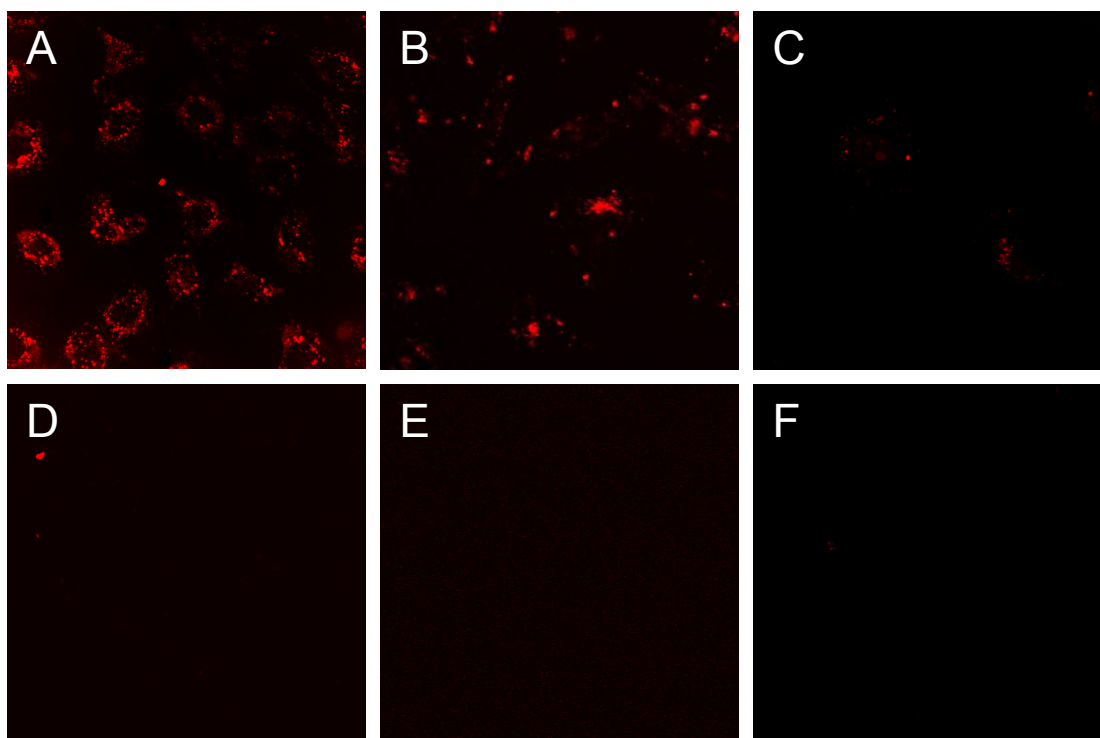


**Figure 3.4.** Uptake of 4  $\mu$ M Cy3-labeled **25** targeting FR $\alpha$  in KB (a), HeLa (b), and HT-1080 (c) cells after 4 h incubation at 37 °C in folic acid depleted media; (d, e, f) Uptake of **25** was successfully blocked in the KB, HeLa and HT-1080 cell lines, respectively, when they were incubated in media containing folic acid.



In order to determine whether **25** could be selectively delivered to FR<sup>+</sup> cells, confocal laser scanning microscopy (CLSM) was performed as shown in Figure 3.4. After 4 h incubation with Cy3-labeled **25**, fluorescence was seen evenly distributed in the perinuclear region of KB cells as expected for receptor-mediated endocytosis (Figure 3.4a). This is desirable as nuclear internalization of imaging agents can cause potential mutagenic effects on healthy cells. Cell uptake of Cy3-labeled **25** in HeLa cells was also confirmed by CLSM after 4 h incubation (Figure 3.4b). The fluorescence intensity was lower in HeLa cells which was expected due to the highest overexpression of FR $\alpha$  in KB cells, followed by HeLa and HT-1080 cells. Uptake of **25** was even lower in HT-1080 (FR<sup>-</sup>) cells, thereby indicating that biosensor **25** was able to discriminate between FR<sup>+</sup> and FR<sup>-</sup> cells (Figure 3.4c). To analyze whether the uptake of **25** was facilitated by folate receptor-mediated endocytosis, **25** was co-incubated with folic acid rich medium in both KB, HeLa, and HT-1080 cells. Because folic acid is known to have a very high affinity for FR $\alpha$ , it was expected to outcompete **25**, thereby blocking uptake. The reduction in fluorescence in Figures 4d-4f indicates that the folic acid did in fact inhibit uptake of **25** and **25** was specifically recognized by the FR receptor. Indeed, the folate recognition moiety subunit was critical for cellular uptake of the biosensor.

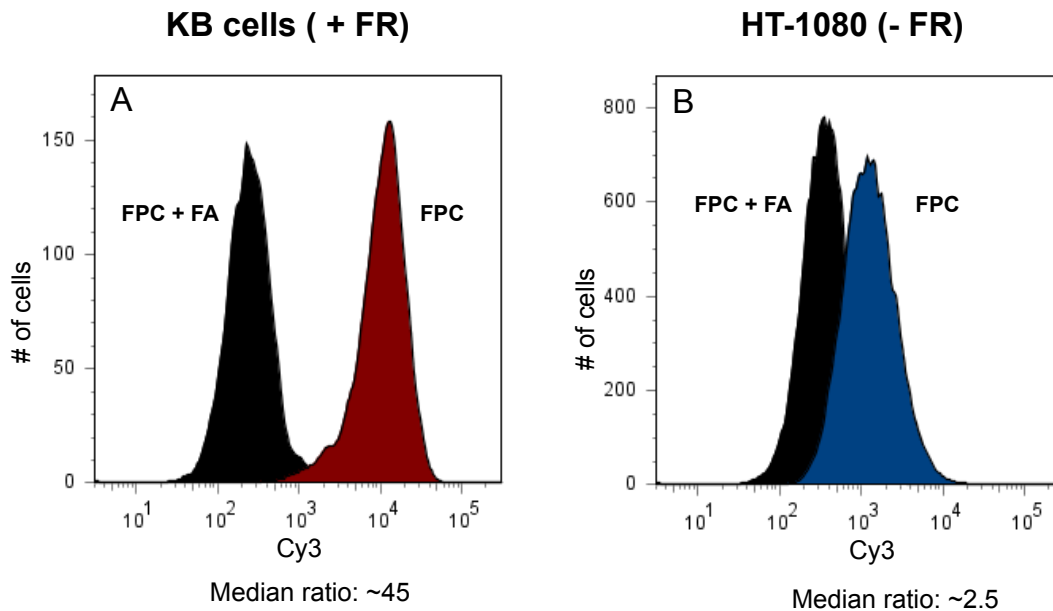


**Figure 3.5.** Monitoring the accumulation of 4  $\mu\text{M}$  Cy3-labeled **25** in (a) HT-1080 (FR-, blue) and (b) KB (FR+, red) cells using flow cytometry. Inhibition of uptake with free folic acid in the medium was indicated in (a) HT-1080 cells (black) and (b) KB cells (black).

In an effort to quantify the selective cellular internalization of **25** in KB and HT-1080 cells, flow cytometry was performed. After 4 h incubation in both KB and HT-1080 cells, there was a dramatic increase in cell-associated fluorescence. When biosensor **25** was co-incubated with excess folic acid, the increase in median fluorescence intensity was much lower than when folic acid was absent. This was in agreement with the results from the CLSM studies, where uptake was significantly lowered when excess folic acid was present. In the absence of folic acid, the median cell-associated fluorescence intensity was approximately 45-fold higher in KB cells and 2.5-fold higher in HT-1080 cells. Therefore, it was determined that the median fluorescence intensity in KB cells was approximately 10-fold higher than in HT-1080 cells. This was expected because KB cells are known to overexpress FR $\alpha$  compared to HT-1080 cells,<sup>45,46</sup> [ENREF\\_42](#) and shows that biosensor **25** was able to selectively target cancer cells overexpressing the intended receptors.

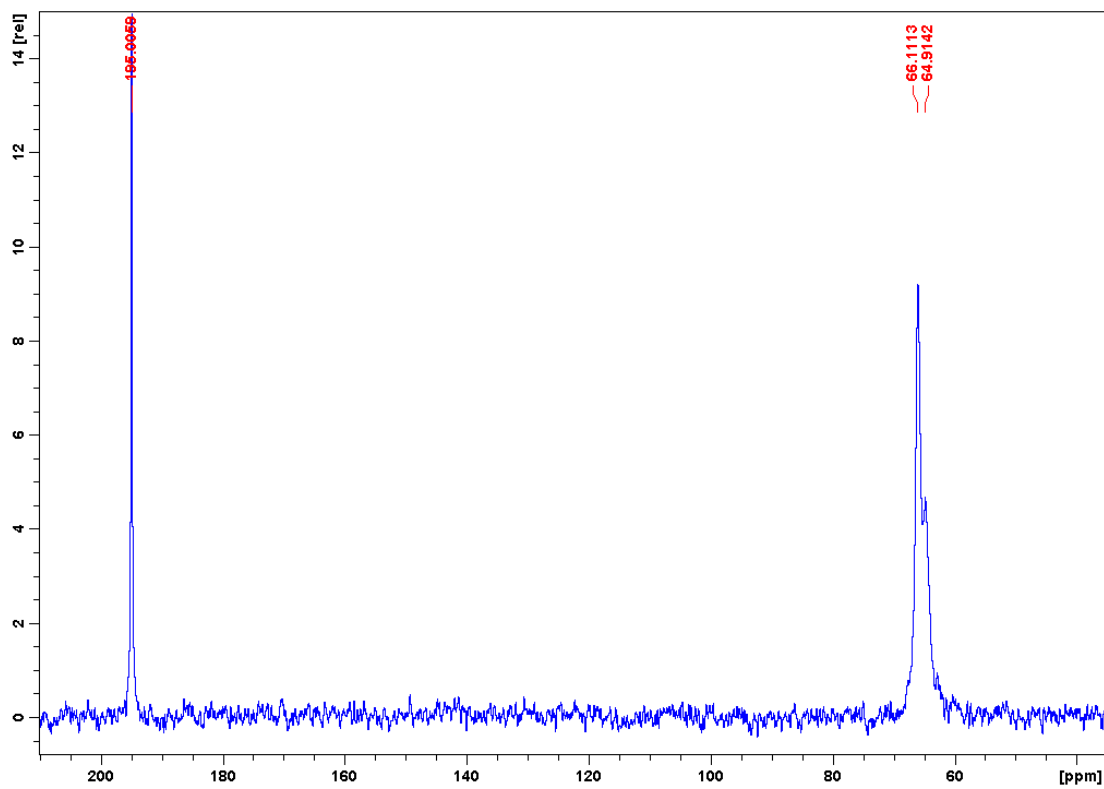


**Figure 3.6.** Hyperpolarized  $^{129}\text{Xe}$  NMR spectrum of 60  $\mu\text{M}$  **24** in acetate buffer at pH 5.0 (40 scans; S/N  $\approx$ 30:1 at 50 Hz line broadening)

Hyperpolarized  $^{129}\text{Xe}$  NMR spectrum of **24** was performed at 60  $\mu\text{M}$  in both PBS buffer at pH 7.5 and acetate buffer at pH 5.0 using a 10 mm probe and a BURP pulse. Figure 3.6 shows  $^{129}\text{Xe}$  NMR chemical shifts of 64.91 and 66.11 ppm due to the presence of the two diastereomers for biosensor **24**. This was due to the chirality of the three components, folate, peptide and cryptophane-A (LLL and LLR). Cryptophane-A is a chiral molecule and the racemic mixture of enantiomers encapsulating xenon has been reported to give rise to a single NMR resonance.<sup>47</sup> However, upon conjugation of chiral moieties to this racemic mixture of cryptophanes, diastereomers are formed. Previous examples of xenon biosensors that contain multiple diastereomers include the biotin-conjugated cryptophane developed by Spence et al.<sup>10</sup> The biosensor consisted of four diastereomers due to the chiral cryptophane-A, L-amino acids, and maleimide center formed when the biotin was conjugated to the rest of the biosensor (RLR, RLL, LLR, LLL).<sup>10</sup> This resulted in 4 distinct peaks in the  $^{129}\text{Xe}$  NMR spectrum. Similarly, the enzyme-responsive MMP-7 biosensor developed in our lab also indicated the presence of two diastereomers that were separated by 0.6 ppm. This was due to the chirality of the two components, peptide and cryptophane-A (RL and LL).<sup>14,47,48</sup> Carbonic anhydrase targeting cryptophane biosensors also developed in our lab are hypothesized to form diastereomers when the two enantiomers that make up the biosensor interact with the chiral protein surface.<sup>15,49</sup> Since for multiplexing purposes it would be preferable to only have single NMR resonances for biosensors targeting different biomarkers, the synthesis of enantiomerically pure cryptophanes is currently underway in our lab and will be discussed in further detail in Chapter 5.

$^{129}\text{Xe}$  NMR experiments were also performed with **24** and folate binding protein (FBP) to determine the change in the chemical shift upon binding to the protein. FBP is an expensive membrane-bound protein and is known to aggregate at low micromolar concentrations.<sup>50</sup> Specifically, the MW of the monomeric protein is 29,000 Da and increases to approximately 300,000 Da during aggregation.<sup>50</sup> Although it would have been desirable to perform the  $^{129}\text{Xe}$  NMR experiments at nanomolar concentrations, due to the sensitivity limitations of our system, micromolar concentrations had to be used. To minimize aggregation, all the NMR experiments were carried out at pH 5.0 in acetate buffer as it is known that the protein experiences lower aggregation in this buffer than at pH 7.0.<sup>50,51</sup> In the first trial, 30  $\mu\text{M}$  FBP was mixed with 60  $\mu\text{M}$  of the biosensor. Although the spectrum indicated the presence of the cryptophane peak, there was no new peak indicating that the biosensor was bound to FBP. In a second trial, the sample was allowed to equilibrate for 30 min and vortexed to ensure good mixing. The results were similar to those of trial 1 where no distinct bound signal was observed. In a third trial, a lower concentration of biosensor (30  $\mu\text{M}$ ) was mixed in an NMR tube with 30  $\mu\text{M}$  FBP but again no new bound peak was observed, only dilution of the free cryptophane peak. Additionally, 10% glycerol was added to the buffer for all  $^{129}\text{Xe}$  NMR experiments to prevent foaming and stabilize the protein. The lack of a cryptophane bound peak could be due to several reasons: a) protein aggregation that prevents folate binding,<sup>50</sup> b) when cryptophane associates with FBP, Xe is unable to gain access, and c) the cryptophane itself may preclude the folate recognition moiety from binding to the protein. All these reasons would lead to a loss in the  $^{129}\text{Xe}$  bound signal. Our lab's improving capabilities in hyperpolarized  $^{129}\text{Xe}$  NMR spectroscopy will soon make it possible to perform these

measurements in live cells, which will help to troubleshoot the potential problems outlined above.

## CONCLUSION

In summary, a novel water-soluble folate-conjugated cryptophane biosensor was synthesized and characterized. The folate moiety had been selectively protected to ensure that only the  $\alpha$ -carboxylate group was available to bind to FR $\alpha$ . Confocal imaging with KB (FR+) and HT-1080 (FR-) cells indicated the selective uptake of the biosensor via folate receptor-mediated endocytosis into cells overexpressing FR $\alpha$ . Flow cytometry analysis indicated that uptake was 45-fold higher in KB cells and 2.5-fold higher in HT-1080 cells than when competing excess folate was in solution. Also, the median fluorescence intensity was approximately 10-fold higher in KB cells than in HT-1080 cells, which motivates the use of this folate-conjugated cryptophane for *in vivo* biosensing in cells overexpressing FR $\alpha$ . Cytotoxicity assays indicated that in the relevant ranges required for confocal and flow cytometry analysis (0-10  $\mu$ M), the viability was greater than 80% in both cells lines.  $^{129}\text{Xe}$  NMR spectroscopy as well cellular spectroscopy studies that can be performed using low concentration of proteins and cells are currently underway and will be discussed in Chapter 5.



## EXPERIMENTAL PROCEDURES

### Reagents

*Sigma-Aldrich:* Dimethyl sulfoxide (DMSO), dimethylformamide (DMF), folate binding protein (FBP), folic acid, methanol, triisopropylsilane (TIS), 2,6-lutidine, piperidine, 3-(4,5-dimethyl-2-thiazolyl)-2,5-diphenyl-2H-tetrazolium bromide (MTT);

*Fisher:* sodium chloride, copper(II) sulfate, trifluoroacetic acid (TFA), diethyl ether (Et<sub>2</sub>O), glutathione

*Alfa Aesar:* Cesium carbonate, L-glutathione

*Novabiochem:* 2-(1H-benzotriazole-1-yl) 1,1,3,3-tetramethyluronium hexafluorophosphate (HBTU), N-Hydroxybenzotriazole (HOBt), N-methylmorpholine (0.4 M), Fmoc-15-amino-4,7,10,13 tetraoxapentadecanoic acid ((PEG)<sub>3</sub>), Rink amide resin, Fmoc-protected amino acids including Fmoc-L-Lys(ivDde)-OH, Fmoc-L-Lys(Boc)-OH, Fmoc-L-Arg(Pbf)-OH, Fmoc-Cys(tButhio)-OH, N-methylmorpholine (0.4 M)

*GE Healthcare:* Cy3 monoreactive dye pack

*Calbiochem:* Tris(2-carboxyethyl)phosphine hydrochloride (TCEP-HCl)

*Invitrogen:* RPMI-1640 medium, folate-depleted RPMI-1640 medium, Dulbecco's phosphate buffered saline (DPBS)

For biological assays, all solutions were prepared using deionized water purified by Mar Cor Premium grade Mixed Bed Service Deionization.

**General Methods.** All organic reactions were carried out under nitrogen atmosphere.  $^1\text{H}$  NMR (500.14 MHz) and  $^{13}\text{C}$  NMR (125.77 MHz) spectra were obtained on a Bruker AMX 500 spectrometer at the University of Pennsylvania NMR facility. Electrospray ionization (ESI) mass spectrometry was performed in low-resolution mode on a Micromass LC Platform and in high resolution mode on a Micromass Autospec while *matrix-assisted laser desorption/ionization spectrometry* (MALDI) was performed on a Bruker Daltonic Ultraflex III MALDI-TOF-TOF at the Mass Spectrometry Center in the Chemistry Department at the University of Pennsylvania. Column chromatography was performed using 60 Å porosity, 40-75  $\mu\text{m}$  particle size silica gel from Sorbent Technologies. Thin layer chromatography (TLC) was performed using silica gel plates with UV light at 254 nm for detection. HPLC analysis was performed on an Agilent 1100 system equipped with a quaternary pump and diode array detector using a Varian Microsorb-MV 300-5 C8 column (4.6  $\times$  250 mm, 5  $\mu\text{m}$ ). The gradient eluent was composed of two solvents: 0.1% aqueous TFA (solvent A) and a 0.1% solution of TFA in  $\text{CH}_3\text{CN}$  (solvent B). UV-visible spectra were measured using a diode-array Agilent 89090A spectrophotometer.

**Synthesis of 22.** Peptide **22** (Scheme 3.5) was prepared by solid-phase synthesis using standard Fmoc amino acid protection chemistry on Rink Amide resin (0.1 mmol scale). Couplings of Fmoc-protected amino acids to the resin were carried out with HBTU and N-methylmorpholine to generate the activated ester. The resin was swelled in DMF (10 min) prior to synthesis. Amino acids were then added sequentially until 3-azidopropionic acid was attached at the N-terminus as the final step. All residues were coupled onto resin

by the following procedure: removal of Fmoc group (20% piperidine solution in DMF, 2 × 5 min), wash (DMF, 6 × 30 s), activation (amino acid/HBTU/N-methylmorpholine, 1 × 30 s) coupling (amino acid/HBTU/N-methylmorpholine, 1 × 60 min), rinse (DMF, 3 × 30 s). The peptide was swelled in DMF for 10 min and the orthogonal lysine was deprotected by washing the resin five times with 4% hydrazine in DMF. The resin was dried and the peptide was cleaved using a mixture of TFA, TIS, and water (90/5/5) at rt for 4 h. The reaction mixture was filtered using a peptide vessel, concentrated and the peptide was precipitated by the addition of ether. The cleavage cocktail removed side chain protecting groups from all amino acids except for the *t*-butylthiol-protected cysteine. Semi-preparative HPLC purification of **22** was accomplished using the following gradient: time 0, A/B = 95/5; 0-45 min, linear increase to A/B = 50/50; 45-47 min, linear increase to A/B = 20/80; 47-56 min, linear change to A/B = 20/80; 56-57 min, linear increase to A/B = 95/5; 57-72 min, linear change to A/B = 95/5. MALDI MS calculated for peptide **22**, C<sub>72</sub>H<sub>141</sub>N<sub>31</sub>O<sub>16</sub>S<sub>2</sub> (M + H<sup>+</sup>) 1761.06; found 1760.91.

**Synthesis of 7.**  $\alpha$ -[2-(Trimethylsilyl)ethoxy]-2-*N*-[2-(trimethylsilyl)-ethoxycarbonyl]folic acid (**7**) was prepared according to literature procedure<sup>41</sup> and matched the reported physical constants and NMR spectra.

**Synthesis of 21.** Monopropargyl cryptophane was prepared according to literature procedure<sup>14</sup> and matched the reported physical constants and NMR spectra.

**Synthesis of 23.** Peptide **22** on the Sieber Amide resin (30 mg, maximum 0.0201 mmol azidopeptide, 1 equiv.) was allowed to swell in DMF (500  $\mu$ L) in a 10 mL peptide vessel for 10 min. The solution was filtered and 1 mL of 4% hydrazine in DMF was added to deprotect the ivDde group on the orthogonally protected lysine. This was repeated 5 times and the absorption of the filtrate at 290 nm was monitored using a UV-vis spectrum to ensure that the deprotection had taken place. The resin was then dried under vacuum. **22** was then added to a mixture of **7** (0.0402 mmol, 2 equiv.), HBTU (0.0603 mmol, 3 equiv.), HOBt (0.0905 mmol, 4.5 equiv.), DIEA (0.1206 mmol, 6 equiv.) in dry DMF. The reaction was stirred overnight at room temperature under nitrogen. Once the reaction was complete, the resin was carefully transferred to a fritted reaction vessel and washed sequentially with DMF, CH<sub>2</sub>Cl<sub>2</sub>, MeOH, 1:1 MeOH/CH<sub>2</sub>Cl<sub>2</sub> and MeOH before drying under vacuum. The peptide coupled to folate **23** was cleaved from the resin using a mixture of TFA, TIS, and water (90/5/5) at rt for 4 h. The reaction mixture was filtered using a peptide vessel, concentrated and the peptide was precipitated by the addition of ether. The cleavage cocktail removed side chain protecting groups from all amino acids except for the *t*-butylthiol-protected cysteine. Semi-preparative HPLC purification of **23** was accomplished using the following gradient: time 0, A/B = 95/5; 0-45 min, linear increase to A/B = 50/50; 45-47 min, linear increase to A/B = 20/80; 47-56 min, linear change to A/B = 20/80; 56-57 min, linear increase to A/B = 95/5; 57-72 min, linear change to A/B = 95/5. MALDI MS calculated for peptide-folate conjugate **23**, C<sub>91</sub>H<sub>158</sub>N<sub>38</sub>O<sub>21</sub>S<sub>2</sub> (M + H<sup>+</sup>) 2184.19; found 2184.05.

**Synthesis of 24.** Monopropargylated cryptophane (20 mg, 0.02186 mmol, 2 equiv.) in 900  $\mu$ L dry DMSO was added to **23** (18.2 mg on solid support, maximum 0.01093 mmol azido-peptide, 1 equiv.) and allowed to stir for 10 min. 2,6-lutidine (0.0219 mmol, 1 equiv.) was added and the reaction mixture was degassed. Sodium ascorbate (0.4372 mmol, 40 equiv.) was added dropwise, the mixture was degassed and finally an aqueous solution of copper(II) sulfate (0.0054 mmol, 0.5 equiv.) was added. The suspension was degassed with  $N_2$  and stirred at rt for 24 h. The resin was then carefully transferred to a fritted reaction vessel and washed sequentially with  $CH_2Cl_2$ , MeOH, water, and 1:1 MeOH/ $CH_2Cl_2$  before drying under vacuum. The [3+ 2] cycloaddition reaction between the azide-terminated folate-peptide **23** and monopropargylated cryptophane generated the folate-peptide-cryptophane conjugate **24** which was cleaved from the resin using a mixture of TFA, TIS, and water (90/5/5) at rt for 4 h. The reaction mixture was filtered using a peptide vessel, concentrated, and the peptide was precipitated by the addition of ether. The cleavage cocktail removed side chain protecting groups from all amino acids except for the *t*-butylthiol-protected cysteine. Semi-preparative HPLC purification of **24** was accomplished using the following gradient: time 0, A/B = 95/5; 0-65 min, linear increase to A/B = 30/70; 65-68 min, linear increase to A/B = 20/80; 68-70 min, linear increase to A/B = 5/95. MALDI MS calculated for **24**,  $C_{147}H_{211}N_{38}O_{32}S_2$  ( $M + H^+$ ) 3102.61; found 3103.08.

**Synthesis of 25.** Cys-protected folate-peptide-cryptophane conjugate **24** was dissolved in PBS buffer (100 mM, pH 7.1) at a concentration of 60  $\mu$ M. The GE protocol was followed to deprotect the *t*-butylthiol group and label the cysteine with the Cy3-maleimide construct. TCEP (0.0006 mmol, 10 equiv.) was added to a 1 mL PBS solution

containing **24** and degassed. The solution was stirred for 40 min to which was added Cy3 dye dissolved in 50  $\mu\text{L}$  dry DMSO. The reaction was degassed and stirred under nitrogen at rt for 16 h. The reaction mixture was purified by HPLC using the following gradient: For Cy3-labeled **25**: time 0, A/B = 95/5; 0-65 min, linear increase to A/B = 30/70; 65-68 min, linear change to A/B = 20/80; 68-70 min, A/B = 5/95. MALDI MS calculated for  $\text{C}_{180}\text{H}_{253}\text{N}_{42}\text{O}_{42}\text{S}_3$  (Cy3-I) ( $\text{M} + \text{H}^+$ ) 3771.81; found 3771.59. Extinction coefficients used to determine solution concentrations of Cy3-labeled **25** was  $\epsilon_{280}$  38,000  $\text{M}^{-1} \text{cm}^{-1}$  and  $\epsilon_{552}$  150,000  $\text{M}^{-1} \text{cm}^{-1}$  in water.

**Cell Culture.** KB, HeLa and HT-1080 cells were obtained from Dr. Jerry Glickson (University of Pennsylvania Medical School, Philadelphia, PA). All cells were grown in 25  $\text{cm}^2$  tissue culture flasks in RPMI-1640 with 25 mM HEPES supplemented with 2 mM L-glutamine, 15% fetal calf serum, 100 units of penicillin, and 100 units of streptomycin. Cells were subcultured on a weekly basis.

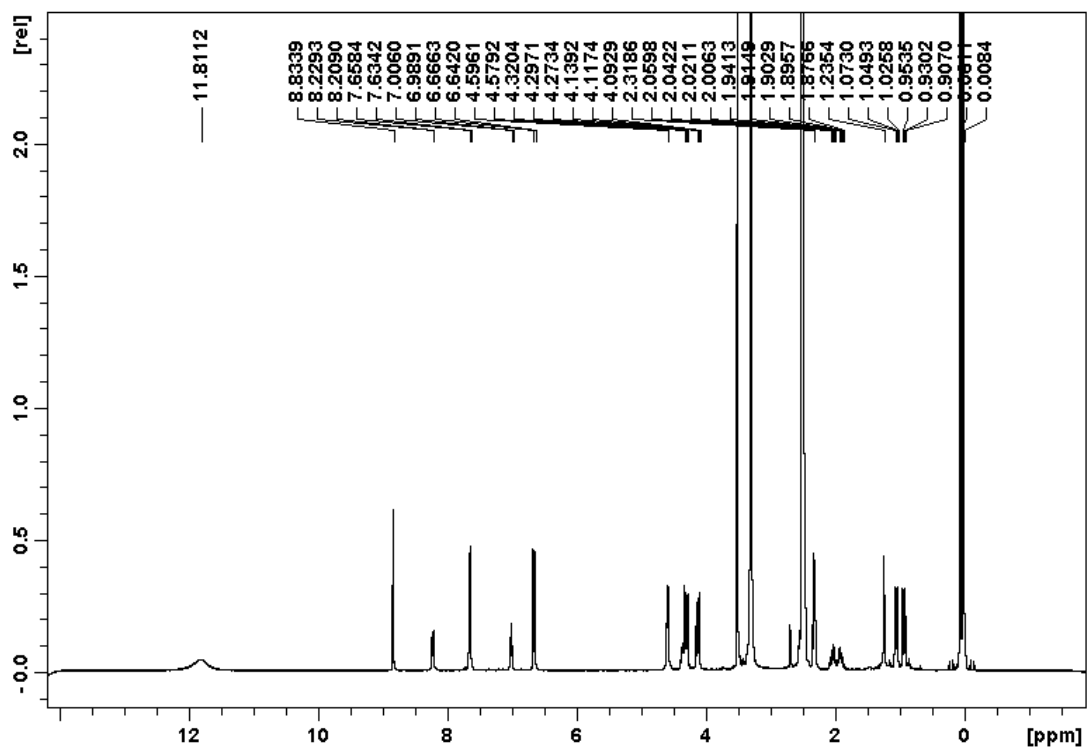
**Cell Viability (MTT) Assay.** In 96 well plates, 25,000 KB and HT-1080 cells were plated per well and allowed to grow overnight. A stock solution of nonfluorescently labeled folate-peptide-cryptophane conjugate **24** was added to wells in triplicate at final concentrations of 0, 2, 10, 25, 50, 75, and 100  $\mu\text{M}$  and incubated for 24 h in the dark. The medium was aspirated and the cells were washed thrice with DPBS before being treated with 20  $\mu\text{L}$  of MTT for 3 h. The medium was removed and DMSO was added to solubilize the resulting crystals. A plate reader was used to record the absorbance at 540 nm. Absorbance readings were subtracted from the value of wells containing untreated

cells, and the reduction in cell growth was calculated as a percentage of control absorbance in the absence of any treatment. Data show the mean of at least three independent experiments  $\pm$  SD.

**Cell Uptake Studies.** KB, HeLa and HT-1080 cells were grown to confluence on LabTek 8-well microscope slides with glass coverslip bottoms at a density of 50,000 cells per plate. The cells were grown in folate-depleted media or 24 h prior to incubation with 4  $\mu$ M solution of Cy3-labeled **25** for 4 h at 37 °C. For blocking studies, cells were grown in media containing folic acid for 24 h prior to incubation with **25** under the same conditions mentioned above. The medium was removed and the cells were washed three times with DPBS. Cells were visualized using an Olympus FV1000 confocal laser scanning microscope with 543 nm (HeNe) laser excitation and Cy3 emission filter under 40 $\times$  magnification (Olympus UApo/340 40 $\times$ , 1.15 W).

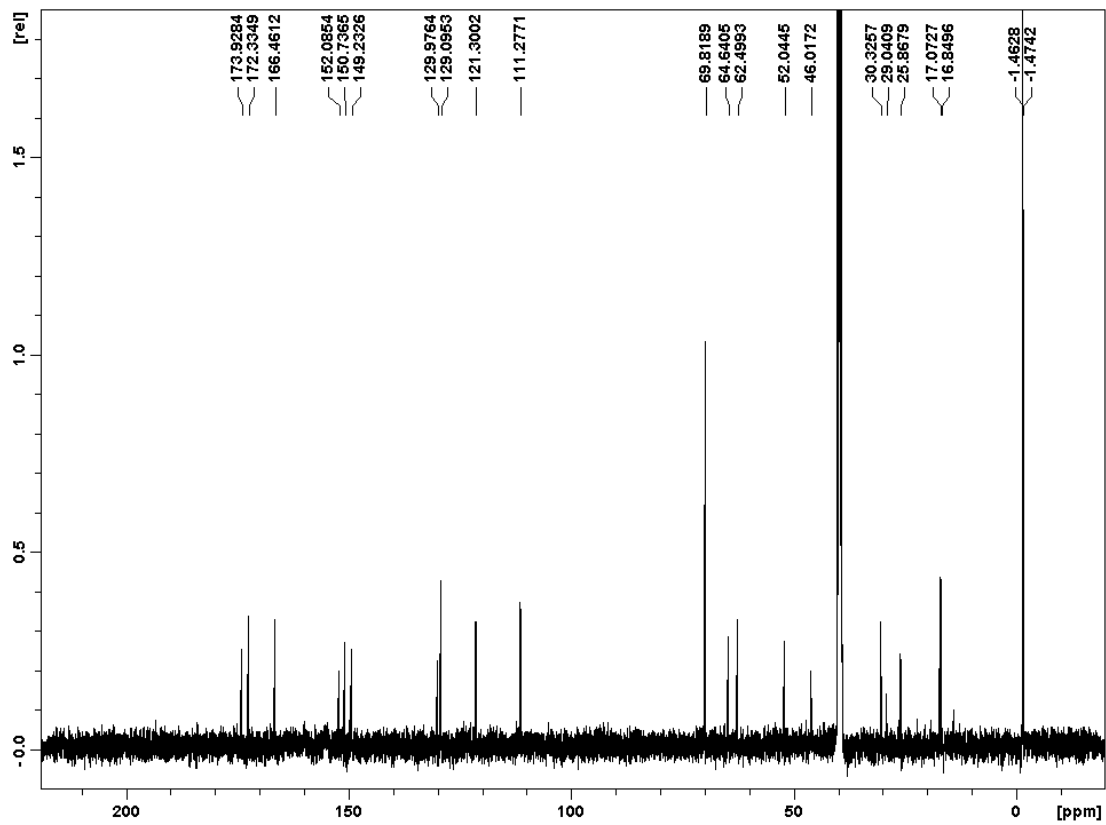
**Flow Cytometry Experiments.** KB and HT-1080 cells were seeded in T25 flasks each containing 10<sup>6</sup> cells and grown for 1 day in folate-depleted RPMI-1640 medium. The cells were incubated for 4 h with 4  $\mu$ M **25** (1.3 mL/flask). For blocking studies, 4  $\mu$ M **25** was added in the presence of medium containing folic acid. The medium was aspirated and cells washed 3 times with 2 mL of PBS. The cells were detached using trypsin-EDTA and centrifuged. The supernatant was aspirated and resuspended in 650  $\mu$ L 10% FBS in Dulbecco's PBS and immediately analyzed on a BD LSRII machine at the Flow Cytometry Laboratory, Abramson Cancer Center, at the University of Pennsylvania.

$^1\text{H}$  NMR of the folate recognition moiety (7) in  $\text{d}_6$ -DMSO at 298K

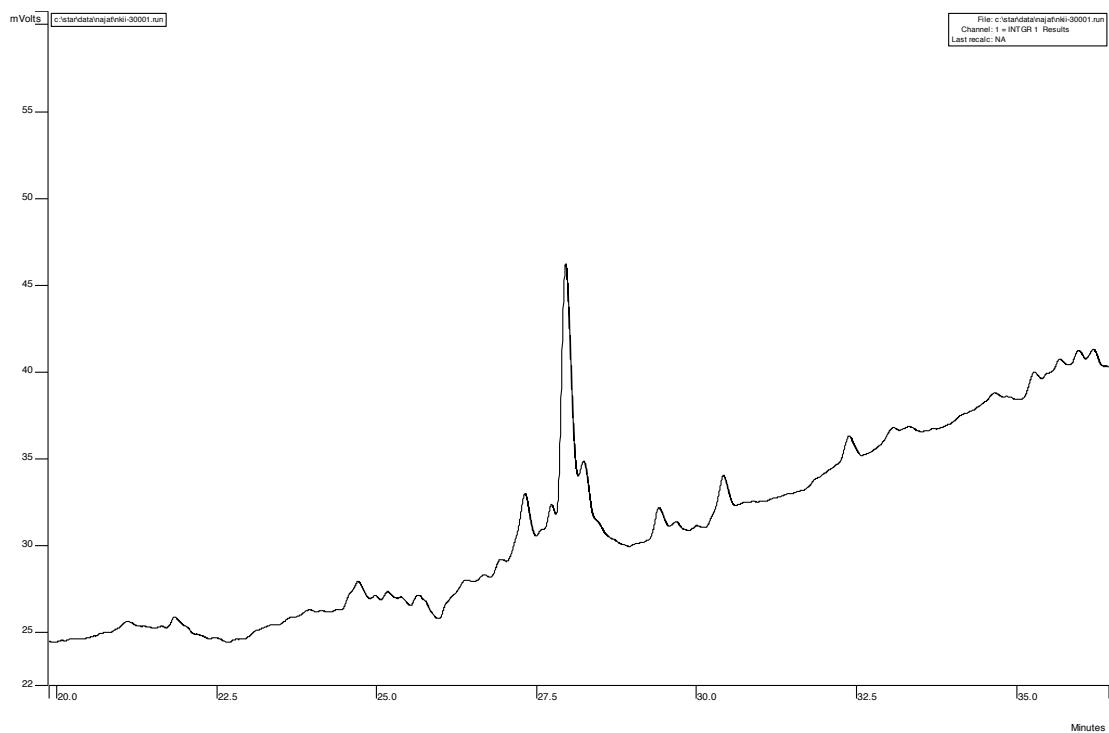




$^{13}\text{C}$  NMR of the folate recognition moiety (7) in  $\text{d}_6$ -DMSO at 298K

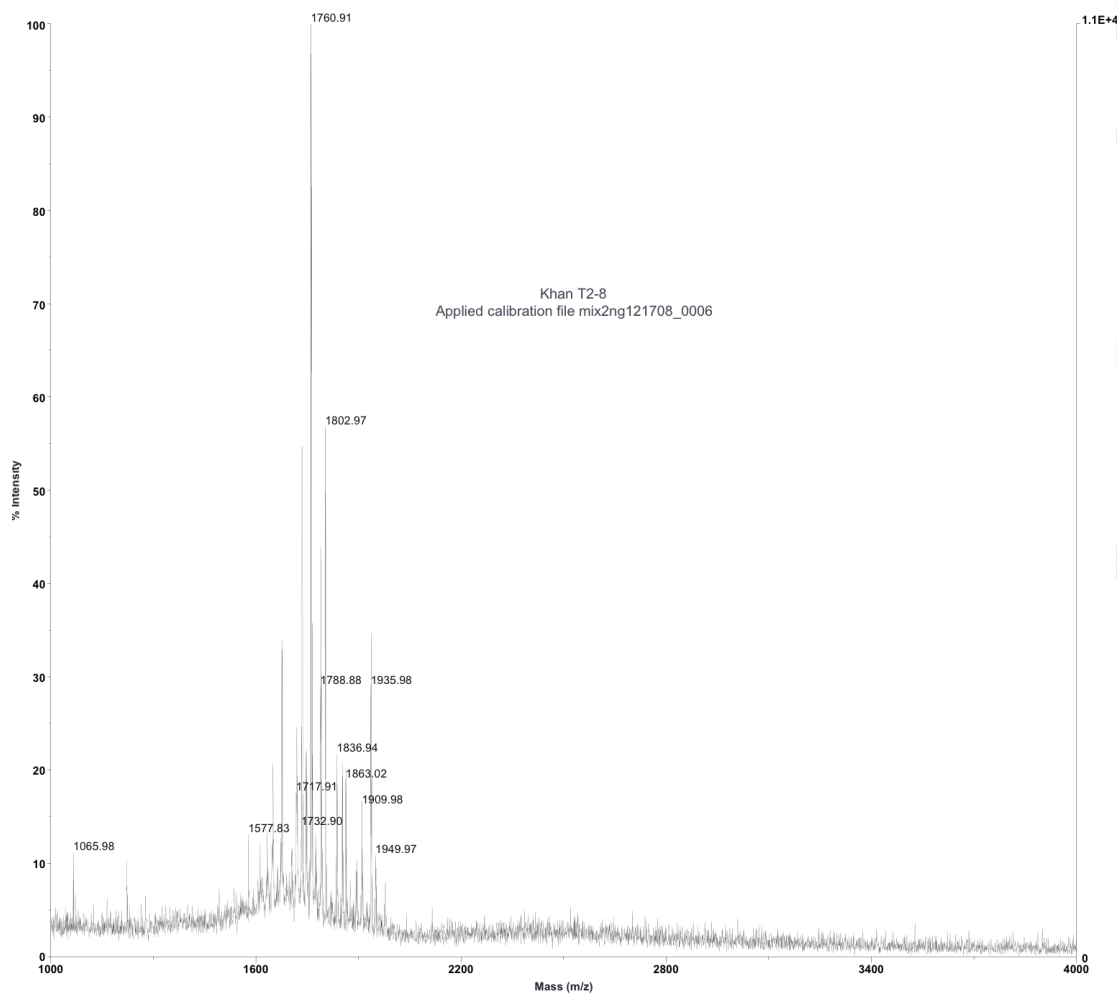


## HPLC purification trace for compound **22** (peptide)

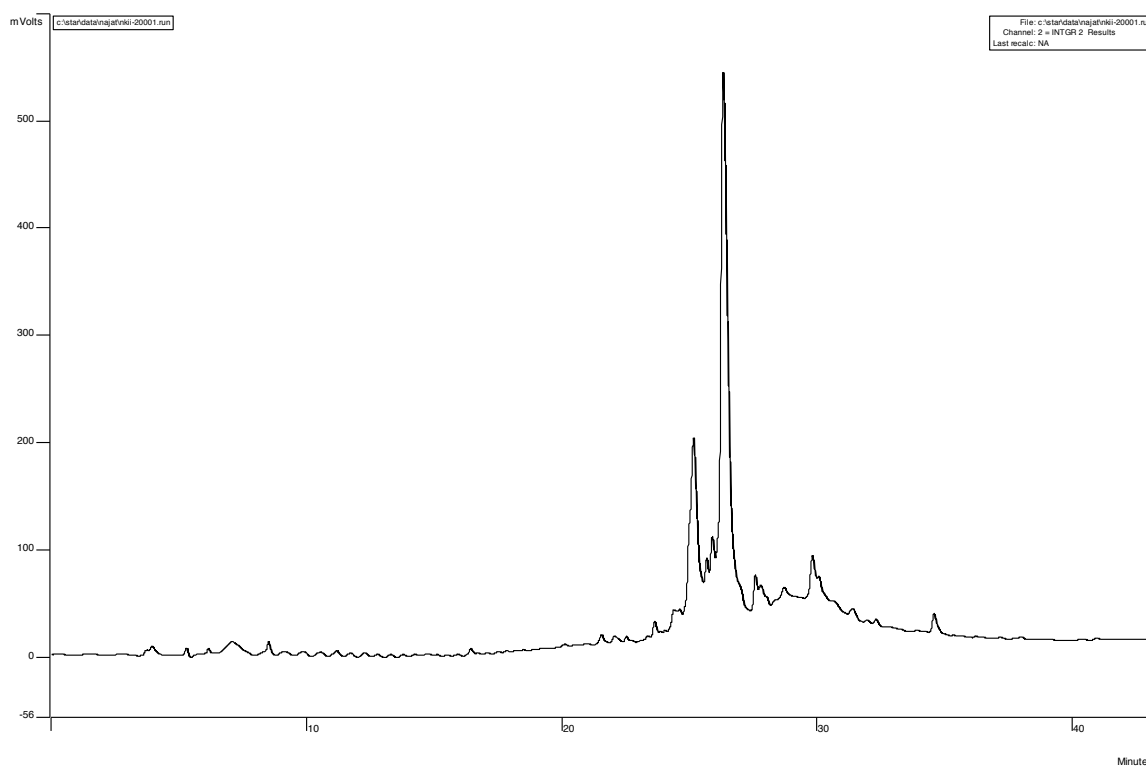


Semi-preparative HPLC purification of **22** was accomplished using the following gradient at 280 nm: time 0, A/B = 95/5; 0-45 min, linear increase to A/B = 50/50; 45-47 min, linear increase to A/B = 20/80; 47-56 min, linear change to A/B = 20/80; 56-57 min, linear increase to A/B = 95/5; 57-72 min, linear change to A/B = 95/5. Retention time: 27.96 min.

# MALDI spectrum of purified compound **22** (peptide)

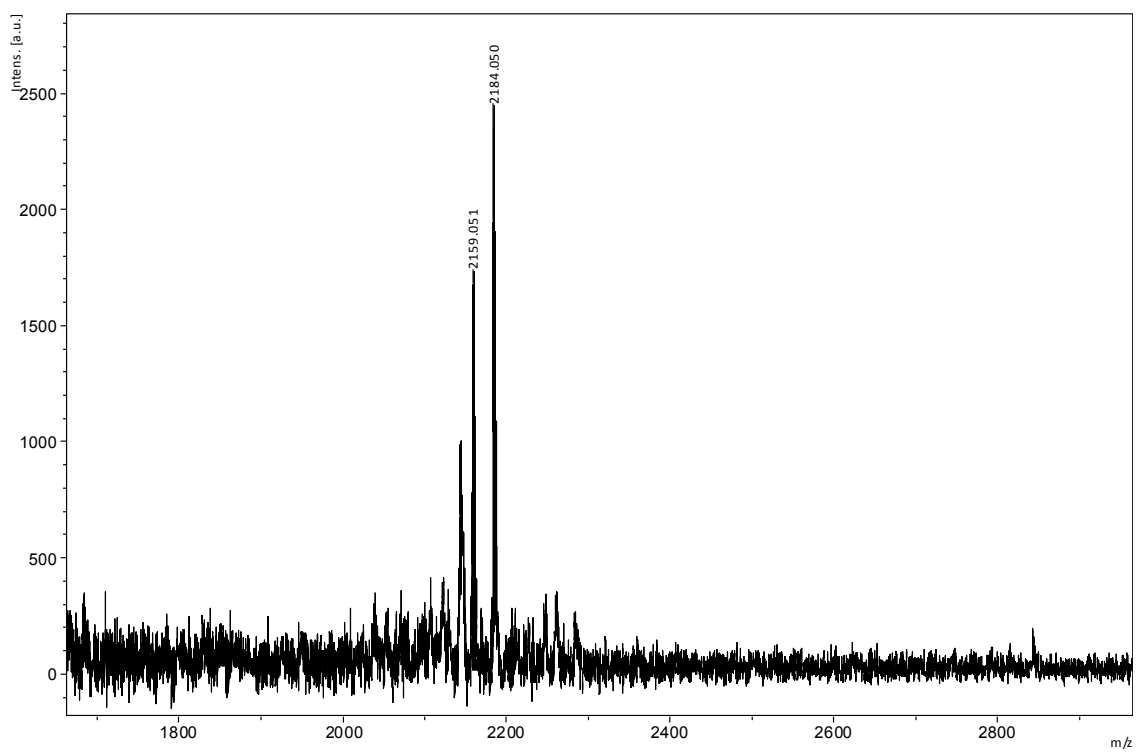


## HPLC purification trace for compound **23** (peptide-folate conjugate)

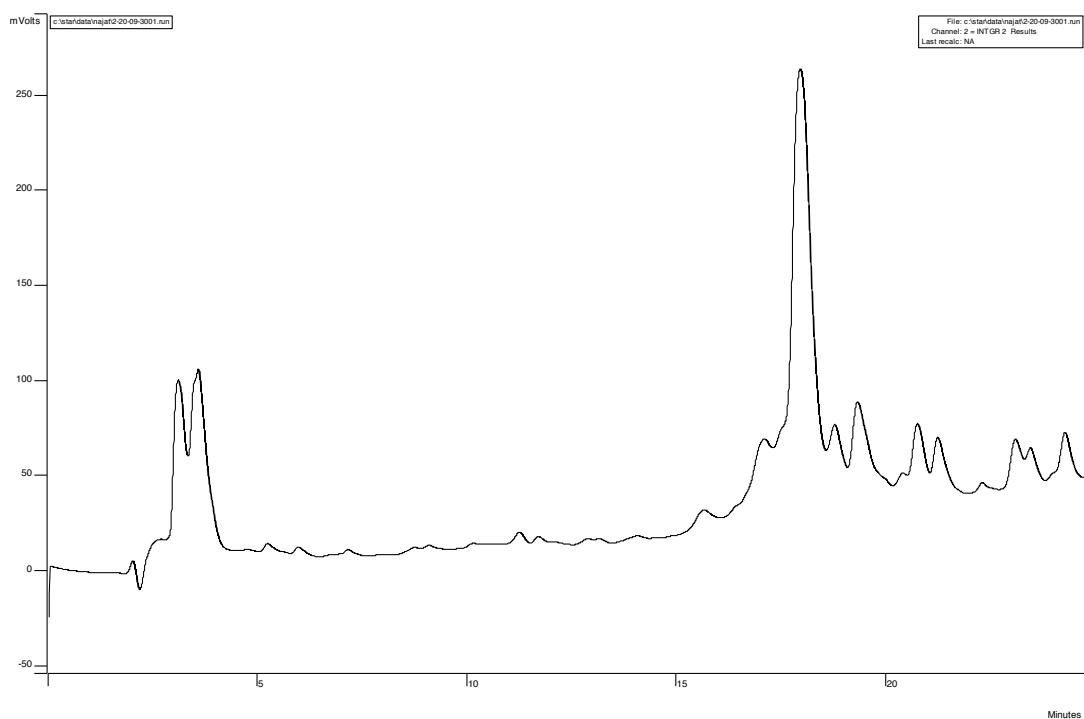


Semi-preparative HPLC purification of **23** was accomplished using the following gradient at 280 nm: time 0, A/B = 95/5; 0-45 min, linear increase to A/B = 50/50; 45-47 min, linear increase to A/B = 20/80; 47-56 min, linear change to A/B = 20/80; 56-57 min, linear increase to A/B = 95/5; 57-72 min, linear change to A/B = 95/5. Retention time: 26.31 min.

MALDI spectrum for purified compound **23** (peptide-folate conjugate)

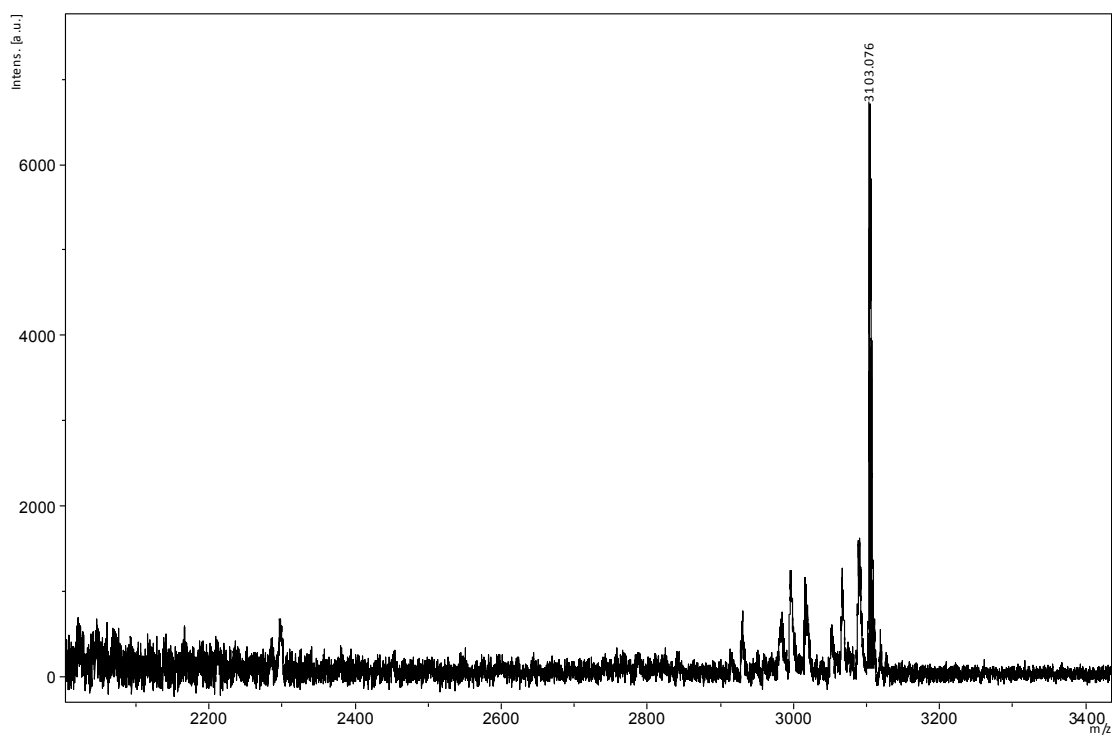


## HPLC trace for compound **24** (peptide-folate-cryptophane conjugate)

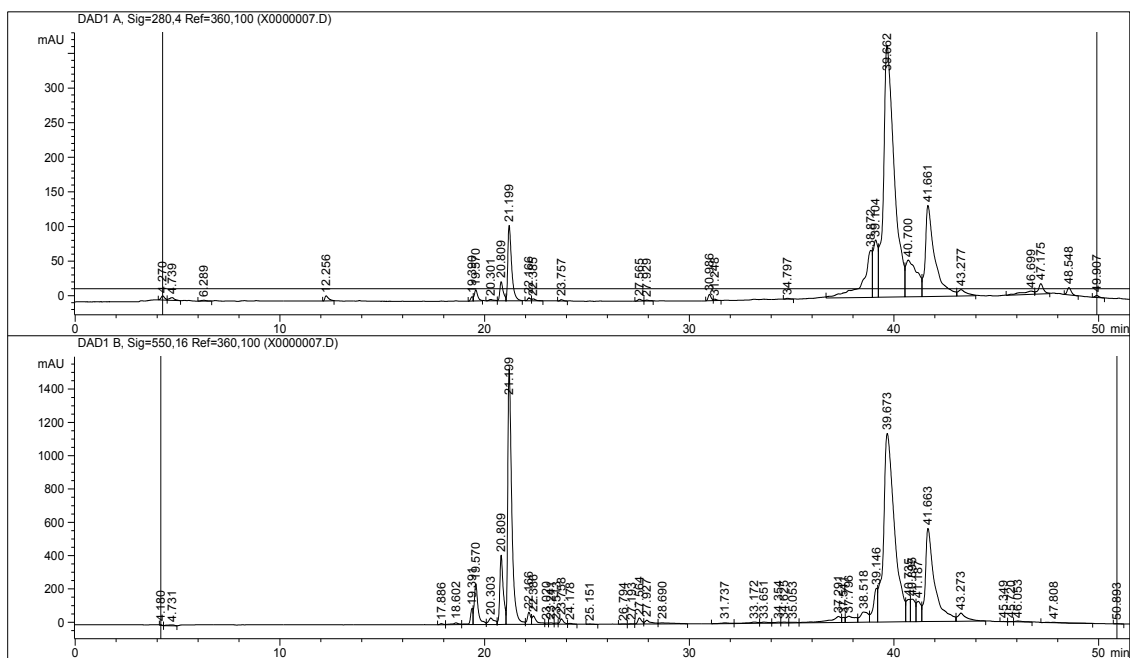


Semi-preparative HPLC purification of **24** was accomplished using the following gradient at 280 nm: time 0, A/B = 95/5; 0-65 min, linear increase to A/B = 30/70; 65-68 min, linear increase to A/B = 20/80; 68-70 min, linear increase to A/B = 5/95. Retention time: 18.73 min.

MALDI spectrum for purified compound **24** (peptide-folate-cryptophane conjugate)



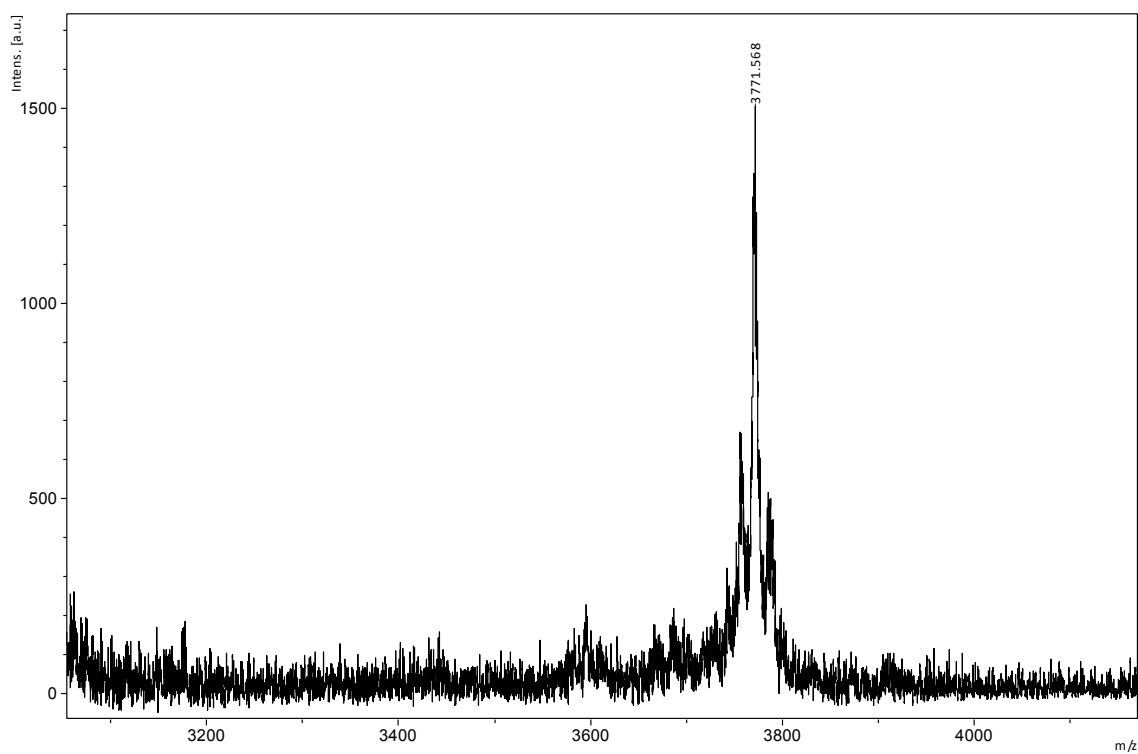
HPLC trace for compound **25** (peptide-folate-cryptophane conjugate)



Semi-preparative HPLC purification of **25** was accomplished using the following gradient at 280 and 550 nm: time 0, A/B = 95/5; 0-65 min, linear increase to A/B = 30/70; 65-68 min, linear change to A/B = 20/80; 68-70 min, A/B = 5/95. Retention time: 39.67 min.



MALDI trace for purified compound **25** (peptide-folate-cryptophane conjugate)



## **ACKNOWLEDGEMENTS**

We thank Dr. Furst for assistance with the NMR and Dr. Jerry Glickson for providing the KB and HT-1080 cell lines. We thank Dr. Qien Wei, Dr. Aru Hill, and Tara Kaufmann for their early contributions to this work. This work was supported by NIH CA110104 and DOD BC061527.

## **AUTHOR CONTRIBUTIONS**

N.S.K. (Najat S. Khan) wrote the manuscript. N.S.K. synthesized and characterized the reported compounds. N.S.K. and G.K.S. (Garry K. Seward) performed the *in vitro* experiments. Y.B. (Yubin Bai) performed hyperpolarized  $^{129}\text{Xe}$  NMR spectroscopy. I.J.D. initiated this project and edited the manuscript.

## REFERENCES

- (1) Sharma, V.; Luker, G. D.; Piwnica-Worms, D. *J. Magn. Reson.* **2002**, *16*, 336-351.
- (2) Degani, H.; Gusic, V.; Weinstein, D.; Fields, S.; Strano, S. *Nat. Med.* **1997**, *3*, 780-782.
- (3) Foster-Gareau, P.; Heyn, C.; Alejski, A.; Rutt, B. K. *Magn. Reson. Med.* **2003**, *49*, 968-971.
- (4) Broome, D. R.; Girguis, M. S.; Baron, P. W.; Cottrell, A. C.; Kjellin, I.; Kirk, G. A. *AJR Am. J. Roentgenol.* **2007**, *188*, 586-592.
- (5) Mugler, J. P., 3rd; Driehuys, B.; Brookeman, J. R.; Cates, G. D.; Berr, S. S.; Bryant, R. G.; Daniel, T. M.; de Lange, E. E.; Downs, J. H., 3rd; Erickson, C. J.; Happer, W.; Hinton, D. P.; Kassel, N. F.; Maier, T.; Phillips, C. D.; Saam, B. T.; Sauer, K. L.; Wagshul, M. E. *Magn. Reson. Med.* **1997**, *37*, 809-815.
- (6) Golman, K.; Zandt, R. I.; Lerche, M.; Pehrson, R.; Ardenkjaer-Larsen, J. H. *Cancer Res.* **2006**, *66*, 10855-10860.
- (7) Hopkins, S. R.; Levin, D. L.; Emami, K.; Kadlecsek, S.; Yu, J.; Ishii, M.; Rizi, R. R. *J. Appl. Physiol.* **2007**, *102*, 1244-1254.
- (8) Clevelanda, Z. I.; Pavlovskayaa, G. E.; Elkinsb, N. D.; Stupica, K. F.; Repineb, J. E.; Meersmann, T. *J. Magn. Reson.* **2008**, *195*, 232-237.
- (9) Hill, P. A.; Wei, Q.; Eckenhoff, R. G.; Dmochowski, I. J. *J. Am. Chem. Soc.* **2007**, *129*, 9262-9263.

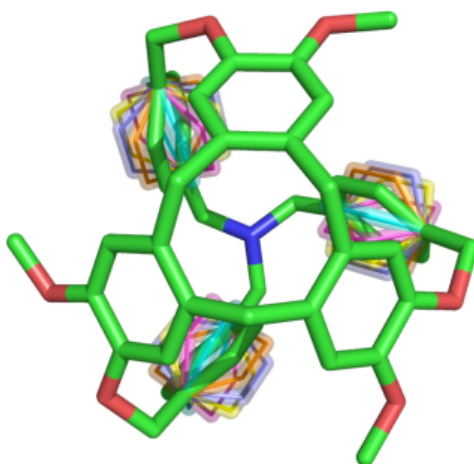
- (10) Spence, M. M.; Rubin, S. M.; Dimitrov, I. E.; Ruiz, E. J.; Wemmer, D. E.; Pines, A.; Yao, S. Q.; Tian, F.; Schultz, P. G. *Proc. Natl. Acad. Sci. U.S.A.* **2001**, *98*, 10654-10657.
- (11) Lowery, T. J.; Garcia, S.; Chavez, L.; Ruiz, E. J.; Wu, T.; Brotin, T.; Dutasta, J. P.; King, D. S.; Schultz, P. G.; Pines, A.; Wemmer, D. E. *Chembiochem* **2006**, *7*, 65-73.
- (12) Ruiz, E. J.; Sears, D. N.; Pines, A.; Jameson, C. J. *J. Am. Chem. Soc.* **2006**, *128*, 16980-16988.
- (13) Hilty, C., Lowery, T. J., Wemmer, D. E., Pines, A. *Angew. Chem. Int. Ed.* **2006**, *45*, 70-73.
- (14) Wei, Q.; Seward, G. K.; Hill, P. A.; Patton, B.; Dimitrov, I. E.; Kuzma, N. N.; Dmochowski, I. J. *J. Am. Chem. Soc.* **2006**, *128*, 13274-13283.
- (15) Chambers, J. M.; Hill, P. A.; Aaron, J. A.; Han, Z.; Christianson, D. W.; Kuzma, N. N.; Dmochowski, I. J. *J. Am. Chem. Soc.* **2009**, *131*, 563-569.
- (16) Schlundt A, K. W., Beyermann M, Sticht J, Guenther S, Höpner S, Falk K, Roetzschke O, Mitschang L, Freund C *Angew. Chem. Int. Ed. Engl.* **2009**, *48*, 4142-4145.
- (17) Seward, G. K.; Wei, Q.; Dmochowski, I. J. *Bioconjug. Chem.* **2008**, *19*, 2129-2135.
- (18) Seward, G. K.; Bai, Y.; Khan, N. S.; Dmochowski, I. J. *Chem. Sci.* **2011**, doi: 10.1039/c1031sc00041a.
- (19) Matherly, L. H.; Goldman, D. I. *Vitam. Horm.* **2003**, *66*, 403-456.
- (20) Qiu, A.; Jansen, M.; Sakaris, A.; Min, S. H.; Chattopadhyay, S.; Tsai, E.; Sandoval, C.; Zhao, R.; Akabas, M. H.; Goldman, I. D. *Cell* **2006**, *127*, 917-928.

- (21) Salazar, M. D.; Ratnam, M. *Cancer Metastasis Rev.* **2007**, *26*, 141-152.
- (22) Elnakat, H.; Ratnam, M. *Adv. Drug Deliv. Rev.* **2004**, *56*, 1067-1084.
- (23) Hilgenbrink, A. R.; Low, P. S. *J. Pharm. Sci.* **2005**, *94*, 2135-2146.
- (24) Campbell, I. G.; Jones, T. A.; Foulkes, W. D.; Trowsdale, J. *Cancer Res.* **1991**, *51*, 5329-5338.
- (25) Weitman, S. D.; Lark, R. H.; Coney, L. R.; Fort, D. W.; Frasca, V.; Zurawski, V. R., Jr.; Kamen, B. A. *Cancer Res.* **1992**, *52*, 3396-3401.
- (26) Sudimack, J.; Lee, R. J. *Adv. Drug Deliv. Rev.* **2000**, *41*, 147-162.
- (27) Bueno, R.; Appasani, K.; Mercer, H.; Lester, S.; Sugarbaker, D. *J. Thorac. Cardiovasc. Surg.* **2001**, *121*, 225-233.
- (28) Chancy, C. D.; Kekuda, R.; Huang, W.; Prasad, P. D.; Kuhnel, J. M.; Sirotnak, F. M.; Roon, P.; Ganapathy, V.; Smith, S. B. *J. Biol. Chem.* **2000**, *275*, 20676-20684.
- (29) Evans, C. O.; Young, A. N.; Brown, M. R.; Brat, D. J.; Parks, J. S.; Neish, A. S.; Oyesiku, N. M. *J. Clin. Endocrinol. Metabo.* **2001**, *86*, 3097-3107.
- (30) Ross, J. F.; Chaudhuri, P. K.; Ratnam, M. *Cancer* **1994**, *73*, 2432-2443.
- (31) Toffoli, G.; Cernigoi, C.; Russo, A.; Gallo, A.; Bagnoli, M.; Boiocchi, M. *Int. J. Cancer* **1997**, *74*, 193-198.
- (32) Wu, M.; Gunning, W.; Ratnam, M. *Cancer Epidemiol. Biomarkers Prev.* **1999**, *8*, 775-782.
- (33) Stover, P. J. *Nutri. Reviews* **2004**, *62*, S3-12; discussion S13.
- (34) Figini, M.; Ferri, R.; Mezzanzanica, D.; Bagnoli, M.; Luisson, E.; Miotti, S.; Canevari, S. *Gene Thera.* **2003**, *10*, 1018-1025.

- (35) Wang, S.; Low, P. S. *J. Control. Release* **1998**, *53*, 39-48.
- (36) Leamon, C. P.; Low, P. S. *Drug Discov. Today* **2001**, *6*, 44-51.
- (37) Wender, P. A.; Mitchell, D. J.; Pattabiraman, K.; Pelkey, E. T.; Steinman, L.; Rothbard, J. B. *Proc. Natl. Acad. Sci. U.S.A.* **2000**, *97*, 13003-13008.
- (38) Punna, S.; Kuzelka, J.; Wang, Q.; Finn, M. G. *Angew. Chem., Int. Ed. Engl.* **2005**, *44*, 2215-2220.
- (39) Rostovtsev, V. V.; Green, L. G.; Fokin, V. V.; Sharpless, K. B. *Angew. Chem., Int. Ed. Engl.* **2002**, *41*, 2596-2599.
- (40) Tornøe, C. W.; Christensen, C.; Meldal, M. *J. Org. Chem* **2002**, *67*, 3057-3064.
- (41) Nomura, M.; Shuto, S.; Matsuda, A. *J. Org. Chem.* **2000**, *65*, 5016-5021.
- (42) Atherton, E., Sheppard, R. C. *Solid-Phase Peptide Synthesis*; Oxford, 1989.
- (43) Leffler, J. E. T., R. D. *J. Am. Chem. Soc.* **1967**, *89*, 5235-5246.
- (44) Kim, I. B.; Shin, H.; Garcia, A. J.; Bunz, U. H. *Bioconjug. Chem.* **2007**, *18*, 815-820.
- (45) Leamon, C. P.; Low, P. S. *Proc. Natl. Acad. Sci. U.S.A.* **1991**, *88*, 5572-5576.
- (46) Moon, W. K.; Lin, Y.; O'Loughlin; T., T., Y. ; Kim, D. E.; Weissleder, R.; Tung, C. H. *Bioconjug. Chem.* **2003**, *14*, 539-545.
- (47) Collet, A. *Tetrahedron* **1987**, *43*, 5725-5759.
- (48) Bartik K, L. M., Dutasta JP, Collet A, Reisse J. *J. Am. Chem. Soc.* **1998**, *120*, 784-791.

- (49) Aaron, J. A.; Chambers, J. M.; Jude, K. M.; Di Costanzo, L.; Dmochowski, I. J.; Christianson, D. W. *J. Am. Chem. Soc.* **2008**, *130*, 6942-6943.
- (50) Kaarsholm, N. C.; Kolstrup, A. M.; Danielsen, S. E.; Holm, J.; Hansen, S. *I. Biochem. J* **1993**, *292 (Pt 3)*, 921-925.
- (51) Holm, J.; Hansen, S. I. *Biosci. Rep.* **2001**, *21*, 745-753.

**CHAPTER 4: MULTIPLE HINDERED ROTATORS IN A  
GYROSCOPE-INSPIRED TRIBENZYLAMINE  
HEMICRYPTOPHANE**



This paper was adapted from a manuscript published in *J. Org. Chem.*

Najat S. Khan,<sup>†</sup> Jose Manuel Perez-Aguilar,<sup>†</sup> Tara Kaufmann, P. Aru Hill, Olena Taratula, One-Sun Lee, Patrick J. Carroll, Jeffery G. Saven\*, Ivan J. Dmochowski\*

<sup>†</sup>These authors contributed equally to this work.

Department of Chemistry, University of Pennsylvania, Philadelphia, 19104



## ABSTRACT

A gyroscope-inspired tribenzylamine hemicryptophane provides a vehicle for exploring the structure and properties of multiple p-phenylene rotators within one molecule. The hemicryptophane was synthesized in three steps in good overall yield using mild conditions. Three rotator-forming linkers were cyclized to form a rigid cyclotrimeratrylene (CTV) stator framework, which was then closed with an amine. The gyroscope-like molecule was characterized by  $^1\text{H}$  NMR and  $^{13}\text{C}$  NMR spectroscopy, and the structure was solved by X-ray crystallography. The rigidity of the two-component CTV-trimethylamine stator was investigated by  $^1\text{H}$  variable-temperature (VT) NMR experiments and molecular dynamics simulations. These techniques identified gyration of the three p-phenylene rotators on the millisecond time scale at  $-93\text{ }^\circ\text{C}$ , with more dynamic but still hindered motion at room temperature ( $27\text{ }^\circ\text{C}$ ). The activation energy for the p-phenylene rotation was determined to be  $\sim 10\text{ kcal mol}^{-1}$ . Due to the propeller arrangement of the p-phenylenes, their rotation is hindered but not strongly correlated. The compact size, simple synthetic route, and molecular motions of this gyroscope-inspired tribenzylamine hemicryptophane make it an attractive starting point for controlling the direction and coupling of rotators within molecular systems.

## INTRODUCTION

Synthetic chemical systems provide means to explore complex phenomena in biological machines<sup>1-8</sup> and also to create novel molecular mechanical components.<sup>9</sup> Designs based on macroscopic devices include brakes, gears, propellers, ratchets, turnstiles, rotors, scissors, and most recently gyroscopes (Figure 4.1).<sup>3,10-14</sup> These molecular systems have been extensively studied in solution, in solid phases, on surfaces and in polymers.<sup>15</sup> One challenge in designing these systems is the required restriction of some molecular degrees of freedom, while allowing specific motions of targeted molecular components.<sup>9</sup> Synthesis of such molecules can also be challenging. Criteria for the construction of molecular gyroscopes have been identified and generally applied: rotary elements (rotators) are attached to a static framework (stator); steric contacts, internal rotation barriers, and interaction with solvent should be minimized to allow low-friction, low-barrier rotary motion; rotating groups are isolated and/or well-separated from each other.

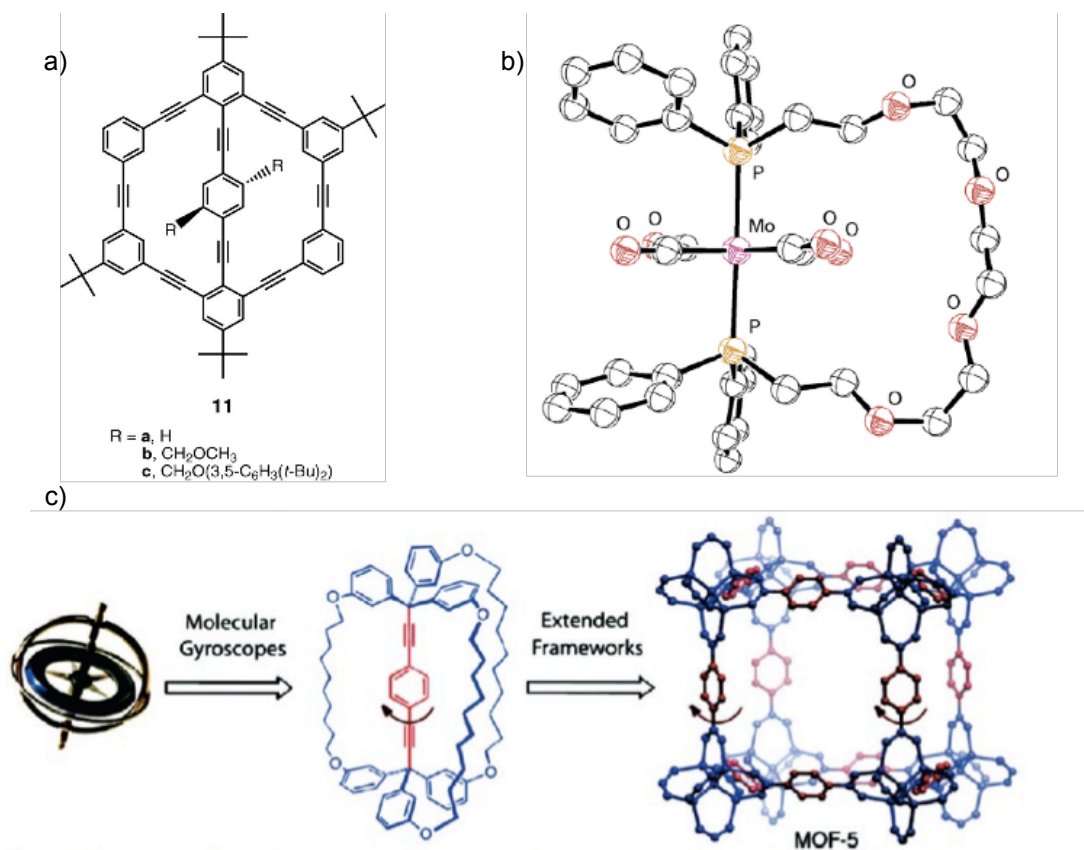
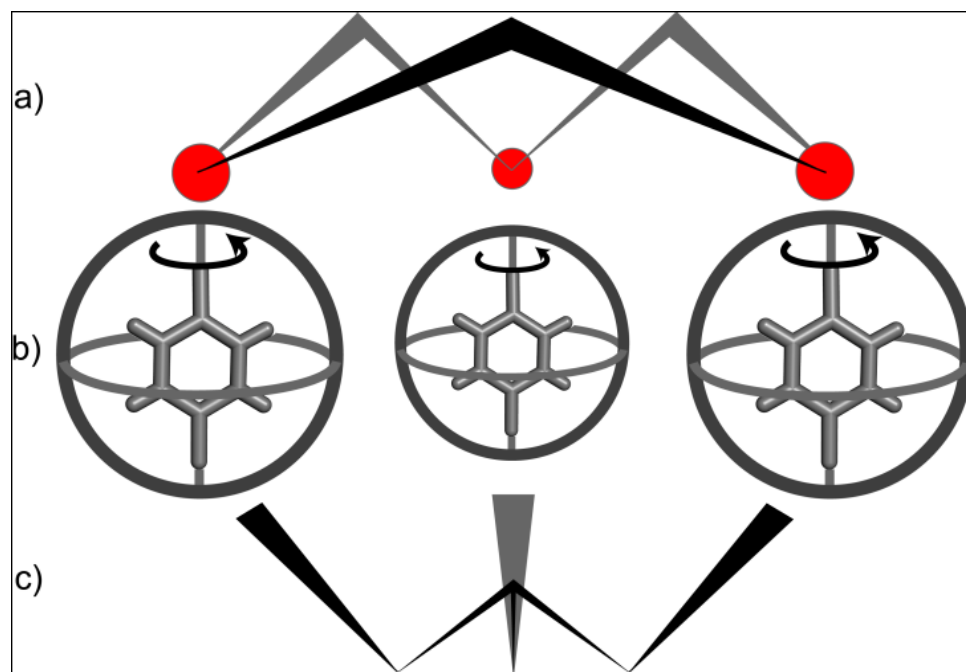


**Figure 4.1.** Examples of molecular components designed to mimic macroscopic devices: a) Molecular “turnstile” developed by Moore and Bedard et al., b) Metal-centered three-spoke molecular gyroscopes developed by Gladysz et al., and c) Solid-state crystals developed by Garcia-Garibay et al. Figures were adapted from Skopek and Sykes et al.<sup>13,14</sup>

One challenge in designing these systems is the required restriction of some molecular degrees of freedom, while allowing specific motions of targeted molecular components.<sup>9</sup> Synthesis of such molecules can also be challenging. Criteria for the construction of molecular gyroscopes have been identified and generally applied: rotary elements (rotators) are attached to a static framework (stator); steric contacts, internal rotation barriers, and interaction with solvent should be minimized to allow low-friction, low-barrier rotary motion; rotating groups are isolated and/or well-separated from each other.

To expand upon these criteria, we designed a gyroscope-inspired framework with cyclotrimeratrylene (CTV) and trimethylamine as the 2-component stator, bridged by three *p*-phenylene rotators (Scheme 4.1). This creates a new application for CTV, which has been used previously for the synthesis of cryptophanes in host-guest chemistry (with biosensing and chiroptical properties),<sup>16-31</sup> supramolecular assemblies, gels and organic microporous polymers.<sup>32</sup> CTV provides a rigid hemicryptophane framework for the synthesis of a novel gyroscope-inspired molecule. Our design incorporates a novel combination of features: (i) efficient, high-yielding synthetic scheme, (ii) multiple, proximate rotators in one covalently bonded molecular system, (iii) exclusion of other molecules and ions from the stator interior that may impede rotator motion, and (iv) hindered rotators experiencing friction through exposure to solvent.

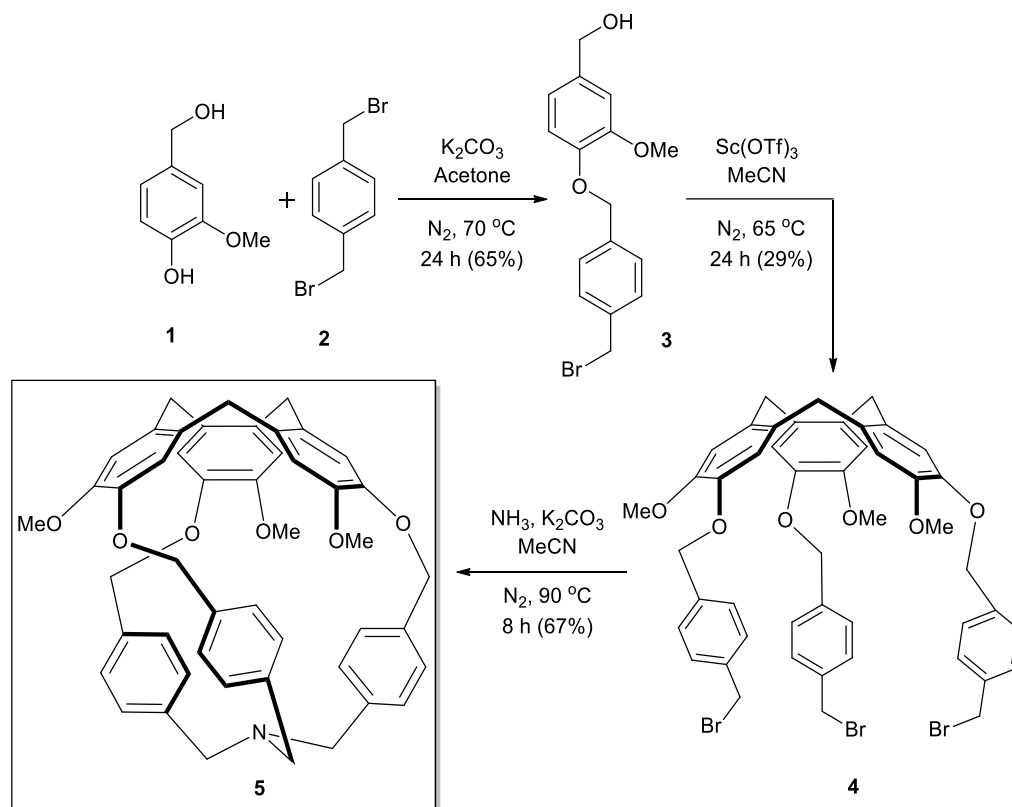


**Scheme 4.1.** Gyroscope-inspired tribenzylamine hemicryptophane (**5**) possesses a rigid stator (a and c) and three rotator groups (b). Arrows illustrate rotation but are not intended to suggest unidirectionality.

Gyroscope-inspired molecular systems have focused largely on approaching barrierless rotation of isolated or sequestered rotors. One of the first examples (also referred to as a molecular turnstile) was synthesized by Moore and Bedard (Figure 4.1a).<sup>33,34</sup> The creative design included a rigid hexa(phenylacetylene) framework that preserved the low barrier of rotation about the 1,4-axis of the substituted *p*-phenylene moiety. Garcia-Garibay and coworkers extended these ideas in the construction of amphidynamic crystals,<sup>11,15,35-54</sup> where the introduction of bulky substituents creates sufficient space in the lattice framework to allow near barrierless rotation of the central *p*-phenylene group (Figure 4.1c). Furthermore, the *p*-phenylene moiety can be functionalized to create a dipole moment that could be used for controlling motion with an external electric field.<sup>11,36-38,42</sup> Following a different approach, Gladysz and coworkers prepared a series of metal-centered molecular gyroscopes in which the rotator is protected by three-spoke structures as part of the stator (Figure 4b). The rotational dynamics of these gyroscopes were studied in solution and their crystal structures indicated sufficient free volume around the rotator to allow low-barrier rotation.<sup>9,55-59</sup> Most recently, Kitagawa et al. designed a self-assembled supramolecular gyroscope where the stator is a heterocapsule formed by noncovalent interactions and the rotator is an encapsulated guest.<sup>60</sup>

Herein, we report a streamlined synthesis of a gyroscope-inspired tribenzylamine hemicryptophane (**5**, Scheme 4.2) involving multiple hindered rotators, where fast rotation is observed by <sup>1</sup>H NMR spectroscopy above a critical temperature. Rotations about the 1,4-axis of the three *p*-phenylene rotators encased in a rigid CTV-

trimethylamine stator were investigated using  $^1\text{H}$  variable temperature (VT) NMR spectroscopy and molecular dynamics (MD) simulations.



Overall Yield (3 steps) = 13%

**Scheme 4.2.** Three-step synthesis of gyroscope-inspired tribenzylamine hemicryptophane

5.



## RESULTS AND DISCUSSION

**Synthesis and X-ray crystal structure of hemicryptophane 5.** In order to synthesize the gyroscope-inspired tribenzylamine hemicryptophane **5**, the linkers (including the rotators) were first cyclized in the rigid CTV framework and then closed with an amine to form the final three-dimensional structure (Scheme 2). Reaction of commercially available vanillyl alcohol **1** and dibromo-*p*-xylene **2** gave the versatile linker **3** in 65% yield. Cyclization of **3** was achieved with a catalytic amount of Sc(OTf)<sub>3</sub> in acetonitrile to afford the “gyroscope scaffold intermediate” **4** in 29% yield. This reaction was based on previous protocols where various 3,4-disubstituted benzyl alcohols were treated with catalytic Sc(OTf)<sub>3</sub> to prepare CTV and cryptophane derivatives.<sup>18</sup> Compound **4** was reacted with 7 N NH<sub>3</sub> in MeOH to give **5** in 67% yield, with an overall yield of 13% for the three steps. Compound **5** was characterized by solution <sup>1</sup>H NMR and <sup>13</sup>C NMR spectroscopy, high-resolution mass spectrometry (using electrospray ionization method) and X-ray crystallography. This short synthetic scheme utilizes mild conditions and results in high overall yields. Moreover, this route provides ample versatility by increasing the number of methylene spacer units or introducing new functional groups on **3** to form rotators with different conformations, rotation barriers, and dipole moments.

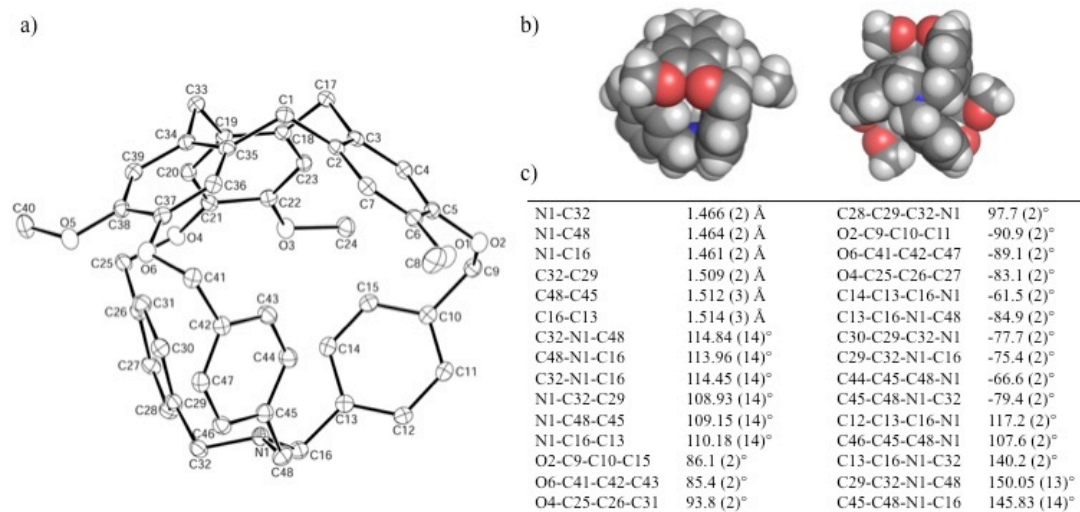
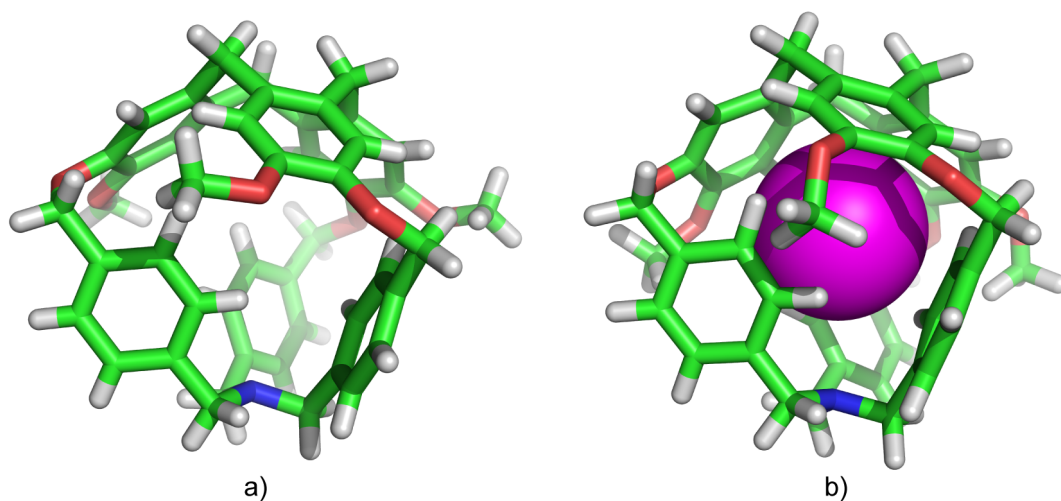


**Figure 4.2.** (a) ORTEP representations for **5** with atom labels. Hydrogen atoms are omitted for clarity. (b) Space-filling side and bottom view of **5**. Atom color code: C is gray, O is red, N is blue, and H is white. (c) Selected bond lengths (Å), angles (°) and dihedral angles (°) of compound **5**.

The X-ray crystal structure of **5** indicates the three rotators adopt a propeller conformation (Figure 4.2a,b). **5** crystallizes in the monoclinic space group  $P2_1/c$  and each unit cell consists of four molecules with two of each enantiomer. In both enantiomers the *p*-phenylene rotators are oriented edgewise into the interior (angled away from the methoxy group *ortho* to them) with an average dihedral angle of  $\sim 88.1^\circ$  for  $O-C_{benzylic}-C_{phenyl}-C_{phenyl}$ ,  $\sim -68.6^\circ$  for  $N-C_{benzylic}-C_{phenyl}-C_{interior-phenyl}$  and  $\sim 107.5^\circ$  for  $N-C_{benzylic}-C_{phenyl}-C_{exterior-phenyl}$  (see Figure 4.2c). The minimal distance from the phenylic proton on *C44* (pointing into the cage) to the plane described by the next aryl ring (*C10* to *C15*) is relatively small at 3.22 Å. After the van der Waals radii for hydrogen and carbon are included,<sup>61</sup> the “clearance” distance is approximately 0.32 Å. The distance from the same proton to the nitrogen atom was even shorter at 2.97 Å, with clearance distance of 0.22 Å when van der Waals radii are included, as the nitrogen is oriented into the interior with an average  $C-N-C$  bond angle of  $114.4^\circ$  (see Figure 4.2c). This propeller-shaped conformation with a pyramidal nitrogen atom where the lone pair is pointed into the cage is similar to the crystal structure of tribenzylamine, where the rigid CTV is not present.<sup>62</sup> It is believed that this conformation is primarily favored due to steric hindrance.<sup>62</sup> Despite the propeller conformation of the rotators and the positioning of the nitrogen atom into the interior of the cage, rotator motion is expected given the observed clearance distances.

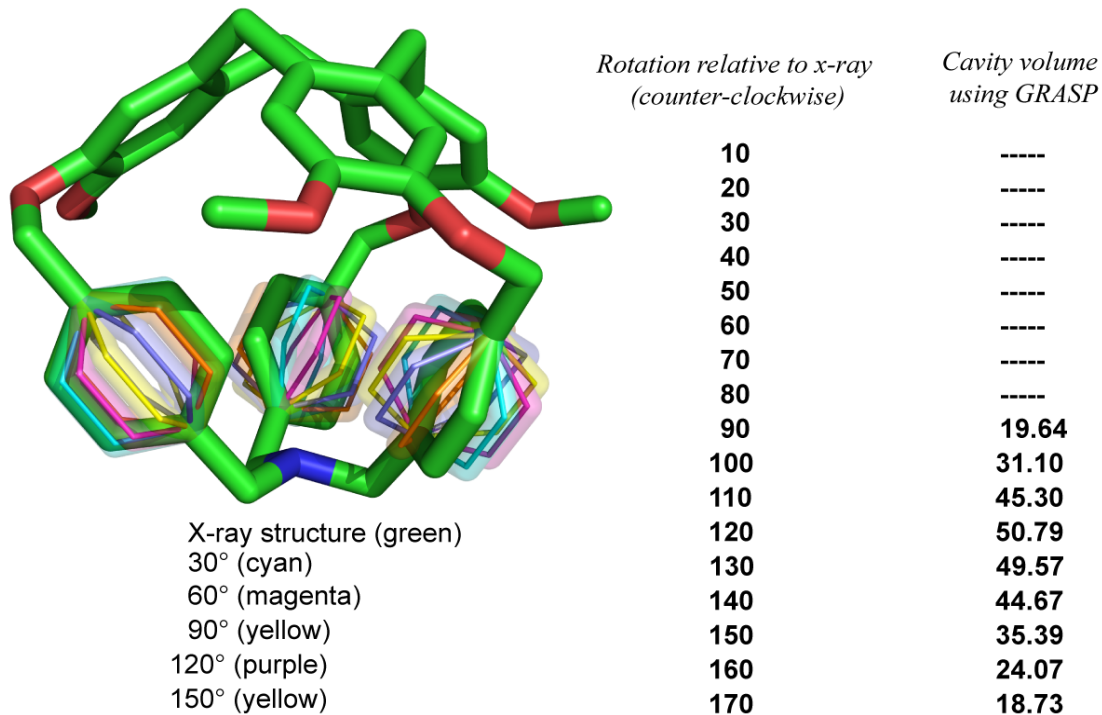
Unlike some previously reported porous gyroscopes,<sup>58</sup> which encountered barriers to rotation due to the intercalation of solvent molecules (or neighboring molecules in solid state), the small internal volume in **5** should prevent guest encapsulation. Indeed, X-

ray crystallography indicated an empty tribenzylamine hemicryptophane, lacking solvent molecules. Small molecules such as helium, dihydrogen, dinitrogen and xenon were not observed to bind to **5** at 1 atm over a range of temperatures, 47 °C to -93 °C (see Experimental procedures section). Molecular dynamics simulations were also in agreement with the experimental findings and suggest that these small molecular species should be excluded from the interior (Figure 4.3).



**Figure 4.3.** Molecular dynamics (MD) simulations were carried out in the absence (a) and presence (b) of the xenon atom (OPLS<sup>63</sup> force field parameter for Xe;  $\epsilon = 0.4330$  kcal mol<sup>-1</sup> and  $r = 2.20$  Å) inside of **5**. Using the crystal structure of **5** as the starting structure, a 50 ns simulation, with a time step of 0.5 fs, was performed for each case in the absence of solvent at 25 °C.<sup>64</sup> The difference of the average potential energies with and without xenon was 0.7 kcal mol<sup>-1</sup>, suggesting that there is no energetic stabilization in the presence of xenon, consistent with **5** having no experimentally observed affinity for Xe.

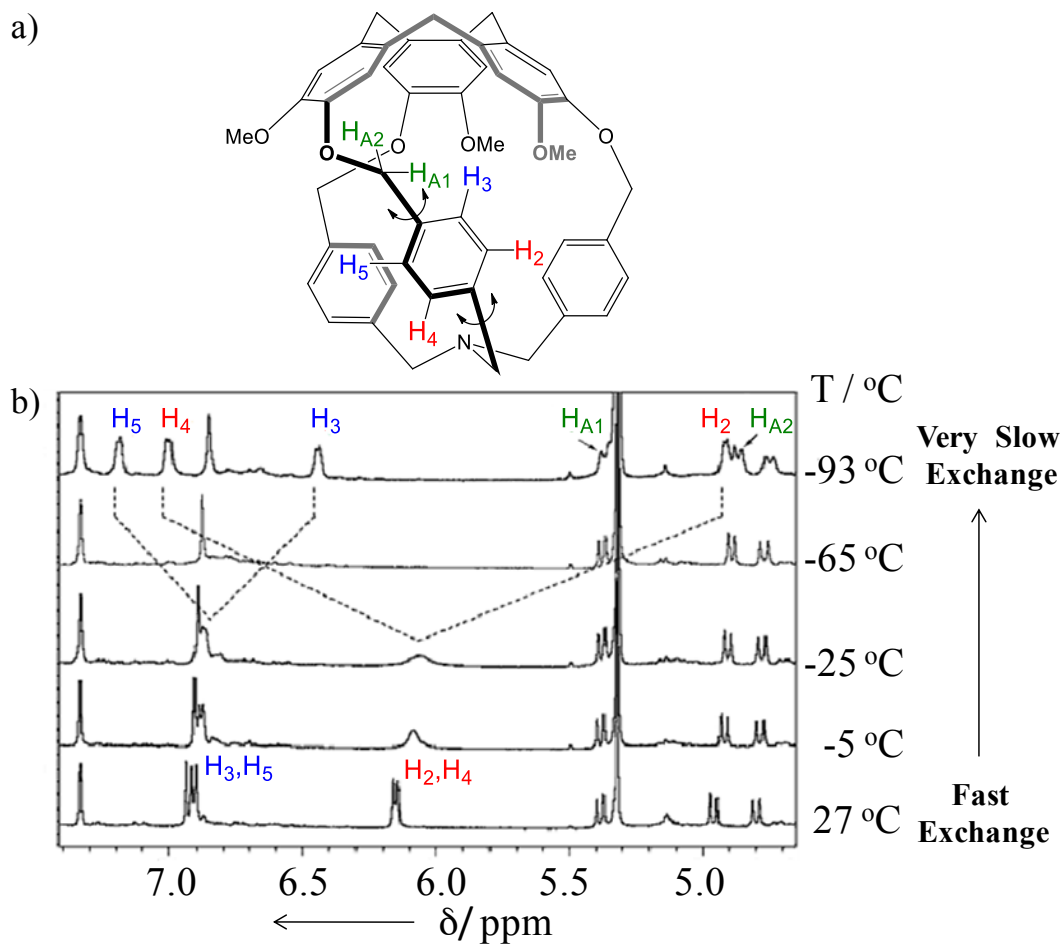
Computational modeling was used to explore effects due to rotation of the *p*-phenylene rotators. GRASP<sup>65</sup> was employed in order to investigate whether a potential interior cavity within **5** emerges with rotation of the rotators. With a probe radius of 1.4 Å, only in improbable, high-energy structures ( $\Delta E > 30 \text{ kcal mol}^{-1}$ , where  $\Delta E$  is the energy relative to the X-ray structure) where the angle of each *p*-phenylene rotator increased by 90° relative to the crystal structure was a cavity identified (Figure 4.4). This suggests that a cavity of sufficient volume to accommodate small guest molecules is essentially nonexistent, thereby preventing the inclusion of small molecules that may hinder *p*-phenylene rotation.



**Figure 4.4.** Structures with different concerted orientation of the *p*-phenylene rotators ( $\alpha = \beta = \gamma$ ). Crystal structure (green), 30° (cyan), 60° (magenta), 90° (yellow), 120° (purple) and 150° (orange). Also the cavity volume values using GRASP are shown. For clarity, hydrogens are not rendered and the high-energy structures ( $\Delta E > 29 \text{ kcal mol}^{-1}$ , where  $\Delta E$  is the energy relative to the X-ray structure) are shown as thin transparent sticks in order to illustrate their low probability.

**<sup>1</sup>H VT-NMR experiments with hemicryptophane 5.** In order to investigate the energy barrier of the rotators in solution phase, we performed a <sup>1</sup>H VT-NMR study of **5** in CD<sub>2</sub>Cl<sub>2</sub> from -93 °C to 27 °C. The NMR spectra in Figure 4.5 indicate that the rotational rate of the *p*-phenylene rotators became slow on the NMR timescale as the temperature was decreased. At 27 °C, the four protons (labeled H<sub>2</sub>, H<sub>3</sub>, H<sub>4</sub> and H<sub>5</sub> in Figure 4.5a) on each of the three rotators were split into two doublets at 6.1 ppm (average signal from H<sub>2</sub> and H<sub>4</sub>) and 6.9 ppm (average signal from H<sub>3</sub> and H<sub>5</sub>). Upon cooling, these doublets became broader and the energy barrier for *p*-phenylene rotation was estimated from equations (1) and (2),<sup>66</sup> see Experimental procedures section, to be 9.2 kcal mol<sup>-1</sup> from the coalescence temperature (ca. -70 °C;  $k_{\text{coalesce}} \approx 2300$  Hz). As the temperature was further reduced to -93 °C, a new pair of doublets of equal intensity (3 protons each) arose for each doublet that coalesced. This led to splitting of the doublet for H<sub>2</sub> and H<sub>5</sub> and also H<sub>3</sub> and H<sub>4</sub>, where H<sub>2</sub> and H<sub>3</sub> shift upfield as they are pointed into the cavity while H<sub>4</sub> and H<sub>5</sub> are oriented away from the cavity. The H<sub>3</sub>-H<sub>5</sub> splitting pattern (Figure 4.5b) evidences that *p*-phenylene rotation at -93 °C is slow on the NMR timescale,  $t_{\text{rot}} > 3$  ms. Similar temperature-dependent behavior was recently reported for a 2,3-dichlorophenylene rotator caged within a polysilaalkane stator.<sup>67</sup> In line with our design, the stator remained rigid throughout the <sup>1</sup>H VT-NMR dataset as indicated by the fact that the integration and splitting pattern of all CTV-trimethylamine proton peaks were constant. It is also interesting to note that protons H<sub>A1</sub> and H<sub>A2</sub> remained diastereotopic throughout the <sup>1</sup>H VT-NMR series (Figure 4.5b). All peaks were assigned by <sup>1</sup>H-<sup>1</sup>H NOESY experiment (Figure 4.6)





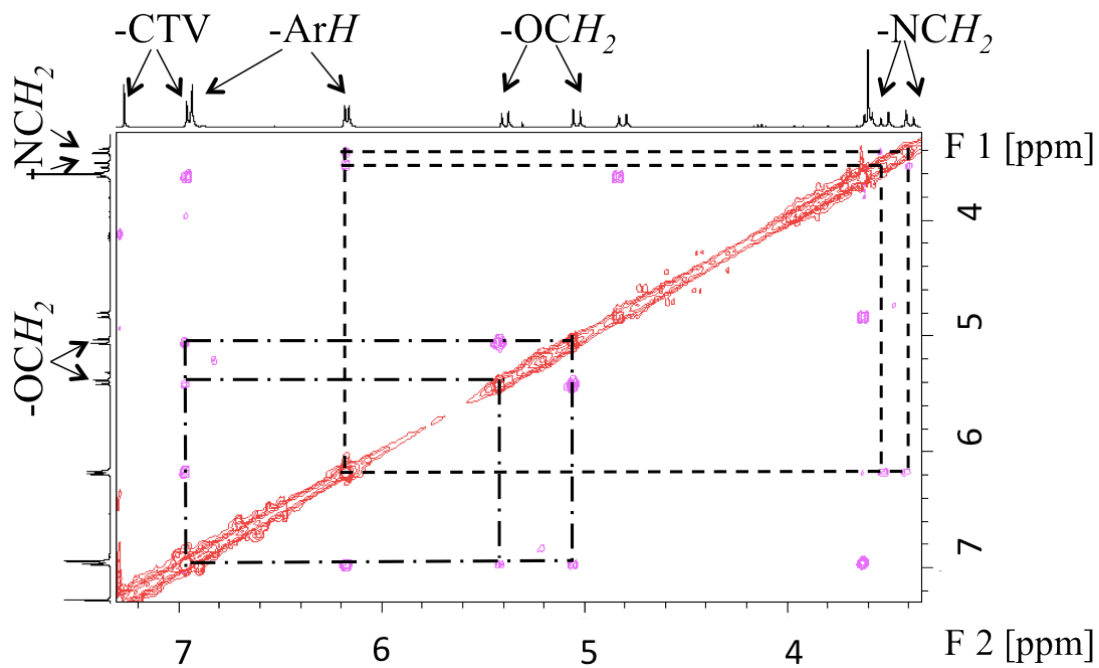


**Figure 4.6.**  $^1\text{H}$ - $^1\text{H}$  NOESY spectrum of **5** in  $\text{CDCl}_3$  at  $27\text{ }^\circ\text{C}$  with 500 MHz spectrometer to determine the assignment of protons.

**Molecular dynamics simulations.** To investigate the conformational fluctuations of the rotators and stator, MD simulations were carried out on **5** (Figure 4.7). One of the crystal structures was used as the initial structure, and the length of the simulations was 50 ns. Equilibration was confirmed by monitoring relaxation of structural parameters (Figure 4.7). Three dihedral angles that reflect the conformations of the rotators were selected: ( $\alpha \equiv NI-C16-C13-C14$ ,  $\beta \equiv NI-C32-C29-C30$  and  $\gamma \equiv NI-C48-C45-C44$ ). The symmetry of the structure yields nearly identical average values of these angles that are in agreement with the values observed in the crystal structure:  $\alpha = -72.3^\circ \pm 10^\circ$ ,  $\beta = -71.8^\circ \pm 10^\circ$  and  $\gamma = -72.8^\circ \pm 10^\circ$ ; the uncertainties (fluctuations) are one standard deviation (Figure 4.8). The MD simulations at 25 °C indicated limited fluctuations within the structure on the nanosecond time scale (Figure 4.9), and the CTV unit that forms the stator remains highly rigid, in agreement with the NMR results noted above. The *p*-phenylene units are not observed to rotate and instead librate in a manner consistent with a hindered rotor that rotates on a time scale  $> 100$  ns. Therefore, simulations, X-ray, and NMR structural data all agree that the propeller-shaped conformation is highly favored in **5**. High temperatures were artificially employed to observe rotation in the simulations: at 527 °C, rotations of the three *p*-phenylenes are frequent, conformations where the rotators are directed edgewise into the interior (similar to what is seen in the crystal structure) are preferentially populated, and no preferred rotational direction in the three *p*-phenylenes is observed.

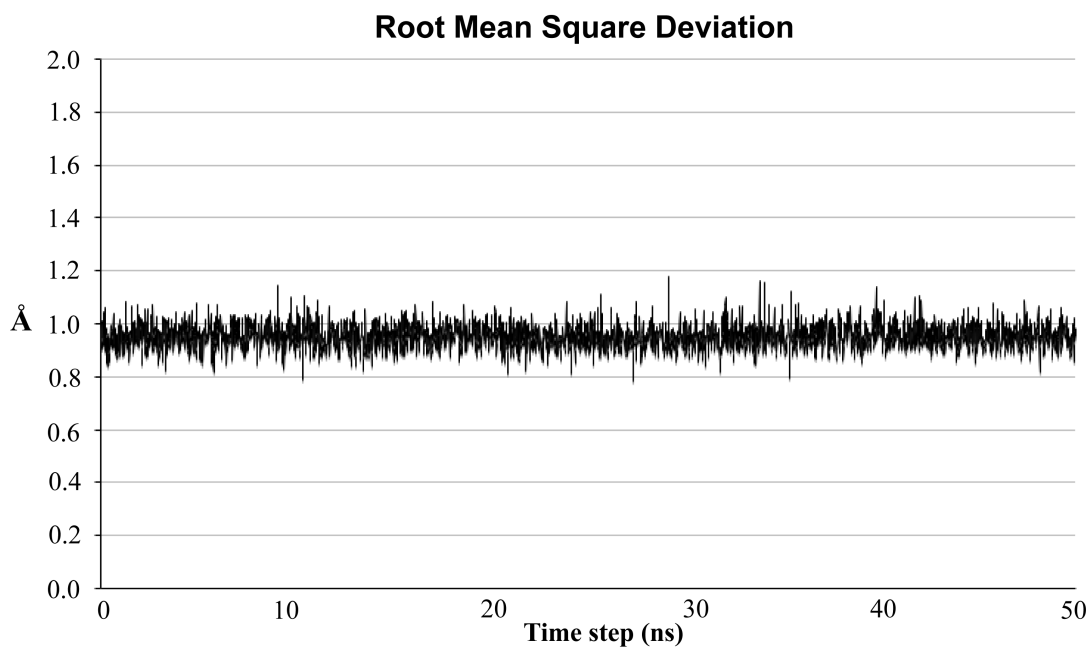


**Figure 4.7.** Structural information related with the equilibration of the systems for the MD simulations. Plotted is the root mean square deviation (RMSD) for the entire system as a function of time step. All-atom MD simulations were carried out in the absence of solvent at 25 °C. The temperature was controlled using Langevin dynamics. The time step of the simulations was 0.5 fs and the length of the simulations was 50 ns.

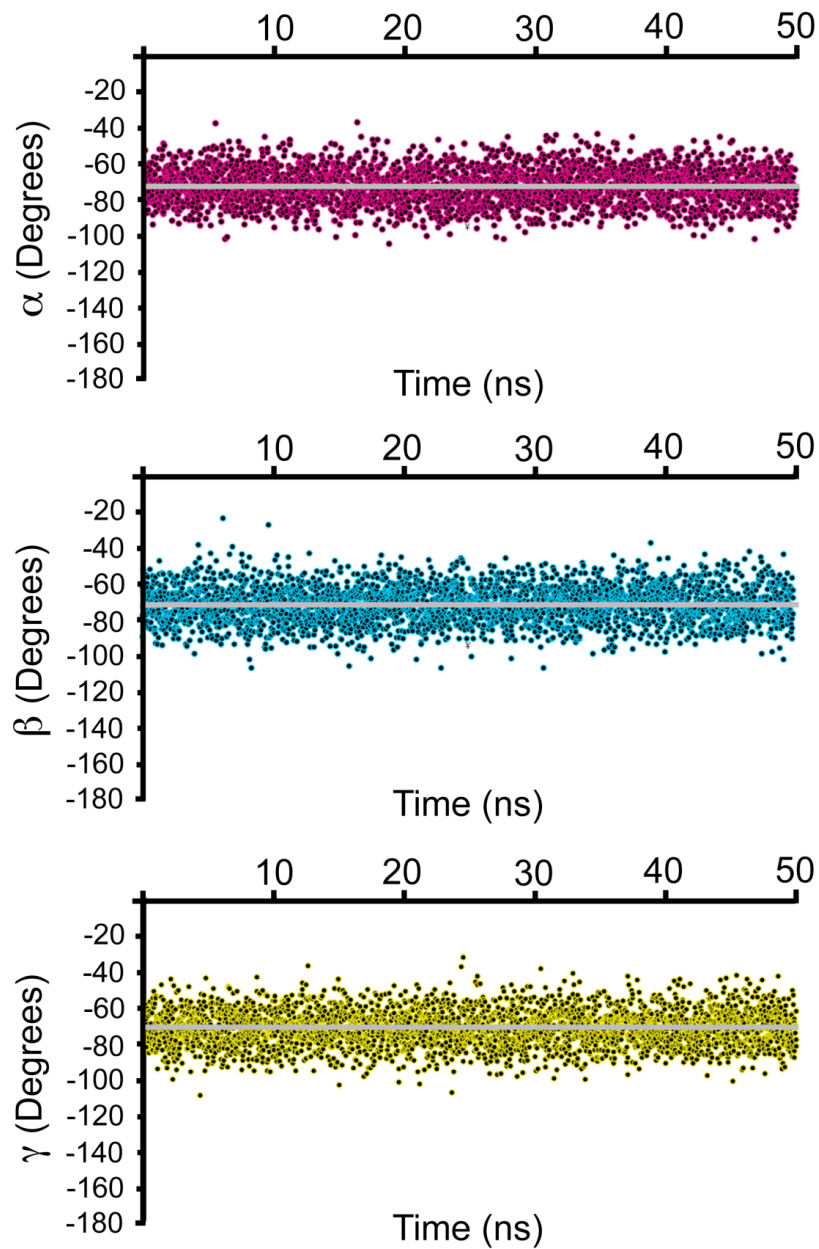


**Figure 4.8.** Plots of the fluctuations in the dihedral angles involving the *p*-phenylene rings in one of the enantiomers of **5** as observed in the molecular dynamics simulations. These three dihedral angles defined as:  $\alpha \equiv N1-C16-C13-C14$ ,  $\beta \equiv N1-C32-C29-C30$  and  $\gamma \equiv N1-C48-C45-C44$ . As mentioned in the main text, the mean and SD values are  $\alpha = -72.3^\circ \pm 10^\circ$ ,  $\beta = -71.8^\circ \pm 10^\circ$  and  $\gamma = -72.8^\circ \pm 10^\circ$ .

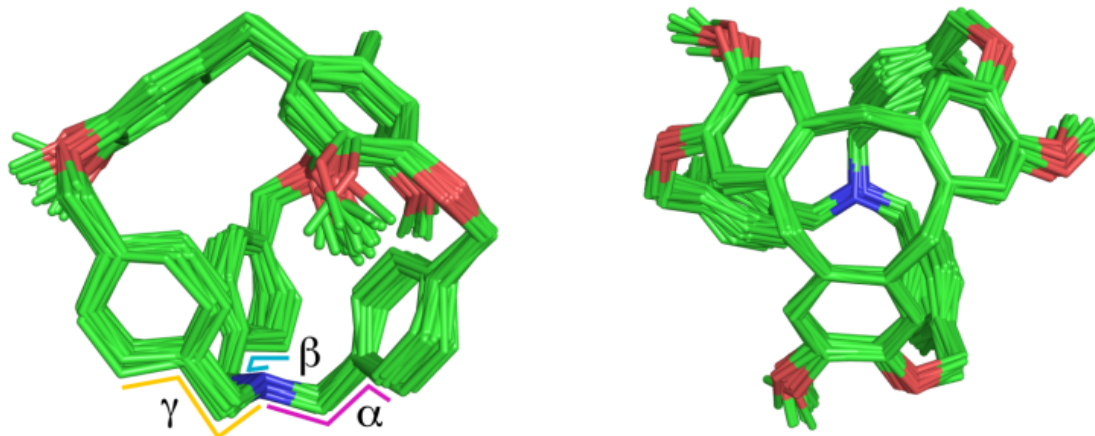


**Figure 4.9.** Orthogonal views of 30 superimposed structures from the MD simulation of **5**. The dihedral angles are indicated:  $\alpha$  (magenta),  $\beta$  (cyan) and  $\gamma$  (yellow).

To investigate further the *p*-phenylene rotation and interactions among the rotators, the crystal structure of **5** was minimized, and the dihedral angle  $\alpha$  was systematically varied (Figure 4.10). The structure was then relaxed via energy minimization, constraining the coordinates of all atoms but those in the two remaining  $\beta$  and  $\gamma$  *p*-phenylene rings. The  $\beta$ -ring is essentially invariant during the rotation. The  $\gamma$ -ring only rotates at most  $19.7^\circ$  to accommodate the  $180^\circ$  rotation of the  $\alpha$ -ring. An energy barrier arises due to the steric interaction between the  $\alpha$ -ring and  $\gamma$ -ring. Interestingly, the rotational energy barrier estimated from this simplistic and highly-constrained calculation ( $\sim 12 \text{ kcal mol}^{-1}$ ) is consistent with the experimental value inferred from the  $^1\text{H}$  VT-NMR experiments ( $\sim 10 \text{ kcal mol}^{-1}$ ). The modeling results suggest that, although not entirely independent, the rotations of the  $\alpha$ - and  $\gamma$ -rings are only weakly coupled.

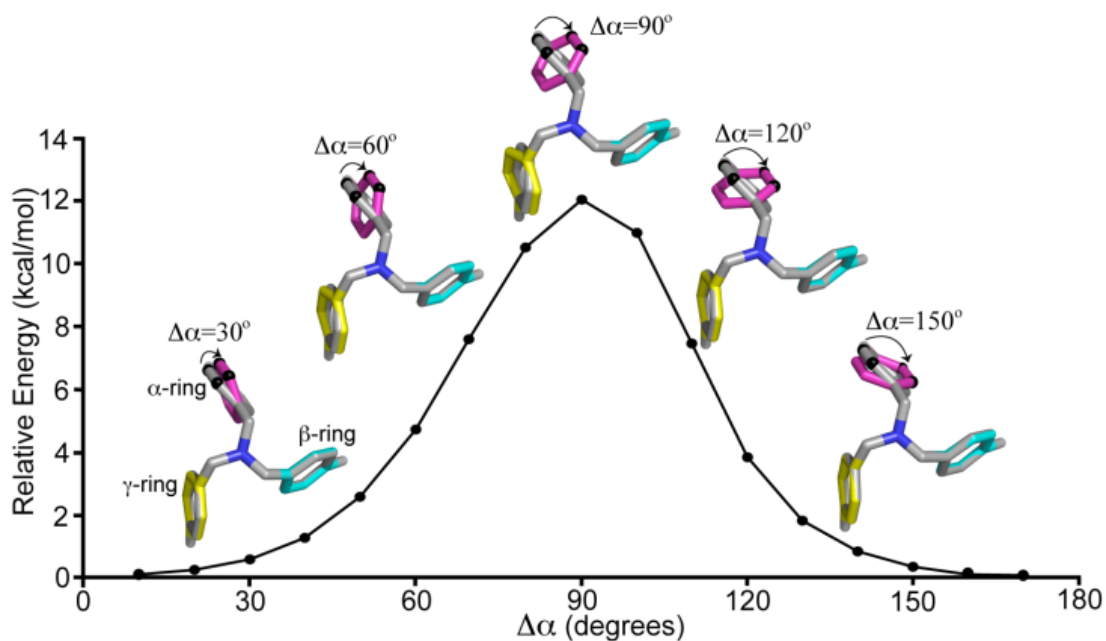


**Figure 4.10.** Minimized energy as a function of  $\Delta\alpha$ , which is rotation of the  $\alpha$  dihedral angle relative to the energy minimized X-ray structure (gray). The crystal structure of **5** was minimized, and the angle  $\alpha$  was varied in  $10^\circ$  increments, driving rotation of the  $\alpha$ -ring (magenta). For each value of  $\Delta\alpha$ , the structure was energy minimized, constraining the coordinates of all atoms but those in the two remaining *p*-phenylene rotators:  $\beta$ -ring (cyan) and  $\gamma$ -ring (yellow). For clarity: the CTV moiety and hydrogens are not shown; two carbons of the  $\alpha$ -ring are rendered black.



## CONCLUSIONS

In summary, a novel gyroscope-inspired tribenzylamine hemicyptophane **5** was synthesized in three steps in good overall yield using mild conditions. This synthetic route offers the possibility of preparing hemicyptophanes with multiple, proximate rotators, where the molecular properties of the rotators can be varied by changing the length and composition of the linkers used to cyclize the “gyroscope scaffold intermediate” **4**. The compact size of the cavity in this system helps to avoid the inclusion of solvent and gaseous molecules that have the potential to inhibit rotation.  $^1\text{H}$  VT-NMR data indicate a critical temperature for the onset of rotation on the sub-millisecond time scale and a hindered, dynamic motion of these three rotators at room temperature. The desired rigidity of the CTV stator and the rotator properties of the *p*-phenylenes were corroborated by  $^1\text{H}$  VT-NMR spectroscopy and MD simulations. As a *p*-phenylene ring rotates, it encounters one of the neighboring *p*-phenylenes, leading to a steric barrier that hinders rotation. Rotation of the rings appears not to be strongly correlated with one another.

The compact size and molecular motions of **5** make it a compelling initial motif from which to engineer unidirectional, potentially coupled rotators for molecular locomotion or transmitting torque. Towards this goal, it may be possible to introduce sterically bulky substituents on the linkers to control the temperatures at which rotation becomes accessible and to favor one direction of rotation. Different substituent groups can also be introduced to create a dipole moment on the rotators, thereby allowing the use of electric

fields to explore rapid conformational response in these systems and to control the direction of rotation.

## EXPERIMENTAL PROCEDURES

**Reagents.** All reactions were carried out in oven-dried glassware under an atmosphere of dry nitrogen. Column chromatography was performed using 60 Å porosity, 40-75 µm particle size silica gel from Sorbent Technologies. Thin layer chromatography (TLC) was performed using silica gel plates with UV light at 254 nm for detection. <sup>1</sup>H NMR (360 and 500 MHz) and <sup>13</sup>C NMR (125 MHz) spectra were acquired on Bruker DMX 360 and AMX 500 spectrometers. Electrospray ionization (ESI) mass spectrometry was performed in high-resolution mode on a Micromass Autospec instrument. All reagents were commercially available and used without further purification, unless otherwise stated.

**[4-(4(bromomethyl)benzyl)oxy-3-methoxyphenyl]methanol (3).** A mixture of vanillyl alcohol **1** (2.5091 g, 16.276 mmol, 1.0 equiv.), dibromo-*p*-xylene **2** (6.4033 g, 24.259 mmol, 1.5 equiv.), and K<sub>2</sub>CO<sub>3</sub> (2.2511 g, 16.288 mmol, 1.0 equiv.) dissolved in acetone (24.0 mL, 0.786 g/mL, 18.9 g) was heated at 70 °C overnight with stirring. The reaction solvent was removed by rotary evaporation. The resulting residue was rinsed in a separatory funnel with a 1:1 mixture of H<sub>2</sub>O (60 mL) and CH<sub>2</sub>Cl<sub>2</sub> (60 mL). The phases were separated and the aqueous layer extracted three times with CH<sub>2</sub>Cl<sub>2</sub> (100 mL). The combined organic layer was washed once with 1 M NaOH (100 mL) and once with saturated NaCl (100 mL). The organic layer was dried over MgSO<sub>4</sub>, filtered, and evaporated under reduced pressure. The crude material was purified by silica gel column chromatography (5:95 Acetone:CH<sub>2</sub>Cl<sub>2</sub> → 20:80 Acetone:CH<sub>2</sub>Cl<sub>2</sub>) to give **3** as white powder (3.5422 g, 65%): m.p. 86-88 °C; <sup>1</sup>H NMR (500 MHz, CDCl<sub>3</sub>, 25 °C) δ = 7.42-

7.38 (m, 4H), 6.96 (s, 1H), 6.85-6.81 (m, 2H), 5.14 (s, 2H), 4.60 (s, 2H), 4.49 (s, 2H), 3.89 (s, 3H), 1.86 (s, 1H);  $^{13}\text{C}$  NMR (125 MHz,  $\text{CDCl}_3$ , 25 °C)  $\delta$  = 149.9, 147.6, 137.6, 137.5, 134.5, 129.4, 127.7, 119.4, 114.1, 111.1, 70.8, 65.4, 56.1, 33.36; HRMS (ESI) calculated for  $\text{C}_{16}\text{H}_{17}\text{BrO}_3$  ( $\text{M}+\text{Na}^+$ ) 359.0259; found 359.0239.

**2,7,12-Tris-(4-bromomethylbenzyloxy)-3,8,13-trimethoxy-10,15-dihydro-5H**

**tribenzo[a,d,g]cyclononene (4).** A mixture of **3** (2.0232 g, 6.0210 mmol, 1.0 equiv.) and  $\text{Sc}(\text{OTf})_3$  (0.0295 g, 0.0599 mmol, 0.01 equiv.) dissolved in MeCN (5.9 mL, 0.786 g/mL, 4.7 g) was heated at 65 °C overnight with stirring. The reaction solvent was removed by rotary evaporation. The resulting residue was extracted twice with  $\text{CH}_2\text{Cl}_2$  (150 mL) and washed three times with sat. NaCl (150 mL). The organic layer was dried over anhydrous  $\text{MgSO}_4$ , filtered, and evaporated under reduced pressure. The crude material was purified by silica gel column chromatography ( $\text{CH}_2\text{Cl}_2 \rightarrow 2:98$  THF: $\text{CH}_2\text{Cl}_2$ ) to give **4** as white powder (0.5571 g, 29%): m.p. 91-93 °C;  $^1\text{H}$  NMR (360 MHz,  $\text{CDCl}_3$ , 25 °C)  $\delta$  = 7.39-7.37 (m, 12H), 6.85 (s, 3H), 6.72 (s, 3H), 5.09 (s, 6H), 4.73 (d, 3H,  $J$  = 13.7 Hz), 4.50 (s, 6H), 3.76 (s, 9H), 3.50 (d, 3H,  $J$  = 13.8 Hz);  $^{13}\text{C}$  NMR (125 Hz,  $\text{CDCl}_3$ , 25 °C)  $\delta$  = 148.6, 147.2, 137.9, 137.5, 132.9, 131.9, 129.4, 127.6, 116.4, 114.0, 71.4, 56.4, 36.6, 33.3; HRMS (ESI) calculated for  $\text{C}_{48}\text{H}_{45}\text{Br}_3\text{O}_6$  ( $\text{M}^+$ ) 954.0766; found 954.0724. The NMR spectra matched the reported literature data.<sup>68</sup>

**Tribenzylamine Hemicryptophane (5).** A mixture of **4** (0.0406 g, 0.0426 mmol, 1.0 equiv.) and  $\text{K}_2\text{CO}_3$  (0.0869 g, 0.629 mmol, 15.0 equiv.) dissolved in MeCN (58 mL, 0.786 g/mL, 46 g) was heated at 90 °C with stirring as 7 N  $\text{NH}_3$  in MeOH (0.0711 mL of

7 N NH<sub>3</sub>, 0.5 mmol, ~12 equiv., in 4.7 mL of MeCN) was added by a syringe pump over 8 h. The reaction solvent was removed by rotary evaporation. The resulting residue was extracted with CH<sub>2</sub>Cl<sub>2</sub> and transferred to a separatory funnel. The organic layer was washed once with a 1:1 mixture of H<sub>2</sub>O (50 mL) and 1 M NaOH (50 mL) and then with 1 M NaOH (50 mL). The aqueous layer was extracted with CH<sub>2</sub>Cl<sub>2</sub> (50 mL) and the combined organic layer was washed with sat. NaCl (50 mL). The organic layer was dried over anhydrous MgSO<sub>4</sub>, filtered, and evaporated under reduced pressure. The crude material was purified by silica gel column chromatography (50:50 CH<sub>2</sub>Cl<sub>2</sub>: hexanes → 50:40:10 CH<sub>2</sub>Cl<sub>2</sub>: hexanes: EtOAc → 60:30:10 CH<sub>2</sub>Cl<sub>2</sub>: hexanes: EtOAc; all with 1% TEA) to give **5** as a white powder (0.0206g, 67%): m.p. (*decom.*) > 250 °C; <sup>1</sup>H NMR (360 MHz, CDCl<sub>3</sub>, 25 °C) δ = 7.34 (s, 3H), 6.96-6.93 (m, 9H), 6.18 (d, 6H, *J* = 7.9 Hz), 5.41 (d, 3H, *J* = 12.1 Hz), 5.06 (d, 3H, *J* = 12.2 Hz), 4.83 (d, 3H, *J* = 13.7 Hz), 3.60 (d, 3H, *J* = 13.8 Hz), 3.58 (s, 9H), 3.54 (d, 3H, *J* = 13.2 Hz), 3.41 (d, 3H, *J* = 13.2 Hz); <sup>13</sup>C NMR (125 MHz, CDCl<sub>3</sub>, 25 °C) δ = 147.7, 143.0, 140.3, 132.9, 131.7, 130.8, 128.4, 127.4, 117.9, 113.9, 68.8, 55.5, 55.3, 34.9; HRMS (ESI) calculated for C<sub>48</sub>H<sub>45</sub>NO<sub>6</sub> (M+H<sup>+</sup>) 732.3326; found 732.3340.

**Crystal growth and X-ray crystallography.** Compound **5** was crystallized by vapor diffusion of diethyl ether or *n*-pentane into toluene. It crystallizes in the monoclinic space group  $P2_1/c$  (systematic absences  $0k0$ :  $k = \text{odd}$  and  $h0l$ :  $l = \text{odd}$ ) with  $a = 17.098(2) \text{ \AA}$ ,  $b = 11.4592(9) \text{ \AA}$ ,  $c = 21.096(2) \text{ \AA}$ ,  $\beta = 113.539(2)^\circ$ ,  $V = 3789.3(6) \text{ \AA}^3$ ,  $Z = 4$  and  $d_{\text{calc}} = 1.283 \text{ g/cm}^3$ . X-ray intensity data were collected on a Rigaku Mercury CCD area detector employing graphite-monochromated Mo- $K_\alpha$  radiation ( $\lambda = 0.71073 \text{ \AA}$ ) at a temperature of  $-130 \text{ }^\circ\text{C}$ . Preliminary indexing was performed from a series of twelve  $0.5^\circ$  rotation images with exposures of 30 s. A total of 336 rotation images were collected with a crystal to detector distance of 35 mm, a  $2\theta$  swing angle of  $-12^\circ$ , rotation widths of  $0.5^\circ$  and exposures of 10 s: scan no. 1 was a  $\phi$ -scan from  $170^\circ$  to  $338^\circ$  at  $\omega = 0^\circ$  and  $\chi = 0^\circ$ . Rotation images were processed using CrystalClear,<sup>69</sup> producing a listing of unaveraged  $F^2$  and  $\sigma(F^2)$  values which were then passed to the CrystalStructure<sup>70</sup> program package for further processing and structure solution on a Dell Pentium III computer. A total of 15571 reflections were measured over the ranges  $5.2 \leq 2\theta \leq 50.02^\circ$ ,  $-16 \leq h \leq 20$ ,  $-13 \leq k \leq 12$ ,  $-23 \leq l \leq 25$  yielding 6601 unique reflections ( $R_{\text{int}} = 0.0261$ ). The intensity data were corrected for Lorentz and polarization effects and for absorption using REQAB<sup>71</sup> (minimum and maximum transmission 0.853, 1.000).

The structure was solved by direct methods (SIR97).<sup>72</sup> Refinement was by full-matrix least squares based on  $F^2$  using SHELXL-97.<sup>73</sup> All reflections were used during refinement ( $F^2$  values that were experimentally negative were replaced by  $F^2 = 0$ ). The weighting scheme used was  $w = 1/[\sigma^2(F_o^2) + 0.0547P^2 + 0.9350P]$  where  $P = (F_o^2 + 2F_c^2)/3$ . Non-hydrogen atoms were refined anisotropically and hydrogen atoms were refined

using a "riding" model. Refinement converged to  $R_1 = 0.0479$  and  $wR_2 = 0.1107$  for 5502 reflections for which  $F > 4s(F)$  and  $R_1 = 0.0599$ ,  $wR_2 = 0.1204$  and  $GOF = 1.078$  for all 6601 unique, non-zero reflections and 500 variables ( $R_1 = \sum ||F_o| - |F_c|| / \sum |F_o|$ ;  $wR_2 = \{\sum w (F_o^2 - F_c^2)^2 / \sum w(F_o^2)^2\}^{1/2}$ ;  $GOF = \{\sum w (F_o^2 - F_c^2)^2 / (n - p)\}^{1/2}$  where  $n$  = the number of reflections and  $p$  = the number of parameters refined). The maximum  $\Delta/\sigma$  in the final cycle of least squares was 0.001 and the two most prominent peaks in the final difference Fourier were +0.173 and -0.253 e/Å<sup>3</sup>.

**Calculating from  $^1\text{H}$  VT-NMR data the energy barrier for *p*-phenylene rotation.**

Equation 1 was used to determine the *p*-phenylene rotation rate at the coalescence temperature:

$$k = \frac{\pi\Delta\nu_0}{\sqrt{2}} \quad (1)$$

where  $k$  is the rate coefficient,  $\Delta\nu_0 = \nu_A - \nu_B$  is the chemical shift difference (in Hz) between the two separate signals at slow exchange (in this case at  $-93\text{ }^\circ\text{C}$  or 180 K). The Arrhenius equation (2) was used to determine the activation energy,  $E_a$ , at the coalescence temperature,  $T$  (in K):

$$\ln(k / \text{Hz}) = -\frac{E_a}{R} \left( \frac{1}{T} \right) + \ln(A / \text{Hz}) \quad (2)$$

where  $A$  is the pre-exponential factor and  $R$  is the universal gas constant.<sup>66</sup>



**Computational methods.** All-atom MD simulations were carried out using NAMD2.<sup>64</sup> The internal bonded parameters were obtained from AMBER-94<sup>74</sup> and the nonbonded parameters were proposed in previous studies.<sup>75-79</sup> Simulations were performed in the absence of solvent at 25 °C and temperature was controlled using Langevin dynamics with a damping coefficient of 5 ps<sup>-1</sup>. The time step of the simulations was 0.5 fs. Relaxation calculations using energy minimization consist of up to 10,000 steps of the conjugate gradient algorithm as implemented in NAMD2; energy was monitored to confirm minimization.<sup>64</sup>

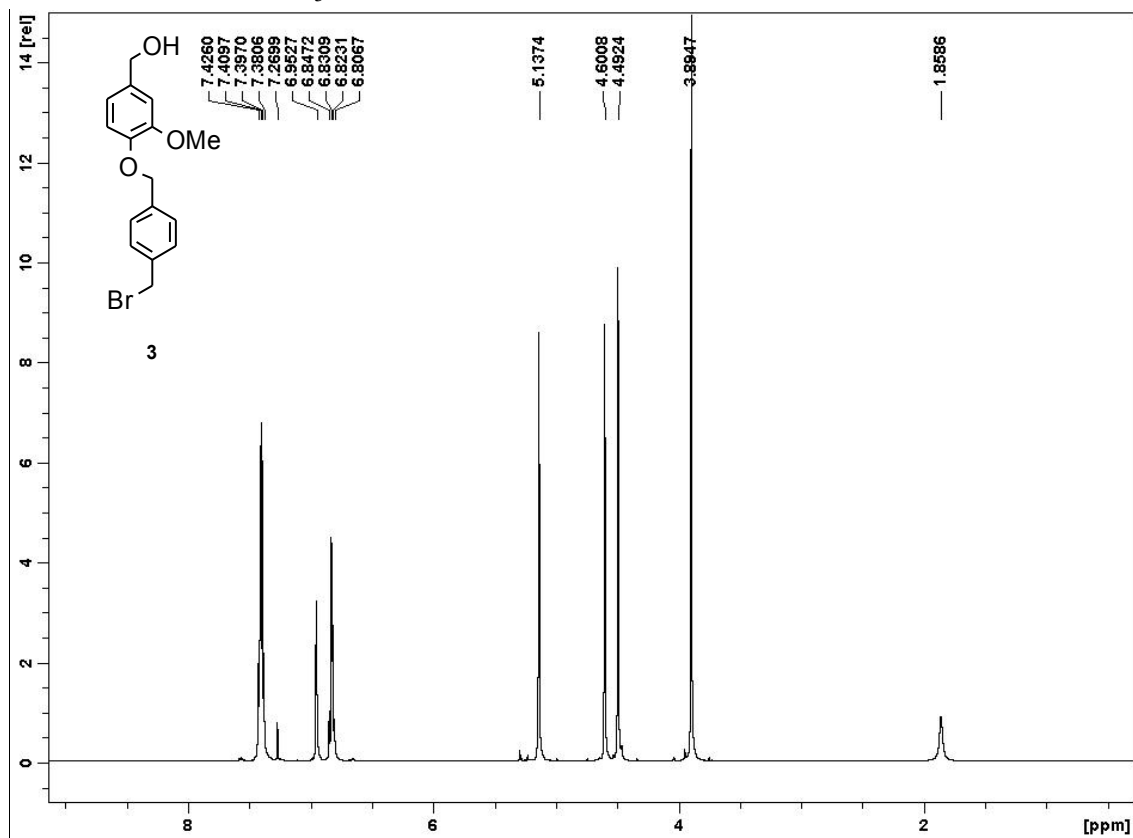
GRASP<sup>65</sup> was employed to investigate a potential interior cavity within **5**. Different conformations were generated by manual rotations of the three *p*-phenylenes. The rotations were systematically performed in 10° increments using one of the crystal structures of **5** as reference. A probe radius of 1.4 Å was used for all calculations.

## **$^1\text{H}$ NMR and $^{129}\text{Xe}$ NMR experiments to determine the binding of He, H<sub>2</sub>, N<sub>2</sub> and Xe to hemicryptophane 5**

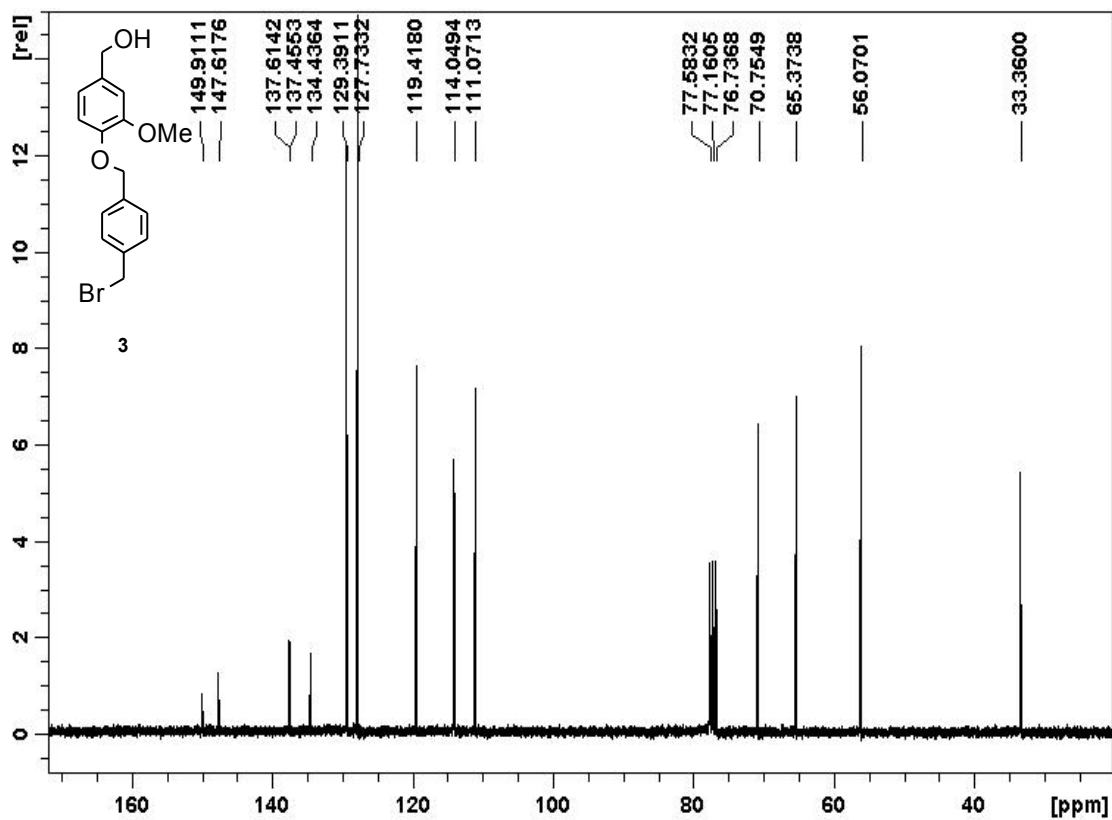
To conduct NMR experiments, 0.0005 g (0.0007 mmol) of hemicryptophane was dissolved in 500  $\mu\text{L}$  of  $\text{CDCl}_3$  or  $\text{CH}_2\text{Cl}_2$  to provide a final concentration  $\sim 1.4$  mM. In order to determine encapsulation for He, H<sub>2</sub> and N<sub>2</sub>,  $^1\text{H}$  NMR experiments were performed. For Xe, a hyperpolarized  $^{129}\text{Xe}$  NMR spectrum was collected. For detailed Experimental procedures for hyperpolarized  $^{129}\text{Xe}$  NMR spectroscopy, please refer to the Supporting Information in Chambers et al.<sup>19</sup> For these NMR experiments, the hemicryptophane solution was loaded into a 5-mm stopcock-sealable NMR tube. The samples were degassed using the freeze-pump-thaw method. The gas (e.g., He, H<sub>2</sub>, N<sub>2</sub>) was then bubbled into the sample tube for a few minutes, sealed, shaken and allowed to equilibrate for 1, 3, 24 and 48 h. Hyperpolarized  $^{129}\text{Xe}$  NMR spectra were collected in the minutes following bubbling with hyperpolarized  $^{129}\text{Xe}$ .

No evidence of binding was observed for He, H<sub>2</sub>, N<sub>2</sub> or Xe due to the absence of spectral changes in the  $^1\text{H}$  and  $^{129}\text{Xe}$  NMR spectra when each of these gases was introduced.  $^1\text{H}$  variable temperature (VT) NMR spectroscopy was also performed for He, H<sub>2</sub>, and N<sub>2</sub> at temperatures ranging from  $-93$   $^\circ\text{C}$  to  $47$   $^\circ\text{C}$ . None of these spectra indicated binding even at the lowest temperature, further confirming that these gas molecules were not encapsulated by the hemicryptophane.

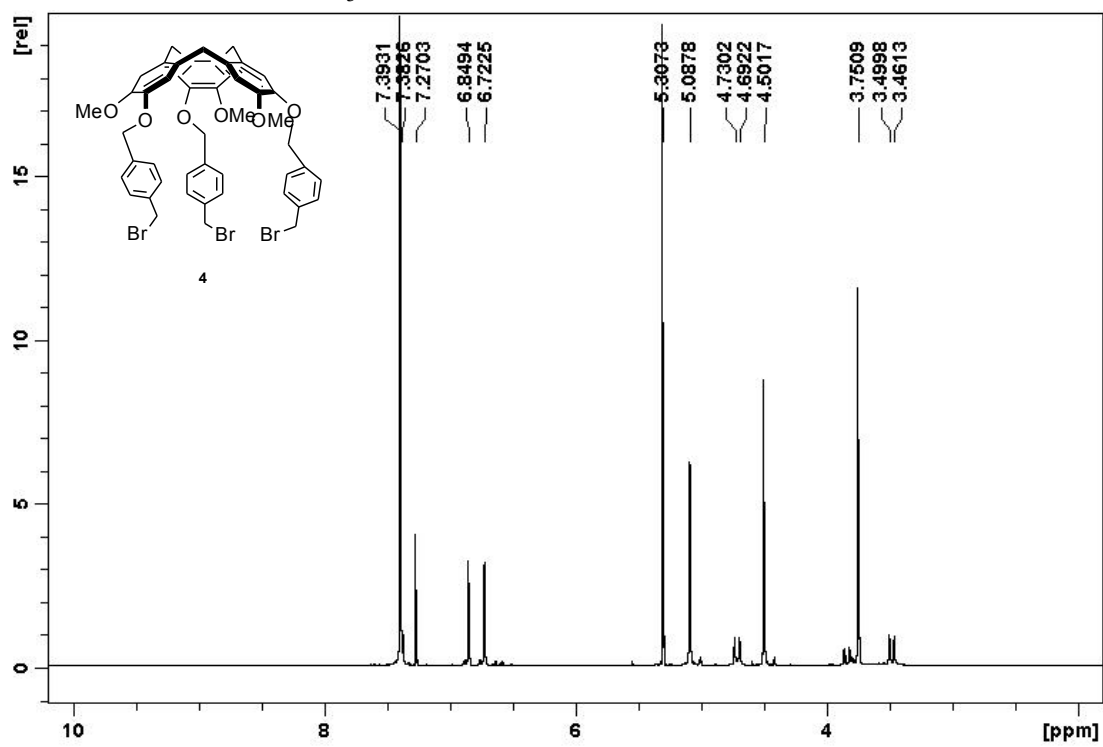
$^1\text{H}$  NMR of **3** in  $\text{CDCl}_3$  at  $25^\circ\text{C}$



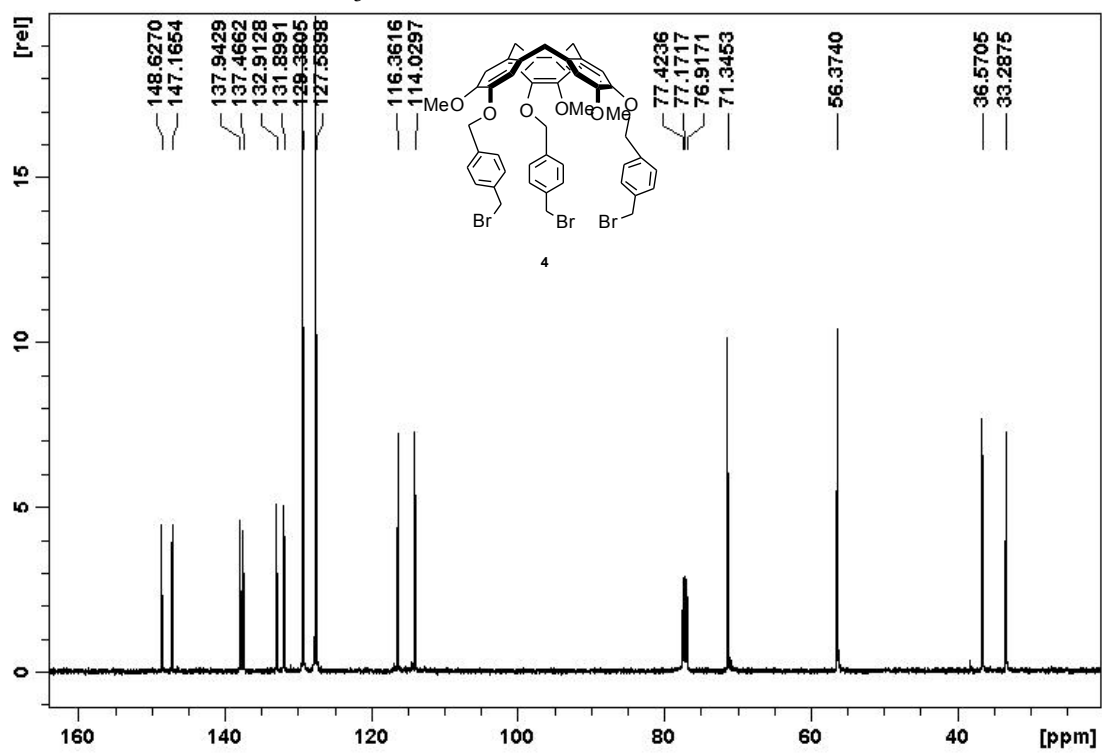
$^{13}\text{C}$  NMR of **3** in  $\text{CDCl}_3$  at  $25^\circ\text{C}$



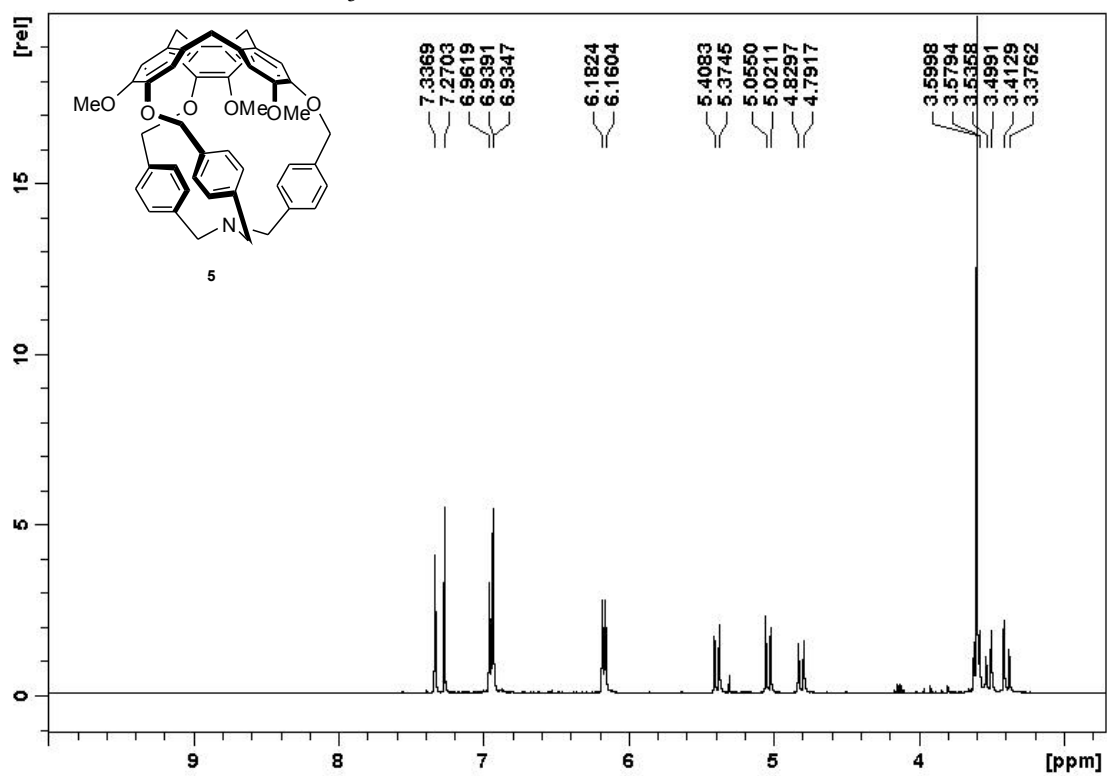
<sup>1</sup>H NMR of **4** in CDCl<sub>3</sub> at 25 °C



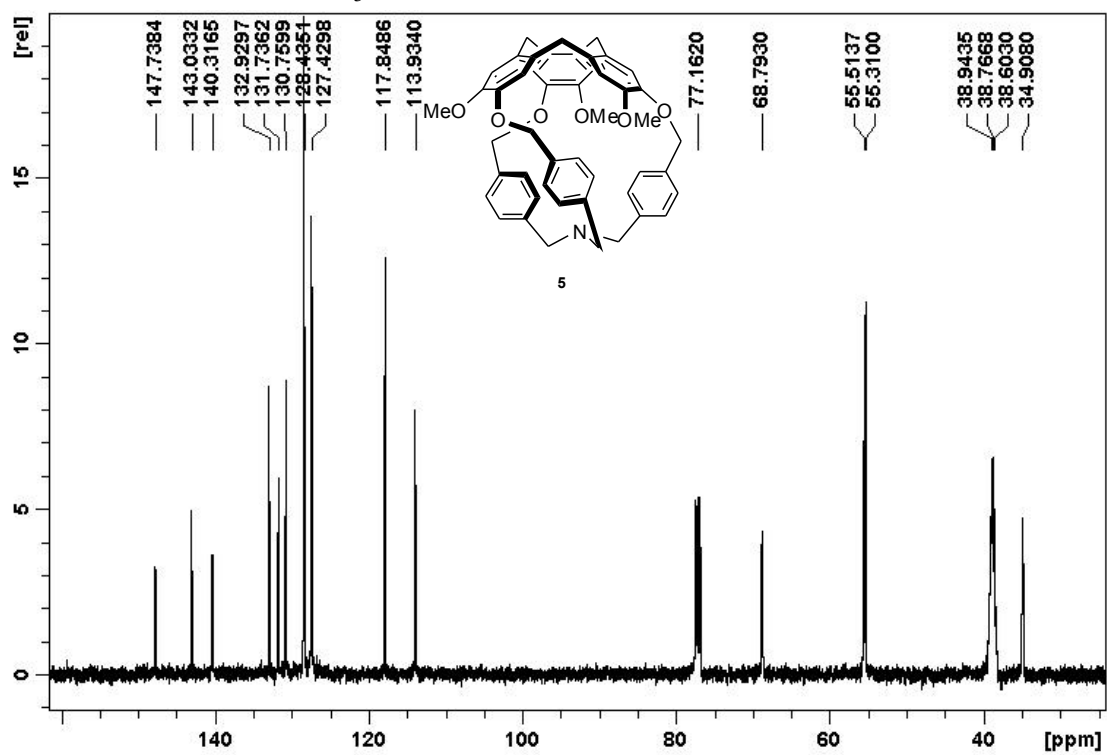
$^{13}\text{C}$  NMR of 4 in  $\text{CDCl}_3$  at 25 °C



<sup>1</sup>H NMR of **5** in CDCl<sub>3</sub> at 25 °C



$^{13}\text{C}$  NMR of **5** in  $\text{CDCl}_3$  at  $25^\circ\text{C}$





## **ACKNOWLEDGEMENTS**

I.J.D. appreciates support from the DOD (W81XWH-04-1-0657), NIH (CA110104), NSF (CHE-0840438), a Camille and Henry Dreyfus Teacher-Scholar Award, and UPenn Chemistry Department. J.G.S. acknowledges support from NSF (DMR08-32802). We thank Laura Spece for her early contributions to this work. Molecular structures in Figures 4.2, 4.3, 4.4, 4.9 and 4.10 were generated using PyMOL.<sup>80</sup>

## **AUTHOR CONTRIBUTIONS**

N.S.K. and J. M. P-A. co-wrote the manuscript. N.S.K. and T. K. synthesized and characterized the reported compounds. N.S.K. performed the <sup>1</sup>H VT-NMR, NOESY and NMR binding experiments. J. M. P-A. performed the molecular dynamic simulation calculations and O-S. L. performed initial computational studies. P.A.H. crystallized compound **5** while and O.T. helped synthesize precursors. I.J.D. initiated this project and co-edited the manuscript with J. S.

## REFERENCES

- (1) Boyer, P. D. *Biosci. Rep.* **1998**, *18*, 97-117.
- (2) Elston, T.; Wang, H.; Oster, G. *Nature* **1998**, *391*, 510-513.
- (3) Kelly, T. R.; Sestelo, J. P. *Struct. Bond.* **2001**, *99*, 19-53.
- (4) Nakanishi-Matsui, M.; Sekiya, M.; Nakamoto, R. K.; Futai, M. *Biochim. Biophys. Acta.* **2010**, *1797*, 1343-1352.
- (5) Rice, S.; Lin, A. W.; Safer, D.; Hart, C. L.; Naber, N.; Carragher, B. O.; Cain, S. M.; Pechatnikova, E.; Wilson-Kubalek, E. M.; Whittaker, M.; Pate, E.; Cooke, R.; Taylor, E. W.; Milligan, R. A.; Vale, R. D. *Nature* **1999**, *402*, 778-784.
- (6) Sindelar, C. V.; Downing, K. H. *Proc. Natl. Acad. Sci. U.S.A.* **2010**, *107*, 4111-4116.
- (7) Terashima, H.; Kojima, S.; Homma, M. *Int. Rev. Cell. Mol. Biol.* **2008**, *270*, 39-85.
- (8) Woolley, D. M. *Biol. Rev. Camb. Philos. Soc.* **2010**, *85*, 453-470.
- (9) Kay, E. R.; Leigh, D. A.; Zerbetto, F. *Angew. Chem. Int. Ed. Engl.* **2007**, *46*, 72-191.
- (10) Day, A. I.; Blanch, R. J.; Arnold, A. P.; Lorenzo, S.; Lewis, G. R.; Dance, I. *Angew. Chem. Int. Ed. Engl.* **2002**, *41*, 275-277.
- (11) Garcia-Garibay, M. A. *Proc. Natl. Acad. Sci. U. S. A* **2005**, *102*, 10771-10776.
- (12) Iwamura, H.; Mislou, K. *Acc. Chem. Res.* **1988**, *21*, 175-182.
- (13) Michl, J.; Sykes, C. H. *ACS Nano.* **2009**, *3*, 1042-1048.

- (14) Skopek, K.; Hershberger, M. C.; Gladysz, J. A. *Coord. Chem. Rev.* **2007**, *251*, 1723-1733.
- (15) Karlen, S. D.; Godinez, C. E.; Garcia-Garibay, M. A. *Org. Lett.* **2006**, *8*, 3417-3420.
- (16) Bartik K, L. M., Dutasta JP, Collet A, Reisse J. *J. Am. Chem. Soc.* **1998**, *120*, 784-791.
- (17) Brotin, T.; Dutasta, J. P. *Eur. J. Org. Chem.* **2003**, *6*, 973-984.
- (18) Brotin, T.; Roy, V.; Dutasta, J. P. *J. Org. Chem.* **2005**, *70*, 6187-6195.
- (19) Chambers, J. M.; Hill, P. A.; Aaron, J. A.; Han, Z.; Christianson, D. W.; Kuzma, N. N.; Dmochowski, I. J. *J. Am. Chem. Soc.* **2009**, *131*, 563-569.
- (20) Collet, A. *Comp. Supramol. Chem.* **2** **1996**, 325-365.
- (21) Fogarty, H. A.; Berthault, P.; Brotin, T.; Huber, G.; Desvaux, H.; Dutasta, J. P. *J. Am. Chem. Soc.* **2007**, *129*, 10332-10333.
- (22) Gautier, A.; Mulatier, J. C.; Crassous, J.; Dutasta, J. P. *Org. Lett.* **2005**, *7*, 1207-1210.
- (23) Gosse, I.; Dutasta, J. P.; Perrin, M.; Thozet, A. *New J. Chem.* **1999**, *23*, 545-548.
- (24) Hill, P. A.; Wei, Q.; Eckenhoff, R. G.; Dmochowski, I. J. *J. Am. Chem. Soc.* **2007**, *129*, 9262-9263.
- (25) Hill, P. A.; Wei, Q.; Troxler, T.; Dmochowski, I. J. *J. Am. Chem. Soc.* **2009**, *131*, 3069-3077.
- (26) Martinez, A.; Robert, V.; Gornitzka, H.; Dutasta, J. P. *Chem. Eur. J.* **2010**, *16*, 520-527.

- (27) Mynar, J. L.; Lowery, T. J.; Wemmer, D. E.; Pines, A.; Frechet, J. M. J. *Am. Chem. Soc.* **2006**, *128*, 6334-6335.
- (28) Schlundt, A.; Kilian, W.; Beyermann, M.; Sticht, J.; Guenther, S.; Höpner, S.; Falk, K.; Roetzschke, O.; Mitschang, L.; Freund, C. *Angew. Chem.* **2009**, *121*, 4206-4209.
- (29) Seward, G. K.; Wei, Q.; Dmochowski, I. J. *Bioconjug. Chem.* **2008**, *19*, 2129-2135.
- (30) Spence, M. M.; Rubin, S. M.; Dimitrov, I. E. *Proc. Nat. Acad. Sci. U.S.A.* **2001**, *98*, 10654-10657.
- (31) Wei, Q.; Seward, G. K.; Hill, P. A.; Patton, B.; Dimitrov, I. E.; Kuzma, N. N.; Dmochowski, I. J. *J. Am. Chem. Soc.* **2006**, *128*, 13274-13283.
- (32) Hardie, M. J. *Chem. Soc. Rev.* **2010**, *39*, 516-527.
- (33) Kottas, G. S.; Clarke, L. I.; Horinek, D.; Michl, J. *Chem. Rev.* **2005**, *105*, 1281-1376.
- (34) Moore, J. S.; Bedard, T. C. *J. Am. Chem. Soc.* **1995**, *117*, 10662-10671.
- (35) Cizmeciyan, D.; Yonutas, H.; Karlen, S. D.; Garcia-Garibay, M. A. *Solid. State Nucl. Magn. Reson.* **2005**, *28*, 1-8.
- (36) Dominguez, Z.; Dang, H.; Strouse, M. J.; Garcia-Garibay, M. A. *J. Am. Chem. Soc.* **2002**, *124*, 7719-7727.
- (37) Dominguez, Z.; Dang, H.; Strouse, M. J.; Garcia-Garibay, M. A. *J. Am. Chem. Soc.* **2002**, *124*, 2398-2399.
- (38) Dominguez, Z.; Khuong, T. A.; Dang, H.; Sanrame, C. N.; Nunez, J. E.; Garcia-Garibay, M. A. *J. Am. Chem. Soc.* **2003**, *125*, 8827-8837.

- (39) Garcia-Garibay, M. A. *Angew. Chem. Int. Ed. Engl.* **2007**, *46*, 8945-8947.
- (40) Garcia-Garibay, M. A. *Nat. Mater.* **2008**, *7*, 431-432.
- (41) Garcia-Garibay, M. A.; Dang, H. *Org. Biomol. Chem.* **2009**, *7*, 1106-1114.
- (42) Godinez, C. E.; Zepeda, G.; Garcia-Garibay, M. A. *J. Am. Chem. Soc.* **2002**, *124*, 4701-4707.
- (43) Godinez, C. E.; Zepeda, G.; Mortko, C. J.; Dang, H.; Garcia-Garibay, M. A. *J. Org. Chem.* **2004**, *69*, 1652-1662.
- (44) Gould, S. L.; Tranchemontagne, D.; Yaghi, O. M.; Garcia-Garibay, M. A. *J. Am. Chem. Soc.* **2008**, *130*, 3246-3247.
- (45) Jarowski, P. D.; Houk, K. N.; Garcia-Garibay, M. A. *J. Am. Chem. Soc.* **2007**, *129*, 3110-3117.
- (46) Karlen, S. D.; Garcia-Garibay, M. A. *Chem. Commun.* **2005**, 189-191.
- (47) Karlen, S. D.; Ortiz, R.; Chapman, O. L.; Garcia-Garibay, M. A. *J. Am. Chem. Soc.* **2005**, *127*, 6554-6555.
- (48) Khuong, T. A.; Dang, H.; Jarowski, P. D.; Maverick, E. F.; Garcia-Garibay, M. A. *J. Am. Chem. Soc.* **2007**, *129*, 839-845.
- (49) Khuong, T. A.; Nunez, J. E.; Godinez, C. E.; Garcia-Garibay, M. A. *Acc. Chem. Res.* **2006**, *39*, 413-422.
- (50) Kuzmanich, G.; Natarajan, A.; Chin, K. K.; Veerman, M.; Mortko, C. J.; Garcia-Garibay, M. A. *J. Am. Chem. Soc.* **2008**, *130*, 1140-1141.
- (51) Nunez, J. E.; Natarajan, A.; Khan, S. I.; Garcia-Garibay, M. A. *Org. Lett.* **2007**, *9*, 3559-3561.

- (52) O'Brien, Z. J.; Karlen, S. D.; Khan, S.; Garcia-Garibay, M. A. *J. Org. Chem.* **2010**, *75*, 2482-2491.
- (53) Rodriguez-Molina, B.; Ochoa, M. E.; Farfan, N.; Santillan, R.; Garcia-Garibay, M. A. *J. Org. Chem.* **2009**, *74*, 8554-8565.
- (54) Rodriguez-Molina, B.; Pozos, A.; Cruz, R.; Romero, M.; Flores, B.; Farfan, N.; Santillan, R.; Garcia-Garibay, M. A. *Org. Biomol. Chem.* **2010**, *8*, 2993-3000.
- (55) Nawara, A. J.; Shima, T.; Hampel, F.; Gladysz, J. A. *J. Am. Chem. Soc.* **2006**, *128*, 4962-4963.
- (56) Shima, T.; Hampel, F.; Gladysz, J. A. *Angew. Chem. Int. Ed. Engl.* **2004**, *43*, 5537-5540.
- (57) Skopek, K.; Barbasiewicz, M.; Hampel, F.; Gladysz, J. A. *Inorg. Chem.* **2008**, *47*, 3474-3476.
- (58) Wang, L.; Hampel, F.; Gladysz, J. A. *Angew. Chem. Int. Ed. Engl.* **2006**, *45*, 4372-4375.
- (59) Wang, L.; Shima, T.; Hampel, F.; Gladysz, J. A. *Chem. Commun.* **2006**, 4075-4077.
- (60) Kitagawa, H.; Kobori, Y.; Yamanaka, M.; Yoza, K.; Kobayashi, K. *Proc. Natl. Acad. Sci. U.S.A.* **2009**, *106*, 10444-10448.
- (61) Bondi, A. *J. Phys. Chem.* **1964**, *68*, 441-451.
- (62) Iwasaki, F.; Iwasaki, H. *Acta Cryst.*, **1972**, *B28*, 3370-3376.
- (63) Jorgensen, W. L.; Maxwell, D. S.; TiradoRives, J. *J. Am. Chem. Soc.* **1996**, *118*, 11225-11236.

- (64) Phillips, J. C.; Braun, R.; Wang, W.; Gumbart, J.; Tajkhorshid, E.; Villa, E.; Chipot, C.; Skeel, R. D.; Kale, L.; Schulten, K. *J. Comput. Chem.* **2005**, *26*, 1781-1802.
- (65) Nicholls, A.; Sharp, K. A.; Honig, B. *Proteins* **1991**, *11*, 281-296.
- (66) Sandstrom, J. *Dynamic NMR Spectroscopy*; Academic Press, 1983.
- (67) Setaka, W.; Ohmizu, S.; Kira, M. *Chem. Lett.* **2010**, *39*, 468-469.
- (68) van Strijdonck, G. P. F.; van Haare, J. A. E. H.; Hönen, P. J. M.; van den Schoor, R. C. G. M.; Feiters, M. C.; van der Linden, J. G. M.; Steggerdab, J. J.; Nolte, R. J. M. *J. Chem. Soc., Dalton Trans.* **1997**, 449-461.
- (69) CrystalClear *Rigaku Corporation* **1999**.
- (70) CrystalStructure *Rigaku Corporation* **2002**.
- (71) Jacobsen, R. A., REQAB4 (Personal Communication).
- (72) Altomare, A.; Burla, M.; Camalli, M.; Cascarano, G.; Giacovazzo, C.; Guagliardi, A.; Moliterni, A.; Polidori, G.; Spagn, R. *J. Appl. Cryst.* **1999**, *32*, 115-119.
- (73) Sheldrick, G. M. *University of Göttingen, Germany.* **1997**.
- (74) Cornell, W. D.; Cieplak, P.; Bayly, C. I.; Gould, I. R.; Merz, K. M.; Ferguson, D. M.; Spellmeyer, D. C.; Fox, T.; Caldwell, J. W.; Kollman, P. A. *J. Am. Chem. Soc.* **1995**, *117*, 5179-5197.
- (75) Kirchhoff, P. D.; Bass, M. B.; Hanks, B. A.; Briggs, J. M.; Collet, A.; McCammon, J. A. *J. Am. Chem. Soc.* **1996**, *118*, 3237-3246.
- (76) Kirchhoff, P. D.; Dutasta, J. P.; Collet, A.; McCammon, J. A. *J. Am. Chem. Soc.* **1997**, *119*, 8015-8022.

- (77) Kirchoff, P. D.; Dutasta, J. P.; Collet, A.; McCammon, J. A. *J. Am. Chem. Soc.* **1999**, *121*, 381-390.
- (78) Potter, M. J.; Kirchoff, P. D.; Carlson, H. A.; McCammon, J. A. *J. Comput. Chem.* **1999**, *20*, 956-970.
- (79) Rizzo, R. C.; Jorgensen, W. L. *J. Am. Chem. Soc.* **1999**, *121*, 4827-4836.
- (80) DeLano, W. L. *The PyMOL molecular graphics system* **2002**.



## CHAPTER 5: SUMMARY AND FUTURE DIRECTIONS

This thesis aimed to look at the role of cryptophanes and their derivatives in host-guest chemistry (Chapter 2),  $^{129}\text{Xe}$  NMR biosensing for early cancer detection (Chapter 3), and the emerging field of molecular devices (Chapter 4).

Chapter 2 focused on the development of a new water-soluble tris-(triazole)ethylamine cryptophane (TTEC) and its binding affinity for two noble gases: xenon and radon. TTEC was determined to be the tightest xenon binder to date ( $K_A = 42,000 \text{ M}^{-1}$  at 293 K in buffer). Preliminary computational studies by Lu Gao in the Saven lab predict that TTEC should have the strongest binding affinity for xenon, at least in part because it has the lowest occupancy of water molecules inside the cavity ( $\sim 0.5$ ) when compared to other anionic cryptophanes (e.g., Huber's hexaacid cryptophanes,<sup>1</sup> TAAC,<sup>2</sup> and TTPC).<sup>3</sup> Additionally, simulations showed that the other anionic cryptophanes had a higher population of sodium counter ions around them than TTEC. Since xenon binding requires interior water molecules and solvent cations to be displaced, this lower occupancy of both encourages tighter binding. TTEC also represents the first example of a discrete molecular species binding to radon. The radiometric binding assay developed is extremely versatile and can be used in future studies to determine the binding affinity of a wide variety of water-soluble hosts to radon. Since indoor accumulation of radon may cause a 5-31% increase in lung cancer risk per 100 Bq  $\text{m}^{-3}$  exposure,<sup>4</sup> it is important to understand how radon binding to specific biological molecules may lead to a higher incidence of cancer.

The promising diagnostic applications of  $^{129}\text{Xe}$  gas as a sensitive MRI contrast agent (outlined in Chapters 1 and 3) make the development of tighter xenon binders an important goal. Future studies could include the synthesis of water-soluble cryptophane-A or cryptophane-1.1.1. derivatives where anionic and cationic functional groups could be incorporated at varying distances from the cryptophane core. Because a cationic water-soluble cryptophane (TTEC) shows the highest affinity for xenon to date, this suggests that improved Xe binding may come from incorporating cationic amine groups closer to the cryptophane core (e.g., as in TAAC) or in a smaller host (e.g., cryptophane 1.1.1.). We have shown that the peripheral solubilizing groups can alter the entropic and enthalpic contributions along with the overall binding affinity of the host towards xenon. The kinetics of xenon binding are also extremely important for applications involving ultra-sensitive hyperpolarized  $^{129}\text{Xe}$  detection. These studies will be guided by computational calculations in collaboration with the Saven lab, and include considerations of cryptophane solvation, as well as interactions with cations and anions in solution. Moreover, we anticipate that generating related host molecules with larger dipole moments will lead to much higher xenon affinities. This was one motivation for the generation of hemicyptophanes that incorporate an electron-donating amine. The first-generation hemicyptophane of this type synthesized by our laboratory was too small and rigid to bind Xe but had other favorable physical properties, as described in Chapter 4.

The synthesis of cryptophanes with high binding affinities for xenon plays a central role in our lab's overall goal to develop  $^{129}\text{Xe}$  biosensors for early cancer detection (outlined in Chapter 3). A folate-conjugated xenon biosensor was developed in this thesis, which was readily soluble in water and was successfully delivered to cells overexpressing FR $\alpha$ . The biosensor showed a 10-fold selectivity for KB cells that overexpressed FR $\alpha$ , which is currently the highest level of selectivity reported by a cryptophane biosensor *in vitro*.

In an effort to synthesize a cocktail of biosensors that target a variety of medically relevant biomarkers for multiplexing purposes, integrin  $\alpha_v\beta_3$ -targeting cryptophane biosensors have been developed in our laboratory by Garry Seward.<sup>5,6</sup> Integrin  $\alpha_v\beta_3$  is an important biomarker as it has been shown to be associated with tumor angiogenesis and metastasis<sup>7,8</sup> and similar to the folate receptor, it is overexpressed in a large variety of tumor cells whereas expression is minimal in most normal tissues.<sup>9-11</sup> To target the integrin  $\alpha_v\beta_3$  receptors, the cryptophane was conjugated to a cyclic arginine–glycine–aspartic acid (RGD) moiety by a Huisgen [3+2] cycloaddition reaction. Additionally, to overcome solubility issues, two propionic acid groups were added to the two remaining propargyl groups on the cryptophane (Figure 5.1).<sup>5</sup> The biosensor was successfully delivered into cells and showed a 4-fold selectivity by flow cytometry towards cells overexpressing the targeted receptor.  $^{129}\text{Xe}$  NMR spectroscopy studies were performed and the biosensor indicated a shift of 4 ppm upon binding to the targeted protein.<sup>5</sup>

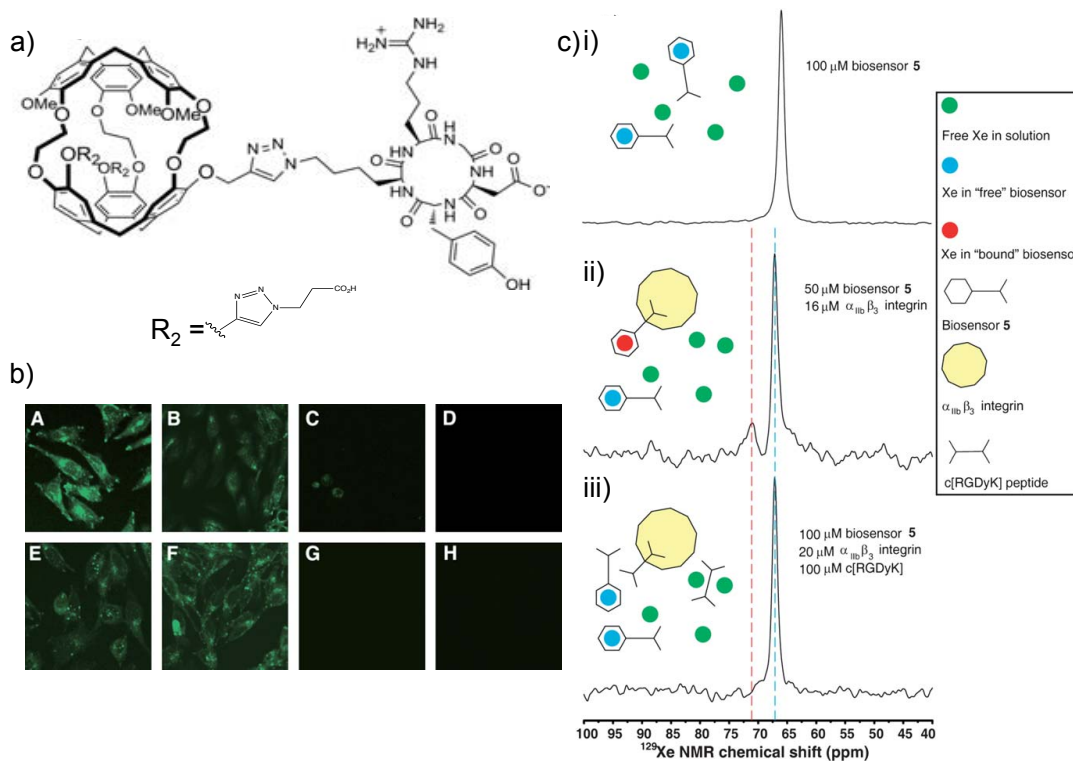


**Figure 5.1.** a) Chemical structure of the c[RGDyK]-labeled cryptophane biosensor, b) Uptake of 1  $\mu\text{M}$  Alexa Fluor 488-labeled c[RGDyK]-cryptophane targeting AsPC-1 cells (A–D) and HFL-1 cells (E–H); (A, E). Targeting of cryptophane was relatively unaffected by coincubation with 10 mM c[RADfK] (B, F). However, uptake was blocked by co-treatment with 10 mM c[RGDyK] peptide (C, G) and 10 mM anti- $\alpha_v$  antibody (D, H), c) Hyperpolarized  $^{129}\text{Xe}$  NMR spectra of i) biosensor alone ( $^{129}\text{Xe}$  NMR chemical shift at 65.8 ppm), ii) biosensor binding to  $\alpha_{IIb}\beta_3$  integrin; the “free” biosensor gave a  $^{129}\text{Xe}$  NMR chemical shift at 67.1 ppm, which was shifted 1.3 ppm downfield from “free” biosensor due to addition of glycerol while the “bound” biosensor appeared at 71.2 ppm, representing a 4.1 ppm downfield shift, iii) blocked by c[RGDyK]; “free” biosensor at the same  $^{129}\text{Xe}$  NMR chemical shift, but no “bound” biosensor was detected. Adapted from Seward et al.<sup>5</sup>

In an effort to perform similar binding experiments with the folate-conjugated xenon biosensor,  $^{129}\text{Xe}$  NMR spectroscopy methods with higher sensitivity need to be employed. In conventional hyperpolarized  $^{129}\text{Xe}$  NMR spectroscopy, most binding studies are performed at micromolar concentrations of cryptophane biosensor, however targets such as the folate binding protein (FBP) and integrin receptors tend to aggregate at such concentrations, which limits the utility of this approach. In recent years, an ultra-sensitive NMR technique called Hyper-CEST (hyperpolarized  $^{129}\text{Xe}$  chemical exchange saturation transfer) has been successfully utilized to detect 0.7 pM virus capsid with 125 cryptophanes attached (87 pM cryptophane equivalent).<sup>12</sup> Hyper-CEST is a technique that can amplify cryptophane cage-related magnetization by using a specific RF pulse that selectively saturates the biosensor-encapsulated Xe magnetization.<sup>13</sup> Following chemical exchange with the free Xe in solution, a high population of depolarized nuclei is accumulated.<sup>13</sup> After several cycles of continuous depolarization of the cage-related magnetization, the signal can be measured indirectly by calculating the difference between initial and final bulk (Xe in solution) magnetization.<sup>13</sup> Yubin Bai in our laboratory has been working on the detection of water-soluble cryptophanes at low concentrations using Hyper-CEST. Recently, we were able to detect TAAC at very low concentrations (1.4 pM), which sets the new lowest detectable concentration for cryptophanes using this technique. Therefore, the next step will involve optimizing the Hyper-CEST conditions and using it to detect NMR resonances produced as a result of the folate-conjugated cryptophane binding to the monomeric FBP at nanomolar or picomolar concentrations.

Another advancement in the use of hyperpolarized  $^{129}\text{Xe}$  gas towards *in vivo* applications includes the ability to perform cellular  $^{129}\text{Xe}$  NMR spectroscopy on a variety of prokaryotic and eukaryotic cells.<sup>14</sup> The cell density in these experiments ranged from 42 to 162 million cells per mL, with typically 0.5 mL sample volumes.<sup>14</sup> The NMR spectra of intact cells from various cell lines were shown to consist of two distinct peaks: peak 1 at 199.5 ppm was assigned to intracellular components whereas peak 2 at 195.5 ppm was assigned to extracellular components (Figure 5.2). Such distinct peak separation may make it possible to differentiate tumor and healthy cells by hyperpolarized  $^{129}\text{Xe}$  NMR spectroscopy due to differences in membrane flexibility or internal pH.<sup>14</sup> Recent studies have also focused on imaging human lungs and quantifying blood flow to human brains using hyperpolarized  $^{129}\text{Xe}$  gas.<sup>15,16</sup> Using conventional  $^1\text{H}$  MRI, lungs are difficult to image due to low proton concentration in the airways. Such limitations make  $^{129}\text{Xe}$  gas a very attractive imaging agent for lungs since it is possible to continuously replenish hyperpolarized  $^{129}\text{Xe}$  gas via inhalation and breath holds.

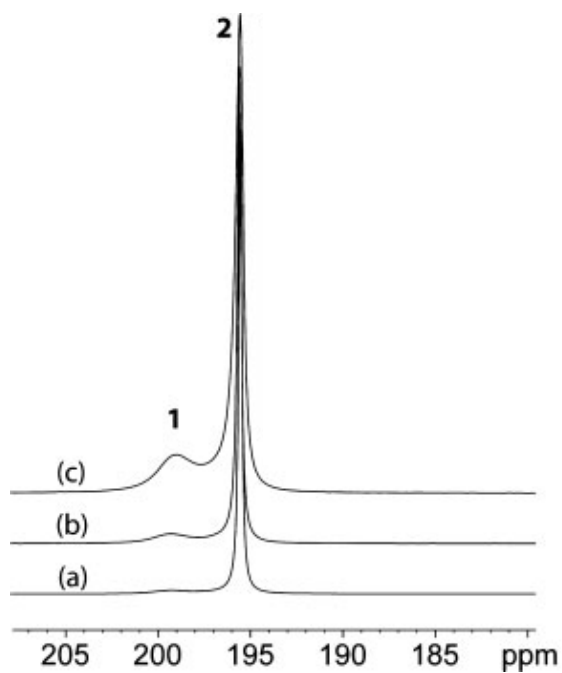


**Figure 5.2.** Hyperpolarized  $^{129}\text{Xe}$  NMR spectra of (a) 42 million cells/mL; (b) 83 million cells/mL; (c) 167 million cells/mL with K562 cells in phosphate-buffered saline at 277 K. Each sample contained approximately 5 mM of dissolved xenon. Figure was adapted from Boutina et al.<sup>14</sup>

The ability to perform cellular NMR imaging using hyperpolarized  $^{129}\text{Xe}$  gas has also motivated the development of cryptophane-based pH biosensors in the Dmochowski group. Intracellular pH is critical for various functions in cells such as proliferation and apoptosis,<sup>17-21</sup> endocytosis,<sup>18</sup> and multidrug resistance.<sup>22</sup> However, abnormal changes in pH due to modifications in cellular functions, growth and division have been associated with cancer<sup>23</sup> and Alzheimer's.<sup>24</sup> Therefore, the development of  $^{129}\text{Xe}$  biosensors that can clearly distinguish changes in both intra- and extracellular pH would assist in the sensitive detection of various diseases.

To develop such a biosensor, a recent design from our laboratory included conjugating a GALA peptide to tripropargyl cryptophane by utilizing the Huisgen [3+2] cycloaddition reaction. The water-soluble GALA peptide consists of 30 amino acids (WEAALAEALAEALAEHLAEALAEALEALAA) with a repeat sequence of glutamic acid-alanine-leucine-alanine (Figure 5.3a).<sup>25</sup> The apolar leucines confer relatively high hydrophobicity, the polar glutamic acids add a pH-dependent component to the hydrophobicity and net charge while the alanine residues act as spacers between the polar and apolar faces of the helix.<sup>25</sup> It also contains a histidine and tryptophan residue for NMR and fluorescence purposes. GALA is known to interact with the lipid bilayer preferentially at acidic pH as it undergoes a coil to  $\alpha$ -helical transition from pH 5.0 to 7.5.<sup>25</sup> At pH 5.0, some of the glutamic acids (with carboxylate side chains) are protonated, which promotes the formation of an  $\alpha$ -helical coil. At pH 7.5, electrostatic charge repulsions between the deprotonated carboxylates on the glutamic acid residues destabilize the helix. Circular dichroism (CD) measurements performed on GALA



indicated that the molar ellipticity at 222 nm changed dramatically from  $-11,500 \text{ deg cm}^2 \text{ dmol}^{-1}$  at pH 5.1 to  $-4,000 \text{ deg cm}^2 \text{ dmol}^{-1}$  at pH 7.6, which is consistent with a decrease in helical content as the pH was increased (Figure 5.3).<sup>25</sup> This peptide has been used in previous studies for pH-triggered lysis of liposomes, because at pH 5.0 the liposomes leak as GALA becomes incorporated into the vesicle bilayer and aggregates to form a transbilayer pore.<sup>25,26</sup>

Due to xenon's polarizability and sensitivity to molecular environment, we expect that a GALA-conjugated cryptophane will reflect a distinct  $^{129}\text{Xe}$  NMR chemical shift due to the conformational changes in the peptide from pH 5.0 to 7.5. Figure 5.4 shows the potential synthetic scheme for such a biosensor. If the GALA-conjugated cryptophane is not highly water-soluble, 2-azido propionic acid groups could also be "clicked" on to improve solubility, as was done with the integrin and carbonic anhydrase targeting biosensors.<sup>5,27</sup> The synthesis of this biosensor is currently underway.

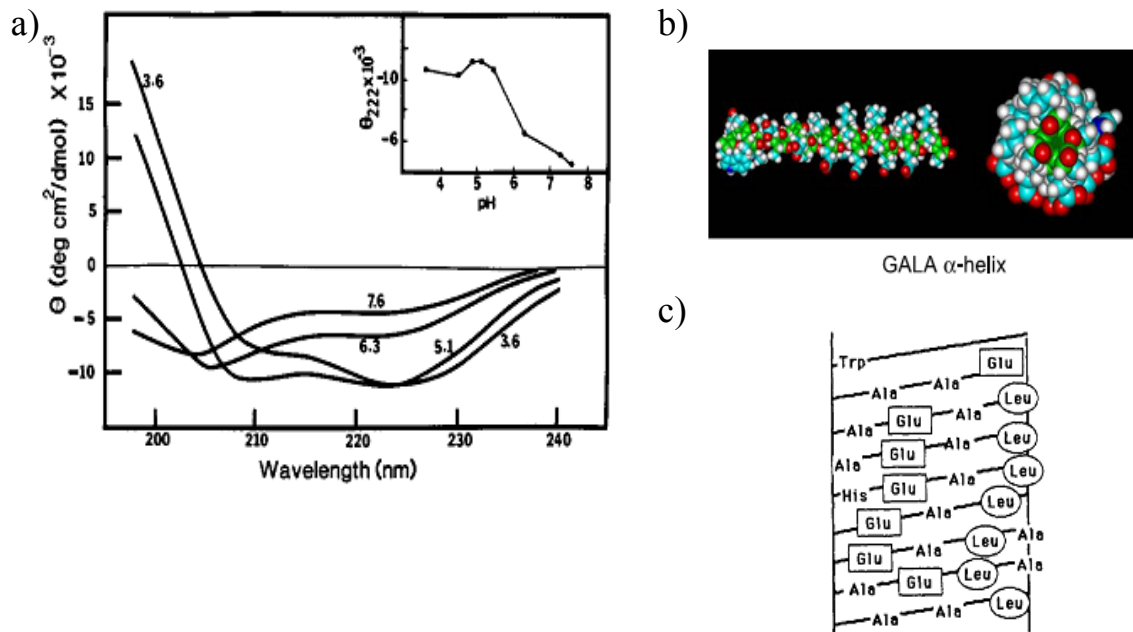


**Figure 5.3.** a) Circular dichroism spectra of GALA in 5 mM TES buffer, 100 mM KCl at varying pH, b) Structural representations of the GALA peptide with side view along the helical axis and end view of the C-terminus. Oxygen, carbon, nitrogen, hydrogen and sulfur atoms are represented by red, light blue, dark blue, white and yellow color, respectively, c) Helical grid representation of GALA demonstrating the stacking of the glutamic acid residues. Figure was adapted from Subbarao and Li, et al.<sup>25,26</sup>

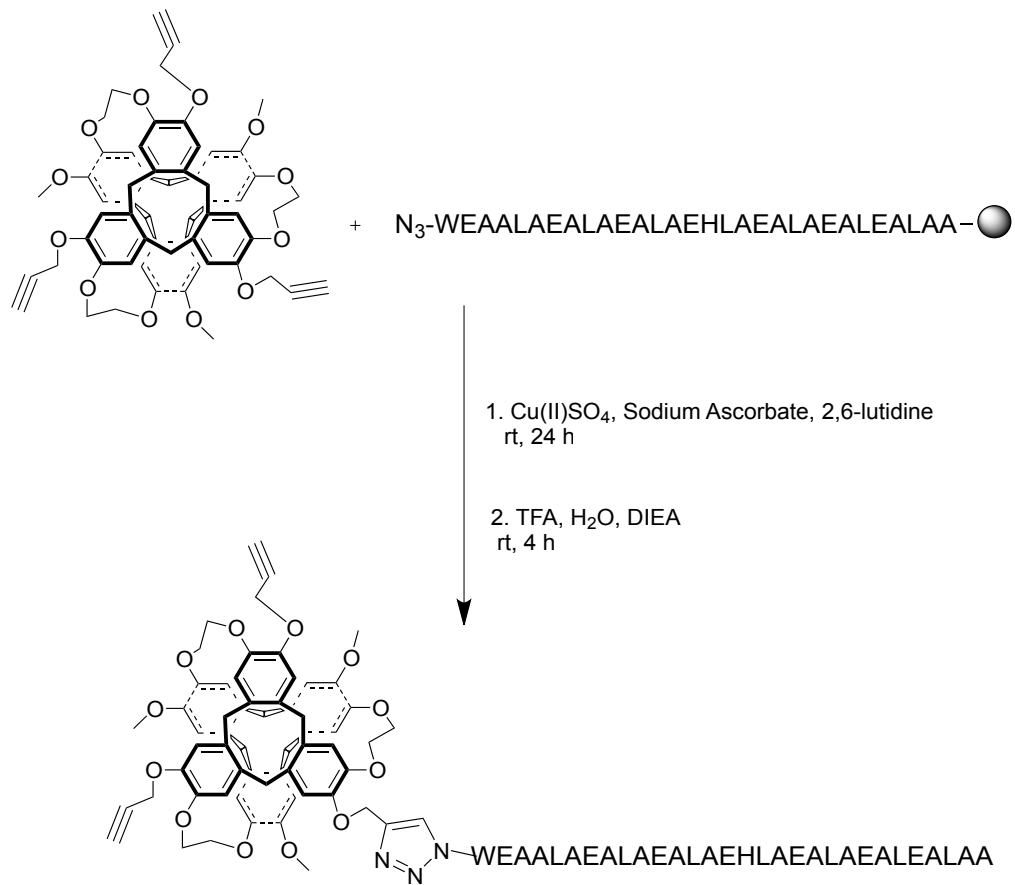


**Figure 5.4.** Synthetic scheme of a GALA-conjugated cryptophane pH sensor.

As mentioned in Chapter 1, our lab has synthesized several carbonic anhydrase (CA)-targeting biosensors where the recognition moiety consisted of a benzenesulfonamide group attached to the cryptophane by a variable-length linker. These biosensors exhibited the largest changes in chemical shifts upon binding to CA (3.0-7.5 ppm) and were able to differentiate between CA I and II isozymes, showing either 1 or 2 “bound” peaks.<sup>27</sup> We hypothesized that this was due to the presence of racemic mixtures (+/-) of enantiomers for the biosensor, which formed diastereomers once bound to the chiral protein. In order to perform multiplexing with hyperpolarized <sup>129</sup>Xe MR imaging and maintain high signal-to-noise, it is pertinent to reduce the number of NMR resonances due to racemic mixtures. To achieve this goal, enantiomerically pure cryptophanes are currently being synthesized by Dr. Olena Taratula in our lab. The synthetic scheme for making enantiomerically pure cryptophanes involves the deprotection of tri-substituted cryptophane using a Pd catalyst to afford tri-hydroxyl cryptophane (Figure 5.5a). Tri-hydroxyl cryptophane can then be reacted with 3 equiv. (S)-Mosher’s acid in the presence of DMAP/Et<sub>3</sub>N. The two resulting cryptophane-A diastereomers **2a** and **2b** functionalized with the three chiral auxiliaries are successfully separated by column chromatography. In previous studies, in an effort to synthesize enantiomerically pure cryptophanes, diastereomers of mono(-)camphanic ester cryptophanes had also been synthesized which required HPLC purification for effective separation.<sup>28</sup> Once the diastereomers are separated using column chromatography, they can be deprotected via basic hydrolysis affording enantiopure tri-hydroxyl cryptophanes (-) **3a** and (+) **3b**. Finally, reaction with 3 equiv. propargyl bromide would give the enantiomerically pure cryptophane (-) **4a** and (+) **4b**. Targeting moieties such as the benzenesulfonamide group or

folate recognition moiety can then be attached by [3+2] cycloaddition to synthesize a variety of enantiomerically pure  $^{129}\text{Xe}$  cryptophane biosensors.

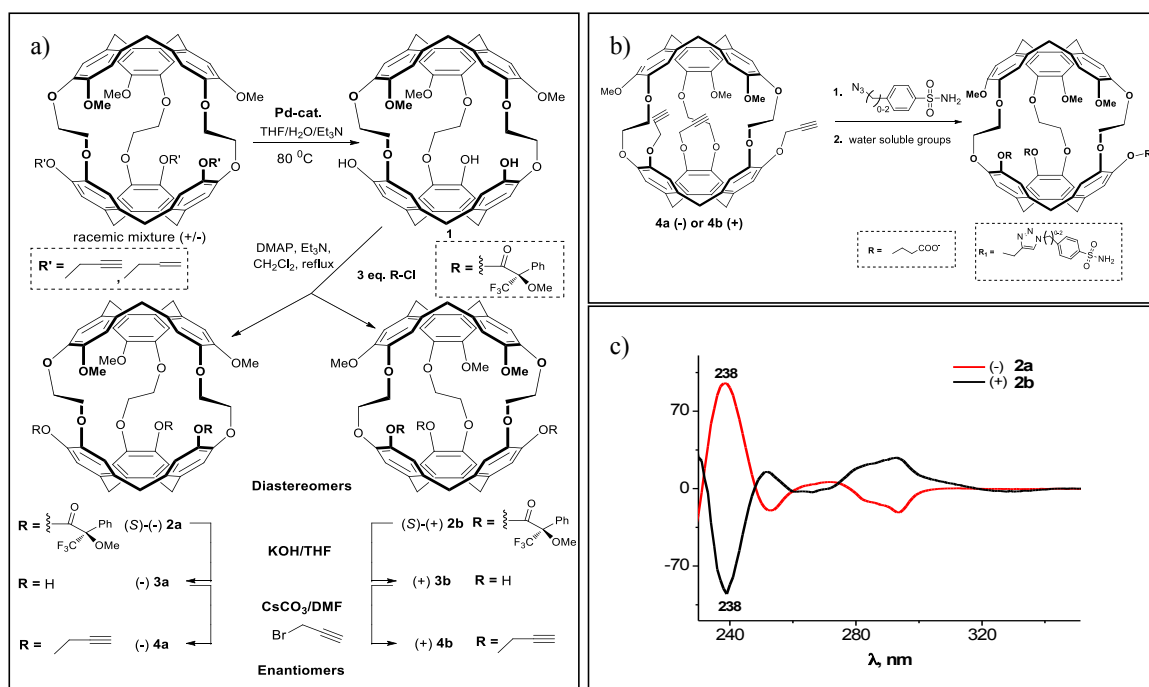


**Figure 5.5.** a) Synthesis of enantiopure tripropargyl cryptophanes, b) Synthesis of future enantiopure CA biosensors, c) Circular dichroism spectra confirming the separation of (+) **2a** and (-) **2a** diastereomers by column chromatography. Figure adapted from Dr. Olena Taratula (Personal communication).

Lastly, in Chapter 4 we outlined a new application for a tribenzylamine hemicryptophane where the cage could be utilized to develop molecular devices. A tribenzylamine moiety was connected to a cyclotrimeratrylene (CTV) unit to form a new hemicryptophane, which resembled a macroscopic gyroscope. Similar to a gyroscope, it had a stator (amine and the CTV unit) with multiple rotators (*p*-phenylene groups). <sup>1</sup>H variable temperature NMR spectroscopy and molecular dynamics simulations were in agreement that the rotation energy barrier of the rotators was approximately 10 kcal/mol. Currently, computational studies are underway in collaboration with the Saven group to determine how structural changes in the cage (e.g., removal of the methoxy groups, incorporation of different moieties with dipole moments or bulkier substituents) may alter the rotational barrier of the *p*-phenylene groups. One can imagine that by engineering hemicryptophanes with rotators that undergo unidirectional motion, it should be possible to direct their movement in solution or on surfaces.

## REFERENCES

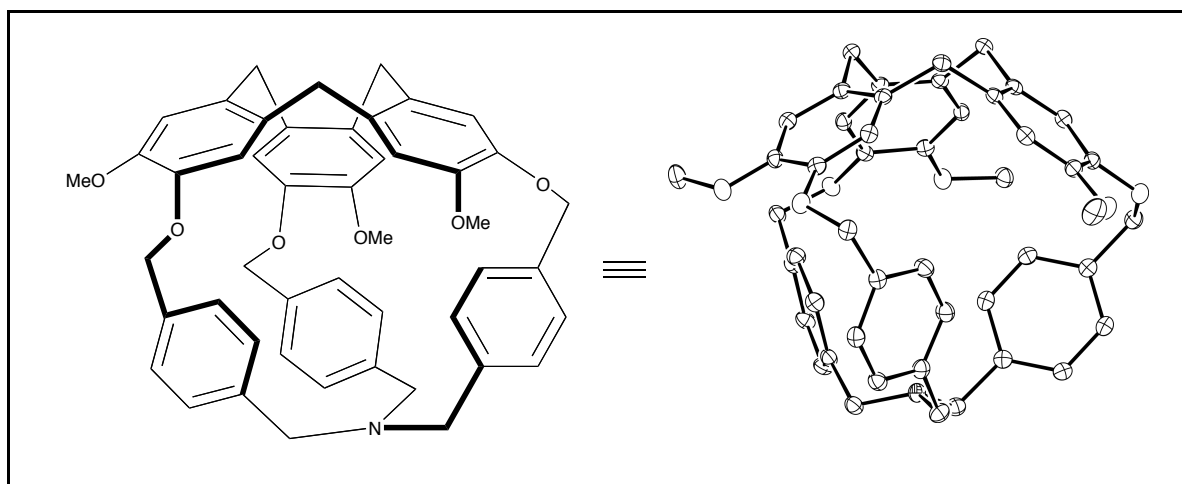
- (1) Huber, G.; Brotin, T.; Dubois, L.; Desvaux, H.; Dutasta, J. P.; Berthault, P. *J. Am. Chem. Soc.* **2006**, *128*, 6239-6246.
- (2) Hill, P. A.; Wei, Q.; Troxler, T.; Dmochowski, I. J. *J. Am. Chem. Soc.* **2009**, *131*, 3069-3077.
- (3) Hill, P. A.; Wei, Q.; Eckenhoff, R. G.; Dmochowski, I. J. *J. Am. Chem. Soc.* **2007**, *129*, 9262-9263.
- (4) Darby, S.; Hill, D.; Auvinen, A.; Barros-Dios, J. M.; Baysson, H.; Bochicchio, F.; Deo, H.; Falk, R.; Forastiere, F.; Hakama, M.; Heid, I.; Kreienbrock, L.; Kreuzer, M.; Lagarde, F.; Mäkeläinen, I.; Muirhead, C.; Oberaigner, W.; Pershagen, G.; Ruano-Ravina, A.; Ruosteenoja, E.; Schaffrath Rosario, A.; Tirmarche, M.; Tomášek, L.; Whitley, E.; Wichmann, H. E.; Doll, R. *Brit. Med. J.* **2005**, *330*, 223-227.
- (5) Seward, G. K.; Bai, Y.; Khan, N. S.; Dmochowski, I. J. *Chem. Sci.* **2011**, doi: 10.1039/c1031sc00041a.
- (6) Seward, G. K.; Wei, Q.; Dmochowski, I. J. *Bioconjug. Chem.* **2008**, *19*, 2129-2135.
- (7) Byzova, T. V.; Goldman, C. K.; Pampori, N.; Thomas, K. A.; Bett, A.; Shattil, S. J.; Plow, E. F. *Mol. Cell* **2000**, *6*, 851-860.
- (8) Byzova, T. V.; Kim, W.; Midura, R. J.; Plow, E. F. *Exp. Cell. Res.* **2000**, *254*, 299-308.
- (9) Cai, W.; Chen, X. *J. Nucl. Med.*, **2008**, 113S-128S.
- (10) Cairns, R. A.; R., K.; Hill, R. P. *Curr. Mol. Med.* **2003**, *3*, 659-671.



- (11) Felding-Habermann, B. *Clin. Exp. Metastasis* **2003**, *20*, 203-213.
- (12) Meldrum, T.; Seim, K. L.; Bajaj, V. S.; Palaniappan, K. K.; Wu, W.; Francis, M. B.; Wemmer, D. E.; Pines, A. *J. Am. Chem. Soc.* **2010**, *132*, 5936-5937.
- (13) Schroder, L.; Lowery, T. J.; Hilty, C.; Wemmer, D. E.; Pines, A. *Science* **2006**, *314*, 446-449.
- (14) Boutina, C.; Desvauxa, H.; Carrierea, M.; Leteurtreb, F.; Jaminb, N.; Boulardb, Y.; Berthault, P. *NMR Biomed.* **2011**, *24*, 1-7.
- (15) Venkatesh, A. K.; Zhao, L.; Balamore, D.; Jolesz, F. A.; Albert, M. S. *NMR Biomed.* **2000**, *13*, 245-252.
- (16) Driehuys, B.; Möller, H. E.; Cleveland, Z. I.; Pollaro, J.; Hedlund, L. W. *Radiology* **2009**, *252*, 386-393.
- (17) Gottlieb, R. A.; Dosanjh, A. *Proc. Natl. Acad. Sci. U. S. A.* **1996**, *93*, 3587-3591.
- (18) Gottlieb, R. A.; Nordberg, J.; Skowronski, E.; Babior, B. M. *Proc. Natl. Acad. Sci. U. S. A.* **1996**, *93*, 654-658.
- (19) Ishaque, A.; Al-Rubeai, M. *J. Immunol. Methods* **1998**, *221*, 43-57.
- (20) Perez-Sala, D.; Collado-Escobar, D.; Mollinedo, F. *J. Biol. Chem.* **1995**, *270*, 6235-6242.
- (21) Han, J.; Burgess, K. *Chem. Rev.* **2010**, *110*, 2709-2728.
- (22) Simon, S.; Roy, D.; Schindler, M. *Proc. Natl. Acad. Sci. U. S. A.* **1994**, *91*, 1128-1132.

- (23) Izumi, H.; Torigoe, T.; Ishiguchi, H.; Uramoto, H.; Yoshida, Y.; Tanabe, M.; Ise, T.; Murakami, T.; Yoshida, T.; Nomoto, M.; Kohno, K. *Cancer Treat. Rev.* **2003**, *29*, 541-549.
- (24) Davies, T. A.; Fine, R. E.; Johnson, R. J.; Levesque, C. A.; Rathbun, W. H.; Seetoo, K. F.; Smith, S. J.; Strohmeier, G.; Volicer, L.; Delva, L.; et al. *Biochem. Biophys. Res. Commun.* **1993**, *194*, 537-543.
- (25) Subbarao, N. K.; Parente, R. A.; Szoka, F. C., Jr.; Nadasdi, L.; Pongracz, K. *Biochemistry* **1987**, *26*, 2964-2972.
- (26) Li, W.; Nicol, F.; Szoka, F. C., Jr. *Adv. Drug Deliv. Rev.* **2004**, *56*, 967-985.
- (27) Chambers, J. M.; Hill, P. A.; Aaron, J. A.; Han, Z.; Christianson, D. W.; Kuzma, N. N.; Dmochowski, I. J. *J. Am. Chem. Soc.* **2009**, *131*, 563-569.
- (28) Brotin, T.; Barbe, R.; Darzac, M.; Dutasta, J. P. *Chem. Eur. J.* **2003**, *9*, 5784-5792.

# APPENDIX A: X-RAY STRUCTURE DETERMINATION OF TRIBENZYLAMINE HEMICRYPTOPHANE



Tribenzylamine hemicryptophane,  $C_{48}H_{45}NO_6$ , crystallizes in the monoclinic space group  $P2_1/c$  (systematic absences  $0k0$ :  $k = \text{odd}$  and  $h0l$ :  $l = \text{odd}$ ) with  $a = 17.098(2)\text{\AA}$ ,  $b = 11.4592(9)\text{\AA}$ ,  $c = 21.096(2)\text{\AA}$ ,  $\beta = 113.539(2)^\circ$ ,  $V = 3789.3(6)\text{\AA}^3$ ,  $Z = 4$  and  $d_{\text{calc}} = 1.283 \text{ g/cm}^3$ . X-ray intensity data were collected on a Rigaku Mercury CCD area detector employing graphite-monochromated Mo-K $\alpha$  radiation ( $\lambda = 0.71073 \text{ \AA}$ ) at a temperature of 143 K. Preliminary indexing was performed from a series of twelve  $0.5^\circ$  rotation images with exposures of 30 seconds. A total of 336 rotation images were collected with a crystal to detector distance of 35 mm, a  $2\theta$  swing angle of  $-12^\circ$ , rotation widths of  $0.5^\circ$  and exposures of 10 seconds: scan no. 1 was a  $\phi$ -scan from  $170^\circ$  to  $338^\circ$  at  $\omega = 0^\circ$  and  $\chi = 0^\circ$ . Rotation images were processed using CrystalClear,<sup>1</sup> producing a listing of unaveraged  $F^2$  and  $\sigma(F^2)$  values which were then passed to the CrystalStructure<sup>2</sup> program package for further processing and structure solution on a Dell Pentium III computer. A total of 15571 reflections were measured over the ranges  $5.2 \leq 2\theta \leq 50.02^\circ$ ,  $-16 \leq h \leq 20$ ,  $-13 \leq k \leq 12$ ,  $-23 \leq l \leq 25$  yielding 6601 unique reflections ( $R_{\text{int}} = 0.0261$ ). The intensity data were corrected for Lorentz and polarization effects and for absorption using REQAB<sup>3</sup> (minimum and maximum transmission 0.853, 1.000).

The structure was solved by direct methods (SIR97).<sup>4</sup> Refinement was by full-matrix least squares based on  $F^2$  using SHELXL-97.<sup>5</sup> All reflections were used during refinement ( $F^2$ 's that were experimentally negative were replaced by  $F^2 = 0$ ). The weighting scheme used was  $w = 1/[\sigma^2(F_o^2) + 0.0547P^2 + 0.9350P]$  where  $P = (F_o^2 + 2F_c^2)/3$ . Non-hydrogen atoms were refined anisotropically and hydrogen atoms were refined

using a "riding" model. Refinement converged to  $R_1 = 0.0479$  and  $wR_2 = 0.1107$  for 5502 reflections for which  $F > 4\sigma(F)$  and  $R_1 = 0.0599$ ,  $wR_2 = 0.1204$  and  $GOF = 1.078$  for all 6601 unique, non-zero reflections and 500 variables.<sup>6</sup> The maximum  $\Delta/\sigma$  in the final cycle of least squares was 0.001 and the two most prominent peaks in the final difference Fourier were +0.173 and -0.253 e/Å<sup>3</sup>.

Table 1 lists cell information, data collection parameters, and refinement data. Final positional and equivalent isotropic thermal parameters are given in Table 2. Anisotropic thermal parameters are in Table 3. Tables 4 and 5 list bond distances and bond angles. Figure 1 is an ORTEP<sup>7</sup> representation of the molecule with 30% probability thermal ellipsoids displayed.

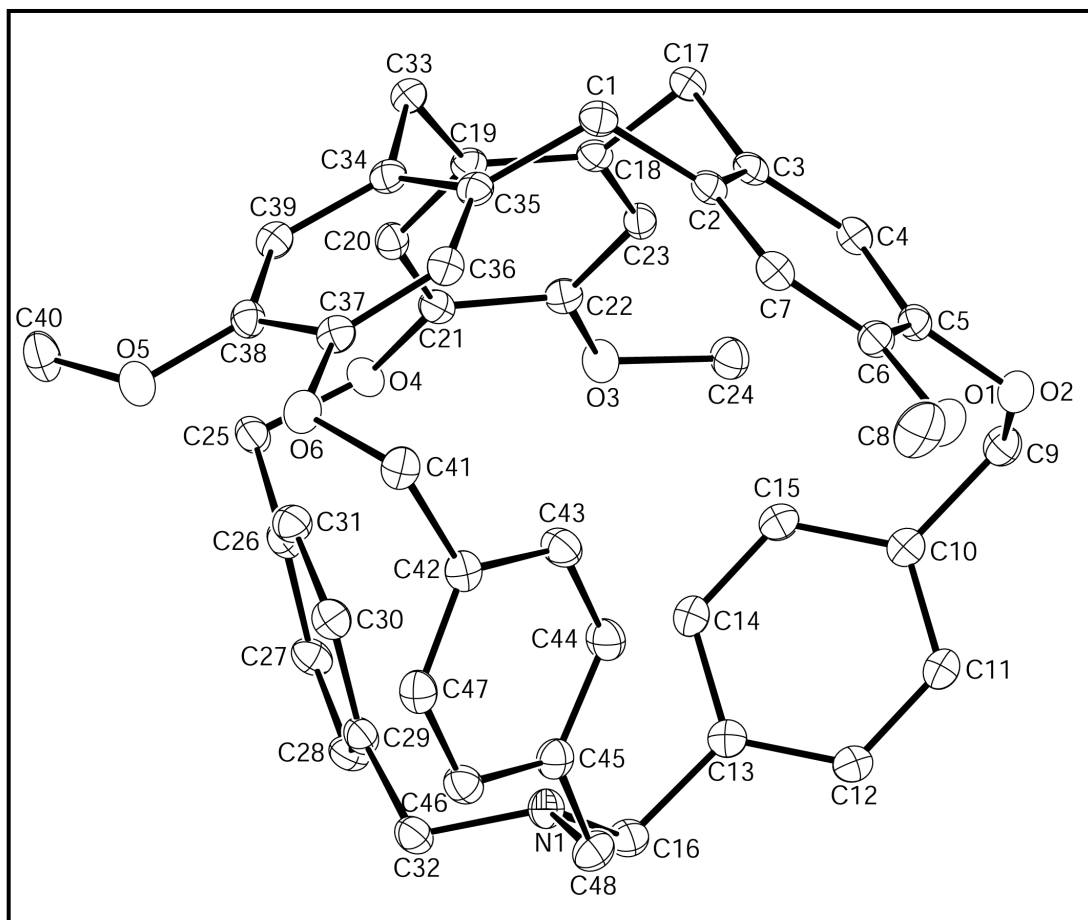


**Figure 1.** ORTEP drawing of the title compound with 30% probability thermal ellipsoids.

**Table 1.** Summary of Structure Determination of Tribenzylamine Hemicryptophane

Formula:	C <sub>48</sub> H <sub>45</sub> NO <sub>6</sub>
Formula weight:	731.85
Crystal class:	monoclinic
Space group:	P2 <sub>1</sub> /c (#14)
Z	4
Cell constants:	
a	17.098(2)Å
b	11.4592(9)Å
c	21.096(2)Å
β	113.539(2)°
V	3789.3(6)Å <sup>3</sup>
μ	0.84 cm <sup>-1</sup>
crystal size, mm	0.40 x 0.30 x 0.15
D <sub>calc</sub>	1.283 g/cm <sup>3</sup>
F(000)	1552
Radiation:	Mo-K <sub>α</sub> (λ = 0.71073Å)
2θ range	5.2 – 50.02°
hkl collected:	-16 ≤ h ≤ 20; -13 ≤ k ≤ 12; -23 ≤ l ≤ 25
No. reflections measured:	15571
No. unique reflections:	6601 (R <sub>int</sub> = 0.0261)
No. observed reflections	5502 (F > 4σ)

No. reflections used in refinement	6601
No. parameters	500
R indices ( $F > 4\sigma$ )	$R_1 = 0.0479$ $wR_2 = 0.1107$
R indices (all data)	$R_1 = 0.0599$ $wR_2 = 0.1204$
GOF:	1.078
Final Difference Peaks, $e/\text{\AA}^3$	+0.173, -0.253



**Table 2.** Refined Positional Parameters for Tribenzylamine Hemicryptophane

Atom	x	y	z	$U_{eq}, \text{\AA}^2$
C1	0.68997(11)	0.3795(2)	0.29839(9)	0.0268(4)
H1a	0.6451	0.3270	0.2672	0.036
H1b	0.7209	0.3367	0.3421	0.036
C2	0.75236(11)	0.40673(14)	0.26512(9)	0.0246(4)
C3	0.84043(11)	0.41596(14)	0.30238(9)	0.0244(4)
C4	0.89146(11)	0.4396(2)	0.26611(9)	0.0264(4)
H4	0.9515	0.4432	0.2911	0.035
C5	0.85851(11)	0.4579(2)	0.19571(9)	0.0261(4)
C6	0.77077(11)	0.4453(2)	0.15789(9)	0.0281(4)
C7	0.71970(11)	0.4191(2)	0.19298(9)	0.0273(4)
H7	0.6602	0.4092	0.1672	0.036
C8	0.65700(13)	0.4318(2)	0.04641(11)	0.0506(6)
H8a	0.6450	0.3517	0.0562	0.076
H8b	0.6468	0.4387	-0.0026	0.076
H8c	0.6196	0.4859	0.0571	0.076
C9	0.97285(11)	0.5726(2)	0.19077(10)	0.0299(4)
H9a	1.0114	0.5752	0.1661	0.040
H9b	1.0073	0.5514	0.2395	0.040
C10	0.93397(10)	0.6912(2)	0.18818(9)	0.0268(4)
C11	0.92045(10)	0.7637(2)	0.13235(9)	0.0276(4)
H11	0.9395	0.7403	0.0977	0.037
C12	0.87924(11)	0.8709(2)	0.12626(9)	0.0276(4)

H12	0.8709	0.9197	0.0877	0.037
C13	0.85038(11)	0.9070(2)	0.17561(9)	0.0270(4)
C14	0.86559(12)	0.8350(2)	0.23278(10)	0.0329(4)
H14	0.8472	0.8591	0.2677	0.044
C15	0.90709(12)	0.7294(2)	0.23933(9)	0.0320(4)
H15	0.9175	0.6821	0.2789	0.042
C16	0.80156(11)	1.0198(2)	0.16882(10)	0.0306(4)
H16a	0.8320	1.0701	0.2094	0.041
H16b	0.7981	1.0620	0.1268	0.041
C17	0.88499(11)	0.4075(2)	0.38059(9)	0.0246(4)
H17a	0.9415	0.3704	0.3932	0.033
H17b	0.8509	0.3577	0.3984	0.033
C19	0.83844(10)	0.5756(2)	0.43743(8)	0.0236(4)
C20	0.85107(10)	0.6909(2)	0.46236(8)	0.0250(4)
H20	0.8110	0.7241	0.4780	0.033
C21	0.91926(11)	0.7572(2)	0.46494(9)	0.0246(4)
C22	0.97914(10)	0.7078(2)	0.44247(9)	0.0255(4)
C23	0.96706(11)	0.5946(2)	0.41771(9)	0.0249(4)
H23	1.0077	0.5611	0.4028	0.033
C18	0.89641(10)	0.5275(2)	0.41390(8)	0.0231(4)
C24	1.10639(11)	0.7335(2)	0.42323(10)	0.0339(5)
H24a	1.1326	0.6623	0.4485	0.051
H24b	1.1508	0.7921	0.4298	0.051
H24c	1.0770	0.7157	0.3739	0.051
C25	0.86890(11)	0.9424(2)	0.49063(9)	0.0284(4)

H25a	0.8923	1.0113	0.5205	0.038
H25b	0.8321	0.8992	0.5088	0.038

C26	0.81656(11)	0.9819(2)	0.41791(9)	0.0271(4)
C27	0.84351(11)	1.0774(2)	0.39113(9)	0.0296(4)
H27	0.8925	1.1200	0.4199	0.039
C28	0.79946(12)	1.1112(2)	0.32269(10)	0.0303(4)
H28	0.8184	1.1773	0.3056	0.040
C29	0.72828(11)	1.0500(2)	0.27887(9)	0.0278(4)
C30	0.70048(11)	0.9553(2)	0.30603(10)	0.0299(4)
H30	0.6515	0.9127	0.2772	0.040
C31	0.74325(11)	0.9228(2)	0.37437(10)	0.0304(4)
H31	0.7225	0.8592	0.3921	0.040
C32	0.68496(12)	1.0772(2)	0.20272(9)	0.0305(4)
H32a	0.6224	1.0698	0.1872	0.041
H32b	0.6981	1.1583	0.1940	0.041
C33	0.76095(11)	0.5109(2)	0.43731(9)	0.0260(4)
H33a	0.7705	0.4260	0.4353	0.035
H33b	0.7550	0.5271	0.4813	0.035
C34	0.67860(10)	0.5436(2)	0.37776(9)	0.0249(4)
C35	0.64710(11)	0.4857(2)	0.31415(9)	0.0249(4)
C36	0.57016(11)	0.5239(2)	0.26292(9)	0.0264(4)
H36	0.5473	0.4828	0.2203	0.035
C37	0.52585(10)	0.6194(2)	0.27182(9)	0.0272(4)

C38	0.55679(11)	0.6754(2)	0.33629(9)	0.0265(4)
C39	0.63139(11)	0.6363(2)	0.38791(9)	0.0264(4)
H39	0.6514	0.6734	0.4318	0.035
C40	0.53370(13)	0.8133(2)	0.41162(10)	0.0403(5)
H40a	0.5307	0.7524	0.4432	0.061
H40b	0.4957	0.8778	0.4109	0.061
H40c	0.5924	0.8420	0.4274	0.061
C41	0.43175(11)	0.6401(2)	0.15108(9)	0.0302(4)
H41a	0.3705	0.6548	0.1232	0.040
H41b	0.4438	0.5575	0.1446	0.040
C42	0.48468(11)	0.7182(2)	0.12638(9)	0.0281(4)
C43	0.56745(11)	0.6877(2)	0.13472(10)	0.0337(4)
H43	0.5880	0.6113	0.1497	0.045
C44	0.61975(11)	0.7673(2)	0.12146(10)	0.0337(4)
H44	0.6761	0.7452	0.1282	0.045
C45	0.59082(11)	0.8795(2)	0.09831(9)	0.0295(4)
C46	0.50707(12)	0.9073(2)	0.08574(9)	0.0318(4)
H46	0.4851	0.9817	0.0673	0.042
C47	0.45492(11)	0.8278(2)	0.09974(9)	0.0312(4)
H47	0.3978	0.8488	0.0909	0.042
C48	0.65400(12)	0.9685(2)	0.09431(9)	0.0329(4)
H48a	0.6841	0.9371	0.0665	0.044
H48b	0.6236	1.0404	0.0716	0.044
N1	0.71561(9)	0.99538(13)	0.16430(7)	0.0281(3)
O1	0.74317(8)	0.45924(12)	0.08764(6)	0.0387(3)

O2	0.90822(8)	0.48420(11)	0.15958(6)	0.0317(3)
O3	1.04669(7)	0.77780(11)	0.44864(7)	0.0318(3)
O4	0.93840(7)	0.86765(10)	0.49263(6)	0.0281(3)
O5	0.50798(8)	0.76623(11)	0.34394(7)	0.0338(3)
O6	0.45025(7)	0.66099(11)	0.22319(6)	0.0310(3)
$U_{eq} = 1/3[U_{11}(aa^*)^2 + U_{22}(bb^*)^2 + U_{33}(cc^*)^2 + 2U_{12}aa^*bb^*\cos\gamma + 2U_{13}aa^*cc^*\cos\beta + 2U_{23}bb^*cc^*\cos\alpha]$				

**Table 3.** Refined Thermal Parameters (U's) for Tribenzylamine Hemicryptophane

Atom	U <sub>11</sub>	U <sub>22</sub>	U <sub>33</sub>	U <sub>23</sub>	U <sub>13</sub>	U <sub>12</sub>
C1	0.0279(9)	0.0225(9)	0.0288(10)	-0.0014(8)	0.0100(8)	-0.0033(8)
C2	0.0275(9)	0.0184(9)	0.0265(9)	-0.0019(7)	0.0093(8)	0.0002(7)
C3	0.0282(9)	0.0172(8)	0.0261(9)	-0.0015(7)	0.0091(8)	0.0015(7)
C4	0.0249(9)	0.0241(9)	0.0289(10)	-0.0028(8)	0.0094(8)	0.0007(8)
C5	0.0291(9)	0.0229(9)	0.0291(10)	-0.0021(8)	0.0145(8)	-0.0004(8)
C6	0.0316(10)	0.0286(10)	0.0219(9)	-0.0001(8)	0.0085(8)	0.0035(8)
C7	0.0238(9)	0.0255(9)	0.0281(10)	-0.0039(8)	0.0054(8)	0.0000(8)
C8	0.0399(12)	0.078(2)	0.0250(11)	-0.0015(11)	0.0035(9)	-0.0016(12)
C9	0.0246(9)	0.0341(10)	0.0326(11)	0.0002(8)	0.0131(8)	-0.0025(8)
C10	0.0224(9)	0.0303(10)	0.0259(10)	-0.0012(8)	0.0079(7)	-0.0033(8)
C11	0.0256(9)	0.0324(10)	0.0254(10)	-0.0042(8)	0.0109(8)	-0.0063(8)
C12	0.0284(9)	0.0273(10)	0.0248(9)	-0.0006(8)	0.0084(8)	-0.0046(8)
C13	0.0228(9)	0.0278(10)	0.0286(10)	-0.0013(8)	0.0085(8)	-0.0040(8)
C14	0.0383(10)	0.0351(11)	0.0293(10)	-0.0006(8)	0.0177(9)	0.0025(9)
C15	0.0367(10)	0.0338(11)	0.0256(10)	0.0043(8)	0.0127(8)	0.0029(9)
C16	0.0313(10)	0.0281(10)	0.0325(10)	0.0004(8)	0.0129(8)	-0.0036(8)
C17	0.0234(9)	0.0223(9)	0.0265(10)	0.0009(7)	0.0082(7)	0.0018(7)
C19	0.0238(9)	0.0259(9)	0.0182(9)	0.0024(7)	0.0053(7)	0.0015(7)
C20	0.0243(9)	0.0284(9)	0.0209(9)	-0.0012(7)	0.0076(7)	0.0029(8)
C21	0.0281(9)	0.0221(9)	0.0196(9)	-0.0014(7)	0.0053(7)	0.0013(8)

C22	0.0232(9)	0.0272(9)	0.0236(9)	0.0012(8)	0.0067(7)	-0.0006(8)
C23	0.0257(9)	0.0269(10)	0.0222(9)	-0.0004(7)	0.0095(7)	0.0042(8)
C18	0.0244(9)	0.0233(9)	0.0177(9)	0.0019(7)	0.0042(7)	0.0023(7)
C24	0.0291(10)	0.0342(11)	0.0416(12)	0.0006(9)	0.0174(9)	0.0017(9)
C25	0.0324(10)	0.0243(9)	0.0283(10)	-0.0015(8)	0.0118(8)	0.0049(8)
C26	0.0296(9)	0.0227(9)	0.0285(10)	-0.0024(8)	0.0112(8)	0.0042(8)
C27	0.0307(10)	0.0228(9)	0.0303(10)	-0.0025(8)	0.0069(8)	0.0002(8)
C28	0.0353(10)	0.0209(9)	0.0337(11)	0.0006(8)	0.0128(9)	0.0011(8)
C29	0.0280(9)	0.0259(10)	0.0287(10)	0.0002(8)	0.0107(8)	0.0064(8)
C30	0.0246(9)	0.0314(10)	0.0312(10)	-0.0012(8)	0.0085(8)	0.0004(8)
C31	0.0289(10)	0.0291(10)	0.0343(11)	0.0026(8)	0.0137(8)	0.0005(8)
C32	0.0317(10)	0.0273(10)	0.0299(10)	0.0008(8)	0.0098(8)	0.0059(8)
C33	0.0280(9)	0.0271(9)	0.0232(9)	0.0013(7)	0.0107(8)	0.0005(8)
C34	0.0237(9)	0.0254(9)	0.0266(10)	0.0019(7)	0.0110(8)	-0.0028(8)
C35	0.0246(9)	0.0235(9)	0.0281(10)	0.0014(8)	0.0120(8)	-0.0037(8)
C36	0.0244(9)	0.0279(9)	0.0256(10)	-0.0043(8)	0.0087(8)	-0.0046(8)
C37	0.0218(9)	0.0300(10)	0.0288(10)	0.0008(8)	0.0092(8)	-0.0030(8)
C38	0.0252(9)	0.0264(10)	0.0299(10)	-0.0024(8)	0.0132(8)	-0.0012(8)
C39	0.0262(9)	0.0281(10)	0.0252(10)	-0.0014(8)	0.0105(8)	-0.0035(8)
C40	0.0394(11)	0.0439(12)	0.0354(11)	-0.0086(9)	0.0124(9)	0.0104(10)
C41	0.0236(9)	0.0389(11)	0.0246(10)	-0.0021(8)	0.0059(8)	0.0000(8)
C42	0.0243(9)	0.0321(10)	0.0244(10)	-0.0042(8)	0.0061(8)	-0.0003(8)
C43	0.0310(10)	0.0295(10)	0.0408(11)	0.0030(9)	0.0145(9)	0.0043(8)
C44	0.0255(9)	0.0360(11)	0.0410(12)	0.0029(9)	0.0147(9)	0.0047(9)
C45	0.0308(10)	0.0331(10)	0.0230(9)	-0.0032(8)	0.0092(8)	-0.0008(8)

C46	0.0347(10)	0.0300(10)	0.0273(10)	-0.0002(8)	0.0088(8)	0.0045(9)
C47	0.0259(9)	0.0373(11)	0.0282(10)	-0.0028(8)	0.0083(8)	0.0028(8)
C48	0.0347(10)	0.0374(11)	0.0253(10)	-0.0001(8)	0.0108(8)	-0.0035(9)
N1	0.0274(8)	0.0297(8)	0.0265(8)	-0.0033(7)	0.0102(7)	-0.0011(7)

O1	0.0343(7)	0.0554(9)	0.0230(7)	0.0001(6)	0.0079(6)	0.0007(7)
O2	0.0349(7)	0.0328(7)	0.0314(7)	-0.0047(6)	0.0173(6)	-0.0031(6)
O3	0.0306(7)	0.0292(7)	0.0399(8)	-0.0068(6)	0.0186(6)	-0.0052(6)
O4	0.0282(6)	0.0234(6)	0.0302(7)	-0.0048(5)	0.0090(5)	0.0005(5)
O5	0.0312(7)	0.0368(8)	0.0320(7)	-0.0039(6)	0.0113(6)	0.0072(6)
O6	0.0230(6)	0.0422(8)	0.0257(7)	0.0001(6)	0.0075(5)	0.0039(6)

The form of the anisotropic displacement parameter is:

$$\exp[-2\pi^2(a^*U_{11}h^2+b^*U_{22}k^2+c^*U_{33}l^2+2b^*c^*U_{23}kl+2a^*c^*U_{13}hl+2a^*b^*U_{12}hk)].$$



**Table 4.** Bond Distances in Tribenzylamine Hemicryptophane, Å

C1-C35	1.524(2)	C1-C2	1.525(2)	C2-C3	1.397(2)
C2-C7	1.403(2)	C3-C4	1.398(2)	C3-C17	1.519(2)
C4-C5	1.378(2)	C5-O2	1.383(2)	C5-C6	1.397(2)
C6-O1	1.373(2)	C6-C7	1.384(3)	C8-O1	1.415(2)
C9-O2	1.449(2)	C9-C10	1.505(3)	C10-C11	1.383(2)
C10-C15	1.401(2)	C11-C12	1.396(3)	C12-C13	1.381(3)
C13-C14	1.397(3)	C13-C16	1.514(3)	C14-C15	1.382(3)
C16-N1	1.461(2)	C17-C18	1.521(2)	C19-C18	1.388(2)
C19-C20	1.406(2)	C19-C33	1.517(2)	C20-C21	1.374(2)
C21-O4	1.378(2)	C21-C22	1.408(2)	C22-O3	1.369(2)
C22-C23	1.383(2)	C23-C18	1.407(2)	C24-O3	1.423(2)
C25-O4	1.452(2)	C25-C26	1.504(2)	C26-C27	1.392(3)
C26-C31	1.398(3)	C27-C28	1.390(3)	C28-C29	1.389(3)
C29-C30	1.396(3)	C29-C32	1.509(2)	C30-C31	1.382(3)
C32-N1	1.466(2)	C33-C34	1.512(2)	C34-C35	1.398(2)
C34-C39	1.401(2)	C35-C36	1.398(2)	C36-C37	1.386(2)
C37-O6	1.375(2)	C37-C38	1.402(2)	C38-C39	1.380(2)
C38-O5	1.383(2)	C40-O5	1.422(2)	C41-O6	1.445(2)
C41-C42	1.506(3)	C42-C47	1.387(3)	C42-C43	1.399(2)
C43-C44	1.381(3)	C44-C45	1.394(3)	C45-C46	1.385(3)
C45-C48	1.512(3)	C46-C47	1.387(3)	C48-N1	1.464(2)

**Table 5.** Bond Angles in Tribenzylamine Hemicyptophane, °

C35-C1-C2	115.01(14)	C3-C2-C7	118.4(2)	C3-C2-C1	123.5(2)
C7-C2-C1	118.1(2)	C2-C3-C4	118.4(2)	C2-C3-C17	124.5(2)
C4-C3-C17	117.1(2)	C5-C4-C3	122.9(2)	C4-C5-O2	123.4(2)
C4-C5-C6	118.9(2)	O2-C5-C6	117.6(2)	O1-C6-C7	125.7(2)
O1-C6-C5	115.6(2)	C7-C6-C5	118.7(2)	C6-C7-C2	122.6(2)
O2-C9-C10	111.67(14)	C11-C10-C15	118.3(2)	C11-C10-C9	119.7(2)
C15-C10-C9	122.0(2)	C10-C11-C12	120.9(2)	C13-C12-C11	120.8(2)
C12-C13-C14	118.4(2)	C12-C13-C16	122.2(2)	C14-C13-C16	119.4(2)
C15-C14-C13	121.0(2)	C14-C15-C10	120.6(2)	N1-C16-C13	110.18(14)
C3-C17-C18	111.11(13)	C18-C19-C20	118.8(2)	C18-C19-C33	123.6(2)
C20-C19-C33	117.6(2)	C21-C20-C19	122.3(2)	C20-C21-O4	125.4(2)
C20-C21-C22	118.9(2)	O4-C21-C22	115.5(2)	O3-C22-C23	125.4(2)
O3-C22-C21	115.6(2)	C23-C22-C21	119.1(2)	C22-C23-C18	122.0(2)
C19-C18-C23	118.8(2)	C19-C18-C17	123.1(2)	C23-C18-C17	118.0(2)
O4-C25-C26	110.73(14)	C27-C26-C31	118.0(2)	C27-C26-C25	119.5(2)
C31-C26-C25	122.4(2)	C28-C27-C26	120.7(2)	C29-C28-C27	121.2(2)
C28-C29-C30	118.1(2)	C28-C29-C32	122.1(2)	C30-C29-C32	119.7(2)
C31-C30-C29	120.8(2)	C30-C31-C26	121.1(2)	N1-C32-C29	108.93(14)
C34-C33-C19	113.77(14)	C35-C34-C39	118.8(2)	C35-C34-C33	123.6(2)
C39-C34-C33	117.6(2)	C34-C35-C36	118.5(2)	C34-C35-C1	123.6(2)
C36-C35-C1	117.9(2)	C37-C36-C35	122.6(2)	O6-C37-C36	125.1(2)
O6-C37-C38	116.3(2)	C36-C37-C38	118.5(2)	C39-C38-O5	124.3(2)
C39-C38-C37	119.2(2)	O5-C38-C37	116.5(2)	C38-C39-C34	122.2(2)
O6-C41-C42	110.92(14)	C47-C42-C43	117.8(2)	C47-C42-C41	120.3(2)
C43-C42-C41	121.8(2)	C44-C43-C42	121.0(2)	C43-C44-C45	120.8(2)

C46-C45-C44	118.3(2)	C46-C45-C48	122.7(2)	C44-C45-C48	118.7(2)
C45-C46-C47	120.8(2)	C46-C47-C42	121.2(2)	N1-C48-C45	109.15(14)
C16-N1-C48	113.96(14)	C16-N1-C32	114.45(14)	C48-N1-C32	114.84(14)
C6-O1-C8	117.5(2)	C5-O2-C9	115.31(13)	C22-O3-C24	117.39(14)
C21-O4-C25	118.46(13)	C38-O5-C40	116.32(14)	C37-O6-C41	118.26(13)

## REFERENCES

- (1) CrystalClear: Rigaku Corporation, **1999**.
- (2) CrystalStructure: Crystal Structure Analysis Package, Rigaku Corp. Rigaku/MSK, **2002**.
- (3) REQAB4: R.A. Jacobsen, **1994**. Private Communication.
- (4) SIR97: Altomare, A.; Burla, M.; Camalli, M.; Cascarano G.; Giacovazzo, C.; Guagliardi, A.; Moliterni, A.G.; Polidori & Spagna, R. *J. Appl. Cryst.* **1992**, 32, 115-119.
- (5) SHELXL-97: Program for the Refinement of Crystal Structures, Sheldrick, G.M. **1997**, University of Göttingen, Germany.
- (6) 
$$R_1 = \sum ||F_o| - |F_c|| / \sum |F_o|$$
- $$wR_2 = \{ \sum w (F_o^2 - F_c^2)^2 / \sum w(F_o^2)^2 \}^{1/2}$$
- $$GOF = \{ \sum w (F_o^2 - F_c^2)^2 / (n - p) \}^{1/2}$$
- where n = the number of reflections and p = the number of parameters refined.
- (7) "ORTEP-II: A Fortran Thermal Ellipsoid Plot Program for Crystal Structure Illustrations". C.K. Johnson, **1976**, ORNL-5138